



**University of Białystok
Faculty of Chemistry
Doctoral School of Exact and Natural Sciences**

Izabela Kurowska

**Diverse strategies of reversible addition-
fragmentation chain transfer polymerization to obtain
polymers with desired properties and architecture**

Doctoral dissertation

Supervisors:

Prof. Agnieszka Zofia Wilczewska

Prof. Mathias Destarac

Białystok, 2024



Acknowledgments

I would like to express my deepest gratitude to my supervisors, Professor Agnieszka Zofia Wilczewska and Professor Mathias Destarac, for their support, guidance, and invaluable mentorship throughout the course of this research.

I extend my sincere thanks to the members of the Department of Polymers and Organic Synthesis at the University of Bialystok and the SOFTMAT laboratory at the University Toulouse III - Paul Sabatier. I am particularly grateful to Dr. Karolina H. Markiewicz, Dr. Iwona Misztalewska-Turkowicz, and Dr. Olivier Coutelier, for their insights and suggestions that significantly expanded my understanding of polymer chemistry.

I would also like to acknowledge my colleagues, especially Pawel Misiak, Dawid Szymczuk, Juan Antonio Rivas Loaiza, Bartosz Maliszewski, Alexis Dupre–Demorsey, Oleksandr Ivanchenko, and Maksym Odnoroh, for their camaraderie, stimulating discussions, and for all the moments we shared in the laboratory.

I would like to extend heartfelt appreciation to my family, especially my parents, for their encouragement and unwavering belief in me. Furthermore, I am deeply grateful to my fiancé for his patience, understanding, and support throughout my studies.



This work was financially supported by:

- ❖ National Science Centre, Poland, grant no. NCN/2016/21/B/ST5/01365
Novel stimuli-responsive block copolymers for smart drug delivery systems (SDDS),
(principal investigator: Prof. Agnieszka Z. Wilczewska)
- ❖ National Science Centre, Poland, grant no. NCN/2019/35/B/ST5/03391
"Two in one" - novel fluorescent polymers for simultaneous imaging and drug
delivery (principal investigator: Prof. Agnieszka Z. Wilczewska)
- ❖ French Ministry for Europe and Foreign Affairs, Eiffel Excellence scholarship
(October 2021 – September 2022)

This work was realized through cooperation with the Department of Experimental Pharmacology and Department of Clinical Pharmacology of the Medical University of Białystok (Prof. Halina Car, Dr. Habil. Katarzyna Niemirowicz-Laskowska, and Dr. Habil. Przemysław Wielgat).

Table of Contents

LIST OF ABBREVIATIONS.....	11
ABSTRACT.....	17
CHAPTER 1. LITERATURE REVIEW	19
1.1. Radical polymerization and reversible-deactivation radical polymerization (RDRP)..	19
1.2. Reversible addition-fragmentation chain transfer (RAFT) polymerization	23
1.2.1. Mechanism of RAFT polymerization.....	24
1.2.2. Monomers	26
1.2.3. Source of radicals	26
1.2.4. Chain transfer agents	27
1.2.5. Modification of the end-groups.....	29
1.3. Photoinduced RAFT polymerization.....	31
1.4. Application of RAFT polymerization in selected fields.....	35
1.4.1. Importance of RAFT polymerization in drug delivery systems	35
1.4.1.1. Thermoresponsive polymers	41
1.4.1.2. PNIPAAm and PNVCL	43
1.4.1.3. Incorporation of lipids into the polymeric structure	48
1.4.2. Application of RAFT polymerization in the synthesis of <i>N</i> -vinylamides	49
1.4.3. Synthesis of ABA triblock polymers.....	52
1.4.3.1. Methods of synthesis.....	52
1.4.3.2. Thermoplastic elastomers.....	54
1.4.3.3. (Meth)acrylic thermoplastic elastomers.....	54
Summary.....	59
RESEARCH OBJECTIVES	61
RESEARCH HYPOTHESES.....	63
RESULTS AND DISCUSSION.....	65
CHAPTER 2. DIGLYCERIDES BASED POLYMERS	65
2.1. Synthesis of diglyceride-based chain transfer agents (CTAs) and monomers	65
2.1.1. Synthesis and characterization of diglyceride-based dithiocarbonate RAFT agents	65
2.1.2. Synthesis and characterization of diglyceride-based monomers	72
2.2. Synthesis and characterization of thermoresponsive polymers with diglyceride moieties.....	77

2.2.1. Synthesis and characterization of thermoresponsive polymers with diglyceride-based chain transfer agents	77
2.2.2. Synthesis and characterization of thermoresponsive polymers with diglyceride-based monomers	88
Summary	96
CHAPTER 3. POLYMERIC NANOPARTICLES BASED ON POLYMERS WITH DIGLYCERIDE MOIETIES	99
3.1. Polymeric nanoparticles based on homopolymers with DGs in the main chain	100
3.2. Polymeric nanoparticles based on copolymers with DGs in the side chains	107
3.2.1. Drug encapsulation and characterization of drug-loaded nanoparticles	109
3.2.2. Drug release study	114
3.2.3. Biological studies	116
3.2.4. The modification of the polymer chain-ends with a fluorescent probe.	117
Summary	121
CHAPTER 4. POLYVINYLAMIDES AND POLYVINYLAMINES	125
4.1. Photoreactors	125
4.2. The influence of light wavelength on polymerization	126
4.3. The influence of light intensity on polymerization	129
4.4. Polymerization with different targeted molar masses	130
4.5. Dithiocarbonate and light-free experiments	133
4.6. Temporal control	133
4.7. The nature of end-groups	134
4.8. Block copolymerization	137
4.8.1. Polymerization with PEG as macro-CTA.....	137
4.8.2. Polymerization with PVP as macro-CTA.....	139
4.8.2.1. Polymerization of <i>N</i> -vinylpyrrolidone (NVP)	139
4.8.2.2. Block copolymerization with NVF	141
4.8.2.3. Hydrolysis of the PNVF segment	144
Summary	146
CHAPTER 5. SYNTHESIS OF ABA TRIBLOCK COPOLYMERS	149
5.1. Synthesis of a hard block: PMMA	149
5.1.1. The influence of light wavelength on polymerization.....	149
5.1.2. The influence of monomer concentration on polymerization	151
5.1.3. The influence of light intensity on the polymerization of MMA	153

5.2. Synthesis of a soft block: PnBA.....	154
5.3. Synthesis of the ABA triblock copolymer	157
Summary	159
CONCLUSIONS AND PERSPECTIVES	161
SUMMARY IN BULLET POINTS	165
EXPERIMENTAL PART	169
CHAPTER 6. METHODS.....	169
CHAPTER 7. SYNTHETIC PROTOCOLS.....	177
7.1. Materials	177
7.2. Drug delivery systems based on polymers with diglyceride moieties	178
7.2.1. Synthesis of (2,2-dimethyl-1,3-dioxolan-4-yl)methyl 2-bromopropanoate (1)	178
7.2.2. Synthesis of 2,3-dihydroxypropyl 2-bromopropanoate (2)	178
7.2.3. Synthesis of 3-((2-bromopropanoyl)oxy)propane-1,2-diyl dipalmitate (3a)..	179
7.2.4. Synthesis of 3-((2-bromopropanoyl)oxy)propane-1,2-diyl dioleate (3b).....	179
7.2.5. Synthesis of 3-((2-((ethoxycarbonothioyl)thio)propanoyl)oxy)propane-1,2-diyl dipalmitate (4a)	180
7.2.6. Synthesis of 3-((2-((ethoxycarbonothioyl)thio)propanoyl)oxy)propane-1,2-diyl dioleate (4b)	180
7.2.7. Synthesis of 3-(benzyloxy)propane-1,2-diol (5).....	181
7.2.8. Synthesis of 3-(benzyloxy)propane-1,2-diyl dipalmitate (6a)	182
7.2.9. Synthesis of 3-(benzyloxy)propane-1,2-diyl dioleate (6b).....	182
7.2.10. Synthesis of 3-hydroxypropane-1,2-diyl dipalmitate (7a).....	183
7.2.11. Synthesis of 3-hydroxypropane-1,2-diyl dioleate (7b).....	183
7.2.12. Synthesis of 3-(acryloyloxy)propane-1,2-diyl dipalmitate (8a).....	184
7.2.13. Synthesis of 3-(acryloyloxy)propane-1,2-diyl dioleate (8b).....	185
7.2.14. General procedure for RAFT polymerization of NIPAAm with diglyceride- based chain transfer agents	185
7.2.15. General procedure for RAFT polymerization of NVCL with diglyceride-based chain transfer agents	185
7.2.16. General procedure for RAFT polymerization with GlyP acrylate	186
7.2.17. General procedure for RAFT polymerization with GlyO acrylate	186
7.2.18. General procedure for RAFT copolymerization with NIPAAm.....	186
7.2.19. General procedure for RAFT copolymerization with NVCL	187

7.2.20. Removing the dithiocarboante-end group by aminolysis	187
7.2.21. The modification of the polymer chain ends with a fluorescent dye	187
7.2.22. Radical polymerization of NVCL	188
7.2.23. Radical polymerization of NIPAAm.....	188
7.3. Polymerization of <i>N</i> -vinylformamide via PI-RAFT technique.....	188
7.3.1. General procedure for the polymerization of NVF with CTA2	188
7.3.2. Synthesis of PNVF-CTA2	190
7.3.3. Chain extension experiment.....	190
7.3.4. General procedure for the synthesis of PEG- <i>b</i> -PNVF block copolymer	191
7.3.5. General procedure for the polymerization of NVP with CTA1	191
7.3.6. General procedure for the polymerization of PVP-CTA1	192
7.3.7. General procedure for the synthesis of PVP- <i>b</i> -PNVF block copolymer	192
7.3.8. Hydrolysis of PVP- <i>b</i> -PNVF.....	193
7.4. Synthesis of ABA triblock copolymers via PI-RAFT technique	193
7.4.1. General procedure for the polymerization of MMA with TTC-bCP	193
7.4.2. General procedure for the polymerization of <i>n</i> BA with TTC-bCP.....	194
7.4.3. General procedure for ABA triblock copolymer synthesis.....	195
7.5. Synthesis of methyl 2-((ethoxycarbonothioyl)thio)propanoate (CTA1)	195
7.6. Synthesis of <i>S</i> -(cyanomethyl) <i>O</i> -ethyl carbonodithioate (CTA2).....	195
LIST OF FIGURES	197
LIST OF SCHEMES	203
LIST OF TABLES	205
SCIENTIFIC ACHIEVEMENTS	207
REFERENCES	211

LIST OF ABBREVIATIONS

5-FU	5-fluorouracil
A4F	asymmetric flow field flow fractionation
AAm	acrylamide
AcOH	acetic acid
ACVA	4,4'-azobis(4-cyanovaleric acid)
AIBN	2,2'-azobis(2-methylpropionitrile)
AIHA	acute immune hemolytic anemia
AN	acrylonitrile
ATR-FTIR	attenuated total reflectance Fourier transform infrared spectroscopy
ATRP	atom transfer radical polymerization
BA	baicalein
BBB	blood-brain barrier
BCl₃	boron trichloride
BDAT	<i>S,S'</i> -bis(α,α' -dimethylacetic acid)trithiocarbonate
BIRP	organobismuthine-mediated radical polymerization
bisMPA	2,2-bis(hydroxymethyl)propionic acid
BSA	bovine serum albumin
CA	cinnamaldehyde
CA4	combretastatin A4 disodium phosphate
CBZ	carbamazepine
CCL	core-cross-linked
CDCl₃	deuterated chloroform
chol	cholesterol
CLRP	controlled/living radical polymerization
CMC	critical micelle concentration
CMRP	cobalt-mediated radical polymerization
CPLL	cyclic-poly(L-lysine)
CPP	cell-penetrating peptide
CPX	ciprofloxacin
CRISPR	clustered regularly interspaced short palindromic repeat system
CS	chitosan
CSIRO	Commonwealth Scientific and Industrial Research Organization
CTA	chain transfer agent
CTA1	methyl 2-((ethoxycarbonothioyl)thio)propanoate
CTA2	<i>S</i> -(cyanomethyl) <i>O</i> -ethyl carbonodithioate
CTA3	bis-(2-methylpropanenitrile)trithiocarbonate
CUR	curcumin
D(Phe-Lys)	dendric phenylalanyllysine
DA	2,3-dimethylmaleic anhydride
DBTTC	<i>S,S</i> -dibenzyl trithiocarbonate
DCC	<i>N,N</i> -dicyclohexylcarbodiimide

DCM	dichloromethane
DGs	diglycerides
DLC	drug loading content
DLE	drug loading efficiency
DLS	dynamic light scattering
DMAEMA	<i>N,N</i> -dimethylaminoethyl methacrylate
DMAP	dimethylaminopyridine
DMF	<i>N,N</i> -dimethylformamide
DMSO	dimethylsulfoxide
DMSO-<i>d</i>₆	deuterated dimethylsulfoxide
DNA	deoxyribonucleic acid
DNR	daunorubicin
DOSY NMR	diffusion-ordered spectroscopy nuclear magnetic resonance
DOX	doxorubicin
DP	degree of polymerization
DSC	differential scanning calorimetry
DT	degenerative transfer process
DTG	derivative thermogravimetry
DTX	docetaxel
DXA	dextran
ELS	electrophoretic light scattering
EPR	permeability and retention effect
ESI-TOF MS	electrospray-ionization time-of-flight mass spectrometry
EtOAc	ethyl acetate
FA	fatty acid
FBS	fetal bovine serum
FDA	Food and Drug Administration
FLA	folic acid
FLU	fluorescein
Fmoc	fluorenylmethoxycarbonyl protecting group
GEM	gemcitabine
GEN	gentamicin
GL	glycine
GlyO-A	3-(acryloyloxy)propane-1,2-diyl dioleate
GlyO-X	3-((2-((ethoxycarbonothioyl)thio)propanoyl)oxy)propane-1,2-diyl dioleate
GlyP-A	3-(acryloyloxy)propane-1,2-diyl dipalmitate
GlyP-X	3-((2-((ethoxycarbonothioyl)thio)propanoyl)oxy)propane-1,2-diyl dipalmitate
GMA	glycidyl methacrylate
GNR	gold nanorods
GO	graphene
HCCA	α -cyano-4-hydroxycinnamic acid
HEMA	2-hydroxyethyl methacrylate

HLB	hydrophilic-lipophilic balance
HMM	high molar mass
HPLC	high-performance liquid chromatography
HPMAAm	<i>N</i> -(2-hydroxypropyl)methacrylamide
ICG	indocyanine green
IMDQ	1-(4-(aminomethyl)benzyl)-2-butyl-1H-imidazo[4,5-c]quinolin-4-amine
IR780	2-[2-[2-chloro-3-[(1,3-dihydro-3,3-dimethyl-1-propyl-2H-indol-2-ylidene)ethylidene]-1-cyclohexen-1-yl]ethenyl]-3,3-dimethyl-1-propylindolium iodide
ITP	iodine transfer polymerization
IUPAC	International Union of Pure and Applied Chemistry
LAM	less activated monomer
LCST	lower critical solution temperature
LEDs	light-emitting diodes
LS	lysozyme
MA	methyl acrylate
Macro-CTA	macromolecular chain transfer agent
MADIX	macromolecular design via interchange of xanthates
MADLS	multiangle dynamic light scattering
MALDI-TOF	matrix-assisted laser desorption ionization-time of flight
MALS	multiangle light scattering
MAM	more activated monomer
MCF-7	estrogen-dependent breast cancer cells
MDA-MB-231	estrogen-independent cancer cells
MMA	methyl methacrylate
MOF	metal-organic framework
mPEG	methoxyl poly(ethylene glycol)
MPLC	medium-pressure liquid chromatography
MS	mass spectrometry
MTX	methotrexate
MWCO	molecular weight cut-off
NaCl	sodium chloride
NaOH	sodium hydroxide
<i>n</i>BA	<i>n</i> -butyl acrylate
NIPAAm	<i>N</i> -isopropylacrylamide
NMP	nitroxide-mediated polymerization
NMR	nuclear magnetic resonance
NMVA	<i>N</i> -methyl- <i>N</i> -vinylacetamide
NO	nitric oxide
NPs	nanoparticles
NPX	naproxen
NR	Nile Red
NVA	<i>N</i> -vinylacetamide

NVC	<i>N</i> -vinylcarbazole
NVCL	<i>N</i> -vinyl caprolactam
NVF	<i>N</i> -vinylformamide
NVP	<i>N</i> -vinylpyrrolidone
OEGA	oligo(ethylene glycol)methylether acrylate
OMRP	organometallic-mediated radical polymerization
ONZ	ornidazole
OVA	ovalbumin
PAA	poly(acrylic acid)
PABMA	poly(4-azidobenzyl methacrylate)
PAcaP	poly(10-(acryloyloxy)decyl-3-oxobutanoate)
PAH	polyacylhydrazide
PALysOH	poly(<i>N</i> -acryloyl-l-lysine)
PAMA	poly(2-aminoethyl methacrylate hydrochloride)
PAMAM	polyamidoamine
PBMA	2-hydroxy-4-methacryloyloxybenzophenone
PBMHH	poly(<i>N</i> -(<i>tert</i> -butoxycarbonyl)- <i>N'</i> -(6-methacryloylaminohexanoyl)hydrazine)
PBS	phosphate buffered saline
PC	pectin
PC7	poly(2-hexamethyleneiminoethanol)
PCA	polycinnamaldehyde
PCSSMA	poly(coumarin-based disulfide-containing monomer)
PD5A	poly(2-diamylamineethyl methacrylate)
PDEAAm	poly(<i>N,N</i> -diethylacrylamide)
PDEAEM	poly(<i>N,N</i> -diethylamineethyl methacrylate)
PDEAEMA	poly(2-(diethylamino)ethyl methacrylate)
PDEGMA	poly(di(ethylene glycol)methyl ether methacrylate)
PDEMA	poly(<i>N,N</i> -dibutylethanolamine)
PDIPAEMA	poly(2-[diisopropylamino]ethyl methacrylate)
PDMA	poly(2-(dimethylamino)ethyl methacrylate)
PDMAAm	poly(<i>N,N</i> -dimethylacrylamide)
PDMAEMA	poly(<i>N,N</i> -dimethylaminoethyl methacrylate)
PDMS	polydimethylsiloxane
PDPA	poly(2-(diisopropylamino)ethyl methacrylate)
PEG	poly(ethylene glycol)
PEGDA	poly(ethylene glycol) diacrylate
PEGMA	poly(ethylene glycol) methyl ether methacrylate
PET-RAFT	photoinduced electron/energy transfer reversible addition-fragmentation chain transfer polymerization
PFMA	poly(pentafluorophenyl methacrylate)
PGEM	polygemcitabine
PHEA	poly(2-hydroxyethylacrylate)
PHODMA	poly(2-(2-(2-hydroxyethyl)disulfanyl)ethyl methacrylate)

PHPMAAm	poly(<i>N</i> -(1,3-dihydroxypropan-2-yl)) methacrylamide
PI-RAFT	photoiniferter reversible addition-fragmentation chain transfer polymerization
PLA	poly(lauryl acrylate)
PMA	poly(methyl acrylate)
PMMA	poly(methyl methacrylate)
PMPC	poly(2-methacryloyloxyethyl phosphorylcholine)
PMVCL	poly(3-methyl- <i>N</i> -vinylcaprolactam)
PMVE	poly(methyl vinyl ether)
PNAGA	poly(<i>N</i> -acryloylglycinamide)
PNALPA	poly(<i>N</i> -acryloyl- <i>L</i> -phenylalanine methyl ester)
PnBA	poly(<i>n</i> -butyl acrylate)
PnBMA	poly(<i>n</i> -butyl methacrylate)
PNIPAAm	poly(<i>N</i> -isopropylacrylamide)
PNMVA	poly(<i>N</i> -methyl- <i>N</i> -vinylacetamide)
PNPCD	poly(2-(2-(2-((4-nitrophenoxy)carbonyloxy)ethyl)disulfanyl)ethyl methacrylate)
PNPs	polymeric nanoparticles
PNVA	poly(<i>N</i> -vinylacetamide)
PNVCL	poly(<i>N</i> -vinylcaprolactam)
PNVF	poly(<i>N</i> -vinylformamide)
POEGMA	poly(oligoethylene glycol)methyl ether methacrylate
PONBA	poly(<i>o</i> -nitrobenzyl acrylate)
PPEGA	poly(poly(ethylene glycol)methyl ether acrylate)
PRE	persistent radical effect
Prg	propargyl
PSAMA	poly(2-methacryloyloxy)ethyl stearate
PSMF	polystyrenemaleic anhydride functionalized with furfuryl amine
PTEGMA	poly(methoxy tri(ethylene glycol) methacrylate)
PTMA	poly(4-(4'-(diphenylamino)-[1,1'-biphenyl]-4-yl)-1-((methacryloyloxy)-methyl)pyridin-1-ium bis((trifluoromethyl)sulfonyl)amide)
PVA	poly(vinyl alcohol)
PVAc	poly(vinyl acetate)
PVAm	polyvinylamine
PVBA	poly(3-vinylbenzylaldehyde)
PVP	poly(<i>N</i> -vinyl pyrrolidone)
RAFT	reversible addition-fragmentation chain transfer
RB	rhodamine
RBC	red blood cells
RDRP	reversible-deactivation radical polymerization
RI	refractive index
ROS	reactive oxygen species
RP	radical polymerization
SBRP	organostibine-mediated living radical polymerization

SBS	polystyrene- <i>b</i> -polybutadiene- <i>b</i> -polystyrene
SDDS	smart drug delivery systems
SEC	size exclusion chromatography
SERM	selective estrogen receptor modulator
siRNA	small interfering RNA
SIS	polystyrene- <i>b</i> -polyisoprene- <i>b</i> -polystyrene
SS	disulfide bridge
St	styrene
TA	transfer agent
TAM	tamoxifen
tBA	<i>tert</i> -butyl acrylate
TEM	transmission electron microscopy
TERP	organotellurium-mediated radical polymerization
TGA	thermogravimetric analysis
THF	tetrahydrofuran
TPE	thermoplastic elastomer
TR-dextran	Texas red-labeled dextran
TT	2-thiazolidine-2-thione
TTC	trithiocarbonate
UHMM	ultrahigh molar mass
UV	ultraviolet
UV-Vis	ultraviolet-visible
VAc	vinyl acetate
β-CD	β-cyclodextrin
<i>C</i>	concentration
<i>D</i>	self-diffusion coefficient
<i>Đ</i>	dispersity
<i>k</i>	rate constant
<i>M_n</i>	number average molar mass
<i>T_{Agg}</i>	aggregation temperature
<i>T_{CP}</i>	cloud point temperature
<i>T_g</i>	glass transition temperature
<i>δ</i>	chemical shift
<i>λ</i>	wavelength
<i>ζ</i>	zeta potential

ABSTRACT

This doctoral dissertation demonstrates the versatile application of reversible addition-fragmentation chain transfer (RAFT) polymerization in synthesizing polymers with desired properties and architectures.

Chapter 1 presents a general literature review on reversible-deactivation radical polymerization (RDRP), focusing on the RAFT method and its photoinduced variant, PI-RAFT. This review also underscores the broad applications of the RAFT technique across diverse fields, including drug delivery systems and materials science.

The results and discussion sections focus on three significant challenges in the field of RAFT polymerization: synthesizing thermoresponsive diglyceride-based polymers, achieving controlled polymerization of *N*-vinylformamide, and enhancing the synthesis of (meth)acrylic ABA triblock copolymers. Chapter 2 delves into the synthesis and characterization of diglyceride-based polymers. The synthesis of novel chain transfer agents (CTAs) and monomers is outlined initially. Their application in RAFT polymerization facilitates the successful creation of homopolymers and block copolymers, which contain one or several diglyceride molecules in their structure and thermoresponsive blocks based on poly(*N*-isopropylacrylamide) (PNIPAAm) or poly(*N*-vinylcaprolactam) (PNVCL). Chapter 3 describes the preparation of thermoresponsive polymeric nanoparticles based on homopolymers or copolymers incorporating diglyceride moieties. The study examines the properties of these nanoparticles, including thermosensitivity, size, shape, and potential as drug carriers. A significant part of the research is devoted to studying photoiniferter RAFT polymerization (PI-RAFT). Chapter 4 evaluates the polymerization of *N*-vinylformamide (NVF) using the PI-RAFT technique. This approach demonstrates control over polymerization, facilitating the synthesis of well-defined homopolymers and block copolymers. The study also explores the hydrolysis of the poly(*N*-vinylformamide) (PNVF) segment, paving the way for future applications of the corresponding polyvinylamine (PVAm). Chapter 5 addresses the synthesis of high molar mass homopolymers based on poly(*n*-butyl acrylate) (*Pn*BA) or poly(methyl methacrylate) (PMMA) and the development of their corresponding (meth)acrylic ABA triblock copolymers using the PI-RAFT technique. The study outlines the influence of variable factors such as light wavelength, monomer concentration, and light intensity on the polymerization process.

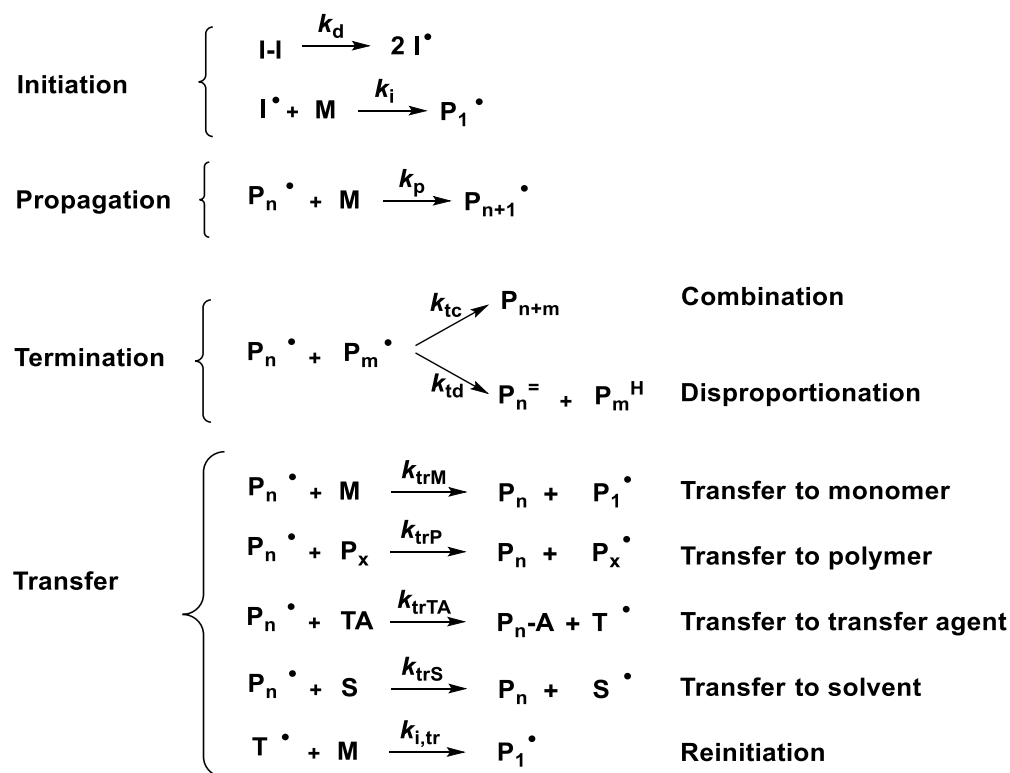
The discussion of results culminates in a section dedicated to conclusions and future perspectives, followed by a summary in bullet points.

The experimental part presents the methods used to identify and characterize the obtained materials (Chapter 6), with subsequent descriptions of synthetic protocols (Chapter 7).

CHAPTER 1. LITERATURE REVIEW

1.1. Radical polymerization and reversible-deactivation radical polymerization (RDRP)

Radical polymerization (RP) is a chain growth process in which the active centers are radicals possessing an unpaired valence electron. RP is a highly versatile technique widely employed in both laboratory-scale and industry settings for producing polymers with high molar masses.¹ Approximately 40–45% of all industrial polymers are obtained through conventional RP methods, owing to their relatively low cost, ease of implementation, and scalability for industrial production.² One of RP's key advantages is its ability to effectively polymerize various types of vinyl monomers with the tolerance of radicals towards various functional groups (e.g., acidic, hydroxy, and amino groups), thus eliminating the need for protecting group chemistry.^{3,4} Moreover, radical polymerization is resilient to impurities and exhibits tolerance towards different reaction conditions. It can be conducted under various temperatures (typically room temperature to 100 °C) and pressures, using different polymerization techniques such as bulk, emulsion, solution, dispersion, or suspension.⁴ A conventional RP process has four main elementary steps: initiation, propagation, termination, and transfer (Scheme 1).^{4,5}



Scheme 1. Mechanism of radical polymerization.

During the initiation stage, two distinct reactions take place. First, primary initiating radicals (I^{\bullet}) are produced. These radicals then react with monomer molecules (M), forming a new active radical (P_1^{\bullet}). The propagation of the polymer chain proceeds through the repetitive addition of multiple monomer units to the active radical center. When two propagating polymer radicals encounter each other, termination occurs either through combination (k_{tc}) (favorable for less hindered monomers like acrylates or styrene) or disproportionation (k_{td}) (favorable for more hindered monomers like methacrylates). The combination is essentially the simple coupling of two radicals. In contrast, during disproportionation, a hydrogen atom adjacent to the radical center is abstracted, resulting in a polymer chain with a saturated end-group and unsaturated macromonomer. Finally, polymer radicals can undergo a chain transfer process toward monomer, polymer (P_x), solvent (S), or specific transfer agents (TAs). The occurrence of unavoidable and irreversible chain transfer/termination reactions leads to polymers with a lack of control over the molar mass and high dispersity ($D < 1.5\text{--}2.0$).^{6,7} Despite many benefits, this is a notable drawback of conventional radical polymerization. Moreover, there is little scope for constructing the complex polymer architectures demanded by many modern applications.⁶

In polymer chemistry, achieving precise control over macromolecular composition, topology, and polymer chain length is crucial for tailoring materials with specific properties and applications. Significant advancements in the field occurred with the introduction of the concept of living polymerization, which was discovered by Szwarc and his coworkers in 1956 during the anionic polymerization of styrene.^{8,9} The living ionic polymerization technique eliminates termination and transfer reactions, ensuring equal growth probability for all polymer chains. Macromolecules obtained through ionic polymerization remain active ("living"), allowing polymerization to continue until all the monomer is consumed. The subsequent addition of other monomers leads to the formation of different structures, such as block copolymers. In general, ionic polymerization enables excellent control over the molar mass distribution and copolymer architectures, making the products highly desirable due to their physicochemical properties and potential applications. However, the industrial-scale application of ionic polymerization proves challenging due to demanding synthesis conditions such as the high purity of monomers and solvents and the need to eliminate moisture and oxygen to prevent undesired termination reactions. Moreover, ionic polymerization is incompatible with a wide range of functional vinyl monomers.¹⁰

The versatility of radical polymerization, including a broader range of monomers and scalable reaction conditions, has fueled interest in developing effective strategies for

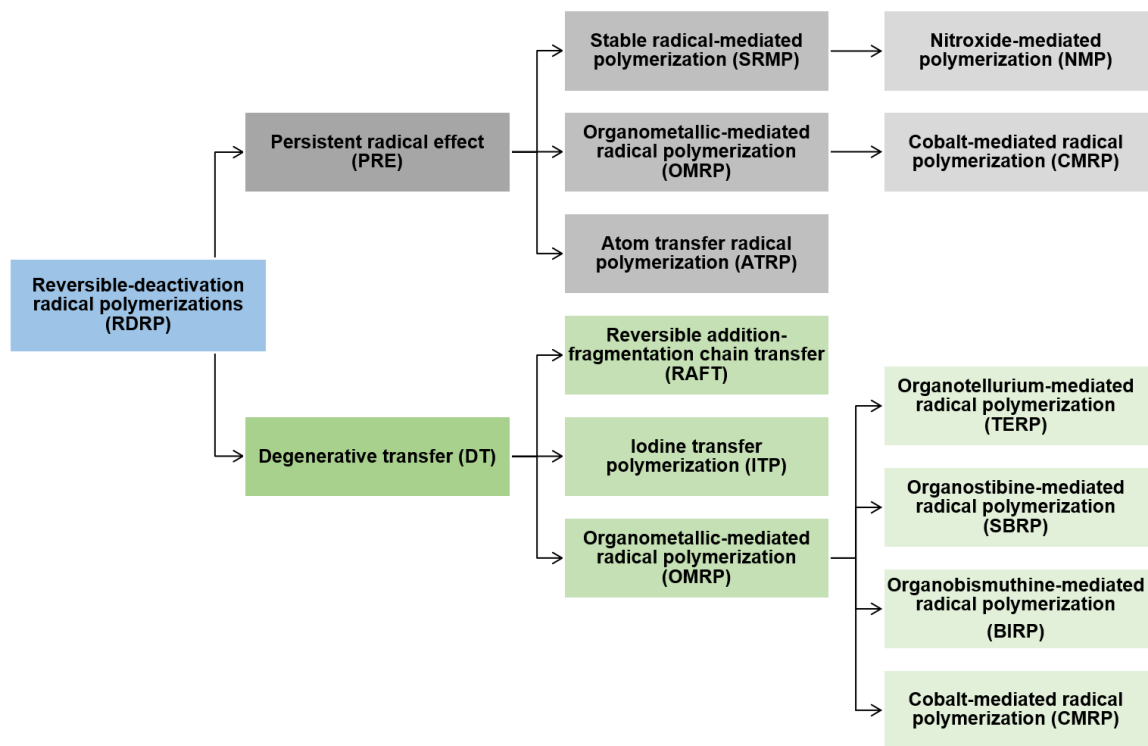
incorporating living characteristics into this process. The breakthrough came during the 1990s with the discovery of new methods for radical polymerization that allowed synthesizing polymer materials with precise molar mass, low dispersity, and diverse structures. These innovative techniques have in common that the propagating species are radicals, and they establish an equilibrium between active (radical) species and dormant species, allowing for the simultaneous growth of all polymer chains with a narrow molar mass distribution.^{6,11} While these systems were often referred to as living radical polymerization, controlled radical polymerization, or controlled/living radical polymerization (CLRP), in 2010, the International Union of Pure and Applied Chemistry (IUPAC) recommended the adoption of the term reversible-deactivation radical polymerization (RDRP) to more accurately describe polymerizations that involve equilibrium between the active and dormant species. The term "living" should only be used for polymerization in which chain termination and irreversible chain transfer are absent. Despite the IUPAC recommendation, the terms "living" and "controlled" are still widely used in the literature.¹²

RDRP encompasses several techniques, including stable radical-mediated polymerization (SRMP), nitroxide-mediated polymerization (NMP), atom transfer radical polymerization (ATRP), iodine transfer polymerization (ITP), reversible addition-fragmentation chain transfer (RAFT) polymerization and organometallic-mediated radical polymerization (OMRP).

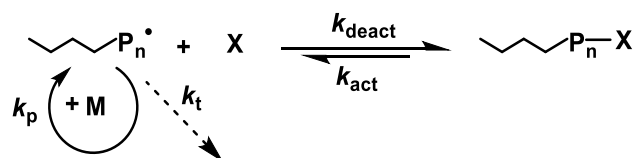
Establishing a dynamic equilibrium between propagating radicals and various dormant species is a fundamental aspect of all RDRP systems (Scheme 2). Radicals can engage in two mechanisms: the persistent radical effect (PRE) or participating in a degenerative transfer process (DT).^{13,14}

As depicted in Scheme 3, the persistent radical effect involves a trapping mechanism in which the propagating radicals (P_n^{\cdot}) undergo the activation-deactivation process facilitated by species X, typically a stable radical or organometallic compound. The dormant species (P_n-X) can be activated (with an activation rate constant, k_{act}) either spontaneously/thermally, in the presence of light, or with an appropriate catalyst (as in ATRP) to reform the growing centers. Radicals can propagate (k_p) or terminate (k_t). However, persistent radicals (X) cannot terminate with each other but can only reversibly cross-couple with the growing species (k_{deact}). As a result, every instance of radical-radical termination leads to the irreversible accumulation of persistent radicals. Consequently, the concentration of radicals and the probability of termination decrease with time. Systems

based on PRE, such as nitroxide-mediated polymerization (NMP), require a stoichiometric amount of mediated species. Atom transfer radical polymerization (ATRP) also operates via the PRE, but less than the stoichiometric amount of transition metal catalyst can be used.¹⁴

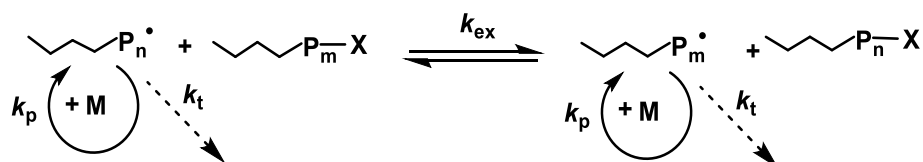


Scheme 2. Activation-deactivation mechanism in RDRP.



Scheme 3. Persistent radical effect.

On the other hand, methods based on degenerative transfer operate by thermodynamically neutral activity exchange between active and dormant species originating from the chain transfer agent (Scheme 4).



Scheme 4. Degenerative transfer.

This exchange occurs via a reversible chain transfer mechanism and leads to the formation of new radical centers.¹⁵ It can proceed through atom transfer (iodine transfer polymerization (ITP), group transfer (TERP, SBRP, or BIRP), and addition-fragmentation chemistry with thiocarbonylthio group (RAFT). In systems employing degenerative transfer, a constant concentration of growing radicals is achieved through initiation and termination processes, similar to conventional RP. Control over molar mass and dispersity is achieved by using appropriate transfer agents (P_m-X or P_n-X) that exchange a group/atom X among all growing chains at a faster rate compared to propagation ($k_{ex} > k_p$). Additionally, it is important to ensure a high concentration ratio of chain transfer agent to the radical initiator.¹⁴

Several variations of the RDRP technique have been developed, each distinguished by its unique reaction mechanisms, reagents, and operating conditions. Each of these techniques offers specific advantages, including the range of monomers it can polymerize, the level of control it offers over the kinetics of polymerization, and the diversity of structures it can produce.¹⁴ In this study, the RAFT method is the fundamental technique for synthesizing polymers with well-defined properties. Therefore, the following section provides a detailed description of this method.

1.2. Reversible addition-fragmentation chain transfer (RAFT) polymerization

RAFT polymerization finds its roots in radical addition reactions in the 1970s, which involved deoxygenating secondary alcohols through their corresponding dithiocarbonates (xanthates).^{16,17} The first reports of the direct use of addition-fragmentation transfer agents to control radical polymerization appeared in the 1980s.^{18,19} Later, in 1995, it was reported that polymerizations of methacrylic monomers in the presence of methacrylic macromonomers exhibited some properties of living polymerization.²⁰ In 1998, the Commonwealth Scientific and Industrial Research Organization (CSIRO) discovered that the use of thiocarbonylthio groups resulted in the production of polymers with controlled molar masses and low dispersities.²¹ This technique was named reversible addition-fragmentation chain transfer (RAFT) polymerization. That same year, Rhodia patented a method for producing polymers with controlled/living characteristics using dithiocarbonates.²² The technique, called MADIX (macromolecular design via interchange of xanthates), can be viewed as a specific case of RAFT polymerization. Since then, there has been a huge development in RAFT polymerization. Presently, a pioneering paper

authored by Chiefari et al. has exceeded 4,500 citations, making it the most cited article in the history of *Macromolecules*.²¹

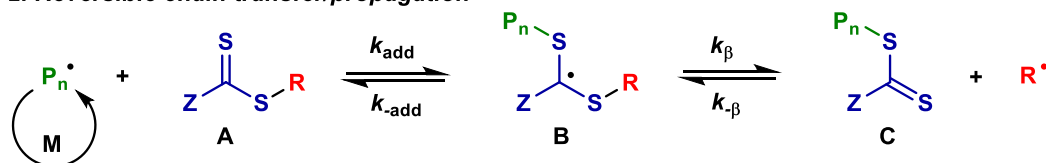
1.2.1. Mechanism of RAFT polymerization

RAFT polymerization involves three key components: a chain transfer agent (CTA), an initiator, and a monomer. The CTA plays a crucial role in controlling the process by allowing for the reversible fragmentation of the growing polymer chains. Meanwhile, the initiator activates the CTA, triggering the polymerization process and initiating a chain reaction, wherein the monomer continuously adds to the growing polymer chain until the reaction is terminated. The mechanism of RAFT polymerization is depicted in Scheme 5. The generated initiator radical (I^{\bullet}) reacts with monomer molecules, resulting in the formation of propagating oligomeric radicals P_n^{\bullet} (step 1). Subsequently, these radicals (P_n^{\bullet}) react with A (chain transfer agent) and add to the C=S group, forming an intermediate radical B (step 2). The presence of the intermediate radical (B) prevents the irreversible termination reaction between the propagating and intermediate radicals, allowing for two types of fragmentation facilitated by the activity of the C=S group. The intermediate radical (B) can return to its initial state to produce a propagating radical (P_n^{\bullet}) and a RAFT agent. At the same time, it may also fragment into a new radical (R^{\bullet}) and a dormant chain (C). These newly formed radicals then reinitiate the polymerization process with the monomer, forming new propagating chains P_m^{\bullet} (step 3). Consequently, a dynamic equilibrium is established between the dormant species (C) and the active propagating radicals P_n^{\bullet} and P_m^{\bullet} (step 4). This equilibrium ensures an equal chance of growth for all chains with equal probability and speed, leading to products with a similar degree of polymerization (DP) and low dispersities. However, due to the high chemical reactivity of radicals, the termination reaction (step 5) is often inevitable. This process happens through either combination or disproportionation. The number of dead polymer chains is determined by the number of active radicals generated from the initiator.^{23,24} This is advantageous, as it allows for easy optimization of the livingness of the polymer by adjusting the initial initiator concentration. Nevertheless, the mode of termination must also be taken into account. Once the RAFT polymerization is complete, the majority of the chains remain living and possess a thiocarbonylthio group at the chain-end. The resulting polymer can serve as a macro-CTA and be extended by adding a new monomer portion.

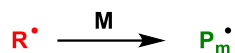
1. Initiation



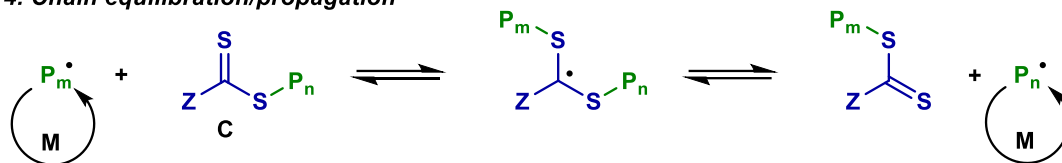
2. Reversible chain transfer/propagation



3. Reinitiation:



4. Chain equilibration/propagation



5. Termination:



Scheme 5. Mechanism of reversible addition-fragmentation chain transfer (RAFT) polymerization.^{23,25,26}

RAFT polymerization provides several benefits, such as its versatility under varied conditions. This method can be applied in bulk,^{27,28} solution,^{29,30} emulsion,^{31,32} dispersion,^{33,34} and suspension^{35,36}. Furthermore, RAFT polymerization can occur within a broad range of temperatures^{23,37} and pressures^{38,39}. Homogeneous RAFT polymerization in bulk or solution follows conditions similar to those for conventional radical polymerization. A CTA, which is soluble in the reaction medium, is added to a mixture containing an initiator, a monomer, and optionally a solvent. Polymerization can be conducted in various organic solvents,³⁷ water,⁴⁰ and other media, such as ionic liquids⁴¹ or supercritical carbon dioxide⁴². While RAFT polymerization offers an array of benefits, it is not without limitations. Like other radical polymerization techniques, RAFT cannot fully eliminate transfer and termination reactions, which can stop the growth of the chain and produce dead chains without CTA-end groups. Moreover, RAFT can sometimes be time-consuming and may not maintain control over dispersity for polymers with high molar masses (with an average molar mass (M_n) higher than 10^5).^{23,43,44}

Several factors influence the appropriate course of the polymerization process, including the source of radicals, the type and activity of the chain transfer agent, and the type and activity of the monomer.

1.2.2. Monomers

The RAFT method provides control over the polymerization of most monomers that can be polymerized by radical polymerization. Exceptions include monomers that react with chain transfer agents, such as primary and secondary amines, which cause the decomposition of the thiocarbonylthio function.^{23,45} RAFT agents exhibit tolerance toward a wide range of functional monomers spanning both hydrophilic and hydrophobic characteristics, containing carboxylic acids, hydroxyl, amide, and tertiary amines or quaternary ammonium groups.⁴⁶

The monomers compatible with the RAFT process can be categorized into two main groups. The first group, known as "more activated" monomers (MAMs), contains compounds in which a double bond is conjugated to an aromatic ring, a carbonyl group, or a nitrile. Examples of MAMs include styrene, vinylpyridines, methyl methacrylate, methyl acrylate, acrylamide, and acrylonitrile. The presence of a conjugated double bond stabilizes the propagating radical, leading to an increase in the propagation rate. The second group, called "less activated" monomers (LAMs), contains compounds with a double bond adjacent to saturated carbon, an oxygen or nitrogen lone pair, or the heteroatom of a heteroaromatic ring. Examples of LAMs include vinyl acetate, *N*-vinylpyrrolidone, and *N*-vinylcarbazole.⁴⁷ The presence of an electron-rich double bond in the polymer chain destabilizes the propagating radical, increasing its reactivity and rendering it susceptible to various side reactions during the polymerization process. These side reactions may include termination by disproportionation or hydrogen abstraction. Therefore, the controlled polymerization of LAMs is more challenging than MAMs.⁴⁸

1.2.3. Source of radicals

The generation of radicals is crucial to the RAFT process. As mentioned above, the initial number of radicals determines the number of dead chains in the system but also impacts the polymerization rate. Several factors influence the requisite number of radicals in the polymerization process, including the nature of the monomer, the overall concentration of the monomer, the solvent properties, and the characteristics of the CTA.⁴⁵ Any source of free radicals can trigger the initiation of RAFT polymerization. The most

common thermal initiators are azo compounds, for example, 2,2'-azobis(2-methylpropanitrile) (AIBN) and 4,4'-azobis(4-cyanovaleric acid) (ACVA). Nevertheless, the radical can be generated by using various approaches. As a result, RAFT polymerization can be fueled by diverse alternative methods, including gamma radiation,⁴⁹ ultrasounds,⁵⁰⁻⁵² metals,⁵³⁻⁵⁶ acids,⁵⁷⁻⁵⁹ enzymes,⁶⁰⁻⁶² electrochemical initiation,⁶³⁻⁶⁵ or light-induced activation. Photopolymerization will be discussed in more detail in the next section of this dissertation.

1.2.4. Chain transfer agents

The thiocarbonylthio group in the CTA is crucial to achieving control over the molar mass in RAFT polymerization. The right choice of CTA enables the adjustment of the polymerization rate, monomer reactivity, and the level of initiating species.⁶⁶ The CTA has two main functionalities: the R group, which should be a good leaving group and allow efficient reinitiation of polymerization, and the Z group, which activates the carbon-sulfur double bond for radical addition and has a stabilizing or destabilizing effect on the intermediate radical. The general structure of the chain transfer agent is shown in Figure 1. Depending on group Z, the main classes of RAFT agents that can be distinguished are trithiocarbonates, dithioesters, dithiocarbonates, and dithiocarbamates.

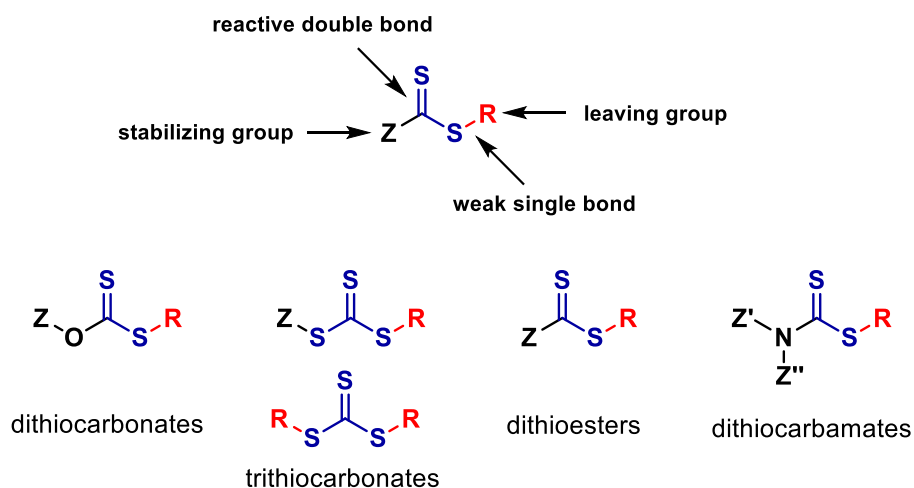


Figure 1. General chemical structure of RAFT chain transfer agents.

The effectiveness of RAFT agents is strongly dependent on the nature of the stabilizing Z group and the leaving group R. A key factor in achieving successful RAFT polymerization is ensuring that the C=S bond is more reactive to radical addition than the C=C bond in the

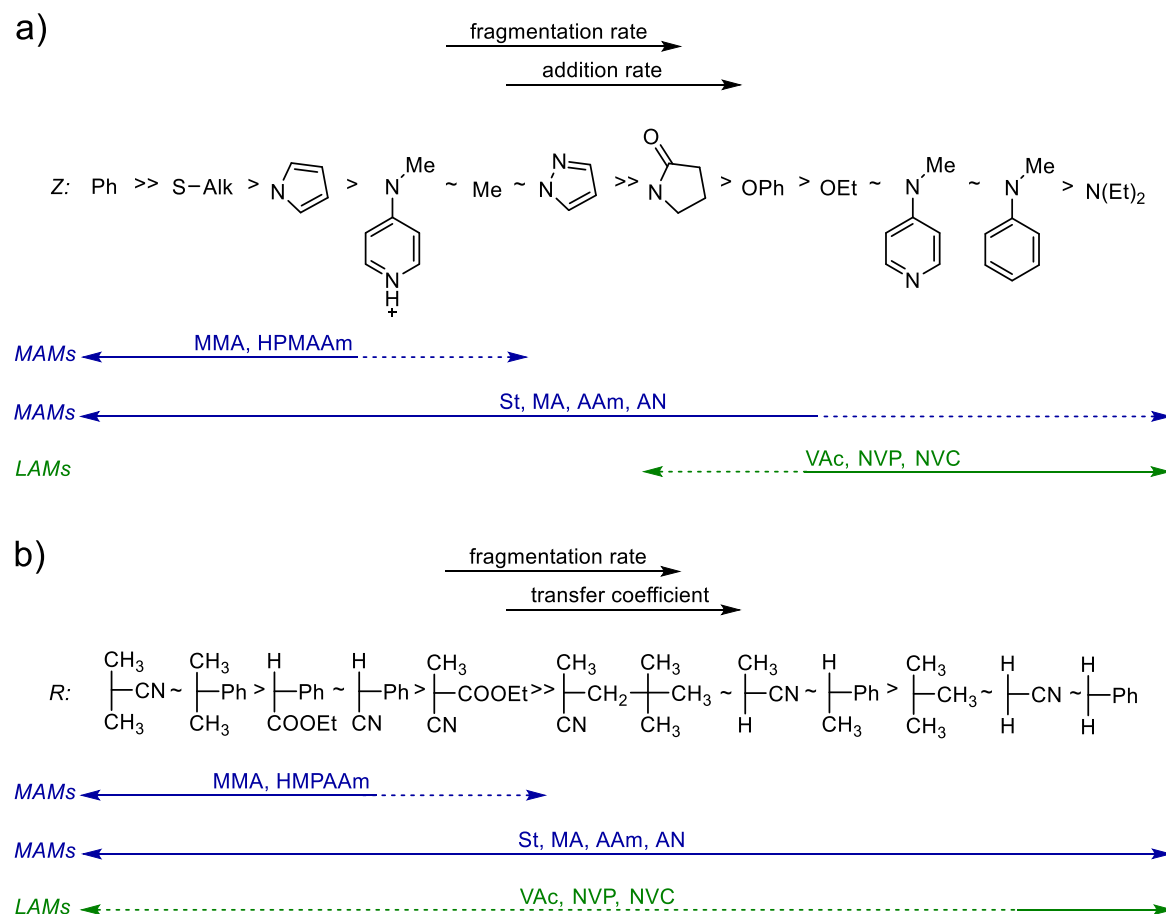
monomer. The correlation between CTA structures and polymerization control has been thoroughly studied in recent years.^{23,26,47,67}

The Z group controls the reactivity of the carbon-sulfur double bond toward free radical addition and the stability of intermediate radicals (Scheme 5).²³ The reactivity of RAFT agents generally decreases in the order of dithiobenzoates > trithiocarbonates \approx dithioalkanoates > dithiocarbonates > dithiocarbamates.⁶⁸ The choice of RAFT agent typically depends on the monomers undergoing polymerization. The more active RAFT agents, such as the dithiobenzoates and trithiocarbonates, have strong stabilizing groups and, therefore, increase the reactivity of C=S toward radical addition. Consequently, they are more effective in controlling the polymerization of MAMs, which produce relatively more stabilized radicals and require a Z group to help stabilize them. In turn, LAMs are poor homolytic groups due to their high reactivity. To facilitate the fragmentation of the propagating radical, they require intermediate radicals that are less stable, for example, dithiocarbonates (Z = *O*-alkyl) or dithiocarbamates (Z = *N*-alkyl) (a compound with the electron-withdrawing group). The lone pair of electrons on oxygen in dithiocarbonates or nitrogen in dithiocarbamates is delocalized in the thiocarbonyl group, deactivating the C=S bond toward radical addition and destabilizing the radical intermediate.²³ In the case of LAMs, the use of more active RAFT agents can result in slow fragmentation, inhibition, or retardation, as they can act as radical traps and limit polymerization.⁴⁷ The general guidelines for the selection of Z groups are presented in Scheme 6a.

The R group, on the other hand, must be a good leaving group compared to the growing polymeric chain. Moreover, it must also act as a good reinitiating species to sustain the polymerization process. The R groups with electron-withdrawing moieties produce a more stable radical upon fragmentation. The general guidelines for the selection of R groups are presented in Scheme 6b.

Until recently, the commercial availability of RAFT transfer agents was limited, but now a wide array of these agents (including trithiocarbonates, dithiocarbamates, dithiobenzoates, and macro-RAFT agents) is readily accessible for research purposes. However, it is important to note that the synthesis of most RAFT agents (especially dithiocarbonates) is not complicated.²³ They can be produced with moderate or very good yields using methods described in the literature.⁴⁷ As an illustration, the simplest methyl 2-((ethoxycarbonothioyl)thio)propanoate (Rhodixan A1, used by Solvay for the industrial production of block copolymers) can be obtained almost quantitatively through

a nucleophilic substitution reaction of a bromo derivative with ethyl-potassium dithiocarbonate.



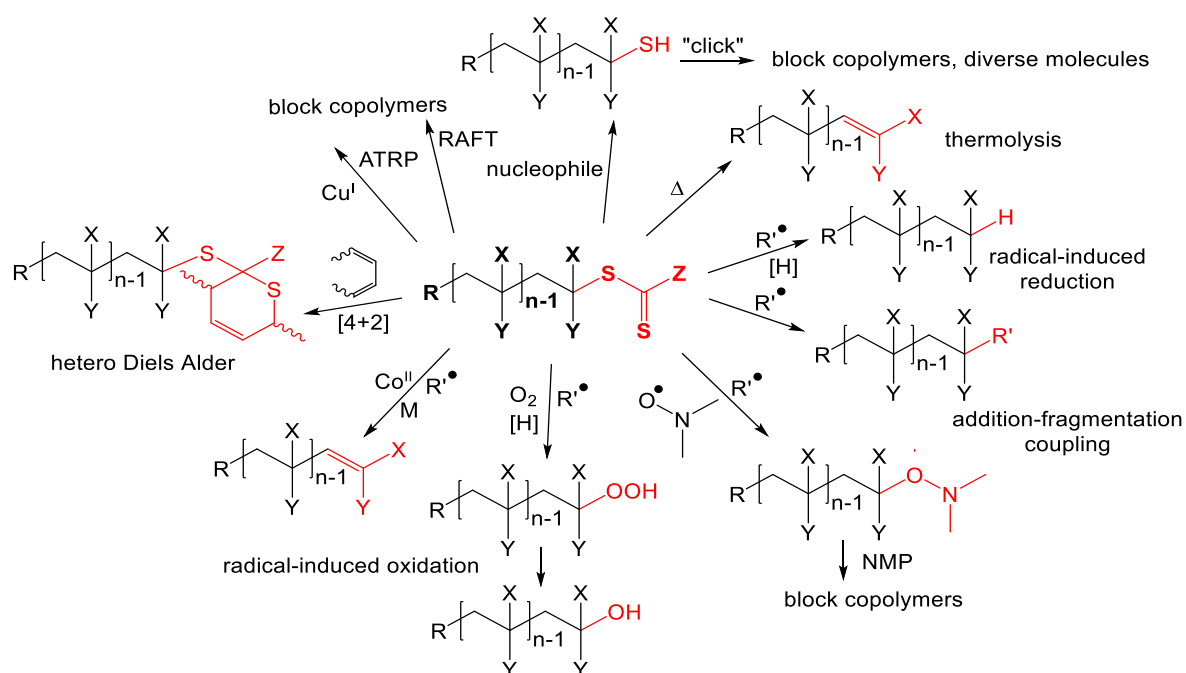
Abbreviations: AAm, acrylamide; AN, acrylonitrile; HPMAAm, *N*-(2-hydroxypropyl)methacrylamide; MA, methyl acrylate; MMA, methyl methacrylate; NVC, *N*-vinylcarbazole; NVP, *N*-vinylpyrrolidone; St, styrene; VAc, vinyl acetate.

Scheme 6. General guidelines for the selection of the a) Z group and b) R groups. A dashed line represents partial control (control of molar mass but poor control over dispersity or substantial retardation in the case of VAc, NVC, or NVP).^{23,47}

1.2.5. Modification of the end-groups

Polymers obtained by RAFT polymerization contain an R group from the starting CTA at one end of the chain and a Z thiocarbonylthio ($-\text{C}(\text{S})\text{S}-$) group at the other end. In many industrial applications, the presence of $-\text{C}(\text{S})\text{S}-$ groups at the ends of polymer chains is undesirable. These groups can alter the color of the product and are susceptible to degradation over time, leading to the release of potentially toxic, low molecular weight sulfur compounds with an unpleasant odor.⁶⁹ It is also known that the thiocarbonylthio group quenches fluorescence, which is a problem in some optoelectronic applications.⁷⁰ Hence,

there is considerable interest in the straightforward elimination or alteration of the CTA species through diverse modifications, as shown in Scheme 7. One of the most well-established approaches to removing RAFT end-groups is the reaction with various nucleophiles, such as amines⁷¹ or hydroxide⁷². In this method, a nucleophile attacks the thiocarbonyl group, forming a thiol group (–SH) at the polymer chain-end. The resulting terminal –SH group presents opportunities for further chemical modifications (e.g., the attachment of fluorescent moieties), yielding diverse molecules. Alternatively, –C(S)S– groups can be readily eliminated by replacing them with a hydrogen atom through radical reduction.^{73,74} Another method to complete the removal of end-groups involves thermal elimination. To prevent thermal degradation, the polymer and any functionality must be stable at temperatures between 120 to 200 °C.⁷⁵ The effectiveness of this method varies depending on the nature of the polymer and the type of the RAFT end-group.⁷⁰ The thiocarbonyl end-group can also react with dienes by Diels-Alder chemistry.^{76,77} Furthermore, the –C(S)S– group can be modified with nitroxide to produce alkoxyamine chain-ends, making them suitable for use in NMP. In addition, thiocarbonylthio compounds can be used as initiators in ATRP.⁷⁰



Scheme 7. Processes for RAFT end-group modifications (R' , radical; $[H]$, hydrogen donor; M , monomer).⁷⁰

1.3. Photoinduced RAFT polymerization

In recent years, various approaches to RAFT polymerization have rapidly developed. One of the fascinating methods is the use of light to initiate polymerization. By employing light, the need for traditional radical initiators, such as azo compounds, can be significantly reduced. Notably, these compounds are unstable and must be kept in the dark at low temperatures to prevent decomposition, thus avoiding the risk of accidental explosion.⁷⁸ Moreover, photo-RAFT offers several advantages, including mild reaction conditions, oxygen tolerance under specific conditions, and precise spatial and temporal control. Furthermore, for example, visible light is an energetically mild and environmentally friendly energy source, supporting greener and more sustainable chemistry. There are typically two strategies for inducing RAFT polymerization with light. The first approach, called photoiniferter reversible addition-fragmentation chain transfer polymerization (PI-RAFT), relies on the direct photodissociation of the chain transfer agent (CTA) to generate the initiating radical. The CTA serves three concurrent roles: initiator, transfer agent, and termination agent, hence the term "ini-fer-ter".⁷⁹ The second method, introduced in 2014 by Boyer and coworkers, is called photoinduced electron/energy transfer reversible addition-fragmentation chain transfer polymerization (PET-RAFT). This technique employs a photocatalyst that captures light and transfers an electron or energy to a CTA, triggering its fragmentation and production of radicals.^{43,80} This dissertation primarily addresses the PI-RAFT strategy, so the PET-RAFT method will not be discussed here. Nevertheless, there are numerous comprehensive reviews dedicated to the PET-RAFT topic.^{43,81-83}

The photoiniferter (PI) process was first introduced to the scientific community by Otsu and coworkers in 1982.^{79,84} They explored the polymerization of methyl methacrylate (MMA) and styrene (St) in the presence of tetraethylthiuram disulfide using thermal activation, and more importantly, in this context, with UV light. However, activating CTA directly under ultraviolet (UV) light presents challenges, notably the loss of end-group fidelity from CTA photolysis. Also, many organic molecules absorb UV light, which raises the potential for unintended side reactions or the degradation of reagents, limiting the yield of the desired product.⁸⁵ As a result, researchers shifted their focus toward using radiation with higher wavelengths (lower energy) from the visible spectrum to minimize side reactions. In 2015, as a validation of this approach, Boyer,⁸⁶ Qiao,⁸⁷ and coworkers independently demonstrated successful RAFT polymerization using blue (435 nm) or green (530 nm) light irradiation. It is worth noting that high energy γ -radiation was also used to activate the chain transfer agents for polymer synthesis. However, this approach faced

challenges related to long reaction times, low conversions, and the potential generation of radicals not only from CTA but also from solvent or monomer.^{45,88,89}

Most chain transfer agents that possess a thiocarbonylthio group, such as dithiobenzoates, trithiocarbonates, dithiocarbonates, and dithiocarbamates, undergo photolysis and produce radicals when irradiated. Undoubtedly, the most popular photoiniferters are dithiocarbonates and trithiocarbonates, which enable PI-RAFT polymerization across both the ultraviolet (UV) and visible regions of the light spectrum.^{45,90,91} The electronic transitions responsible for C–S bond photolysis are the $\pi \rightarrow \pi^*$ and $n \rightarrow \pi^*$ electronic transitions (Figure 2a). The energy gap for the $\pi \rightarrow \pi^*$ transition is notably larger than that for the $n \rightarrow \pi^*$ transition. Thus, the $\pi \rightarrow \pi^*$ transition is observed in the shorter, higher-energy wavelengths of the UV spectrum, whereas the $n \rightarrow \pi^*$ transition is seen in the longer wavelengths, which have lower energies.⁹⁰

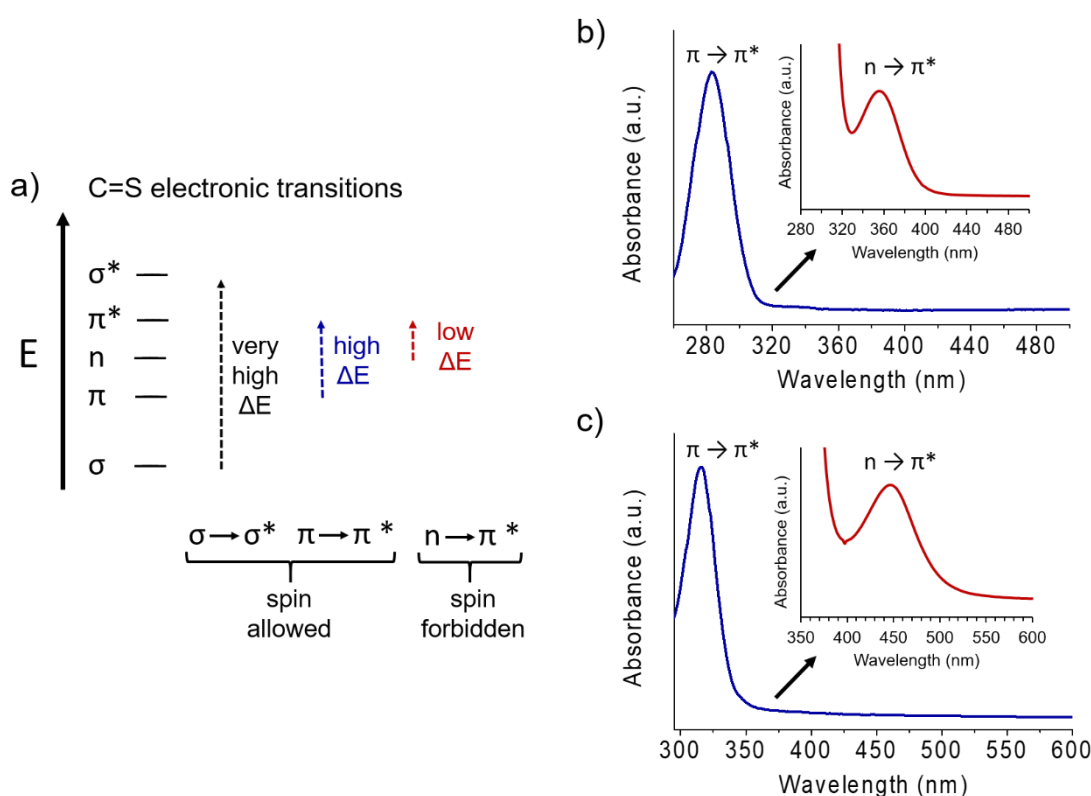
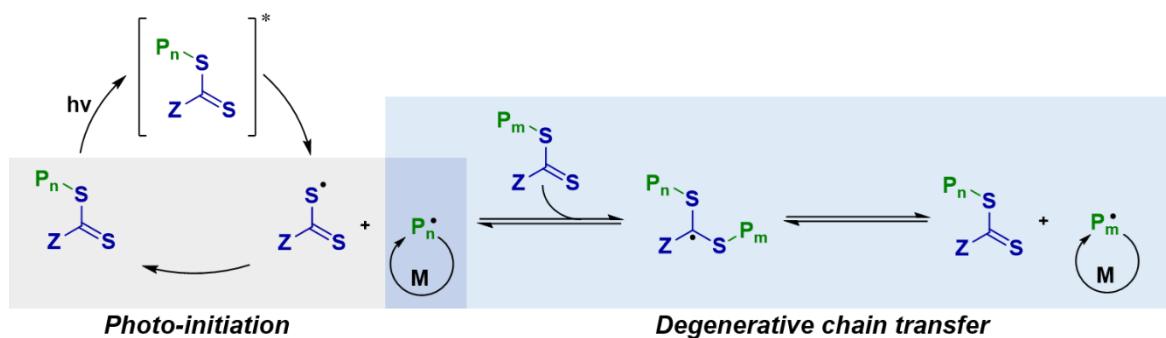


Figure 2. a) The electronic transitions responsible for C–S bond photolysis.⁸⁷ b) UV-Vis spectrum of dithiocarbonate (methyl 2-((ethoxycarbonothioyl)thio)propanoate), c) UV-Vis spectrum of trithiocarbonate (bis-(2-methylpropanenitrile)trithiocarbonate).

Although the band related to the spin forbidden $n \rightarrow \pi^*$ transition is much weaker, it facilitates efficient excitation and photolysis required to start polymerization.^{45,90} The position of the $n \rightarrow \pi^*$ band strongly depends on the type of CTA. Dithiocarbonates (Figure 2b) possess absorption based on the $n \rightarrow \pi^*$ transition in the UV light spectrum ranging from 330–420 nm, while in trithiocarbonates (Figure 2c), the $n \rightarrow \pi^*$ band is located in the visible

range of the spectrum (~400–560 nm). It is important to note that the irradiation wavelength should overlap with the absorption profile of the chain transfer agent. Therefore, dithiocarbonates can be activated under UV, purple, or blue visible light, whereas trithiocarbonates can be activated, for example, with blue or green visible light. In recent years, there has been significant development of the PI-RAFT method. Various RAFT agents, monomers, solvents, and light sources have been employed to synthesize polymers with diverse properties. Selected examples of polymerizations, with particular emphasis on using di- and trithiocarbonates as CTAs and visible light as irradiation sources, are shown in Table 1.

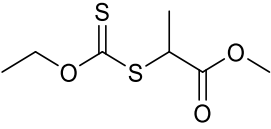
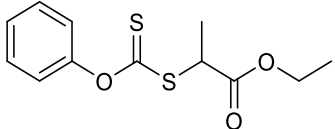
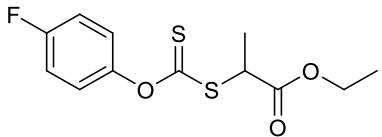
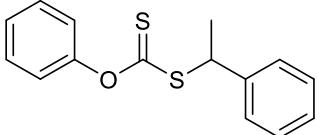
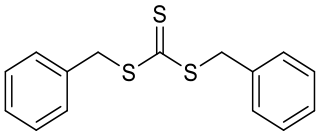
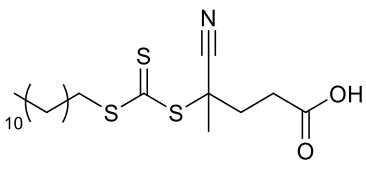
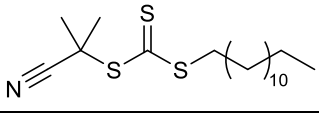
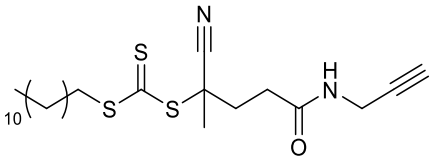
The mechanism of PI-RAFT is illustrated in Scheme 8. The chain transfer agent directly absorbs light, causing an electron in the C=S bond to be excited to a higher energy state. This transition is followed by cleavage of the C–S bond by β -scission, leading to the formation of an initiating/propagating carbon-centered radical and a persistent thiocarbonylthio radical.^{45,90} The propagating radicals (P_n^\bullet) are then engaged in degenerative chain transfer, a pivotal process in RAFT polymerization. In turn, thiocarbonylthio radicals are less reactive and can reversibly deactivate growing polymer chains, as in the case of NMP or ATRP.^{45,83,90}



Scheme 8. Mechanism of PI-RAFT.⁸³

Incorporating light as an external control mechanism in PI-RAFT offers a dynamic and precise tool for modulating the polymerization process. Light is an easily adjustable parameter. Altering parameters such as intensity, wavelength, or duration of irradiation allows fine-tuning of the polymerization rate and pausing or restarting the process.⁸⁵ As a result, this dynamic control provides the means to produce polymers with desired properties suitable for a wide range of applications. PI-RAFT has been successfully applied in 3D printing,^{92,93} production of well-defined nanostructures,^{94,95} surface functionalization,^{96,97} the synthesis of ultrahigh molar mass polymers (UHMM)^{98,99}, and multiblock copolymers¹⁰⁰ synthesis. Further insights on PI-RAFT can be found in recent review papers authored by Hartlieb⁴⁵ and by Kwon and coworkers⁸³.

Table 1. Overview of chain transfer agents, irradiation wavelengths, and monomers in PI-RAFT polymerization.

Chain transfer agent	Irradiation wavelength	Monomer	Reference
	blue (460–470 nm)	VAc	101
	purple (390 nm)	<i>n</i> BA <i>t</i> BA NIPAAm	102
	purple (390 nm)	VAc MA <i>n</i> BA NIPAAm	103
	blue (465 nm) purple (391 nm)	<i>n</i> BA VP <i>n</i> BA VP MA St	104
	blue (460 nm)	OEGA	105
	purple (405 nm) green (530 nm)	PEGDA MMA GMA DMAEMA HEMA	92 86
	blue (460 nm)	AN	106
	blue (460 nm)	PPEGA NIPAAm	107

Abbreviations: AN, Acrylonitrile; *n*BA, *n*-butyl acrylate; *t*BA, *tert*-butyl acrylate; DMAEMA, *N,N*-dimethylaminoethyl methacrylate; GMA, glycidyl methacrylate; HEMA, 2-hydroxyethyl methacrylate; OEGA, oligo(ethylene glycol)methylether acrylate; MA, methyl acrylate; MMA, methyl methacrylate; NIPAAm, *N*-isopropylacrylamide; PEGDA, poly(ethylene glycol) diacrylate; PPEGA, poly(poly(ethylene glycol)methyl ether acrylate); St, styrene; VAc, vinyl acetate.

1.4. Application of RAFT polymerization in selected fields

RAFT polymerization has emerged as a highly versatile method that facilitates the synthesis of polymers with controlled molar mass, narrow dispersity, and tailored end-groups functionality. Precise control over the molar mass and polymerization rate can be achieved by adjusting reaction conditions and the RAFT agent and monomer concentrations. RAFT polymerization enables the synthesis of polymers with complex architectures, such as block copolymers, star polymers, graft copolymers, and comb-like structures (Figure 3). This architectural control allows the design of materials with specific functionalities, self-assembly behavior, and mechanical properties. This section highlights the diverse applications of RAFT polymerization in selected fields, including drug delivery systems, the synthesis of well-defined poly(*N*-vinylamides), and the synthesis of ABA triblock copolymers.

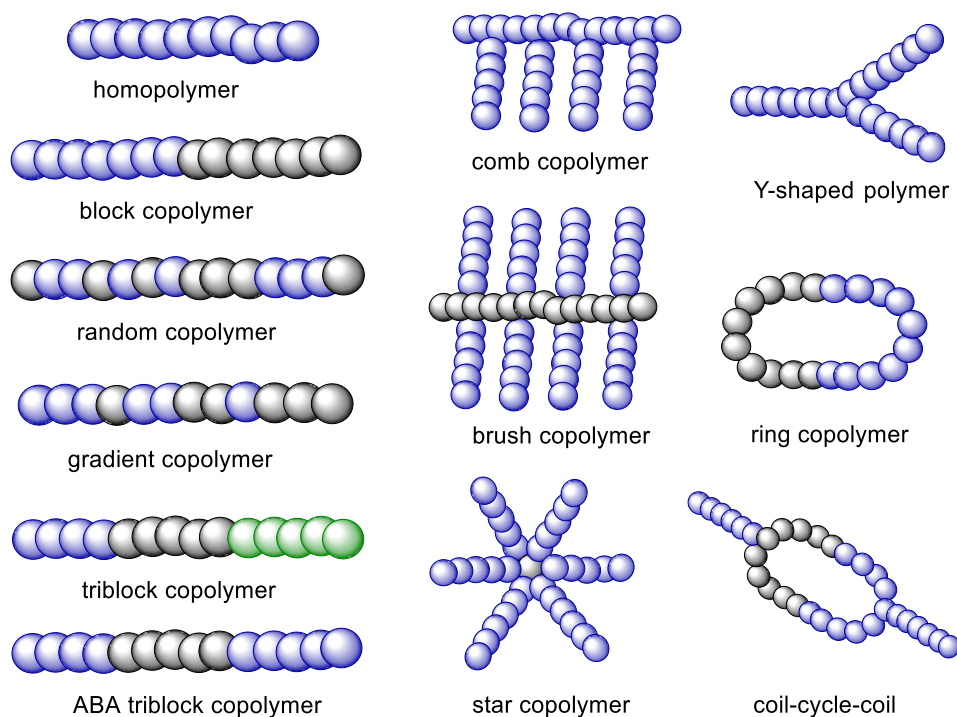


Figure 3. Complex architectures accessible through the RAFT process.

1.4.1. Importance of RAFT polymerization in drug delivery systems

In modern medicine, ensuring the effective and safe administration of therapeutic agents remains of utmost importance. Although conventional therapies have achieved significant milestones, they often suffer from overdosing, leading to potentially undesirable side effects and poorer therapeutic outcomes.¹⁰⁸ The main reason is the poor water solubility

of many therapeutic agents, which compromises their bioavailability. Consequently, there is growing interest in the development and use of more precise smart drug delivery systems (SDDS). SDDS are intelligent platforms that facilitate the targeted and controlled release of therapeutic agents in response to specific physiological or environmental triggers, for example, pH, temperature, enzymes, light, or magnetic field.¹⁰⁹ Temperature is one of the most extensively studied stimuli for drug delivery because it can be easily applied and monitored externally, which will be shown later in this work. SDDS are designed to incorporate therapeutic agents, effectively enhancing their solubility and prolonging their circulation time. They allow the delivery of the appropriate dose of the drug at the precise time and location in the body, maximizing therapeutic effects and minimizing potential adverse reactions. In essence, the goal of SDDS is to improve the efficacy of drugs while ensuring patient safety.^{110,111}

Numerous nanomaterials, including liposomes,^{112,113} metallic nanoparticles (NPs),^{114,115} silica-based materials,^{116–118} and carbon-based materials,^{119,120} have found applications as drug delivery systems. Among these, polymer-based materials have drawn considerable interest due to their versatility and the potential to fine-tune their properties. There are various types of polymeric nanocarriers, such as polymeric nanoparticles, polymeric micelles, polymer conjugates, dendrimers, polymersomes, polyplexes, nanogels, and lipomers.^{110,111,121–123} Examples of such systems are presented in Table 2, which illustrates various polymeric nanocarriers developed specifically through RAFT polymerization. The diversity of drug delivery vehicles, their responsiveness to stimuli, versatility in cargo, and a range of therapeutic applications highlight the importance of RAFT polymerization in the realm of drug delivery. This technique permits precise control over the properties of polymers, enhancing their suitability for drug delivery applications. Polymers can be designed to respond to various stimuli, such as pH, temperature, light, and enzymatic activity. The derived polymers might be tailored to encapsulate diverse cargos, from conventional drugs such as doxorubicin (DOX) and gemcitabine (GEM) to bioactive molecules like DNA and siRNA. Moreover, such polymers can be fine-tuned in terms of size, charge, and molar mass, offering a broad spectrum of applications ranging from combating bacterial infections to anticancer therapies and delivering genes.

The behavior of nanocarriers in complex biological environments, including circulation time, clearance, selective tissue distribution, and intracellular fate, depends on many factors, such as size, shape, charge, and stability. A significant challenge for their distribution is to overcome various biological barriers between organs and surrounding

fluids, e.g., the blood-brain barrier (BBB). The size of nanocarriers has emerged as a critical parameter that influences their behavior in biological systems. Particles smaller than 10 nm in diameter are prone to rapid elimination by the kidneys. On the contrary, those with a diameter greater than 200 nm could activate the body's immune system, leading to their rapid removal from the bloodstream.¹²⁴ Therefore, it can be concluded that 10–200 nm is the ideal size range for drug carriers.¹²⁵ It should be noted that in cancer therapy, particles with diameters within the range of sub-100 nm tend to accumulate effectively at the target sites due to the enhanced permeability and retention effect (EPR).^{126,127} This effect capitalizes on abnormal vasculature in tumor tissues and inflamed regions with pore sizes larger than normal blood vessels.¹²⁸ The surface charge of nanocarriers, represented by the zeta (ζ) potential, is another design feature that can be tailored to prolong circulation lifetimes and selectively enhance accumulation at specific sites. Cationic NPs are generally cleared more rapidly, whereas neutral and slightly negative particles (having ζ potential of -10 to +10 mV) have a prolonged half-life in circulation.^{118,127,129} Positively charged particles generally have a higher affinity for negatively charged cell membranes, which can lead to increased cellular uptake. However, this can also increase nonspecific interactions with various nontarget cells and proteins. Strongly positively charged particles can damage the cell membrane, causing other toxic side effects in normal cells.¹²⁷ It is worth noting that introducing a drug into a carrier can affect its size and zeta potential. The shape of the carrier also impacts the cellular interactions and uptake, but this relationship remains more complex. While some research suggests that spherical particles have better uptake in non-phagocytic cells than non-spherical particles, other studies show the contrary.^{127,130} The optimal size, shape, and charge of carriers may differ depending on the specific disease, its stage, and location. Thus, understanding these intricacies is paramount to harnessing the full potential of nanomaterials for therapeutic purposes.

Table 2. Polymeric nanocarriers developed through the RAFT polymerization.

Polymer	Stimuli	Cargo	M_n (kg mol^{-1}) / D	ζ potential of carrier (mV)	ζ potential with cargo (mV)	Size of carrier (nm)	Size with cargo (nm)	Application	Ref.
Polymeric nanoparticles									
POEGMA- <i>b</i> -PVBA	pH	GEN, NO	13.7/1.13	-	-	-	15.0	antibacterial activity	131
				pH 5.5/7.4					
<i>Pn</i> BMA- <i>b</i> -PDMAEMA- <i>r</i> -PEGMA			24.1/1.42	3.2/0.2		149.4			
<i>Pn</i> BMA- <i>r</i> -PDMAEMA- <i>b</i> -PEGMA	pH	BA, CPX	22.5/1.40	8.6/0.1	-	135.0	-	antibacterial activity	132
<i>Pn</i> BMA- <i>r</i> -PDMAEMA- <i>r</i> -PEGMA			23.7/1.39	2.5/-0.7		167.2			
PAA ₅₀ - <i>b</i> - <i>Pn</i> BA ₃₀₀	temperature	DOX	45.0/1.20	-65.0	-	130.0 100.0 ^e	140.0	cancer therapy	133
chol-PNIPAAm			26.4/1.10	-6.8		21.8	24.1		
chol-PNIPAAm- <i>b</i> -PACacP			29.5/1.07	-5.5		99.7	42.6		
chol-PNIPAAm- <i>s</i> -PACacP	temperature	DOX	32.1/1.04	-3.7	-	81.9	86.4	cancer therapy	134
chol-PACacP- <i>b</i> -PNIPAAm			26.6/1.30	-4.9		30.1	41.6		
Polymeric micelles									
			9.3/1.10			27.0			
PSAMA- <i>b</i> -PNIPAAm	temperature	CBZ	11.4/1.15	-	-	28.0	42.0	cancer therapy	135
			11.4/1.15			31.0			
PEG- <i>b</i> -PSMF-CCL						100			
PEG- <i>b</i> -PSMF	light	ICG	11.0/-	-	-	150	-	ROS-based drug delivery	136
PMPC- <i>b</i> -PDEMA- <i>co</i> -SS-PGEM- <i>co</i> -PTPMA	redox, pH	GEM	17.8/-	14.7 (pH 5)	-	42.9	53.4	cancer therapy	137
PEG-PDMAEMA-PONBA	pH/light	CUR	11.8/1.04	-	-	100.0	140.0	cancer therapy	138
PDPA- <i>b</i> -PNIPAAm- <i>co</i> -PDMAAm			19.0/1.38	0 to 6.0 (pH 5–7.5)		50.0 ^a 700.0 ^b			
<i>Pn</i> BMA- <i>b</i> -PNIPAAm- <i>co</i> -PDMAAm	pH temperature	DOX	16.8/1.35	-3.0 (pH 5–7.5)	-	50.0 ^a 600.0 ^b	-	cancer therapy	139

Polymersomes									
PDMAAm- <i>b</i> -PONBA	light	DOX, NR	20.5/1.25	-	-	200.0 150.0 ^e	-	cancer therapy	140
PMVCL ₅₈ -PVP ₆₅	temperature	DOX	9.9/1.14	-	-	370.0	-	cancer therapy	141
PMVCL ₅₈ -PVP ₉₈			10.1/1.17			220.0			
PEG- <i>b</i> -PDEAEM	pH, light	GNR, DOX	21.0–28.0/ 1.11–1.22	0.5 to 25.0 (pH = 7.4)	-	200.0	-	cancer therapy	142
PEG ₄₅ - <i>b</i> -PCSSMA ₁₅	redox, light	DOX, TR-dextran	10.9/1.22	-	-	220.0	-	treatment of various diseases	143
PEG ₄₅ - <i>b</i> -PCSSMA ₂₂			13.9/1.18			400.0			
PEG ₄₅ - <i>b</i> -PCSSMA ₃₀			17.7/1.13			440.0			
Polymer-drug conjugates									
DA-POEGMA- <i>b</i> -PABMA- <i>co</i> - PAMA@imine-DNR	pH	DNR	-	-	-22.1 to 17.4 (pH 11–1)	137.0 115.0 ^e	-	cancer therapy	144
mPEG- <i>b</i> -PC7- <i>b</i> -PCA	pH	CA	9.6/1.69	-	4.0 to 9.0 (pH 7.4–6.25)	-	200.0–450.0 (pH 7.4–6.5)	cancer therapy	145
PDHPMA-DOX	pH	DOX	95.0/-	-3.8	-	-	21	cancer therapy	146
Dendrimers									
PHPMAAm-GEM	enzyme	GEM	168.0/2.24	-1.4	-	-	45.0–50.0 ^f 55.0–85.0 ^g	cancer therapy	147
bisMPA dendrimer/ PHPMAAm- <i>co</i> -PBMHH-Prg	pH	DOX	268.0/1.10	-1.7	-3.3	20.5	28.5	cancer therapy	148
bisMPA dendron/ PHPMAAM- <i>co</i> - PBMHH-TT			354.0/1.20	-0.3	-2.6	23.9	35.4		
PAMAM/ PHPMAAm- <i>co</i> - PBMHH-TT			456.0/1.30	-2.0	-0.7	27.1	40.4		
Polyplexes									
POEGMA- <i>b</i> -PDIPAEMA	pH, temperature	DNA	33.3/1.21 48.6/1.19 35.1/1.24	-	-30.0 to -13.0 -25.0 to -7.0 -23.0 to -4.0	-	-	gene delivery	149

PNIPAAm-PEG-PDMAEMA	temperature	DNA	52.0/1.8	7.7	-	150.0	-	gene delivery	150
PVAm- <i>b</i> -PNIPAAm	temperature	DNA	5.6/1.3	5.5 ^c	-23.0 ^c	7.8 ^c	156 ^c	gene delivery	151
PVAm- <i>b</i> -PALysOH			13.7/1.5	45.1 ^d	-32.0 ^d	122.0 ^d	223 ^d		
PEGMA- <i>b</i> -PDPA- <i>b</i> -PDMA	pH	siRNA	-	-0.7	9	-	60 ^e	gene delivery	152
mPEG- <i>b</i> -PAMA- <i>b</i> -PD5A/PDEA	pH	siRNA	12.6/1.7	-	32	-	44	gene delivery	153
Nanogels									
PDEGMA- <i>co</i> -PEGMA- <i>co</i> -PHODMA- <i>co</i> -PNPCD	temperature, redox	BSA, LS	31.7/1.1	-	-22.1	-	320.1	protein delivery	154
PmTEGMA- <i>b</i> -PPFPMA	pH	IMDQ	12.0/1.3	-4.0	-	56.3	59.7	nanovaccines	155
		IMDQ, OVA		-4.0	-9.5	56.3	57.3		

Notes: ^ameasured at 37 °C, ^bmeasured at 42 °C, ^cmeasured at 25 °C, ^dmeasured at 50 °C, ^emeasured by TEM, ^fmeasured in PBS, ^gmeasured in FBS.

Abbreviations: BA, baicalein; bisMPA- 2,2-bis(hydroxymethyl)propionic acid; BSA, bovine serum albumin; CA, cinnamaldehyde; CBZ, carbamazepine; CCL, core-cross-linked; chol, cholesterol; CPX, ciprofloxacin; CUR, curcumin; DA, 2,3-dimethylmaleic anhydride; DNR, daunorubicin; DOX, doxorubicin; FBS, fetal bovine serum; GEM, gemcitabine; GEN, gentamicin; GNR, gold nanorods; ICG, indocyanine green; IMDQ, agonist 1-(4-(aminomethyl)benzyl)-2-butyl-1H-imidazo[4,5-c]quinolin-4-amine; LS, Lysozyme; NO, nitric oxide; NR; Nile Red; OVA, ovalbumin; PAA, poly(acrylic acid); PABMA, poly(4-azidobenzyl methacrylate); PAcaP, poly(10-(acryloyloxy)decyl-3-oxobutanoate); PALysOH, poly(N-acryloyl-L-lysine); PAMA, poly(2-aminoethyl methacrylate hydrochloride); PAMAM, polyamidoamine, PBMHH, poly(*N*-(*tert*-butoxycarbonyl)-*N'*-(6-methacryloylamino)hexanoyl)hydrazine); PC7, poly(2-hexamethyleneiminoethanol); PCA, polycinnamaldehyde; PCSSMA, poly(coumarin-based disulfide-containing monomer); PD5A, poly(2-diamylamineethyl methacrylate); PDEAEM, poly(*N,N*-diethylamineethyl methacrylate); PDEGMA, poly(di(ethylene glycol)methyl ether methacrylate); PDEMA, poly(*N,N*-dibutylethanolamine); PDIPAEMA, poly(2-[diisopropylamino]ethyl methacrylate); PDMA, poly(2-(dimethylamino)ethyl methacrylate); PDMAAm, poly(*N,N*-dimethylacrylamide); PDMAEMA, poly(*N,N*-dimethylaminoethyl methacrylate); PDPA, poly(2-(diisopropylamino)ethyl methacrylate); PEG, poly(ethylene glycol); PEGMA, poly(ethylene glycol)methyl ether methacrylate); PFPMA, poly(pentafluorophenyl methacrylate); PGEM, polygemcitabine; PHODMA, poly(2-(2-(2-hydroxyethyl)disulfanyl)ethyl methacrylate); PHPMAAm, poly(*N*-(1,3-dihydroxypropan-2-yl)methacrylamide); PMPC, poly(2-methacryloyloxyethyl phosphorylcholine); PMVCL, poly(3-methyl-*N*-vinylcaprolactam); PnBA, poly(*n*-butyl acrylate); PnBMA, poly(*n*-butyl methacrylate); PNIPAAm, poly(*N*-isopropylacrylamide); PNPCD, poly(2-(2-(2-((4-nitrophenoxy)carbonyloxy)ethyl)disulfanyl)ethyl methacrylate); POEGMA, poly(oligoethylene glycol)methyl ether methacrylate; PONBA, poly(*o*-nitrobenzyl acrylate); Prg, propargyl; PSAMA, poly(2-methacryloyloxyethyl stearate); PSMF, poly(styrenemaleic anhydride) functionalized with furfuryl amine; PTEGMA, poly(methoxy tri(ethylene glycol) methacrylate); PTMA, poly(4-(4'-(diphenylamino)-[1,1'-biphenyl]-4-yl)-1-((methacryloyloxy)-methyl)pyridin-1-ium bis((trifluoromethyl)sulfonyl)amide); PVAm, polyvinylamine; PVBA, poly(3-vinylbenzylaldehyde); PVP, poly(*N*-vinylpyrrolidone); ROS, reactive oxygen species; siRNA, small interfering RNA; TR-dextran, texas red-labeled dextran; TT, 2-thiazolidine-2-thione.

1.4.1.1. Thermoresponsive polymers

Thermoresponsive polymers, well-known for their ability to modify their physical properties with temperature changes, represent a fascinating and common field of study. The use of drug carriers containing thermoresponsive polymers is inspired by the observation that pathological processes in various tissues and organs are associated with local temperature increases by 1–5 °C.¹⁵⁶ For example, tumor microenvironments are characterized by mild hyperthermia exhibiting temperatures 1–2 °C higher than healthy tissue.¹⁵⁷ Additionally, these versatile polymers can serve as carriers for drugs intended to act on external surfaces such as skin and mucous membranes, where the temperature is lower than the body temperature.¹⁵⁸ By carefully designing polymeric carriers, it becomes possible to efficiently release drugs at a specific location within the different temperature ranges associated with pathological processes (Figure 4).

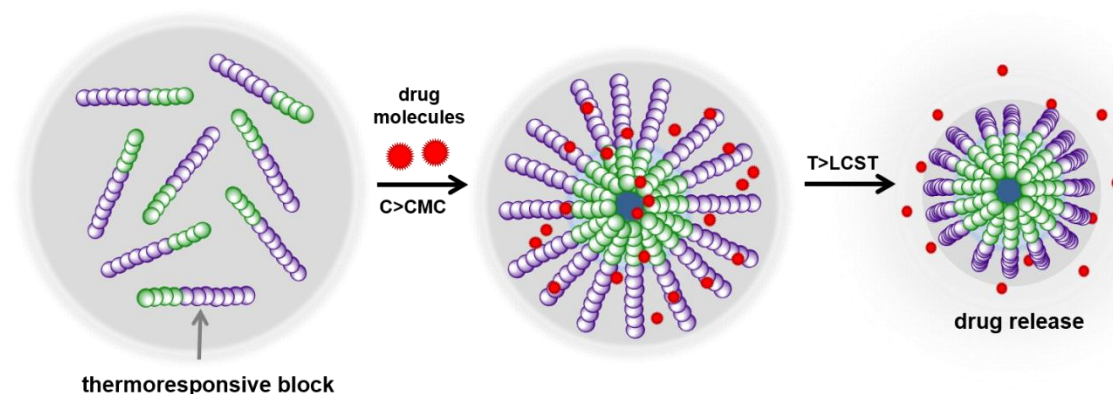


Figure 4. Mechanism of action of thermoresponsive amphiphilic polymers.

Thermoresponsive polymers exhibit phase transitions at specific temperatures known as the lower critical solution temperature (LCST) and the upper critical solution temperature (UCST) (Figure 5). This phenomenon can be described as a sharp change in solubility, accompanied by conformational changes in the polymer structure caused by temperature fluctuations. The LCST is the temperature at which a polymer transitions from a soluble state to an insoluble state upon heating. Below the LCST, the polymer is fully dissolved and exhibits a coil conformation since the hydrophilic groups on the polymer chain interact favorably with the surrounding water molecules. As the temperature increases, the hydrogen bonds between the hydrophilic groups and the solvent weaken, causing the hydrophobic groups to dominate and making polymer-polymer interactions more important.⁷⁴

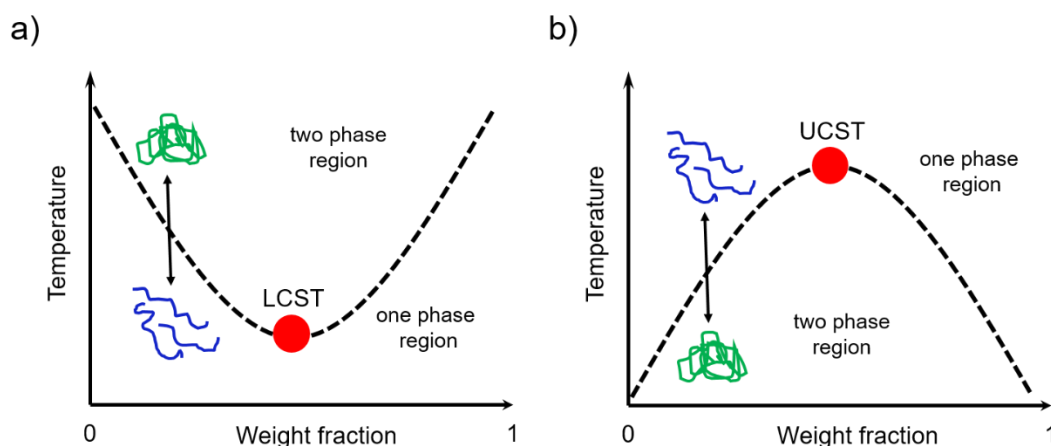


Figure 5. Schematic illustration of phase diagrams for polymer solution a) lower critical solution temperature (LCST) behavior and b) upper critical solution temperature (UCST) behavior.

Consequently, the polymer chains aggregate, adopting a globular conformation, resulting in a turbid suspension. This characteristic behavior of thermoresponsive polymers is often referred to as the "coil-to-globule transition".¹⁵⁹ Examples of polymers exhibiting LCST behavior include poly(*N*-isopropylacrylamide) (PNIPAAm), poly(*N*-vinylcaprolactam) (PNVCL), poly(methyl vinyl ether) (PMVE), and poly(*N,N*-diethylacrylamide) (PDEAAm) are presented in Figure 6. On the contrary, the UCST is the temperature at which the polymer transitions from an insoluble state to a soluble state upon heating. Below the UCST, the polymer is in a collapsed, insoluble state because of strong hydrogen bonds, stronger than those involving the polymer-water interaction. These bonds break with increasing temperature, allowing the polymer to dissolve. A typical UCST system is based on poly(*N*-acryloylglycinamide) (PNAGA) or acrylamide-based copolymers.¹⁶⁰ The application of polymers exhibiting UCST behavior in the biomedical field is less common than those exhibiting LCST behavior, as achieving this behavior under physiological conditions is more challenging.¹⁶¹ It is worth noting that LCST and UCST systems are not restricted to an aqueous solvent environment. Moreover, phase transitions are reversible, allowing the polymers to switch between their soluble and insoluble phases multiple times. Nevertheless, the temperature at which the polymer solubilizes again may be slightly different, resulting in hysteresis of the system.¹⁶⁰

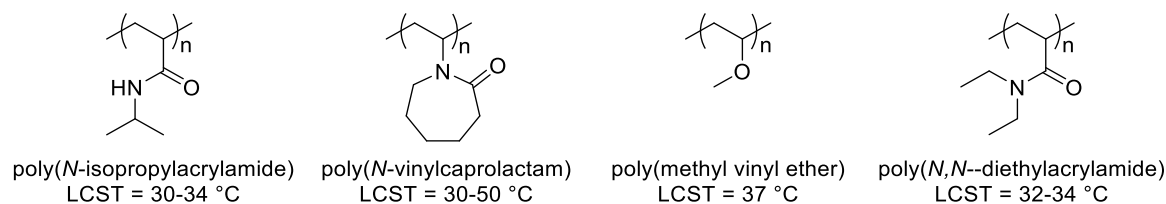


Figure 6. Examples of polymers exhibiting LCST behavior.

It is essential to highlight the significant distinction between LCST/UCST and cloud point temperature (T_{CP}) in the context of thermoresponsive polymers. Often, the terms LCST and T_{CP} are mistakenly used interchangeably. The LCST is the minimum temperature value on the binodal curve, which is generated by plotting multiple cloud points at different concentrations (Figure 5, red spot). On the other hand, T_{CP} refers to the temperature at a specific polymer concentration where a phase transition occurs, causing the cloudiness of the solution. T_{CP} can be located anywhere on the binodal curve.^{159,160}

1.4.1.2. PNIPAAm and PNVCL

Poly(*N*-isopropylacrylamide) (PNIPAAm) and poly(*N*-vinylcaprolactam) (PNVCL) have gained significant attention for their applications in thermoresponsive drug delivery systems. *N*-vinyl caprolactam (NVCL) is a representative of *N*-vinylamides, which will be discussed in the following section. However, in the context of this dissertation, polymers containing PNVCL were specifically utilized as thermoresponsive drug carriers. Hence, a description of PNVCL and its role in drug delivery systems will be provided.

PNIPAAm is widely regarded as the "gold standard" in thermoresponsive SDDS and has undergone extensive research. It exhibits a lower critical solution temperature (LCST) of approximately 32 °C, a crucial feature for biomedical applications due to its proximity to human body temperature. PNIPAAm contains a hydrophobic isopropyl group as well as a hydrophilic amide moiety.¹⁶² PNIPAAm is soluble in organic solvents, such as chloroform, acetone, methanol, and water (below LCST). PNIPAAm can be easily synthesized through reversible-deactivation radical polymerization, allowing for the creation of various structures such as micelles, gels, and grafted surfaces. In addition to controlled delivery, PNIPAAm-based materials are excellent candidates for biosensing, tissue engineering, and wound treatment applications.

PNVCL is another polymer that displays notable properties for biomedical applications. Its transition temperature (32–34 °C) is suitable for biomedical applications.¹⁶³ PNVCL bears both hydrophilic amide groups and a hydrophobic carbon-carbon backbone.¹⁵⁶ It is a non-ionic polymer and exhibits solubility in water and organic solvents. Additionally,

PNVCL is very stable against hydrolysis.¹⁶³ However, PNVCL has been less popular among researchers than PNIPAAm, primarily due to the difficulties in polymerizing NVCL in a controlled fashion.

Table 3 shows various polymers based on PNIPAAm or PNVCL prepared by RAFT polymerization, which are utilized to construct thermoresponsive drug carriers. Carriers based on PNIPAAm and PNVCL are used in various forms, such as nanoparticles, micelles, composites, gels, or grafted surfaces. Cargo molecules carried by these systems include common chemotherapy agents such as doxorubicin (DOX), paclitaxel (PTX), and 5-fluorouracil (5-FU), among others. The effectiveness of these drug carriers is attributed to their ability to respond to changes in temperature, allowing controlled release of drugs at target sites. Cloud point temperatures range from around 31 to 43 °C; thus, they can respond to the human body's temperature. The size of these carriers also varies, from as small as 7 nm to as large as 396 nm. It is worth mentioning that the introduction of a drug molecule into a polymer carrier may affect both its size and T_{CP} . Biological applications are predominantly in cancer therapy, with specific references to colorectal, breast, colon, and liver cancer treatments and broader drug delivery and gene therapy applications.

Table 3. Comprehensive overview of thermoresponsive polymer-based drug delivery systems.

Polymer	Form of carrier	Cargo	M_n (kg mol^{-1})/ D	T_{CP} of carrier ($^{\circ}\text{C}$)	T_{CP} with cargo ($^{\circ}\text{C}$)	Size of carrier (nm)	Size with cargo (nm)	Biological application	Ref.
PNIPAAm									
GO/ β -CD-star-PMMA- <i>b</i> -PNIPAAm	nanocomposites	DTX	15.3/1.17	41.0–43.0	-	<u>61.0 (25 $^{\circ}\text{C}$)</u> <u>112.0 (38 $^{\circ}\text{C}$)</u> <u>85.0 (45 $^{\circ}\text{C}$)</u>	-	cancer therapy	164
mPEG- <i>b</i> -PNIPAAm- <i>b</i> -PDEAEMA- <i>co</i> -PnBMA	polymersomes	<u>DOX</u> <u>PTX</u> DOX, PTX	133.4/1.41	33.0 (pH 7) 41.0 (pH 6.4)	-	172.1	<u>175.5</u> <u>172.1</u> 168.3	cancer therapy	165
PNIPAAm-GMA	MOF	DOX/ CRISPR	-	-	-	75.0–120.0	-	drug/gene delivery	166
PNIPAAm- <i>co</i> -PAA	polymeric nanoparticles	DOX	13.5/-	39.0 ^b	36.0–40.0 ^a 40.0 ^b	45.0 (29 $^{\circ}\text{C}$) 7.0 (47 $^{\circ}\text{C}$)	255.0 ^c 40.0 (29 $^{\circ}\text{C}$) ^d 10.0 (47 $^{\circ}\text{C}$) ^d	cancer therapy	167
PHEA-(FLA)-PHEA- <i>b</i> -PNIPAAm	polymeric nanoparticles	5-FU	<u>13.0/1.65</u> <u>14.7/1.51</u> <u>17.0/1.57</u>	36.1 36.0 35.6	36.5 36.6 36.6	53.1 6.4 8.7	<u>7.7</u> <u>8.0</u> <u>9.4</u>	colorectal cancer therapy	168
PNIPAAm-SS- <i>b</i> -CPLL- <i>b</i> -SS-PNIPAAm	micelles	DOX, IR780	10.1/1.20	36.9	-	180.0	-	colon cancer therapy	169
PNIPAAm- <i>b</i> -PLA	micelles	DTX	22.1/-	32.0–38.0 ^a 34.0 ^b	37.0–40.0 ^a	-	<u>13.0 (25 $^{\circ}\text{C}$)</u> <u>82.0 (40 $^{\circ}\text{C}$)</u> <u>245.0 (42 $^{\circ}\text{C}$)</u>	breast cancer therapy	170
PNIPAAm- <i>b</i> -PNALPA	micelles	DOX	<u>15.3/1.38</u> <u>14.8/1.31</u> <u>16.3/1.30</u>	31.0–33.0	-	<u>123.0</u> <u>220.0</u> <u>296.0</u>	<u>142.0</u> <u>296.0</u> <u>342.0</u>	drug delivery	171
PC/PNIPAAm- <i>s</i> -PAH	hydrogel	DOX/CA4	35.4/-	36.0–43.0	-	-	-	cancer therapy	172
PVA- <i>g</i> -PNIPAAm	hydrogel	5-FU	-	-	-	-	-	drug delivery	173
PNVCL									
GNR@PEG- <i>b</i> -PNVCL	nanoparticles	RB	15.0/1.06	39.0	-	280.0	-	cancer therapy	174
CPP-CS- <i>co</i> -NVCL	nanoparticles	DOX	15.3/-	40.0	-	150.0	166.0	breast cancer therapy	175

PHEA-(FA)-PHEA- <i>b</i> -PNVCL	micelles	5-FU	18.0/1.73	31.0	34.5	8.0	110.0	colon cancer therapy	176
			22.3/1.83	31.0	34.5	50.0	90.0		
			24.2/2.10	31.0	36.0	100.0	10.0		
(PVAc ₁₇ - <i>b</i> -PNVCL ₁₀ - <i>co</i> -PVP ₇) ₆	micelles	MTX	36.5/1.10	40.0	40.0	115.0	123.0	drug delivery	177
(PVAc ₃₀ - <i>b</i> -PNVCL ₂₈ - <i>co</i> -PVP ₁₇) ₆			42.3/1.10	36.0	36.0	234.0	244.0		
PMVCL- <i>co</i> -PNVCL- <i>b</i> -PNVCL- <i>co</i> -PVP	micelles	DOX	31.2/1.41	42.0	46.0	226.0	-	cancer therapy	178
POEGMA ₁₆ - <i>b</i> -PNVCL ₃₉₀	micelles	NR	74.5/1.23	38.5 (H ₂ O) 35.5 (PBS)	-	235.0 (45 °C)	-	drug delivery	179
PAA- <i>g</i> -PNVCL	micelles	ONZ	27.2/1.22	34.0	37.0	-	175.0	cancer therapy	180
PNVCL- <i>b</i> -G _n -Fmoc-GL	micelles	NR	27.1/1.26	35.0–40.0	-	20–140 ^d	-	drug delivery/ biosensors	181
			25.5/1.27	35.0–40.0		165–270 ^d	300–460 ^d		
PNVCL- <i>b</i> - _D (Phe-Lys)	micelles	DOX	4.6/1.22	36.8	-	220.0	252.0	liver cancer therapy	182
			6.6/1.27	38.0		124.0	164.0		
			7.1/1.19	38.0		260.0	283.0		
			8.9/1.18	40.0		159.0	119.0		
PNVCL ₁₀ -PDMS ₆₅ -PNVCL ₁₀	polymersomes	DOX	5.0/1.13	40.0–42.0	-	396.0	470.0	drug delivery	183,184
γ-Fe ₂ O ₃ @DXA- <i>g</i> -PNVCL	nanocomposites	NPX	18.9/1.01	36.2	-	-	213.2–255.3 (from 6 to 48 h)	drug delivery	185

Notes: ^ameasured by UV-Vis, ^bmeasured by DSC, ^cmeasured by AFM, ^dmeasured by TEM.

Abbreviations: 5-FU, 5-fluorouracil; CA4, combretastatin A4 disodium phosphate; CBZ, carbamazepine; CPLL, (cyclic-poly(L-lysine); CPP, cell-penetratin peptide; _D(Phe-Lys), dendric phenylalanyllysine; CRISPR, clustered regularly interspaced short palindromic repeat system; CS, chitosan; DOX, doxorubicin; DTX, docetaxel; DXA, dextran; FLA, folic acid; Fmoc, fluorenylmethoxycarbonyl protecting group; GL, glycine; GMA, glycidyl methacrylate; GNR, gold nanorods; GO, graphene; IR780, 2-[2-[2-chloro-3-[(1,3-dihydro-3,3-dimethyl-1-propyl-2H-indol-2-ylidene)ethylidene]-1-cyclohexen-1-yl]ethenyl]-3,3-dimethyl-1-propylindolium iodide; mPEG, methoxyl poly(ethylene glycol); MTX, methotrexate; NPX, naproxen; NR, Nile red; PAA, poly(acrylic acid); ONZ, ornidazole; PAH, polyacylhydrazide; PBMA, 2-hydroxy-4-methacryloyloxybenzophenone; PC, pectin; PDEAEMA, poly(2-(diethylamino)ethyl methacrylate); PDMS, polydimethylsiloxane; PEG, poly(ethylene glycol); PHEA, poly(2-hydroxyethylacrylate); PLA, poly(lauryl acrylate); PMMA, poly(methyl methacrylate); PMVCL, poly(3-methyl-*N*-vinylcaprolactam); PNALPA, poly(*N*-acryloyl-*L*-phenylalanine methyl ester); PNIPAAm, poly(*N*-isopropylacrylamide); PNVCL, poly(*N*-vinylcaprolactam); POEGMA, poly(oligoethylene glycol)methyl ether methacrylate; PVA, poly(vinyl alcohol); PVAc, poly(vinyl acetate) PVP, poly(*N*-vinylpyrrolidone); MOF, metal-organic framework; ONZ, ornidazole; RB, rhodamine; SS, disulfide bridge, β-CD, β-cyclodextrin.

Despite having similar LCST temperatures, PNIPAAm and PNVCL differ in the mechanisms of the thermoinduced phase transitions and properties. The comparison between the properties of PNIPAAm and PNVCL is shown in Table 4. PNIPAAm shows a type I Flory–Huggins phase change. The LCST of PNIPAAm is independent of molar mass but can be influenced by environmental factors such as pH and polymer concentration. In turn, PNVCL exhibits a "classical" Flory-Huggins thermoresponsive behavior in water (type II).¹⁶³ Consequently, the LCST of PNVCL can be modulated by altering the length of the polymer chains.¹⁸⁶ The LCST of both PNIPAAm and PNVCL can be manipulated by copolymerization to modify the hydrophilic/hydrophobic balance. The introduction of hydrophilic comonomers enhances the energy required to disrupt H-bonding, thereby raising the LCST. In contrast, hydrophobic comonomers decrease LCST.^{156,160} Additionally, the LCST can be influenced by the nature of the end-groups: hydrophilic end-groups tend to increase it, while hydrophobic end-groups have the opposite effect.¹⁵⁶ The biomedical implications of PNIPAAm and PNVCL require meticulous consideration. The amide moiety in PNIPAAm can hydrolyze under acidic conditions, releasing small amide molecules that may be deleterious in biomedical contexts. PNVCL, on the other hand, offers a comparatively safer profile. Its hydrolysis produces non-toxic by-products resulting from caprolactam ring breakage. Furthermore, PNVCL offers additional advantages over PNIPAAm, such as decreased biomolecule interaction and no crystallization tendency.^{156,187} In this work, a thorough comparative study was carried out to juxtapose the properties and biomedical applications of drug delivery systems based on both PNIPAAm and PNVCL.

Table 4. Comparison between physicochemical properties of PNIPAAm and PNVCL.^{156,187}

	PNIPAAm	PNVCL
Thermoresponsivness		
LCST	32 °C	32–50 °C
Dependence on molar mass	independent	dependent
Flory–Huggins phase change	type I	type II
Biocompatibility		
In vitro cytotoxicity	none (before hydrolysis) toxic (after hydrolysis)	none (before hydrolysis) none (after hydrolysis)
In vivo toxicity	systemic toxicity detected	not yet reported
Polymerization and polymers		
RDRP techniques	well-established	in constant development
Well-defined polymers	lots	limited examples

1.4.1.3. Incorporation of lipids into the polymeric structure

All biological membranes are built of lipid bilayers. Their role is essential because their structural components provide the barrier that marks the boundaries of a cell. The structure is called a "lipid bilayer" because it comprises two layers of lipid molecules organized in two sheets.¹⁸⁸ Lipids, including sterols, isoprenoids, fatty acids, diglycerides, and phospholipids, are components of biological membranes.

The critical issue related to the efficiency of smart drug nanocarriers is their interaction with cell membranes. One strategy to improve cellular uptake is the modification of a carrier structure with a cell-penetrating molecule. Interestingly, lipids can serve as cell-penetrating agents due to their inherent nature and interaction with cellular barriers. As an example, using cholesterol-containing polymeric drug carriers led to the disruption of the cell membrane and, as a result, reduced tumor growth.¹⁸⁹

Diglycerides (DGs) (commonly referred to as diacylglycerols), which are esters derived from glycerol and two fatty acids with one remaining free hydroxyl group, show great potential as components in modern drug delivery systems. Although they constitute a minor quantity among the numerous bioactive lipids in biological membranes, they play a significant functional role. DGs are responsible for maintaining cellular homeostasis, acting as second messengers in diverse signaling pathways, including lipid metabolism, protein export, and complex neurotransmission processes.¹⁹⁰⁻¹⁹² Beyond their role as messengers, DGs exert a notable influence on the physicochemical properties of the membrane. They regulate aspects such as membrane curvature, fusion or fission dynamics, and interactions with proteins.^{191,193,194} Notably, DGs exhibit a degree of variability in their structure. They can occur in different stereochemical forms and contain various types of fatty acids (FAs) with different degrees of unsaturation.^{192,195} This structural diversity significantly influences their biological properties and roles within the membrane. For example, DGs containing saturated fatty acids, such as palmitic acid, contribute to the rigidity of the membrane. They promote a more organized and stable structure because they can pack together closely. On the other hand, DGs with unsaturated fatty acids, such as oleic acid, do not pack as tightly, which introduces a level of fluidity into the membrane.

Despite the numerous advantages associated with the use of diglycerides in drug delivery systems, it should be noted that only a limited number of polymers containing diglycerides have been reported so far.¹⁹⁶⁻¹⁹⁸ Diglyceride-terminated poly(oligo(ethylene glycol) acrylates)¹⁹⁶ and acrylamides¹⁹⁷ were synthesized by RAFT polymerizations

mediated by trithiocarbonates based on DGs. However, there is a lack of literature reports on polymers containing diglycerides as side chains. This approach presents an intriguing opportunity for further exploration. Previous studies demonstrated that the presence of multiple long alkyl chains, working in synergy along the polymer chain, disrupts the cytoplasmic membrane of microorganisms and leads to the loss of cytoplasmic constituents, ultimately resulting in their death.¹⁹⁹

In this context, part of this doctoral thesis concerns the synthesis of polymers containing diglycerides in different parts of the chain, aiming to explore further the potential of diglycerides in polymeric drug delivery systems. These aspects will be discussed in Chapters 2 and 3 of this dissertation.

1.4.2. Application of RAFT polymerization in the synthesis of *N*-vinylamides

N-vinylamides are water-soluble monomers in which nitrogen is directly attached to the vinyl group. They belong to the group of "less activated" monomers (LAM) and can be classified into two types, cyclic and noncyclic, according to the nature of the amide group in their constitutive monomers (Figure 7).

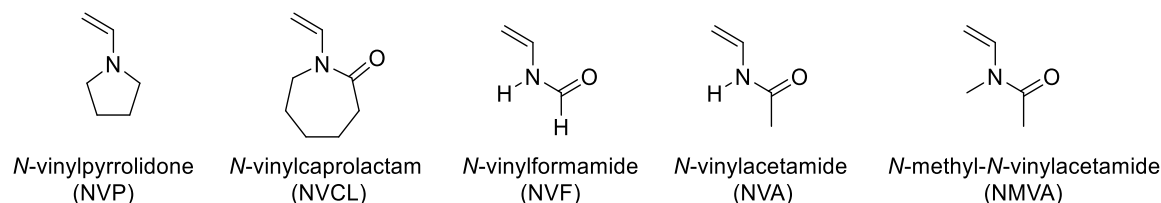
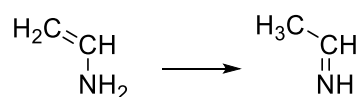


Figure 7. Chemical structures of *N*-vinylamides.

N-vinylpyrrolidone (NVP) and *N*-vinylcaprolactam (NVCL) are the most commonly used examples of cyclic *N*-vinylamides, frequently referred to as *N*-vinyl lactams. Noncyclic *N*-vinylamide monomers involve *N*-vinylformamide (NVF), *N*-vinylacetamide (NVA), and *N*-methyl-*N*-vinylacetamide (NMVA). Synthesizing *N*-vinylamides in a controlled manner is challenging despite their easy polymerization through radical polymerization. This difficulty arises because of the high reactivity of the generated radical species, which is attributed to their nonconjugated nature (lack of resonance stabilization) and strong electron-donating pendant groups. The high reactivity of the propagating radicals derived from *N*-vinyl monomers led to an inability to suppress unfavorable chain transfer and termination reactions.^{48,200}

Noncyclic *N*-vinylamides play a crucial role as precursors for the synthesis of homopolymers and copolymers with a wide range of applications in diverse fields, such as the biomedical field,^{201,202} petroleum industry,^{203,204} and batteries^{205,206}. Notably, their hydrolysis led to the formation of water-soluble polyvinylamines (PVAm). It is important to emphasize the significant role of poly(*N*-vinylformamide) (PNVF), the simplest member of the *N*-vinylamide family, as a key starting compound in the synthesis of polyvinylamines with reactive primary amino groups.²⁰⁷

Polyvinylamine (PVAm) is a cationic polymer with the highest content of primary amine groups of any polymer.²⁰⁸ PVAm possesses attractive properties such as pH-sensitivity, nontoxicity, and the ability to bind metals. PVAm has become a valuable material with many applications, including biomedicine,^{209–211} functionalization of nanoparticles surface,^{208,212,213} water purification,²¹⁴ membranes for carbon dioxide capture,^{215,216} and textile chemicals²¹⁷. It should be clarified that PVAm cannot be synthesized directly from the corresponding vinylamine monomer, as it is impossible to isolate it due to imine-enamine tautomerization (Scheme 9).^{218,219} The vinylamine monomer undergoes a change in the configuration of the bond, forming a more stable imine by moving its carbon-carbon double bond to the carbon-nitrogen bond. PVAm must be synthesized by indirect methods. For example, the introduction of primary amine groups into a polymer can be achieved by the Hofmann rearrangement of polyacrylamide,²²⁰ or hydrazinolysis of poly(*N*-vinylphthalimide).^{221,222} However, extensive research has shown that the simplest precursor for the production of polyvinylamines is the aforementioned poly(*N*-vinylformamide). The hydrolysis of PNVF proceeds under mild reaction conditions, both acidic and alkaline. In comparison, PNVA and PNMVA hydrolyzed to PVAm under harsh reaction conditions (6 mol L⁻¹ aqueous HCl at 120 °C for 64 h) and often did not achieve 100% conversion.^{223,224} Therefore, they are considered less attractive for synthesizing functional polyvinylamines.



Scheme 9. Imine-enamine tautomerization of vinylamine.

Although the RAFT polymerization of cyclic *N*-vinylamides has been extensively studied and documented,^{177,225–228} achieving precise control over noncyclic *N*-vinylamides has been more challenging. To date, only a few articles have been published on the RDRP polymerization topic of these compounds. Debuigne and coworkers described controlled polymerization of *N*-vinylacetamide and *N*-methylvinylacetamide through cobalt-mediated

radical polymerization (CMRP).²²⁴ Fan and Yamago showed the successfully controlled polymerization of NVF, NVA, and NMVA by organotellurium-mediated radical polymerization (TERP).²²⁹ Interestingly, RAFT polymerization has only been used for the synthesis of a few examples of noncyclic *N*-vinylamides. The work published by Destarac and coworkers sheds new light on the polymerization of noncyclic *N*-vinylamides using the RAFT method.²³⁰ In-depth research consisted of selecting the polymerization conditions, which in turn allowed to obtain homopolymers based on PNMVA and copolymers with a PNMVA block in a controlled manner. Also, few reports focused on the RAFT polymerization of NVF-based copolymers. Beckmann and coworkers demonstrated the synthesis of PEG-*b*-PNVF block copolymers using a dithiocarbonate-terminated PEG as macro-CTA.²³¹ However, the conversion of NVF was relatively low, and the obtained copolymers exhibited high dispersities ranging from 1.7 to 2.3. Another similar strategy was proposed by Barsbay and coworkers to obtain poly(acrylic acid)-*b*-poly(*N*-vinylformamide) (PAA-*b*-PNVF) copolymer.²¹² They utilized dithiocarbonate functionalized PAA as macro-CTA, which was subsequently chain extended with NVF. In this case, the molar masses were close to the theoretical assumption, and the polymers exhibited relatively low dispersities. Notably, the homopolymerization behavior of NVF was not investigated in either of the mentioned studies, as NVF was used only as the second block. Pich and coworkers also applied RAFT polymerization to prepare a series of statistical copolymers based on cyclic poly(*N*-vinylamides), including *N*-vinylcaprolactam, *N*-vinylpiperidine, and *N*-vinylpyrrolidone, with a maximum content of NVF of 50%.²³² Although polymerization proceeded in a controlled manner, the focus of the authors primarily lay on low molar mass copolymers with $M_n \sim 10 \text{ kg mol}^{-1}$.

Recently published manuscripts by Destarac and coworkers (which also includes the author of this dissertation) have presented a comprehensive study for the first time to understand better the potential of NVF monomer in traditional thermally activated RAFT²³³ and PI-RAFT polymerization²³⁴. The research focused on the homopolymerization of NVF and the synthesis of corresponding block copolymers. In the study involving thermally-activated RAFT, the reactions were conducted in DMSO at 35 °C, with a dithiocarbonate as the chain transfer agent. These conditions facilitated the synthesis of PNVF with molar mass up to $M_n \sim 80 \text{ kg mol}^{-1}$ and low dispersities ($D < 1.4$). Additionally, well-defined block copolymers with a PNVF-based segment were successfully synthesized. As an example, poly(*N*-vinylcaprolactam)-*b*-poly(*N*-vinylformamide) (PNVCL-*b*-PNVF) was hydrolyzed, yielding the original thermoresponsive and pH-sensitive poly(*N*-vinylcaprolactam)-*b*-

poly(*N*-vinylamine) (PNVCL-*b*-PVAm), thus demonstrating the remarkable potential of the RAFT approach in developing complex architectures based on PVAm. The polymerization of NVF through PI-RAFT polymerization constitutes a significant part of this doctoral dissertation. A detailed discussion of this process will be presented in Chapter 4.

1.4.3. Synthesis of ABA triblock polymers

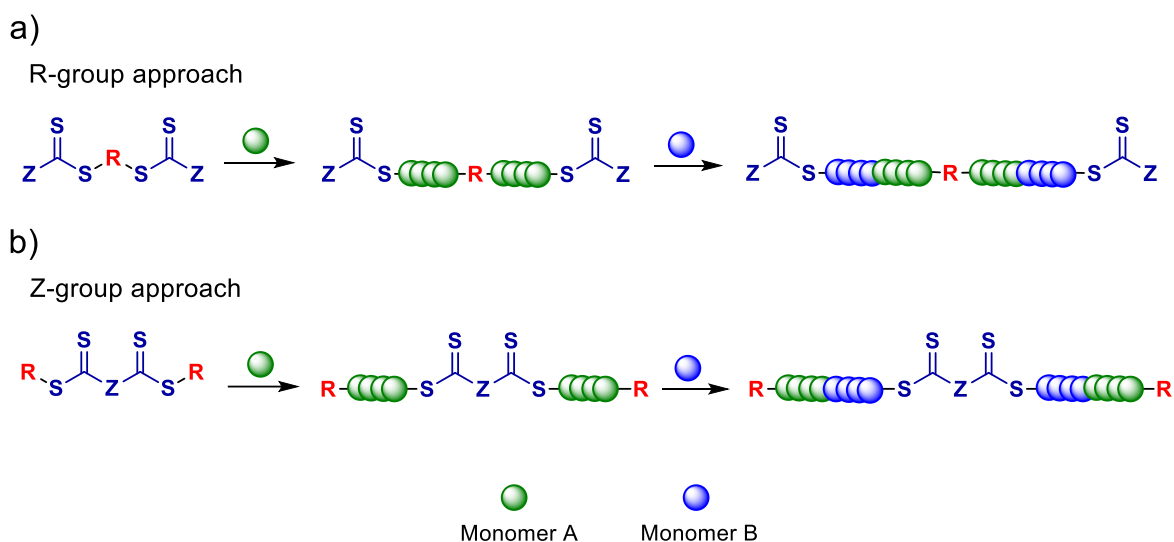
Among the various copolymer architectures, block copolymers stand out due to their ability to combine distinct properties within a single molecule. Block copolymers are composed of covalently linked polymer segments that can be arranged in various configurations.^{235,236} The simplest is the diblock copolymer, typically denoted as AB, where A and B represent different types of repeating monomer units. The more complex form, triblock copolymers, consists of three segments and can be symmetric (ABA or BAB) or asymmetric (ABC), with each letter representing a different type of repeating monomer unit.^{235,237} It has been shown that the sequence of blocks influences the properties of the copolymer, such as self-assembly,^{238,239} phase separation,^{240,241} and mechanical properties.^{242,243} Numerous studies concerning the synthesis of triblock copolymers via anionic²⁴⁴ and RDRP methods^{243,245,246} have already been reported. This thesis focuses mainly on the synthesis of triblock ABA copolymers using RAFT polymerization; therefore, it will be discussed in more detail.

1.4.3.1. Methods of synthesis

The synthesis of triblock copolymers requires precise control over the polymerization process. In this context, RAFT polymerization has emerged as a robust and versatile technique. Various strategies have been employed for the synthesis of ABA-type copolymers by RAFT.²⁴⁷ One approach includes the conversion of α,ω -telechelic homopolymers into macro-CTA. This process usually involves a homopolymer with functionalities such as hydroxy, carboxylic acid, or thiol at the chain end and demands a high purity of the reagents. The other method relies on the sequential addition of a monomer to a monofunctional CTA. Although this method is effective, it requires three distinct reaction steps and is restricted to monomers exhibiting similar reactivity. A notable advancement in this field of synthesis of ABA-type triblock copolymers is the employment of difunctional CTAs, which allows for the synthesis of triblock copolymers in two steps (and potentially a pentablock in three steps, etc.).^{238,246,248} This approach facilitates the precise synthesis of highly symmetrical ABA block copolymers, where both arms have identical composition and length.²⁴⁹ There are two

main approaches in this methodology, each based on the specific type of difunctional CTA used: the difunctional R-group approach or the difunctional Z-group approach (Scheme 10, Table 5).^{250,251} In the R-group approach, polymer chain propagation occurs at both ends of the CTA. The process starts with the addition of monomer A, followed by monomer B. This results in the formation of a BAB triblock copolymer, characterized by having the thiocarbonylthio moiety at both ends and the R group at the center, as depicted in Scheme 10a. In contrast, the Z-group approach involves the chain propagation from the core of the CTA. Starting with monomer A and then adding monomer B results in an ABA triblock copolymer, where the thiocarbonylthio group is located at the center and the R group at each end of the polymer chain (Scheme 10b).

ABA-type triblock copolymers synthesized using RAFT have been found to be useful in a variety of applications (Table 5). Amphiphilic triblock copolymers possess the ability to self-assemble into different nanostructures, such as micelles with distinct morphologies (e.g., vesicles and ring shape).²³⁹ This makes them good candidates for drug delivery systems, where they can encapsulate drugs^{248,252} or siRNA.²⁵³ Furthermore, ABA triblock copolymers, consisting of outer hard amorphous or semicrystalline blocks (A) and an inner thermodynamically immiscible soft segment (B) that exhibits a glass transition temperature (T_g) below ambient temperature, are important in the production of high-performance thermoplastic elastomers (TPEs).



Scheme 10. Synthesis of ABA-type triblock copolymers via RAFT polymerization using difunctional CTAs: a) R-group approach, b) Z-group approach.

1.4.3.2. Thermoplastic elastomers

Thermoplastic elastomers combine the elastomeric properties of rubbers and the processability and recyclability of thermoplastics; therefore, they can be molded when heated.²⁵⁴ TPEs are typically composed of a two-phase system in which glassy domains are dispersed in a continuous rubbery phase (Figure 8).^{255–257} The choice of monomer pairs and their ratio (generally >50% elastomer)²⁵⁴ directly dictate the T_g range, which defines the operational temperature scope of thermoplastic elastomers. TPEs first emerged in the 1940s, and their utilization has been expanding in recent decades, attributed to their ability to be efficiently recycled and their functionality in a variety of applications such as adhesives, automotive components, coatings, fibers, and medical devices.^{243,258} Moreover, they are an integral part of the shift toward a renewable plastic economy, reducing dependence on petroleum-based feedstocks.²⁵⁵ The most studied and widely used are styrenic TPEs, such as polystyrene-*b*-polybutadiene-*b*-polystyrene (SBS) and polystyrene-*b*-polyisoprene-*b*-polystyrene (SIS). However, these TPEs present limitations regarding UV stability and oxidative resistance arising from unsaturated bonds in polydiene soft blocks.²⁴³ Moreover, hard block segments of polystyrene are confined by a relatively low T_g (65–90 °C), which restricts their upper service temperature.²⁵⁸

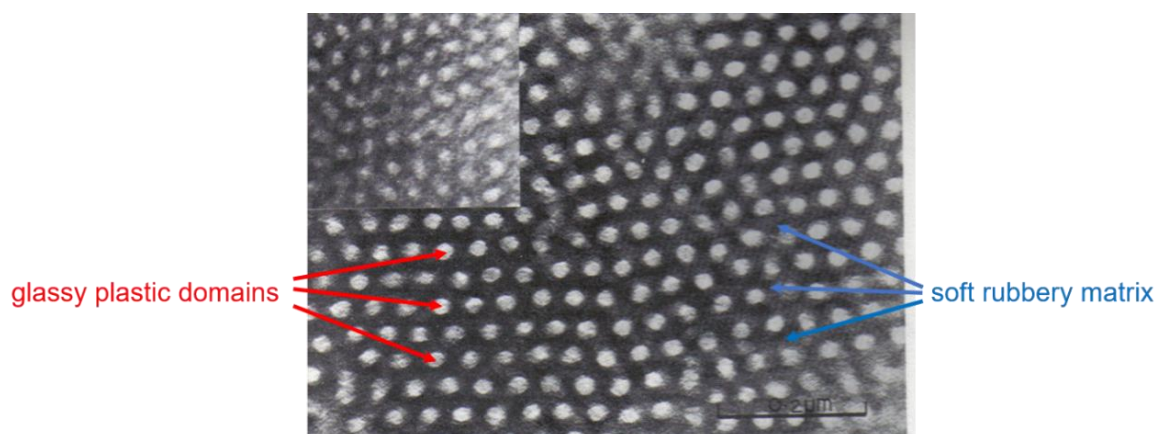


Figure 8. Structure illustration of thermoplastic elastomers.²⁵⁷

1.4.3.3. (Meth)acrylic thermoplastic elastomers

The growing interest in high-performance TPEs has driven advancements in the field, including the development of (meth)acrylic-based materials such as methacrylate–acrylate–methacrylate (hard–soft–hard) ABA copolymers (Table 5). It should be noted that all (meth)acrylic TPEs offer numerous advantages, such as optical transparency, adhesion

versatility, weatherability, oil resistance, printability, compatibility with fillers, abrasion resistance, and low viscosity.^{243,259}

Acrylates and methacrylates differ significantly in their radical formation during propagation. Acrylates form secondary radicals, while methacrylates produce more stable tertiary radicals.^{260,261} This stability of tertiary radicals reduces the reactivity of the propagating end, leading to slower polymerization compared to acrylates.^{260,261} Additionally, methacrylates exhibit greater steric hindrance, further slowing polymerization.²⁶² Monomers known for producing stabilized tertiary propagating radicals with enhanced steric stabilization, and therefore better leaving group ability, should be polymerized prior to those yielding stabilized secondary radicals.²⁵¹ Consequently, the synthesis of methacrylate–acrylate–methacrylate triblock copolymers requires a difunctional CTA agent that will allow the creation of the outer polymethacrylate segments first, followed by the soft central block that links the two hard domains (Z-group approach). The simplest examples of difunctional CTAs as precursors of ABA-type block copolymers operating by the Z-group approach are symmetrical trithiocarbonates (TTCs) (Figure 1).²⁴⁹ However, a significant challenge in synthesizing methacrylate–acrylate–methacrylate ABA triblock copolymers was the moderate reactivity of accessible symmetrical TTCs for polymerization of methacrylates. For example, one of the most frequently reported symmetrical TTCs, *S,S'*-bis(α,α' -dimethylacetic acid)trithiocarbonate (BDAT) (Table 5, entry 5–10), resulted in relatively high dispersities ($D = 1.4–1.7$) during the polymerization of methacrylates.^{263,264} In the case of terpene methacrylates, polymerization yielded polymers with higher than expected molar masses and relatively high dispersities ($D = 1.5–1.8$).²⁶⁵ Also, the commercially available *S,S*-dibenzyl trithiocarbonate (DBTTC) (Table 5, entries 3–4) is unsuitable for methacrylate polymerization due to insufficient radical stabilization of the leaving groups.^{265,266} To overcome these challenges, Destarac and coworkers developed the synthesis of a new symmetrical RAFT agent, bis-(2-methylpropanenitrile)trithiocarbonate (TTC-bCP) (Table 5, entry 11).²⁴⁶ The tertiary leaving groups (2-cyanopropan-2-yl) in this CTA provide an optimal fragmentation rate for methacrylates polymerization (Scheme 6). As a result, TTC-bCP allowed the successful synthesis of polymethacrylate blocks with controlled molar masses ($M_n \sim 40 \text{ kg mol}^{-1}$) and narrow molar mass distributions ($D < 1.09$), as well as ABA triblock copolymers with a high molar mass ($M_n = 135 \text{ kg mol}^{-1}$) and remarkably low dispersity ($D = 1.04$). These findings open new perspectives in the synthesis of methacrylate–acrylate–methacrylate ABA copolymers.

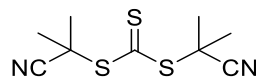
From the point of view of TPEs, the synthesis of high molar mass (HMM) polymers is very attractive, as mechanical and thermal properties are generally improved with increasing molar mass, which enhances intermolecular forces and chain entanglement density.^{267–269} As mentioned earlier in the literature review, a significant drawback of RDRP polymerization is the difficulty in synthesizing HMM polymers with molar mass (M_n) higher than 100 kg mol^{-1} . These difficulties arise due to the occurrence of unavoidable termination reactions, which lead to the formation of dead polymers and consequently to a widening of the molar mass distribution ($D > 1.5$). However, this challenge was overcome by maximizing the rate of propagation (k_p) relative to termination (k_t).⁹⁹ Several approaches achieved this effect, for example, by implementing heterogeneous reaction conditions^{270,271} or high pressure^{272,273}. An alternative approach is the use of photoiniferter polymerization (PI).^{23,98,99} This method eliminates the need for traditional low molar mass radical initiators, which reduces termination events and enables the synthesis of HMM polymers under homogeneous conditions. Moreover, PI polymerization has additional benefits, such as the ability to proceed at room temperature and pressure and to maintain high monomer concentrations, further helping to minimize termination events.²³

In this context, part of this doctoral thesis concerns the preparation of (meth)acrylic ABA triblock copolymers. The synthesis of already known homopolymers (*n*BA and MMA) and their ABA triblock copolymer of high molar mass using the PI-RAFT polymerization will be discussed in Chapter 5 of this dissertation.

Table 5. Characteristics and applications of ABA-type triblock copolymers.

Lp.	Polymer	CTA	Properties	Application	Ref.
R-group approach					
1.	PMOS- <i>b</i> -PIBVE- <i>b</i> -PMOS		-thermal stability up to ~345 °C -superior strength, elongation, and recovery	thermoplastic elastomers	274
2.	PDHF- <i>b</i> -PIBVE- <i>b</i> -PDHF				
Z-group approach					
3.	PS- <i>b</i> -PEHA- <i>b</i> -PS		-good thermal stability -viscoelastic properties of copolymers influenced by their composition and thermal treatment	thermoreponsive materials	275
4.	PS- <i>b</i> -PMY- <i>b</i> -PS		-good tensile properties -recyclable and reusable	thermoplastic elastomers	276
5.	PAAm- <i>b</i> -PNIPAAm- <i>b</i> -PAAm		-thermoreponsiveness -the creation of nanocomposite materials with tunable optical properties	devices for temperature monitoring	238
6.	PMA- <i>b</i> -PnBA- <i>b</i> -PMA		-good tensile properties and adhesive behavior, comparable to commercial pressure-sensitive adhesives	pressure-sensitive adhesives/thermoplastic elastomers	265
7.	PHPMA- <i>b</i> -PS- <i>b</i> -PHPMA		-tendency to self-assemble -copolymer-based nanoparticles decrease the <i>n</i> -hexane/water interfacial tension	emulsifiers	277
8.	PDMAAm- <i>b</i> -PDAAAm- <i>b</i> -PDMAAm		-thermoreponsiveness -tendency to self-assemble, sphere-to-worm micellar transition at the LCST point	drug delivery	252
9.	PNIPAAm- <i>b</i> -PODA- <i>b</i> -PNIPAAm		-thermoreponsiveness -tendency to self-assemble into highly stable micelles	drug delivery	248
10.	PtBA- <i>b</i> -PTFEA- <i>b</i> -PtBA		-tendency to self-assemble	hydrophobic materials	278

11.

PMMA-*b*-P*n*BA-*b*-PMMA-behaved as an elastomer up to
temperatures of 110–120 °C

thermoplastic elastomers 246

Abbreviations: PAAm, polyacrylamide; PDAAAm, poly(diacetone acrylamide); PDHF, poly(2,3-dihydrofuran); PDMAAm, poly(*N,N*-dimethylacrylamide); PEHA, poly(2-ethylhexyl acrylate); PHPMA, poly(2-hydroxypropyl methacrylate); PIBVE, poly(isobutyl vinyl ether); PMA, poly(α -pinene methacrylate); PMMA, poly(methyl methacrylate); PMOS, poly(*p*-methoxystyrene); PMY, poly(β -myrcene), PNIPAAm, poly(*N*-isopropylacrylamide); PODA, poly(*n*-octadecylacrylate); P*n*BA, poly(*n*-butyl acrylate), PS, polystyrene; P*t*BA, poly(*tert*-butylacrylate); PTFEA, poly(2,2,2-trifluoroethyl acrylate).

Summary

Reversible deactivation radical polymerization (RDRP) involves a spectrum of robust methods for the synthesis of well-defined polymers. Among these, reversible addition-fragmentation chain transfer (RAFT) polymerization stands out as one of the most versatile. RAFT polymerization operates based on a mechanism involving the reversible addition-fragmentation transfer of chain transfer agents (CTAs), which can be classified as dithioesters, trithiocarbonates, dithiocarbamates, or dithiocarbonates. Notably, this method facilitates the production of polymers from numerous monomer types in organic solvents or water under moderate pressure and temperature conditions. A distinguishing feature of RAFT polymerization is its high tolerance to various functional groups. Furthermore, it offers end-groups that can be profitably transformed into various functionalities (such as thiols) that may be helpful for further modifications (e.g., the attachment of fluorescent moieties). RAFT allows for precise control over molar mass and polymer architecture, making it ideal for creating complex structures such as block, star, and graft copolymers, which have wide-ranging applications from drug delivery to materials science. Innovations in RAFT, including photoinduced RAFT polymerization, have expanded its applicability, offering advantages such as mild reaction conditions and eco-friendliness.

Despite the significant advancements in RAFT polymerization, this method still encounters challenges. Through a literature review, three key areas have been identified where further research and development are critical.

1. While diglycerides show promise in drug delivery systems because of their integral role in cellular homeostasis and membrane interaction, there is a notable gap in the literature regarding thermoresponsive diglyceride-based polymers synthesized through RAFT polymerization.
2. While RAFT polymerization of cyclic *N*-vinylamides is well-documented, precise control over the polymerization of noncyclic *N*-vinylamides such as *N*-vinylformamide remains a challenge.
3. While RAFT polymerization is effective for synthesizing ABA-type triblock copolymers, it still faces challenges in the synthesis of (meth)acrylic-based copolymers.

RESEARCH OBJECTIVES

The overall goal of this dissertation is to exploit the diverse strategies of reversible addition-fragmentation chain transfer (RAFT) polymerization to prepare polymers with desired properties and architecture.

The general objectives of this research are:

- **Developing thermoresponsive drug delivery systems based on diglycerides.**
- **Exploring the polymerization of *N*-vinylformamide employing the PI-RAFT technique.**
- **Investigating the synthesis of high molar mass (meth)acrylic ABA triblock copolymers employing the PI-RAFT technique.**

The specific objectives of this research are:

PART I. Developing thermoresponsive drug delivery systems based on diglycerides.

1. Formation of thermoresponsive polymers with diglyceride moieties using the RAFT technique:
 - Synthesis of chain transfer agents with diglyceride moieties.
 - Synthesis of monomers with diglyceride moieties.
 - Synthesis of various thermoresponsive polymers via the RAFT polymerization.
2. Formation of polymeric nanoparticles and encapsulation of biologically active compounds in selected thermoresponsive materials.
3. Physicochemical characterization of polymers and polymeric nanoparticles: NMR, ATR-FTIR, TEM, TGA, UV-Vis, ELS, DLS, and SEC.
4. Biological studies of selected stimuli-responsive polymeric nanoparticles and their conjugates with biologically active compounds.
5. Development of models of dependence of nanocarrier properties, such as thermoresponsiveness and biological properties on their structure.

PART II. Exploring the polymerization of *N*-vinylformamide employing the PI-RAFT technique.

1. In-depth examination of polymerization and influencing variables, e.g., light wavelength, light intensity, and presence of light.
2. Investigation of polymerization control at different targeted molar masses of PNVF.

3. Validating the presence of dithiocarbonate end-groups, affirming the "living" nature of the polymer.
4. Synthesis of block copolymers incorporating PNVF segments.
5. Selective hydrolysis of the PNVF block of the copolymer into the corresponding polyvinylamine.
6. Physicochemical characterization of the obtained polymers: NMR, SEC, and A4F.

PART III. Investigating the synthesis of high molar mass (meth)acrylic ABA triblock copolymers employing the PI-RAFT technique.

1. Optimization of PI-RAFT polymerization conditions (light wavelength, monomer concentration, and light intensity) on the polymerization of MMA and *n*BA using the PI-RAFT.
2. Establishing a methodology for synthesizing high molar mass ABA triblock copolymers.
3. Physicochemical characterization of the obtained polymers: NMR and SEC.

RESEARCH HYPOTHESES

PART I. Developing thermoresponsive drug delivery systems based on diglycerides.

1. The application of chain transfer agents and monomers derived from diglycerides in RAFT polymerization will yield well-defined polymers containing one or more diglyceride molecules in their structure.
2. The synthesized thermoresponsive polymers will form polymeric nanoparticles (PNPs) with desired physicochemical properties, including stability, size uniformity, and thermoresponsive behavior.
3. The type of diglyceride (derived from palmitic or oleic acid) and the thermoresponsive block (PNIPAAm or PNVCL) will influence the physicochemical and biological properties of PNPs.
4. The nanoparticles prepared from thermoresponsive polymers with diglyceride moieties will be able to encapsulate biologically active compounds, such as the anticancer drugs doxorubicin and tamoxifen.
5. The thermoresponsive properties of PNPs, achieved through the incorporation of the PNIPAAm or PNVCL segments, will enable controlled drug release in response to temperature changes.
6. The structure and composition of PNPs will influence the encapsulation efficiency and release profile of drugs.
7. Incorporating diglyceride moieties into polymeric nanoparticles will enhance their biocompatibility and interaction with cell membranes, potentially improving the efficiency of drug delivery systems.
8. PNPs loaded with anticancer drugs will exhibit cytotoxic effects against breast cancer cell lines while maintaining compatibility with normal cells.
9. The insertion of fluorescent dye into polymers/nanoparticles will enable their tracing within biological systems.

PART II. Exploring the polymerization of *N*-vinylformamide employing the PI-RAFT polymerization.

1. The utilization of purple light-emitting diodes (LEDs) will enable NVF polymerization, yielding polymers with predetermined molar masses and low molar mass distributions.

2. The exclusion of dithiocarbonate as a RAFT agent or lack of purple light will prevent NVF polymerization.
3. Polymers derived by the PI-RAFT method will possess dithiocarbonate end-groups, corroborating their "living" nature.
4. The synthesis of block copolymers with PNVF segments via PI-RAFT polymerization, using PEG and PVP as macro-CTAs, will proceed in a controlled manner.
5. Hydrolysis of PNVF segments will result in conversion to corresponding PVAm, underpinning future advancements and explorations of the potential applications of the synthesized polymer.

PART III. Investigating the synthesis of high molar mass (meth)acrylic ABA triblock copolymers employing the PI-RAFT technique.

1. The use of the novel RAFT agent TTC-bCP in PI-RAFT polymerization will enhance the synthesis and control of MMA, *n*BA, and their ABA triblock copolymers.
2. The polymerization conditions will significantly influence the control of MMA and *n*BA polymerization.
3. Optimized light conditions will enable the synthesis of ABA triblock copolymers with a well-defined high molar mass and low dispersity.

RESULTS AND DISCUSSION

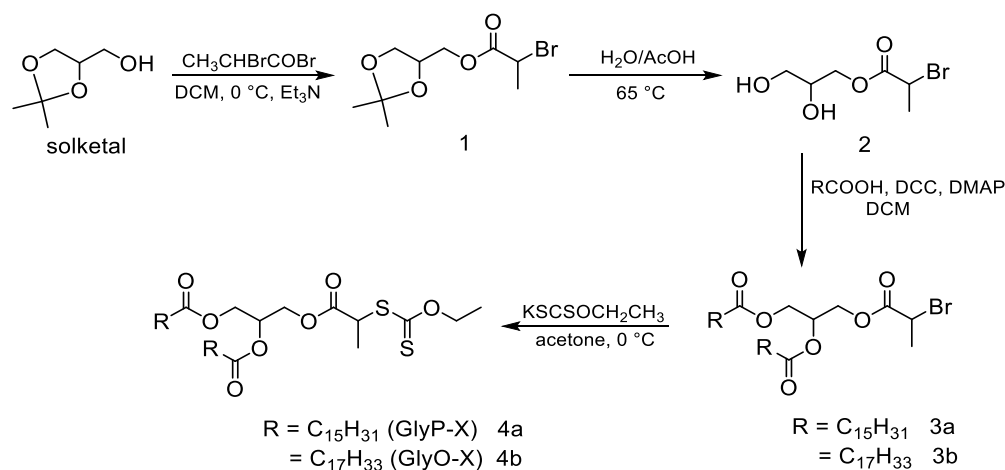
CHAPTER 2. DIGLYCERIDES BASED POLYMERS

2.1. Synthesis of diglyceride-based chain transfer agents (CTAs) and monomers

This section of the work aimed to synthesize chain transfer agents and monomers based on diglycerides for use in RAFT polymerization to obtain novel drug carriers. The diglycerides chosen for this study were of two types: saturated, containing palmitic acid, and unsaturated, based on oleic acid. The original diglyceride-based CTAs and monomers were synthesized via multistep synthetic pathways. As starting material, commercially available and inexpensive solketal (2,2-dimethyl-1,3-dioxolane-4-methanol) was used.

2.1.1. Synthesis and characterization of diglyceride-based dithiocarbonate RAFT agents

The diglyceride-based CTAs were synthesized via a four-step synthetic pathway (Scheme 11). The initial step involved the reaction of the hydroxyl group of solketal with 2-bromopropionyl bromide in anhydrous dichloromethane (DCM). This was followed by the conversion of dioxolane **1** into diol **2** through simple hydrolysis with aqueous acetic acid (AcOH) at 65 °C. Esters (**3a** and **3b**) were then synthesized through Steglich esterification utilizing palmitic or oleic acid, respectively, in the presence of dimethylaminopyridine (DMAP) as a catalyst and dicyclohexylcarbodiimide (DCC) as a coupling agent.²⁷⁹ Finally, the original dithiocarbonate chain transfer agents, GlyP-X (**4a**) and GlyO-X (**4b**) were obtained by a well-established nucleophilic substitution of bromine with *O*-potassium ethylcarbonate in acetone. The use of readily available starting materials and mild reaction conditions allowed for the successful preparation of these CTAs on a gram scale. The final products (GlyP-X and GlyO-X) were obtained as yellowish solids in the case of the palmitic acid derivative and yellow oil in the case of the oleic acid derivative. After each reaction step, the products were purified by medium pressure liquid chromatography (MPLC) and analyzed by nuclear magnetic resonance (¹H NMR, ¹³C NMR) and attenuated total reflectance Fourier transform infrared spectroscopy (ATR-FTIR). The final products (GlyP-X and GlyO-X) were also characterized by mass spectrometry (MS), thermogravimetric analysis (TGA), and differential scanning calorimetry (DSC).



Scheme 11. Synthesis of chain transfer agents.

The structure of the products after each step of the reaction was confirmed by NMR spectroscopy. The comparison of NMR spectra for the GlyP-X and GlyO-X synthesis pathways is shown in Figures 9 and 10, respectively. After the reaction with 2-bromopropionyl bromide, the ^1H NMR spectrum of compound **1** showed signals at 1.8 and 4.3 ppm, corresponding to the CH_3 and CH_3CHBr groups, respectively. In addition, the ^{13}C NMR spectrum of compound **1** displayed a new signal at 170 ppm, attributed to the carbonyl group. Successful deprotection of the hydroxyl group in compound **2** was verified by the presence of a broad signal at 3.1 ppm in the ^1H NMR, which corresponded to the $-\text{OH}$ groups, and the absence of the signal in the ^{13}C NMR spectrum at 110 ppm attributed to the quaternary carbon atom. After esterification, characteristic resonance signals from the diglyceride segment appeared. The ^1H NMR spectra of compounds **3a** and **3b** revealed the triplet of the end of the fatty acid tails at 0.9 ppm and the signals from the methylene groups at 1.3 ppm, 1.4 ppm, and 2.6 ppm. In addition, the ^{13}C NMR spectra showed new signals from carbonyl atoms at ~ 175 ppm, methylene groups in the range of 20–35 ppm, and methyl groups at 14 ppm. The ^1H NMR spectra of diglyceride-based CTAs (**4a**, **4b**) possessed signals at 4.5–4.7 ppm and 1.6 ppm ascribed to the methylene and methyl protons of the *O*-ethyl dithiocarbonate moiety. In turn, the ^{13}C NMR spectra exhibited a characteristic signal from the $\text{C}=\text{S}$ group at 212 ppm. Observations of the synthetic routes of two chain transfer agents were similar. However, the presence of unsaturated bonds in the oleic moieties in compounds **3b** and **4b** led to the appearance of additional signals at 2.1 and 5.3 ppm in the ^1H NMR spectra and a signal at 130 ppm in the ^{13}C NMR spectra.^{280,281}

ATR-FTIR additionally confirmed the structure of the products. The comparison of ATR-FTIR spectra for the GlyP-X and GlyO-X synthesis pathways is shown in Figure 11. The total disappearance of the solketal peak corresponding to the –OH stretching vibrations in the 3400–3600 cm^{-1} range was observed in the ATR-FTIR spectrum of compound **1** after the reaction with 2-bromopropionyl bromide. Furthermore, the other characteristic peaks appeared at 1740 cm^{-1} and 1330 cm^{-1} , which can be correlated with the C=O and C–Br vibrations. Acidic hydrolysis led to the appearance of a broad peak in spectrum **2** at 3350 cm^{-1} ascribed to the free hydroxyl groups. After esterification with fatty acids, additional peaks appeared in the **3a** and **3b** spectra. The bands at 2954–2850 cm^{-1} and 1460 cm^{-1} , corresponding to the C–H stretching and deformation vibrations, respectively, were observed. The presence of the dithiocarbonate group in the final products GlyP-X (**4a**) and GlyO-X (**4b**) was confirmed by the presence of two additional characteristic peaks of the *O*-ethyl dithiocarbonate group at $\sim 1220 \text{ cm}^{-1}$ and 1050 cm^{-1} . As expected, the ATR-FTIR spectra of the two synthetic paths were similar. The main difference was that the additional absorption band at 3006 cm^{-1} visible in the spectra of **3b** and **4b** ascribed to a double bond in the oleate moiety.

The thermal stability and decomposition behavior of the diglyceride-based CTAs, GlyP-X and GlyO-X, were evaluated using thermogravimetric analysis. As depicted in Figure 12, the results showed that both CTAs underwent decomposition in two distinct stages. The first stage, between 250 and 300 $^{\circ}\text{C}$, was attributed to the decomposition of dithiocarbonate groups, as evidenced by a weight loss consistent with the calculated mass loss of the dithiocarbonate moiety alone (13–14%). The second stage, with a maximum decomposition rate of approximately 410 $^{\circ}\text{C}$, corresponded to the decomposition of diglyceride groups.²⁸² To investigate the thermal properties of GlyP-X and GlyO-X further, differential scanning calorimetry measurements were conducted. The results revealed differences in their thermal and structural characteristics. In the case of GlyP-X, an endothermic melting peak was observed during the heating step, and an exothermic crystallization peak was observed during the cooling step, as shown in Figure 13.

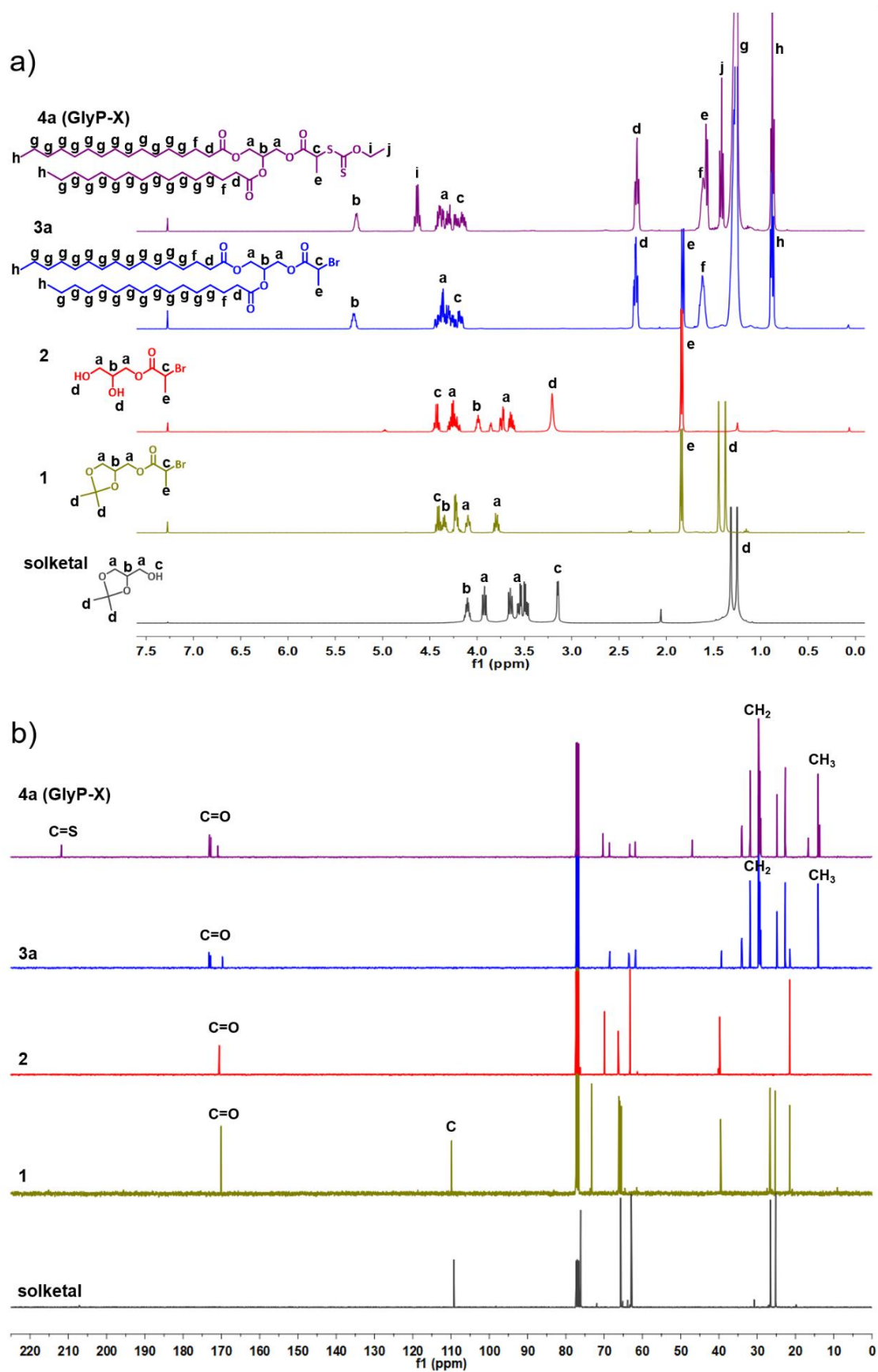


Figure 9. Comparison of a) ^1H NMR spectra (400 MHz, CDCl_3) and b) ^{13}C NMR spectra (100 MHz, CDCl_3) for the synthetic route of RAFT agent with palmitic acid derivative (GlyP-X).

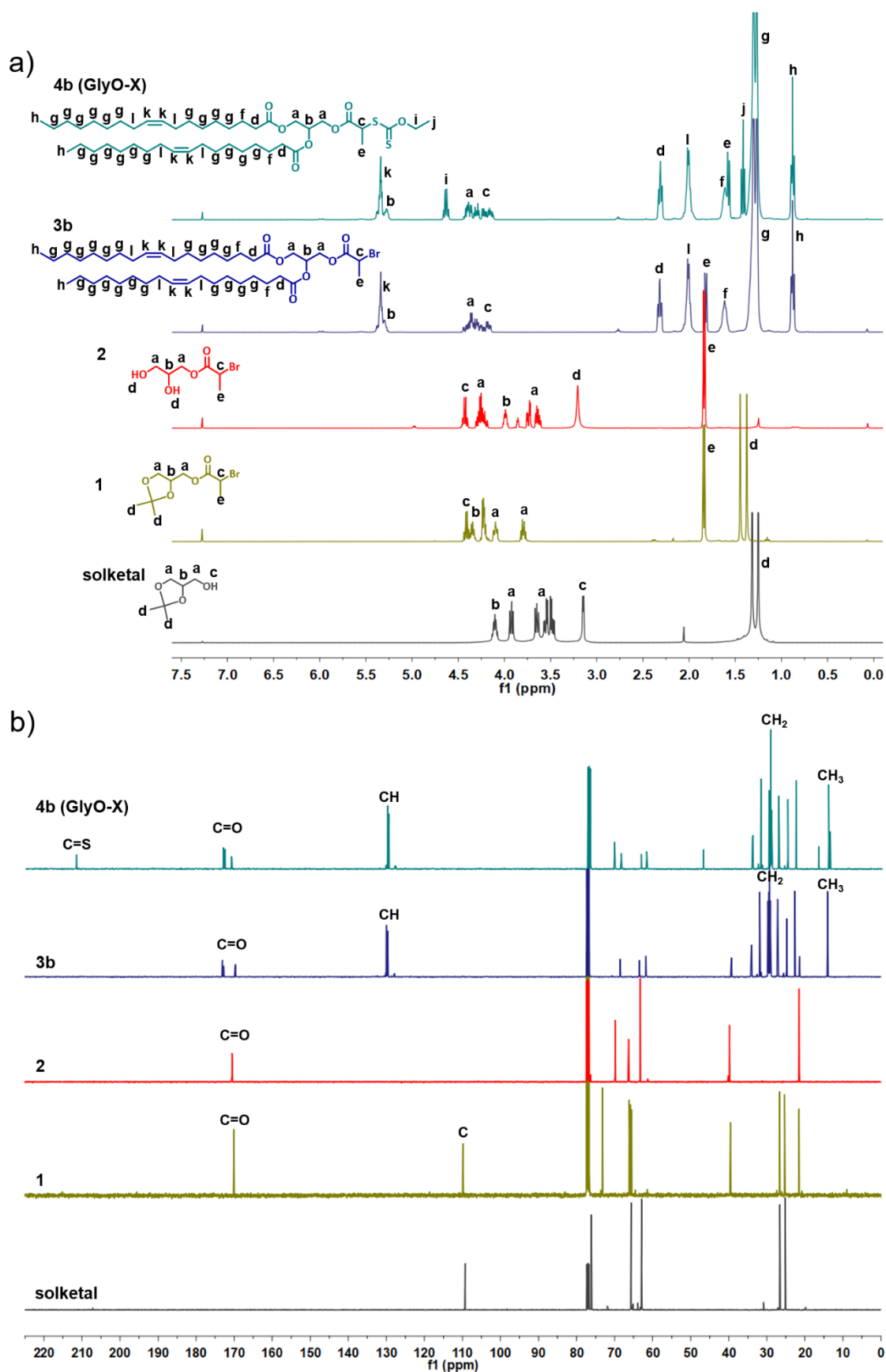


Figure 10. Comparison of the a) ^1H NMR spectra (400 MHz, CDCl_3) and b) ^{13}C NMR spectra (100 MHz, CDCl_3) for the synthetic route of RAFT agent with oleic acid derivative (GlyO-X).

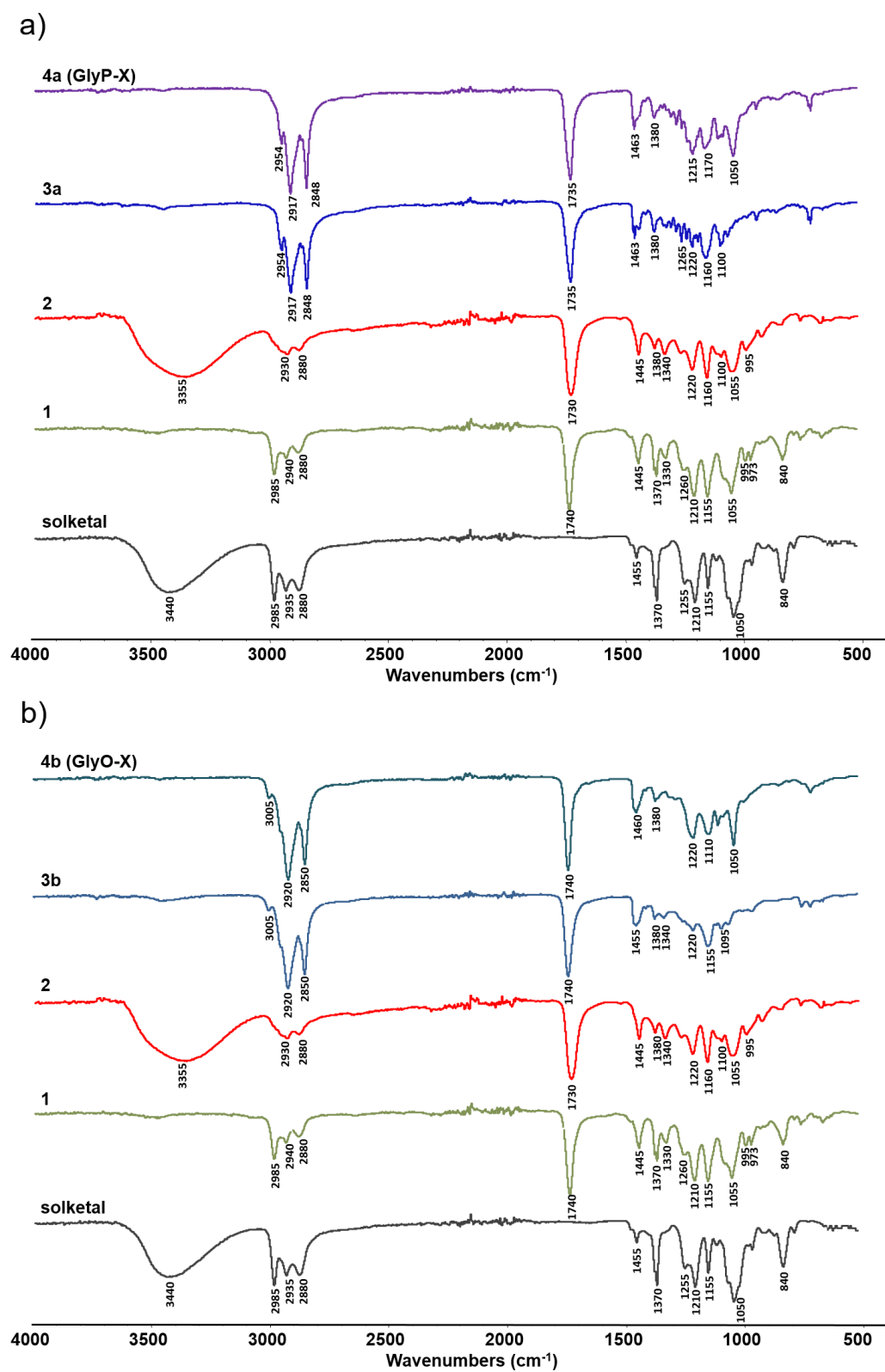


Figure 11. Comparison of ATR-FTIR spectra for the synthetic routes of RAFT agents with a) palmitic acid derivative (GlyP-X) and b) oleic acid derivative (GlyO-X).

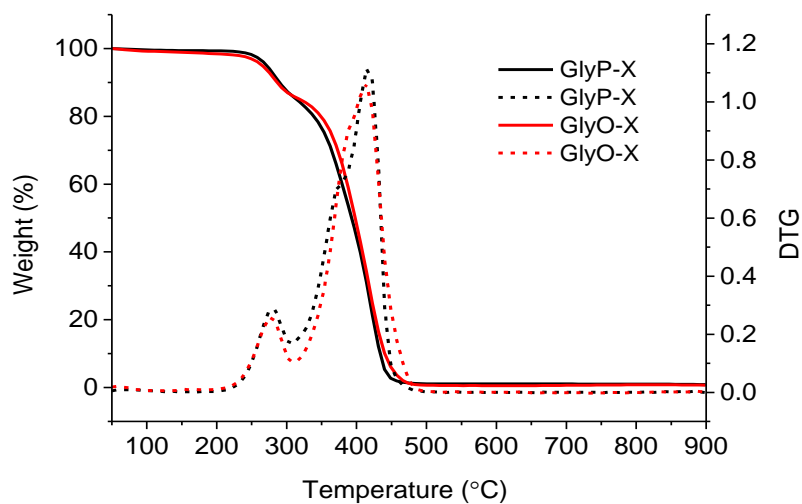


Figure 12. TG and DTG curves of synthesized RAFT agents: GlyP-X and GlyO-X.

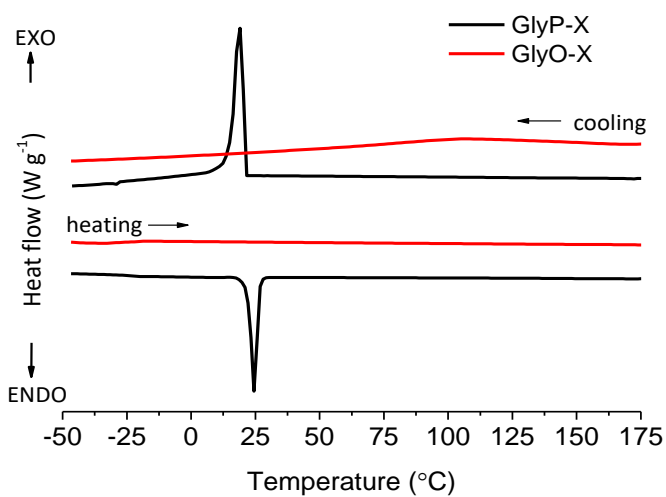
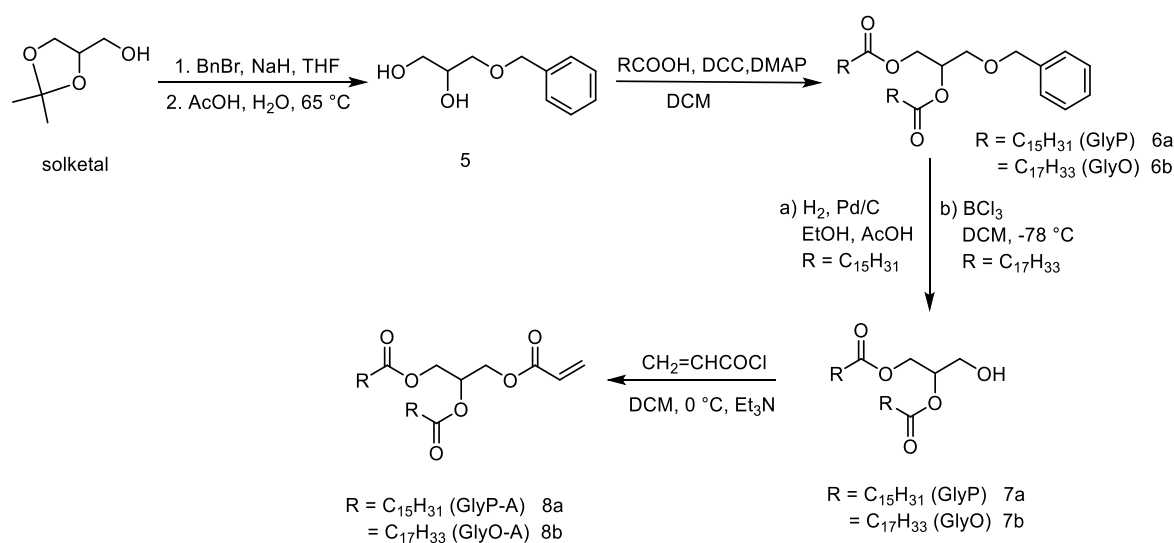


Figure 13. DSC curves of chain transfer agents: GlyP-X (black trace) and GlyO-X (red trace).

2.1.2. Synthesis and characterization of diglyceride-based monomers

Diglyceride-based monomers were synthesized through a four-step synthetic pathway, as outlined in Scheme 12. The initial step involved the protection of the hydroxyl group of solketal with benzyl bromide in THF. Subsequently, dioxolane was converted to diol **5** by hydrolysis with aqueous acetic acid at 65 °C. Next, esters **6a** and **6b**, containing either palmitic or oleic acid, were prepared through Steglich esterification under mild conditions.¹⁸ The benzyl group of the palmitic acid derivative was then deprotected by hydrogenation to produce alcohol **7a**. In turn, due to the presence of unsaturated bonds in oleic acid, which would become saturated in the hydrogenation process, the hydroxyl function of the oleic acid derivative was obtained using BCl_3 in DCM at -78 °C.^{19,20} This method did not induce any side reactions in double bonds of oleate moieties, which confirms the effectiveness of the synthetic procedure. The final step involved the reaction of compounds **7a** and **7b** with acryloyl chloride at 0 °C, forming original diglyceride-based monomers, GlyP-A (**8a**) and GlyO-A (**8b**). The palmitic acid derivative was obtained as a white solid (GlyP-A), while the oleic acid derivative was obtained as a yellowish oil (GlyO-A).



Scheme 12. Synthesis of diglyceride-based monomers.

The products were characterized by nuclear magnetic resonance (^1H NMR, ^{13}C NMR) and attenuated total reflectance Fourier transform infrared spectroscopy (ATR-FTIR) at each step of the synthesis. In addition, the final products were also analyzed by mass spectrometry (MS).

The structure of the products after each reaction was confirmed by NMR spectroscopy. A comparison of the NMR spectra for the synthesis of GlyP-A and GlyO-A is shown in

Figures 14 and 15, respectively. In the ^1H NMR spectrum from compound **5**, signals of the benzyl group were observed at 7.2–7.5 ppm and 4.5 ppm. Additionally, the ^{13}C NMR spectrum possessed peaks from the benzyl group at 137.6, 128.4, and 127.7 ppm. After esterification, characteristic signals of the fatty acid segment appeared. The ^1H NMR spectra of compounds **6a** and **6b** showed the triplet attributed to the end of the fatty acid tails at 0.9 ppm, the broad peak of the methylene groups at 1.3 ppm, and the signals at 1.6 and 2.6 ppm. The ^{13}C NMR spectra exhibited signals from carbonyl atoms at ~ 175 ppm, methylene groups in the range of 20–35 ppm, and methyl groups at 14 ppm. The disappearance of a peak at 7.2–7.5 ppm in ^1H NMR, along with the signals in the ^{13}C NMR spectra at 137.6, 128.4, and 127.7 ppm of compounds **7a** and **7b**, confirmed a successful deprotection of the hydroxyl group. The ^1H NMR spectra of the final monomers GlyP-A (**8a**) and GlyO-A (**8b**) exhibited characteristic signals of vinyl protons ranging from 5.8 to 6.5 ppm. Also, the ^{13}C NMR spectra showed signals from the carbonyl in the acrylate group at 165.5 ppm and signals at 131.5 and 127.7 ppm correlated to the acrylate double bond. The NMR spectra for both synthetic paths showed high similarity. However, for compounds **6b**, **7b**, and **8b**, signals attributed to a double bond in the oleate moiety were observed. In the ^1H NMR spectra, additional peaks at 2.1 ppm and 5.3 ppm and a signal at 130 ppm in the ^{13}C NMR spectra were present.^{281,283}

The synthesized compounds were also characterized by ATR-FTIR spectroscopy (Figure 16). The spectrum of compound **5** exhibited a broad peak at 3350 cm^{-1} , indicating the presence of free hydroxyl groups. The esterification with fatty acids led to the appearance of additional peaks in the spectra of compounds **6a** and **6b**, including bands at $2915\text{--}2850\text{ cm}^{-1}$ and 1400 cm^{-1} , which correspond to C–H stretching and deforming vibrations, respectively. The other characteristic peaks appeared at 1740 cm^{-1} and 1720 cm^{-1} , which can be correlated with the C=O stretching of the ester bonds. After hydrolysis, the ATR-FTIR spectra of compounds **7a** and **7b** exhibited a peak at 3550 cm^{-1} , which indicated the presence of free hydroxyl groups. The ATR-FTIR spectra of monomers **8a** and **8b** showed a peak at 1635 cm^{-1} , which is characteristic of the terminal acrylate double bonds. The ATR-FTIR spectra for the two synthetic paths were nearly identical. However, the spectra of compounds **6b**, **7b**, and **8b** possessed an additional absorption band at 3004 cm^{-1} , which corresponds to C–H stretching vibrations of unsaturated --HC=CH-- bonds in the oleic moieties.

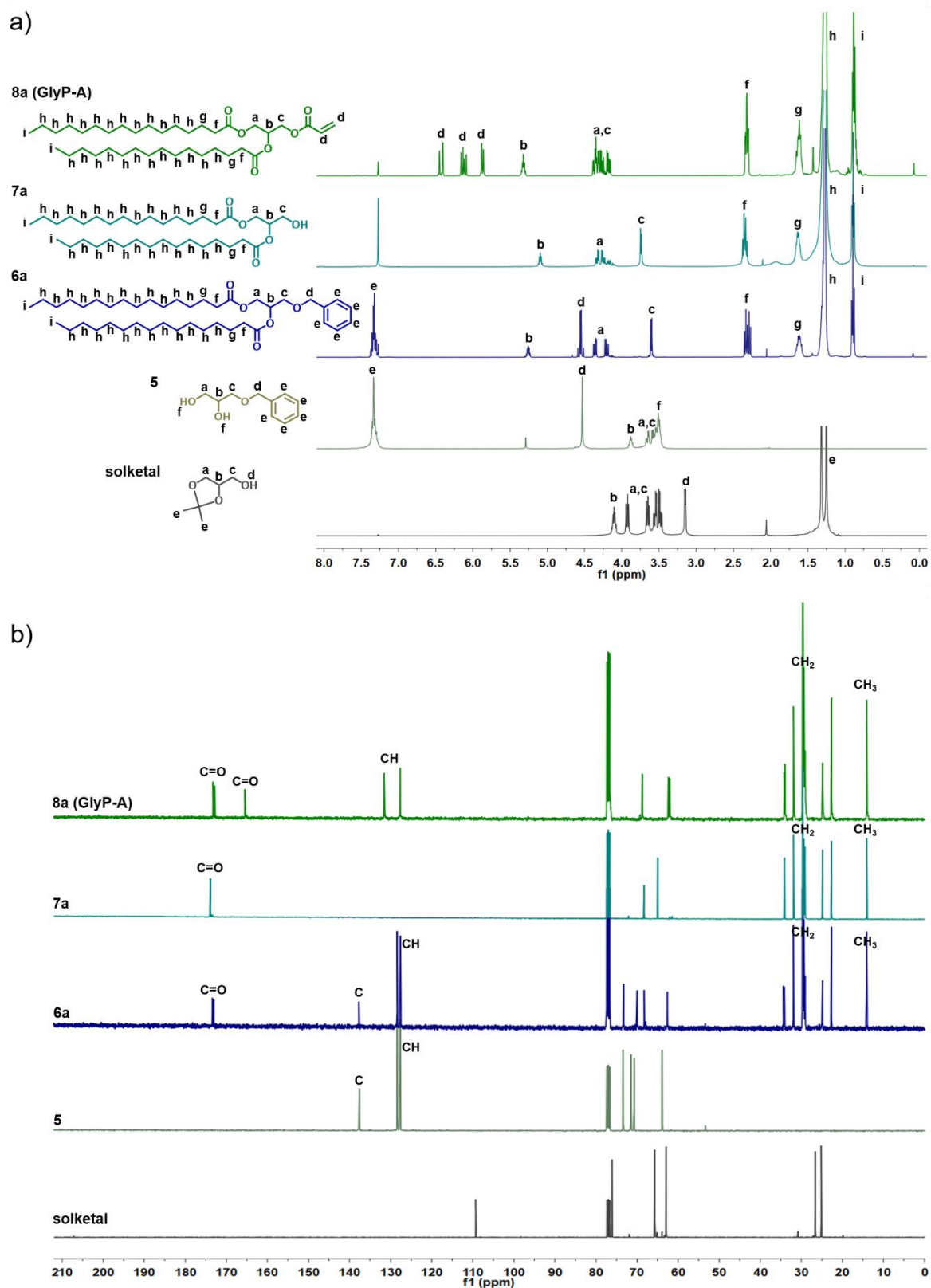


Figure 14. Comparison of the a) ^1H NMR spectra (400 MHz, CDCl_3) and b) ^{13}C NMR spectra (100 MHz, CDCl_3) for the synthetic route of monomer with palmitic acid derivative (GlyP-A).

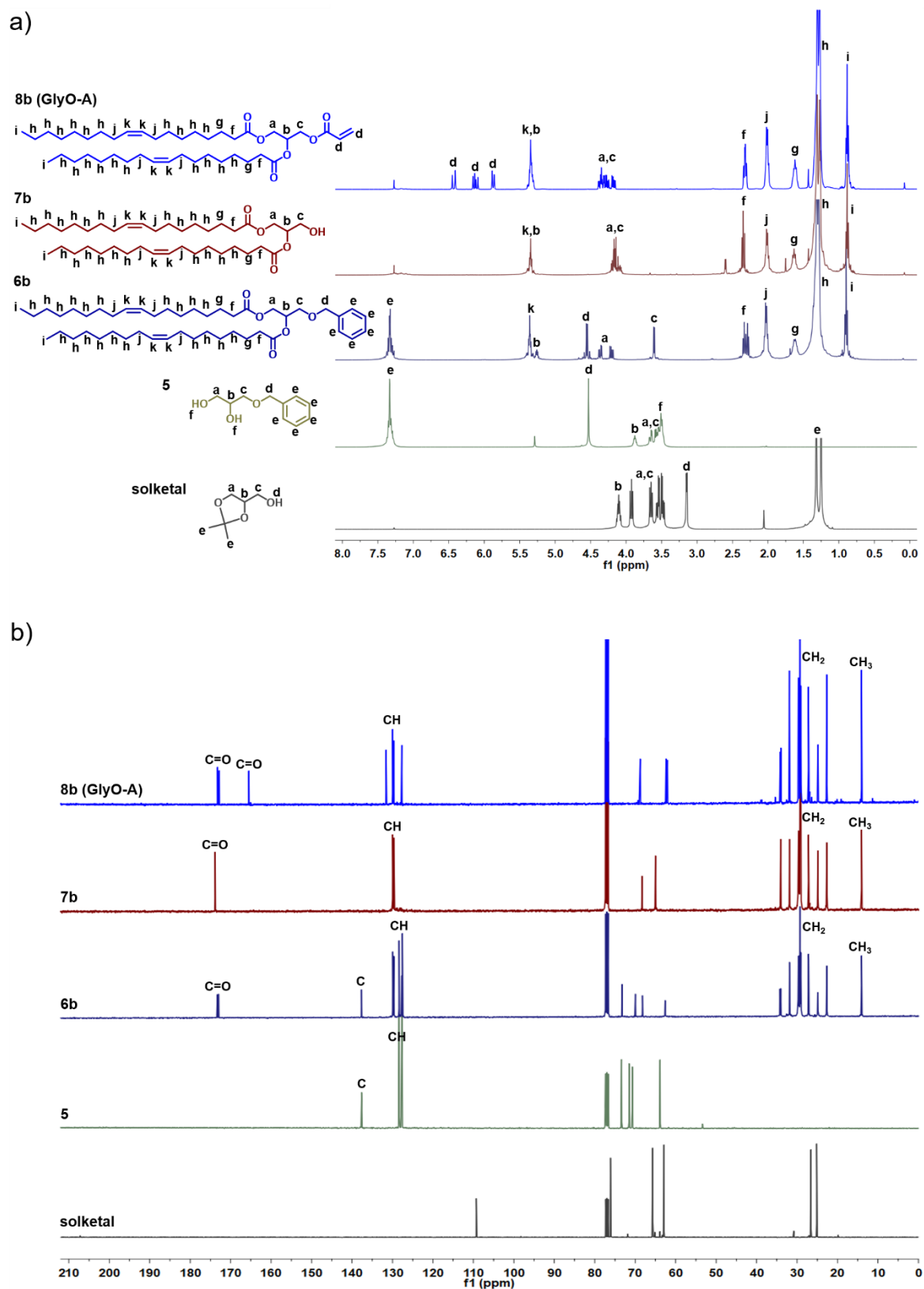


Figure 15. Comparison of the a) ^1H NMR spectra (400 MHz, CDCl_3) and b) ^{13}C NMR spectra (100 MHz, CDCl_3) for the synthetic route of monomer with oleic acid derivative (GlyO-A).

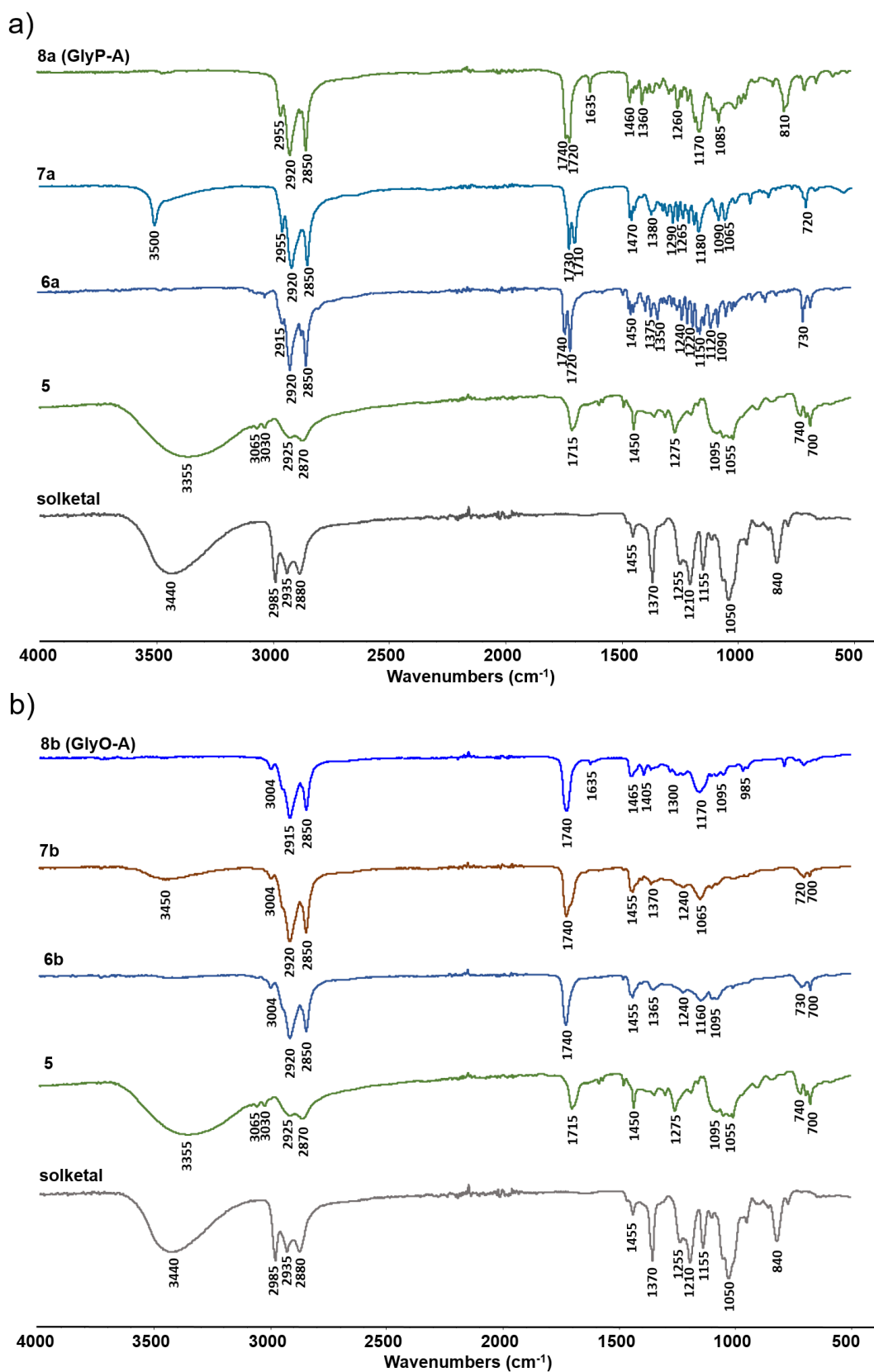


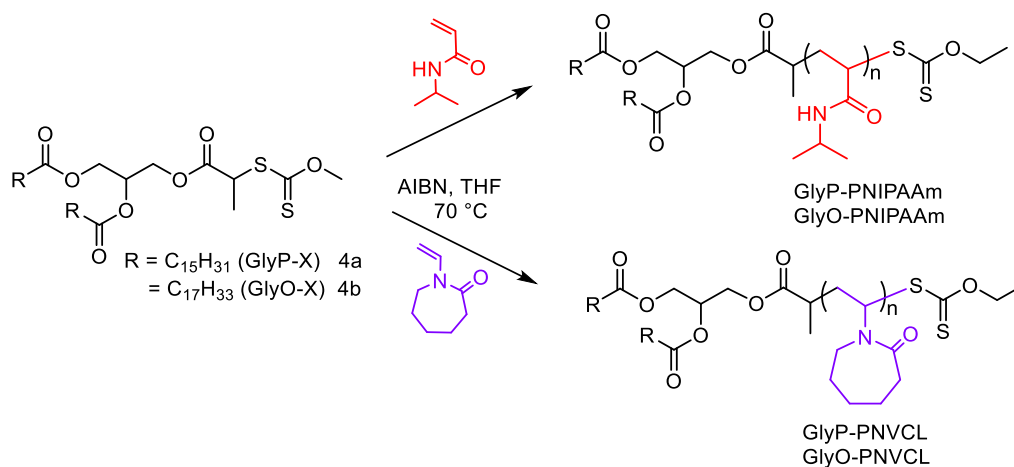
Figure 16. Comparison of ATR-FTIR spectra for the synthetic routes of monomers with a) palmitic acid derivative (GlyP-A) and b) oleic acid derivative (GlyO-A).

2.2. Synthesis and characterization of thermoresponsive polymers with diglyceride moieties

This part of the work aimed to obtain new classes of thermoresponsive lipid-polymer conjugates containing one or more diglyceride molecules in the polymeric structure. For this purpose, chain transfer agents (CTAs) and monomers derived from diglycerides containing palmitic or oleic acid moieties, synthesized in the previous section of this work, were applied in RAFT polymerization. The polymers were designed to be amphiphilic and thermoresponsive by incorporating water-soluble segments based on poly(*N*-vinylcaprolactam) (PNVCL) or poly(*N*-isopropylacrylamide) (PNIPAAm).

2.2.1. Synthesis and characterization of thermoresponsive polymers with diglyceride-based chain transfer agents

At first, *N*-isopropylacrylamide (NIPAAm) and *N*-vinylcaprolactam (NVCL) were polymerized in the presence of diglyceride-based chain transfer agents, GlyP-X and GlyO-X (Scheme 13). Detailed experimental conditions for all polymerizations are presented in Table 6. The block lengths of the polymers were varied by adjusting the molar ratio of CTA to the monomer. Polymerizations were carried out in tetrahydrofuran (THF) at 70 °C, using 2,2'-azobis(2-methylpropionitrile) (AIBN) as the thermal initiator. NIPAAm polymerizations were carried out for 3 hours, and the resulting products were purified by precipitation from cold hexane. For NVCL, polymerizations took 16 hours, and the polymers were precipitated from cold pentane. In addition, PNIPAAm and PNVCL were obtained by radical polymerization and further used as the model system without the diglyceride function.



Scheme 13. Synthesis of thermoresponsive polymers with diglyceride-based dithiocarbonates by RAFT polymerization.

The crude reaction mixtures were analyzed by ^1H NMR spectroscopy to calculate monomer conversions (Table 6). For PNIPAAm, the integration of the signal at 3.9 ppm was compared to the peak of the vinyl group at 6.2 ppm. In PNVCL, the integration ratio of the two protons ($-\text{NCH}_2-$) at 3.1 ppm was compared with the residual vinyl proton at 7.3 ppm. The conversion was high in all cases (greater than 89%). However, NVCL conversions were higher than those calculated for NIPAAm, reaching more than 99% in most experiments. This may be related to the different polymerization times. Diglyceride-terminated PNIPAAms with higher molar masses (5, 10, 20 kg mol^{-1}) were dissolved in chloroform and precipitated in cold hexane. Polymers with lower molar masses (2 kg mol^{-1}) could not be purified by this method because of the high proportion of the hydrophilic part that causes solubility in hexane. Because of their structure, they were also not soluble in water. Therefore, they could not be purified by dialysis either. PNVCL-based homopolymers with higher molar masses (5, 10, 20 kg mol^{-1}) were dissolved in chloroform and precipitated in cold pentane. As with PNIPAAms, polymers with lower molar masses (2 kg mol^{-1}) could not be purified by simple precipitation or dialysis.

Subsequently, the polymers were characterized by size exclusion chromatography (SEC), ^1H NMR, ATR-FTIR, TGA, and DSC. To give a clear presentation of the results, they were divided into four groups according to the type of CTA and thermoresponsive block.

The SEC results indicated the high efficiency of diglyceride-based CTAs in controlling the polymerization of NIPAAm and NVCL (Figure 17). This is in good agreement with the literature, where dithiocarbonate-type chain transfer agents were successfully applied in the RAFT polymerization of NVCL²⁸⁴ and NIPAAm²⁸⁵. However, the chromatograms of the polymers with the lower PNVCL molar mass (2 and 5 kg mol^{-1}) showed a small shoulder at 25 min. The SEC-RI chromatograms smoothly shifted toward lower elution times with increased molar mass for both PNIPAAm and PNVCL. It should be noted that regardless of the CTA used, the dispersity values of PNVCL ($1.05 < D < 1.23$) are lower than those of PNIPAAm ($1.18 < D < 1.42$). This difference can be attributed to the comparatively faster reversible transfer process of the *O*-ethyl dithiocarbonate terminal group in the case of NVCL²⁸⁴ compared to NIPAAm²⁸⁶.

Table 6. Comparative properties and synthesis details of polymerizations.

Polymer	[GlyP-X] ₀ or [GlyO-X] ₀ (mmol L ⁻¹)	[AIBN] ₀ (mmol L ⁻¹)	M/CTA/I	Conversion ^a (%)	M _{n,th} ^b (kg mol ⁻¹)	SEC ^d		T _g ^e (°C)	HLB ^f	CMC ^g (mg mL ⁻¹)
						M _n (kg mol ⁻¹)	Đ			
GlyP-PNIPAAm _{2k}	223	22.3	20/1/0.1	93	2.85	4.00	1.18	107.7	17.16	-
GlyP-PNIPAAm _{5k}	91.4	9.14	49/1/0.1	92	5.83	8.09	1.24	124.8	18.60	7.9·10 ⁻³
GlyP-PNIPAAm _{10k}	45.2	4.52	99/1/0.1	89	10.70	12.54	1.22	131.2	19.09	1.0·10 ⁻²
GlyP-PNIPAAm _{20k}	22.8	2.28	196/1/0.1	89	19.60	16.40	1.28	134.7	19.31	1.6·10 ⁻²
GlyO-PNIPAAm _{2k}	223	22.3	20/1/0.1	90	2.83	3.74	1.28	105.8	16.68	-
GlyO-PNIPAAm _{5k}	91.4	9.14	49/1/0.1	91	5.82	8.51	1.20	126.3	18.54	6.3·10 ⁻³
GlyO-PNIPAAm _{10k}	45.2	4.52	99/1/0.1	91	10.97	10.63	1.36	132.3	18.83	8.9·10 ⁻³
GlyO-PNIPAAm _{20k}	22.7	2.27	197/1/0.1	90	20.80	14.37	1.42	136.6	19.14	2.8·10 ⁻²
GlyP-PNVCL _{2k}	257	103	14/1/0.4	>99	2.67	1.97	1.05	120.0	14.23	-
GlyP-PNVCL _{5k}	99.8	40	36/1/0.4	>99	5.71	5.00	1.14	133.0	17.73	5.6·10 ⁻⁴
GlyP-PNVCL _{10k}	49.9	20	72/1/0.4	>99	10.70	11.40	1.09	161.7	19.00	4.0·10 ⁻³
GlyP-PNVCL _{20k}	24.9	9.98	144/1/0.4	>99	20.60	19.35	1.18	172.2	19.41	6.3·10 ⁻³
GlyO-PNVCL _{2k}	257	103	14/1/0.4	>99	2.73	1.26	1.08	128.4	10.16	-
GlyO-PNVCL _{5k}	99.8	40	36/1/0.4	95	5.56	4.57	1.16	133.5	17.29	8.9·10 ⁻⁴
GlyO-PNVCL _{10k}	49.9	20	72/1/0.4	95	10.30	8.19	1.22	149.2	18.49	1.2·10 ⁻³
GlyO-PNVCL _{20k}	24.9	9.98	144/1/0.4	>99	20.60	19.03	1.23	170.3	19.35	1.6·10 ⁻³

Notes: xk stands for $M = x \text{ kg mol}^{-1}$, e.g., 2k = 2 kg mol⁻¹, [NIPAAm]₀ = 4.47 mol L⁻¹, [NVCL]₀ = 3.59 mol L⁻¹, ^adetermined by ¹H NMR in CDCl₃, ^bM_{n,th} for PNIPAAm: ([NIPAAm]₀/[GlyP-X]₀ or [GlyO-X]₀)·Conv·M_{NIPAAm}+M_{GlyP-X} or M_{GlyO-X}, M_{n,th} for PNVCL: ([NVCL]₀/[GlyP-X]₀ or [GlyO-X]₀)·Conv·M_{NVCL}+M_{GlyP-X} or M_{GlyO-X}, ^dmeasured by SEC-RI-MALS, ^edetermined by DSC from the second heating run with a heating rate of 10 °C min⁻¹, ^fdetermined by Griffin's method using an equation: HLB = 20·(1 - MI/M) with MI the molar mass of the hydrophobic part and M the molar mass of the entire polymer, ^gdetermined by fluorescence measurement, M_{NIPAAm} = 113 g mol⁻¹, M_{NVCL} = 139.2 g mol⁻¹, M_{GlyP-X} = 745.2 g mol⁻¹, M_{GlyO-X} = 796.5 g mol⁻¹.

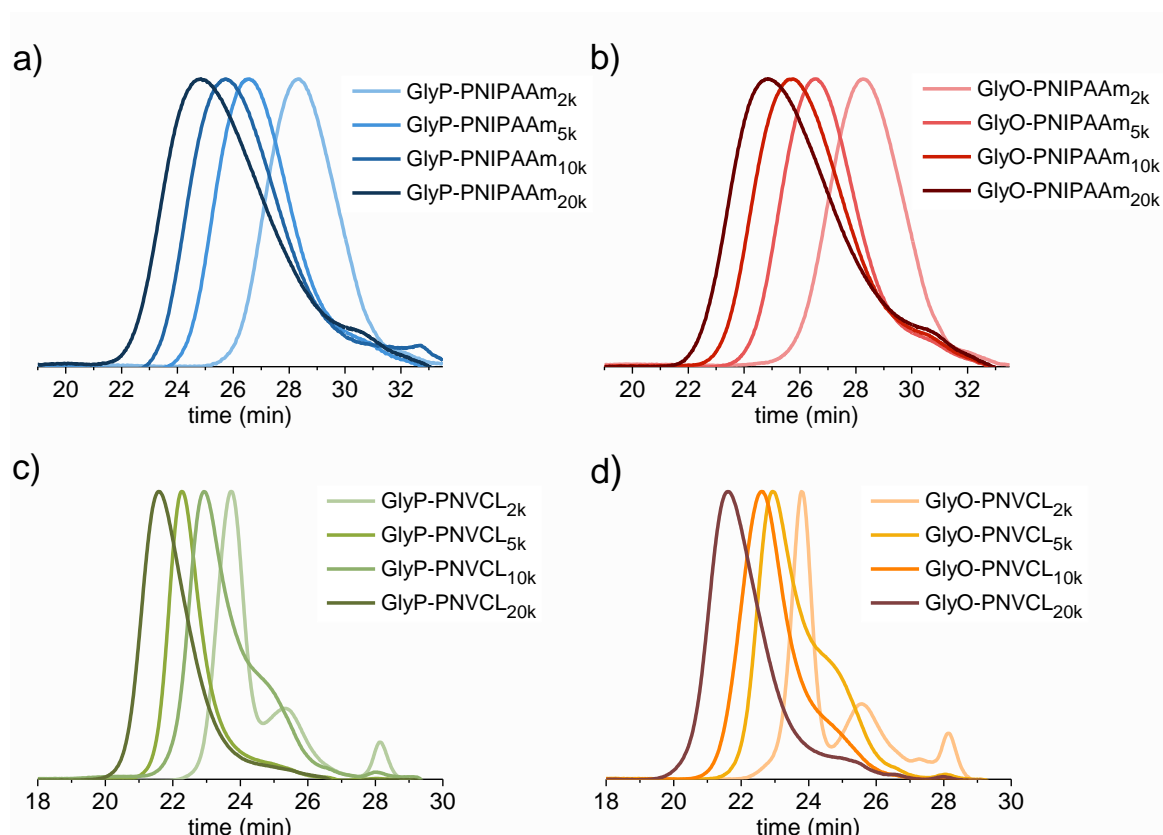
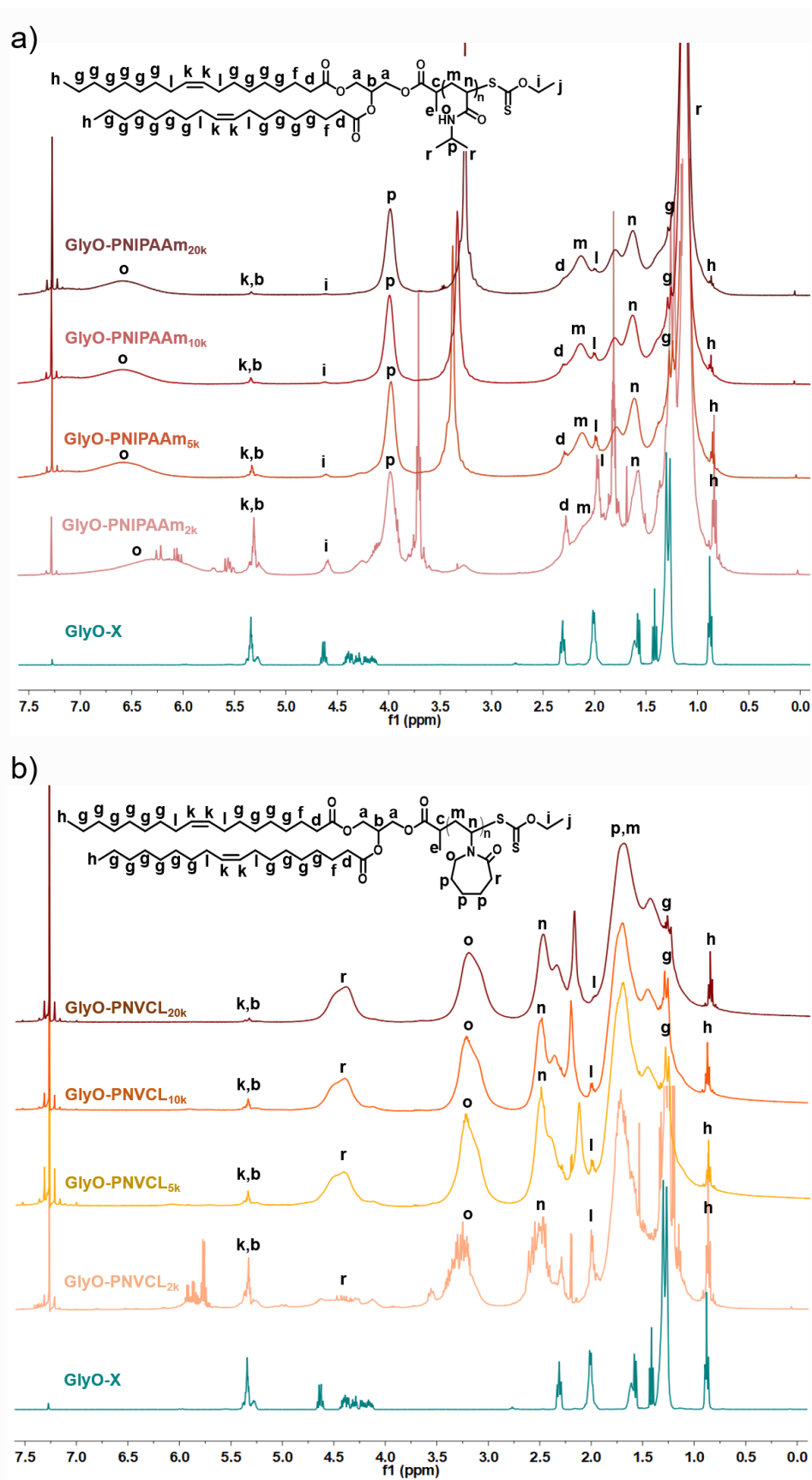


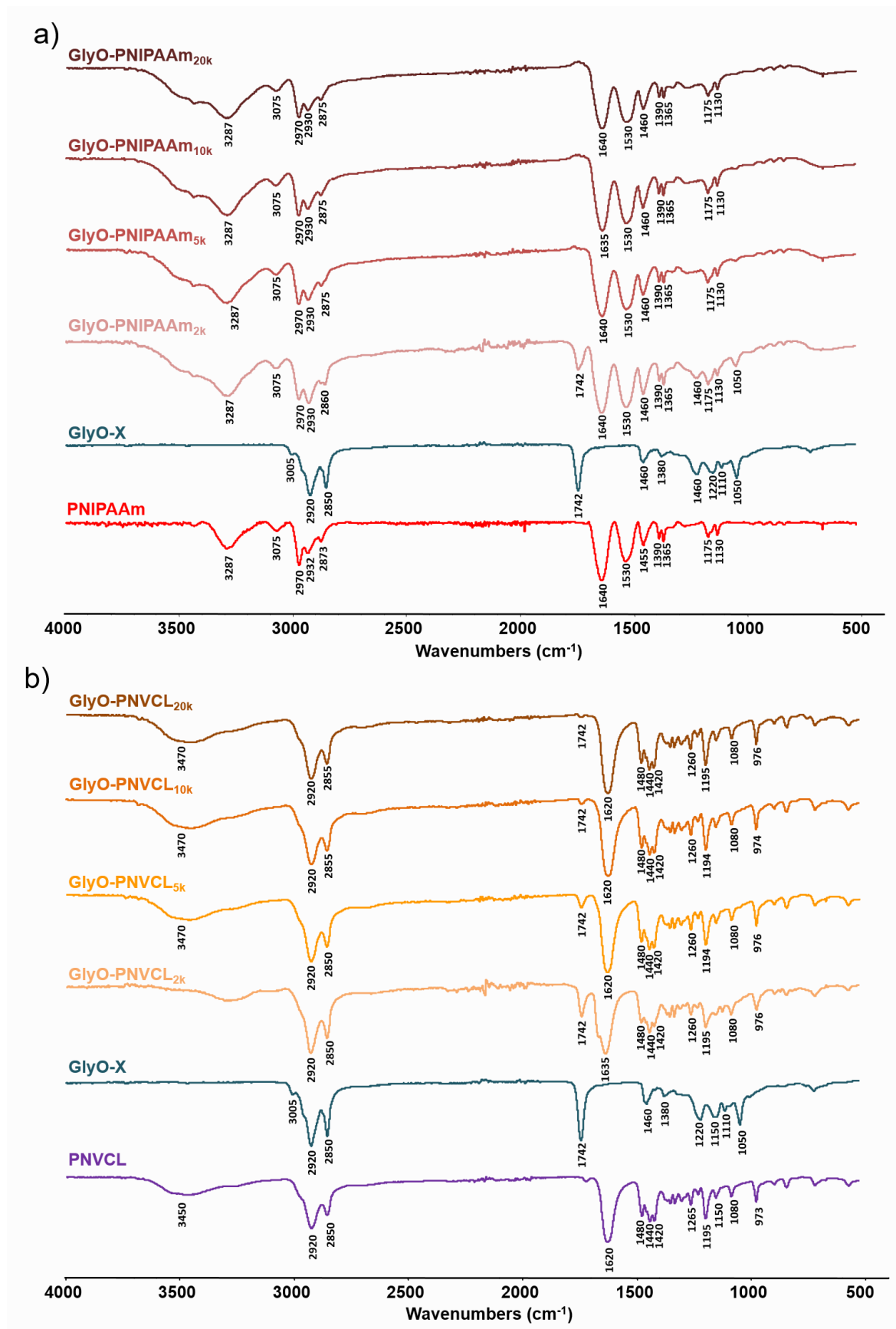
Figure 17. SEC chromatograms of homopolymers.

The ^1H NMR analysis of the polymers confirmed the presence of diglyceride tails in their structure. The NMR spectra of two selected groups of compounds (GlyO-PNIPAAm and GlyO-PNVCL) are presented in Figure 18. A triplet from the end of the lipid chain of CTAs at 0.9 ppm and the signal from the methylene groups at 1.35 ppm were observed. Furthermore, in polymerizations with GlyO-X, characteristic signals at 5.3 ppm and 2.0 ppm provided evidence that the internal double bonds of the oleate moiety did not react during RAFT polymerization.^{287,288} However, the intensity of the signals of the diglyceride moiety decreases with increasing molar mass of PNIPAAm or PNVCL. The ^1H NMR spectra displayed a high similarity in each measurement series, regardless of the length of the PNVCL or PNIPAAm chain. The appearance of broad signals characteristic of the polymer backbone was observed in all cases. PNIPAAm-based homopolymers exhibited a peak at 4.0 ppm ascribed to the $-\text{CH}-$ group and the signals in the range of 1.0–2.4 ppm from the polymer backbone. In turn, PNVCL-based homopolymers showed characteristic peaks in the range of 4.2–4.6 ppm, 3.0–3.3 ppm, 2.2–2.6 ppm, and 1.5–2.0 ppm. Moreover, ^1H NMR spectroscopy for PNIPAAm-based homopolymers confirmed the presence of the dithiocarbonate group as the chain-end, where characteristic signals at 4.5–4.7 ppm corresponding to the methylene of the *O*-ethyl dithiocarbonate group were observed.

ATR-FTIR analysis of the polymers showed trends similar to those of the NMR results. Selected ATR-FTIR spectra for two groups of compounds (GlyO-PNIPAAm and GlyO-PNVCL) are shown in Figure 19. The presence of diglyceride moieties was confirmed in the spectra of the polymers with the lowest molar mass based on the signal at 1740 cm^{-1} . Regardless of the length of the PNVCL or PNIPAAm chain, the spectra were similar. ATR-FTIR spectra of PNIPAAm-based homopolymers displayed peaks at 3280 cm^{-1} , 1655 cm^{-1} , and 1545 cm^{-1} , correlated with stretching vibrations of N–H, C=O (amide I), and N–H bending vibrations (amide II), respectively. For homopolymers based on PNVCL, a carbonyl vibrational peak in the lactam at 1630 cm^{-1} was observed, along with the signals from the C–N group at 1480 cm^{-1} and CH_2 at 1440 cm^{-1} .²⁸⁹

TGA and DSC were performed to evaluate the thermal properties of the synthesized polymers. The TGA curves of all polymers exhibited a slight weight loss (around 2%) in the temperature range up to $150\text{ }^\circ\text{C}$, which can be attributed to the removal of absorbed moisture. Polymers of the lowest molar mass (2 kg mol^{-1}) displayed a two-stage decomposition with the maximum decomposition rate at approximately 200 and $400\text{ }^\circ\text{C}$, which is particularly evident in the cases of PNVCL polymers. The first stage is likely related to the removal of dithiocarbonate moieties and oligomeric fractions, whereas the second stage is attributed to the degradation of the PNVCL or PNIPAAm chains. Polymers of higher molar mass (5 , 10 , 20 kg mol^{-1}) showed only a significant weight loss ($<95\%$) in the temperature range of PNIPAAm ($3\text{--}420\text{ }^\circ\text{C}$) or PNVCL ($400\text{--}470\text{ }^\circ\text{C}$) depolymerization.^{289,290} Generally, the degradation temperature increased, and the maximum degradation rate shifted to higher temperatures with an increasing number of repeating units in the polymer chain (Figure 20). Furthermore, the glass transition temperature (T_g) values determined by DSC for all polymers increased with increasing M_n of PNIPAAm or PNVCL (Table 6, Figure 21).





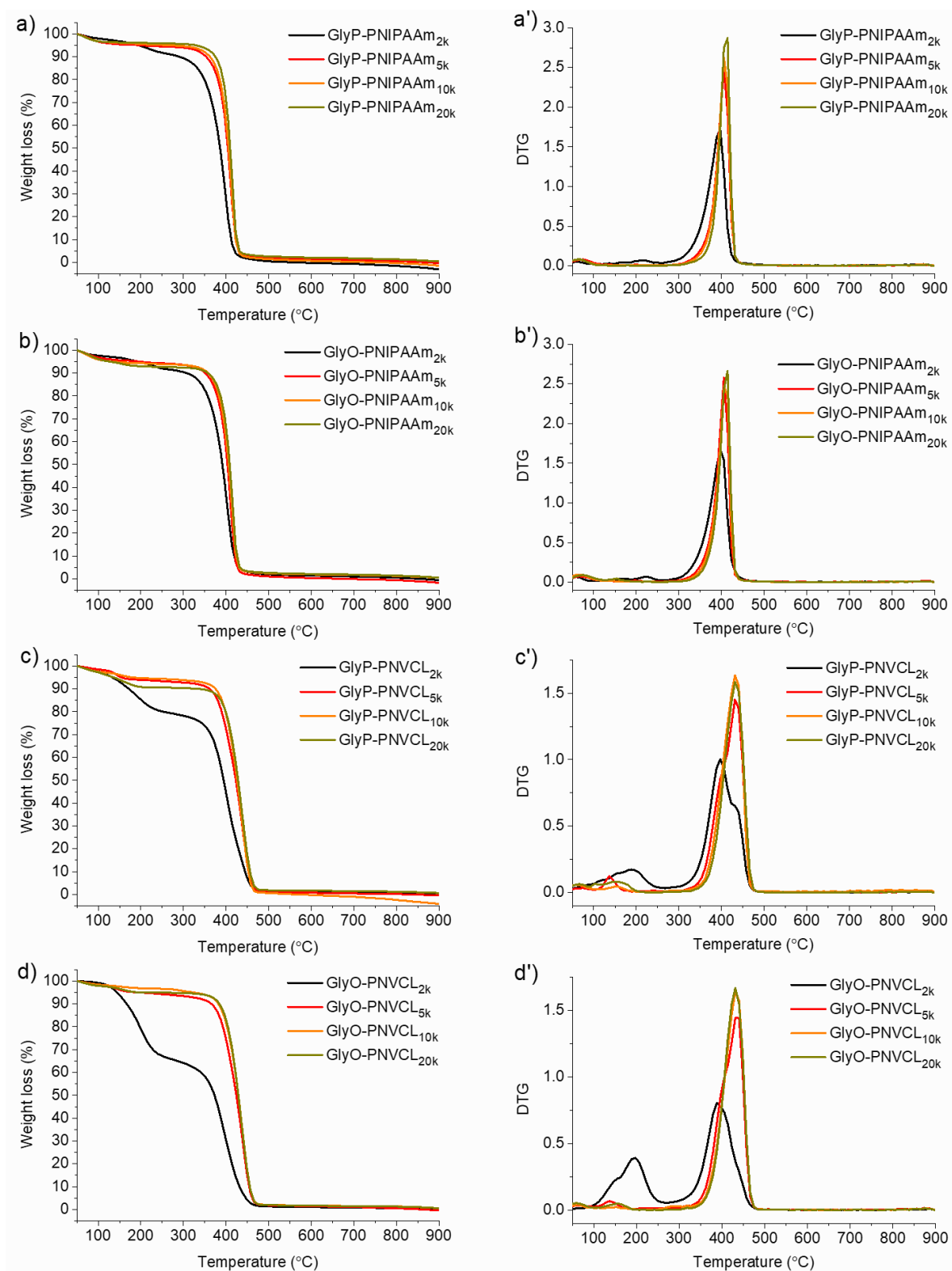


Figure 20. TG and DTG curves of the studied homopolymers.

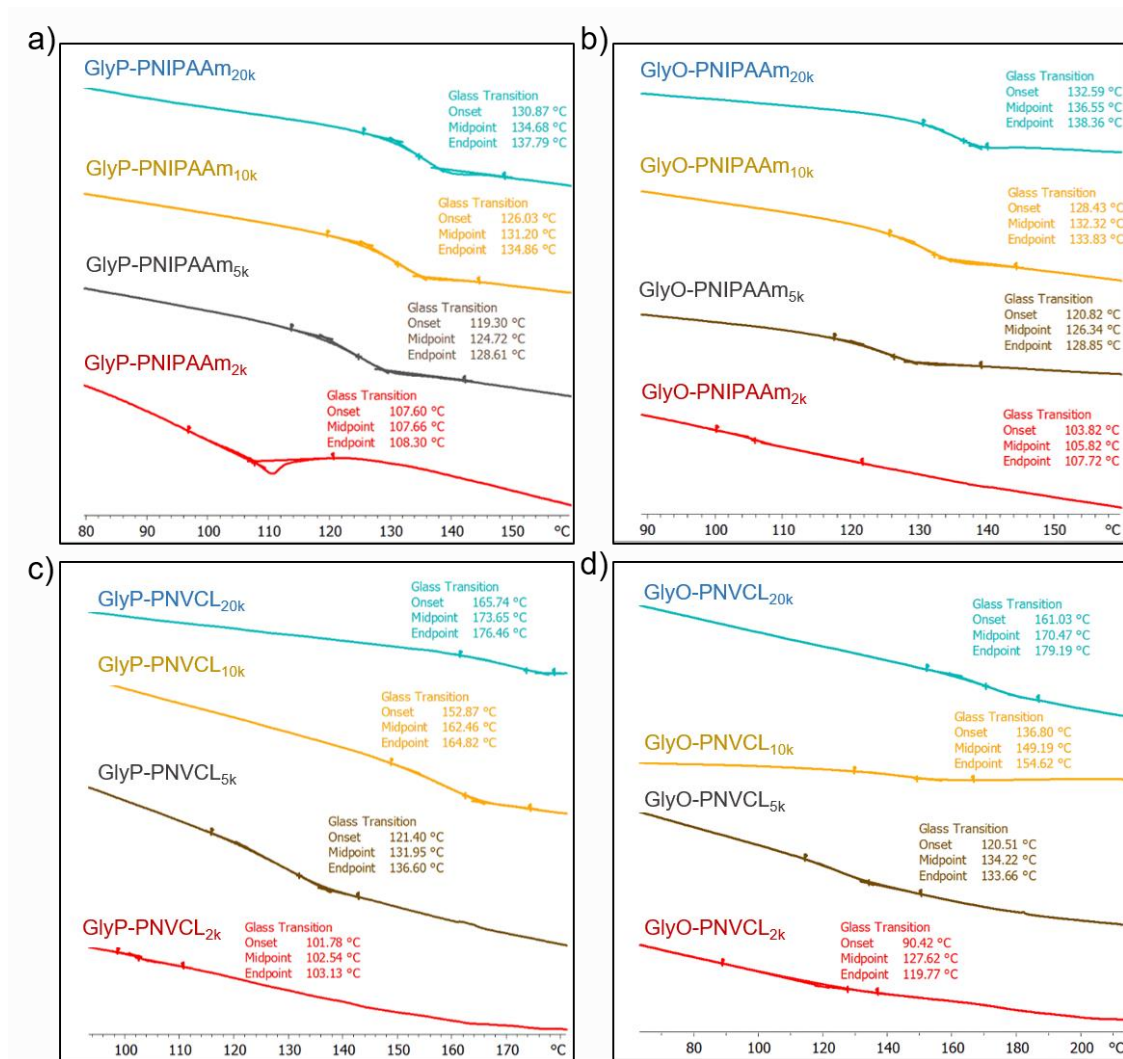


Figure 21. Glass transition temperatures of polymers determined by DSC: a) GlyP-PNIPAAm, b) GlyO-PNIPAAm, c) GlyP-PNVCL, and d) GlyO-PNVCL.

The addition of a diglyceride moiety to the termini of hydrophilic PNIPAAm or PNVCL chains imparts amphiphilic properties, enabling self-organization in an aqueous medium. The hydrophilic part is responsible for hydration and swelling, while the hydrophobic moieties minimize water contact, which is energetically unfavorable.²⁹¹ At first, the amphiphilic properties of the polymers were predicted by calculating the hydrophilic-lipophilic balance (HLB) values using the method developed by Griffin (Table 6).²⁹² HLB values can be used to predict the solubilizing properties of surfactants and polymers.²⁹³ The HLB values were calculated by determining the weight fractions of the hydrophobic and hydrophilic groups, according to the mathematical equation: $20 \cdot (1 - MI/M)$, where MI is the molar mass of the hydrophobic part, and M is the molar mass of the whole polymer. The HLB value is a numerical value between 0 and 20, where 0 represents highly hydrophobic molecules, and a value of 20 denotes hydrophilic ones. HLB values of diglyceride-

terminated polymers ranged from 10.16 to 19.41, with longer hydrophilic blocks resulting in higher HLB values. With increased HLB values, the polymers become more hydrophilic and form more thermodynamically stable interactions with water. It should be noted that the HLB value is a theoretical indicator of amphiphilic properties and does not take into account certain factors, such as the hydrophilicity and hydrophobicity of the molecules, the influence of temperature, concentration or interactions with other molecules.^{294,295}

The critical micelle concentration (CMC) is a vital parameter in the characterization of amphiphilic properties. Critical micelle concentration measures the concentration of a polymer in a solution at which it begins to form micelles. The CMC can be determined using pyrene as a fluorescent probe. The method is based on the fact that the fluorescence intensity of pyrene is sensitive to the local environment. Pyrene is a hydrophobic molecule that is not fluorescent in aqueous solutions. However, when it is incorporated into the core of the micelle, the pyrene molecules are shielded from the solvent and can fluoresce. As the concentration of surfactant increases, the number of micelles in the solution also increases. As a result, the fluorescence of pyrene is higher. At the CMC, a sharp increase in fluorescence is observed, indicating that micelles are forming. The CMC is generally lower for surfactants with a higher degree of hydrophobic character and higher for surfactants with a higher degree of hydrophilic character. The resulting polymeric micellar systems, where the core is hydrophobic, may include biologically active substances with poor water solubility. As previously mentioned, the polymers with a molar mass of 2 kg mol⁻¹ were insoluble in water due to a hydrophilic/hydrophobic balance that was too low. Therefore, it was not possible to study their properties in aqueous solvents. All polymers with higher molar masses of 5, 10, and 20 kg mol⁻¹ were used for further research. Critical micelle concentrations were determined by fluorescence measurement using pyrene as a probe and ranged from 8.0·10⁻⁴ to 1.6·10⁻² mg mL⁻¹ (Table 6, Figure 22). As expected, the longer the hydrophilic block, the higher the CMC values, indicating a lower tendency to form micelles. As the length of the polymer chain increases, the number of hydrogen bonds between repeating units of the hydrophilic block and water molecules increases, resulting in greater solubility in water and a higher CMC value.²⁹⁶⁻²⁹⁸ A similar trend was observed for PEG-lipid conjugates²⁹⁹, poly(*N*-vinylpyrrolidone)s with stearyl or palmityl chain-end^{299,300} or poly(2-methyl-2-oxazoline)s terminated with hydrophobic alkyl group.^{301,302}

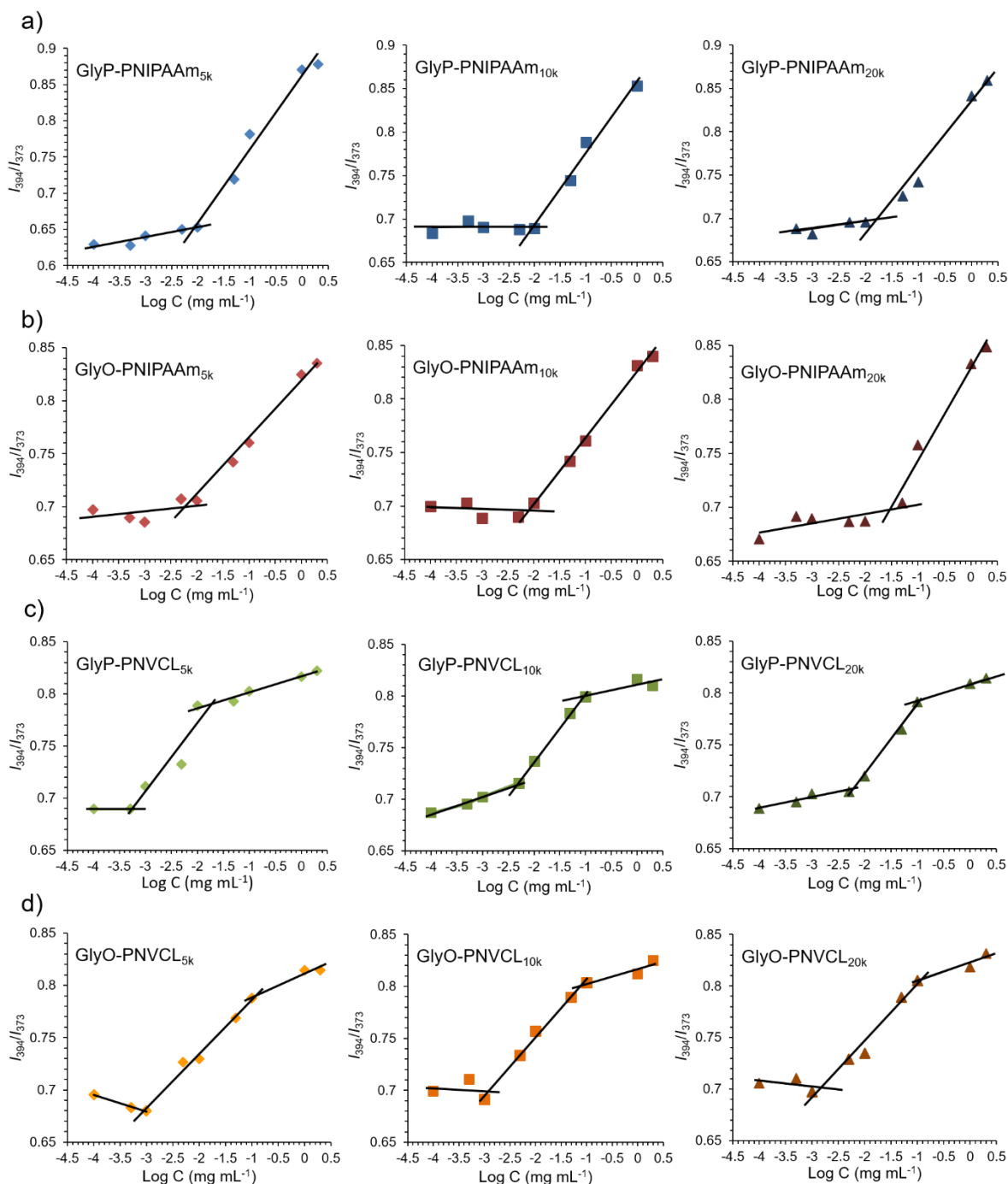


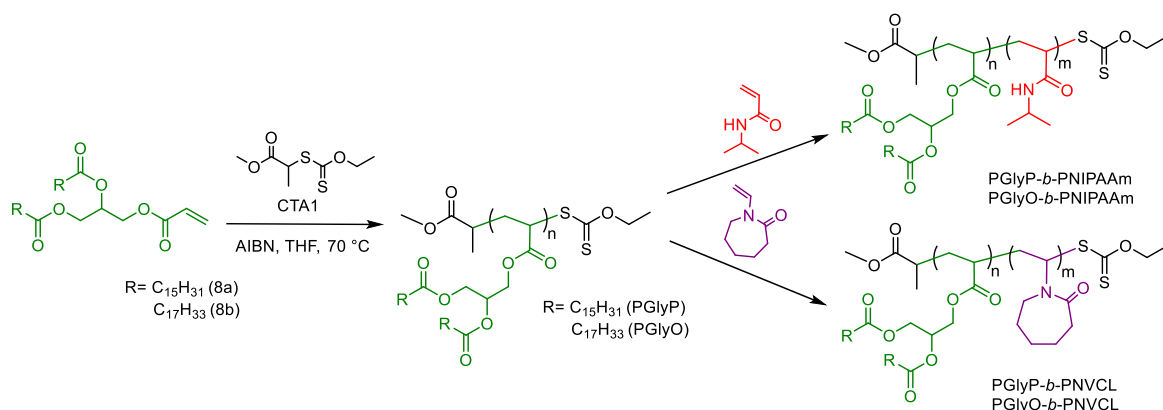
Figure 22. Intensity ratios (I_{394}/I_{373}) from pyrene emission spectra plotted with a concentration of polymers a) GlyP-PNIPAAm, b) GlyO-PNIPAAm, c) GlyP-PNVCL, d) GlyO-PNVCL.

It was also noted that the CMC values for amphiphilic PNVCL-based polymers were lower than those of PNIPAAm-based counterparts, which can be attributed to the lower hydrophilicity of PNVCL.^{158,303,304} The molecular structure of PNVCL does not possess strong self-associated hydrogen bonds, in contrast to PNIPAAm. The carbonyl group in PNVCL can only participate in hydrogen bonding with water molecules due to the absence of H-donors in its molecular structure.^{305,306} Considering that the obtained polymeric

nanoparticles will be further used for biomedical applications and may be diluted, e.g., in the body fluids, all experiments on polymeric particles were carried out well above the designated CMCs.

2.2.2. Synthesis and characterization of thermoresponsive polymers with diglyceride-based monomers

Polymers containing several diglyceride molecules in the side chains were synthesized by the RAFT method in two steps (Scheme 14). At first, homopolymers of PGlyP or PGlyO were obtained using diglyceride-based monomers and the well-known methyl 2-((ethoxycarbonylthio)thio)propanoate (CTA1) as a chain transfer agent. Crude reaction mixtures were analyzed by ^1H NMR spectroscopy. The NMR spectra showed that the monomer conversion for GlyP-A was 93% after 6 h. In the case of PGlyO, the polymerization was carried out for 16 h, and the monomer conversion reached 95%. Polymers were further purified by precipitation in cold methanol. The molar mass distributions of the homopolymers were narrow ($D < 1.3$), and good agreement was observed between the theoretical and average molar masses obtained from size exclusion chromatography (Table 7 and Figure 23). ^1H NMR and IR spectra also confirmed the successful homopolymerization. The ^1H NMR spectra showed the disappearance of vinyl proton signals ranging from 5.8 to 6.5 ppm, while broader peaks than those of the corresponding monomers were present (Figures 24a and 25a). As expected, in the case of the ATR-FTIR spectra of the homopolymers, the band ascribed to the acrylate double bond at 1635 cm^{-1} disappeared (Figures 24b and 25b).



Scheme 14. Synthesis of thermoresponsive polymers with diglyceride-based monomers by RAFT polymerization.

In the second step, *N*-isopropylacrylamide (NIPAAm) and *N*-vinylcaprolactam (NVCL) were polymerized in the presence of PGlyP and PGlyO as macro-CTAs. The detailed experimental conditions for all polymers are depicted in Table 7. The conversions determined by ^1H NMR spectroscopy were greater than 88% in all cases. The resulting copolymers were purified by precipitation in cold diethyl ether (polymers with the PNIPAAm block) or pentane (polymers with the PNVCL block) and characterized by SEC, ^1H NMR, ATR-FTIR, TGA, and DSC. For all samples, a shift of the chromatograms of block copolymers to a lower elution time was observed, which indicated the transformation of diglyceride-based macro-CTAs into copolymers (Figure 23).

For copolymers with PNIPAAm block, the molar masses determined by SEC were in good agreement with theoretical values. In the case of PNVCL-based copolymers, the M_n values were lower than the theoretical ones (Table 7). This can be explained by chain transfer to solvent, which dictates an upper limit in the accessible molar mass. However, for all copolymers, the molar mass distributions were narrow ($D < 1.4$).

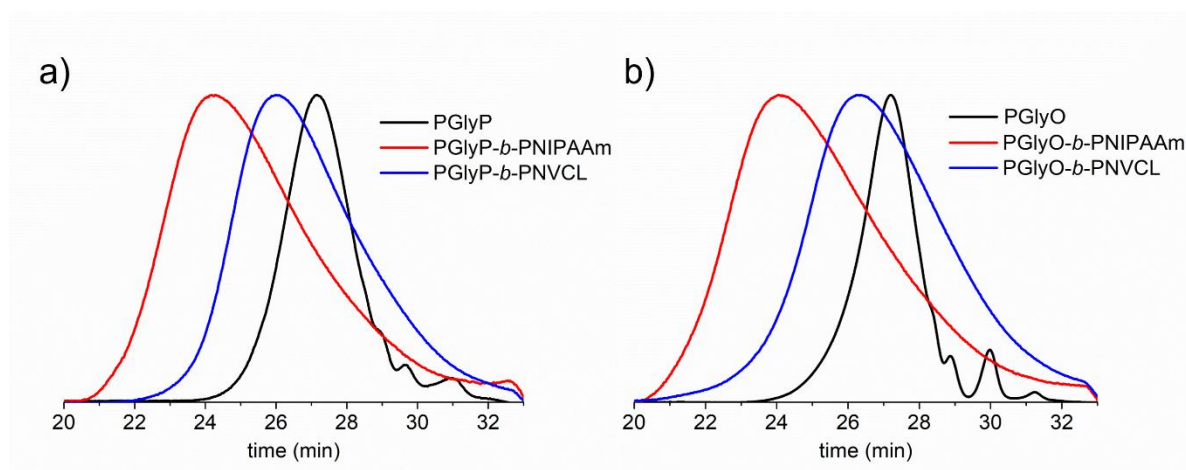


Figure 23. SEC-RI chromatograms of diglyceride-based homopolymers and copolymers.

Table 7. Comparative properties and synthetic details of polymerization for PGlyP, PGlyO, and their copolymers.

Polymer	[CTA] ₀ (mol L ⁻¹)	[Monomer] ₀ (mol L ⁻¹)	[AIBN] ₀ (mol L ⁻¹)	Conversion ^a (%)	$M_{n,th}^b$ (kg mol ⁻¹)	SEC ^c		Max. degradation rate ^d (°C)	Residue at 600 °C ^d (%)	T_g^e (°C)	HLB ^f	CMC ^g (mg mL ⁻¹)
						M_n (kg mol ⁻¹)	\bar{D}					
PGlyP	0.0803	0.803	0.530	95	6.14	4.83	1.17	400	2.0	-	-	-
PGlyO	0.0741	0.741	0.608	93	6.48	6.32	1.26	405	3.3	-	-	-
PGlyP- <i>b</i> -PNIPAAm	0.0167	4.425	0.00167	93	32.65	33.96	1.40	415	1.8	136.5	19.14	0.014
PGlyP- <i>b</i> -PNVCL	0.0167	3.592	0.00668	93	32.70	19.82	1.33	435	1.8	174.5	19.24	0.007
PGlyO- <i>b</i> -PNIPAAm	0.0167	4.425	0.00167	88	32.67	28.36	1.31	415	2.5	135.5	19.22	0.018
PGlyO- <i>b</i> -PNVCL	0.0167	3.590	0.00668	89	32.99	19.02	1.35	435	2.3	165.1	19.33	0.007

Notes: ^acalculated from ¹H NMR in CDCl₃, ^b $M_{n,th} = [\text{Monomer}]_0 / [\text{CTA}]_0 \cdot M_{\text{Monomer}} \cdot \text{Conv.} + M_{\text{CTA}}$, ^cmeasured by SEC-RI-MALS, ^ddetermined by TGA, ^edetermined by DSC from the second heating run with a heating rate of 10 °C min⁻¹, ^fdetermined by Griffin's method using an equation: $\text{HLB} = 20 \cdot (1 - MI/M)$ with MI the molar mass of the hydrophobic part and M the molar mass of the whole polymer, ^gdetermined by fluorescence measurement.

Successful block copolymerization was also confirmed by ^1H NMR spectroscopy (Figures 24a and 25a). In the spectra of all copolymers, signals from the diglyceride-based block, such as the triplet from the lipid chain-end of CTAs at 0.9 ppm and the signal from the methylene groups at 1.35 ppm, were observed. Furthermore, the ^1H NMR results showed the presence of the broad signals characteristic of the PNIPAAm or PNVCL segment. PNIPAAm-based homopolymers exhibited a peak at 4.0 ppm ascribed to the $-\text{CH}-$ group and the signals in the range of 1.0–2.4 ppm from the polymer backbone. Conversely, homopolymers of PNVCL exhibited distinctive peaks within the ranges of 4.2–4.6 ppm, 3.0–3.3 ppm, 2.2–2.6 ppm, and 1.5–2.0 ppm. As expected, ATR-FTIR analysis (Figures 24b and 25b) of the copolymers showed a trend similar to the NMR results. The ATR-FTIR spectra of copolymers containing PNIPAAm showed broad bands at 3285 cm^{-1} , 1635 cm^{-1} , and 1530 cm^{-1} , correlated to stretching vibrations of N–H, C=O (amide I), and N–H bending vibrations (amide II), respectively. For copolymers based on PNVCL, a characteristic carbonyl band in the lactam at 1630 cm^{-1} , signals from the stretching vibrations of the C–N group at 1480 cm^{-1} and CH_2 at 1440 cm^{-1} were observed. In the spectra of all copolymers, the band at $\sim 1740\text{ cm}^{-1}$ confirmed the presence of a diglyceride-based block.

The thermal behavior of copolymers was investigated using thermogravimetric analysis and differential scanning calorimetry (Figure 26 and Figure 27). The decomposition of PGlyP and PGlyO polymers occurred in a single step within the temperature range of 350–450 °C, with the maximum decomposition rate at 400 °C for PGlyP and 405 °C for PGlyO. The TGA curves of the copolymers revealed a slight weight loss (<5%) below 200 °C due to the removal of adsorbed moisture and a significant weight loss (>90%) between 350 and 470 °C due to depolymerization. The maximum decomposition rate varied depending on the copolymer type, with values of 415 °C for PNIPAAm-based copolymers and 435 °C for those with PNVCL block. DSC measurements showed that the glass transition temperature (T_g) values for the synthesized copolymers were similar to those reported for PNIPAAm or PNVCL¹⁹⁸ (Table 7). However, this method could not determine the T_g values for PGlyP and PGlyO. Nevertheless, differences in thermal and structural characteristics were observed for both homopolymers. In the case of PGlyP, the DSC heating and cooling curves revealed peaks related to the melting and crystallization of the sample (Figure 27).

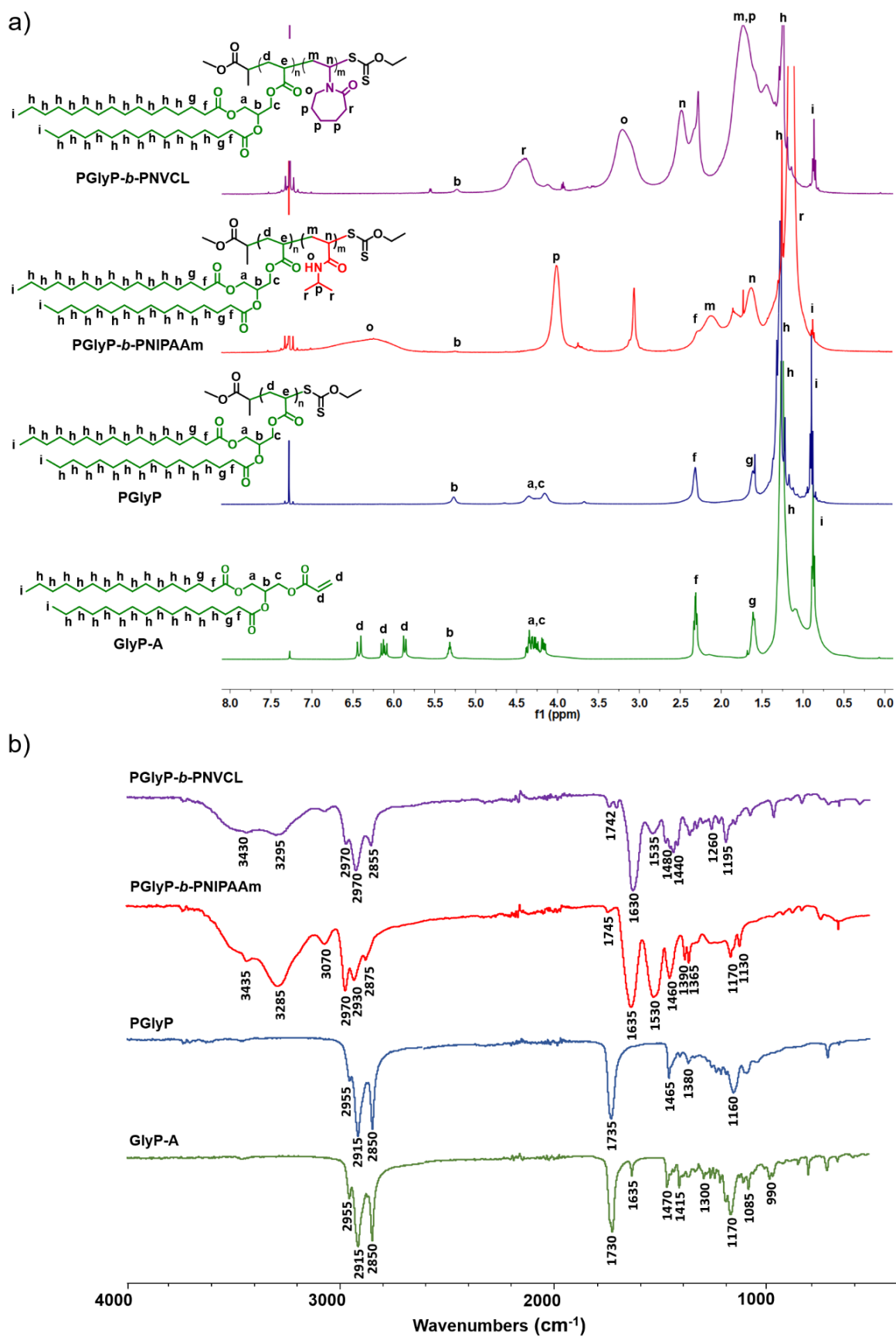


Figure 24. Comparison of a) ¹H NMR spectra (400 MHz, CDCl₃) and b) ATR-FTIR spectra for polymers containing the palmitic acid derivative (GlyP-A).

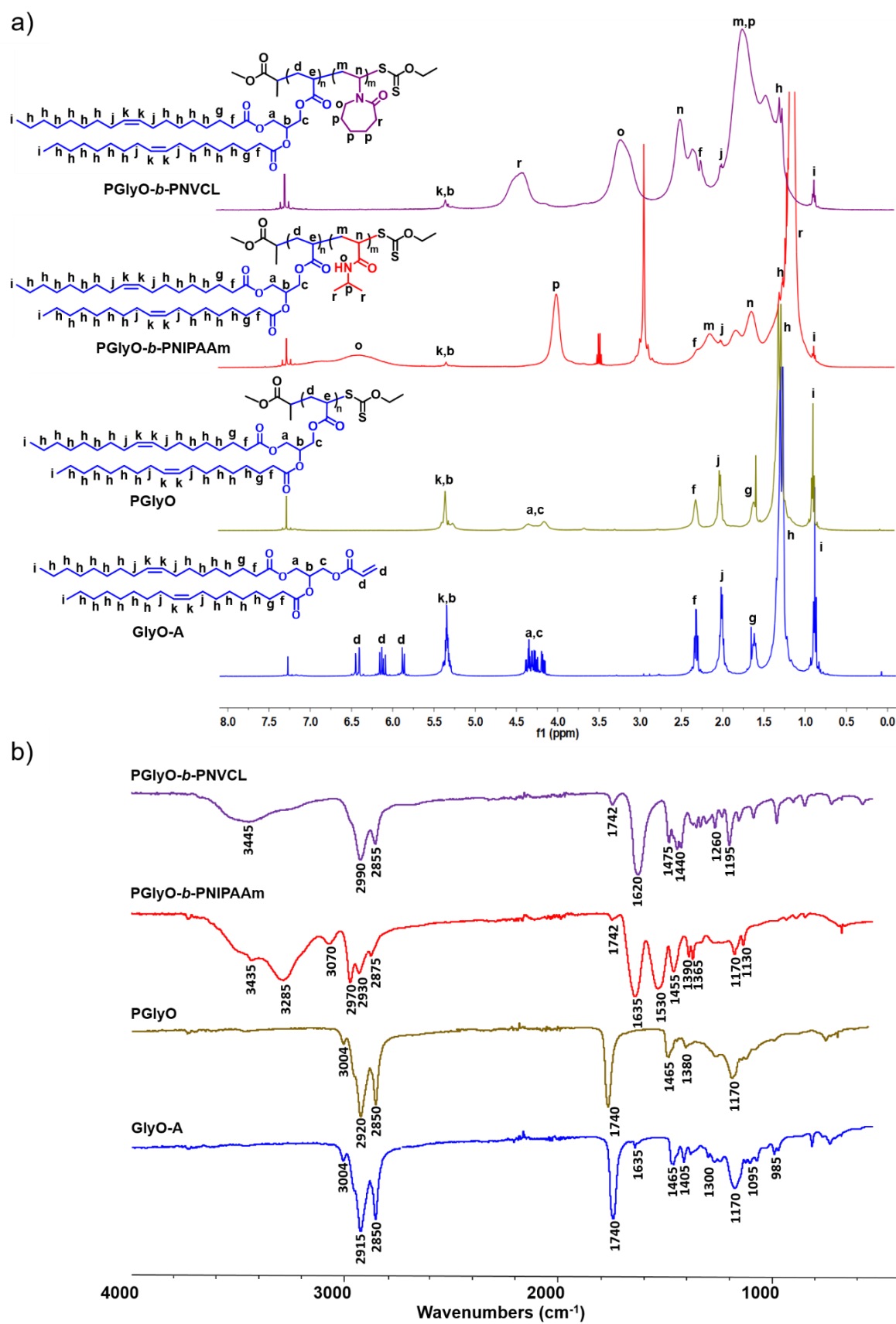


Figure 25. Comparison of the a) ^1H NMR spectra (400 MHz, CDCl_3) and b) ATR-FTIR spectra for polymers containing the oleic acid derivative (GlyO-A).

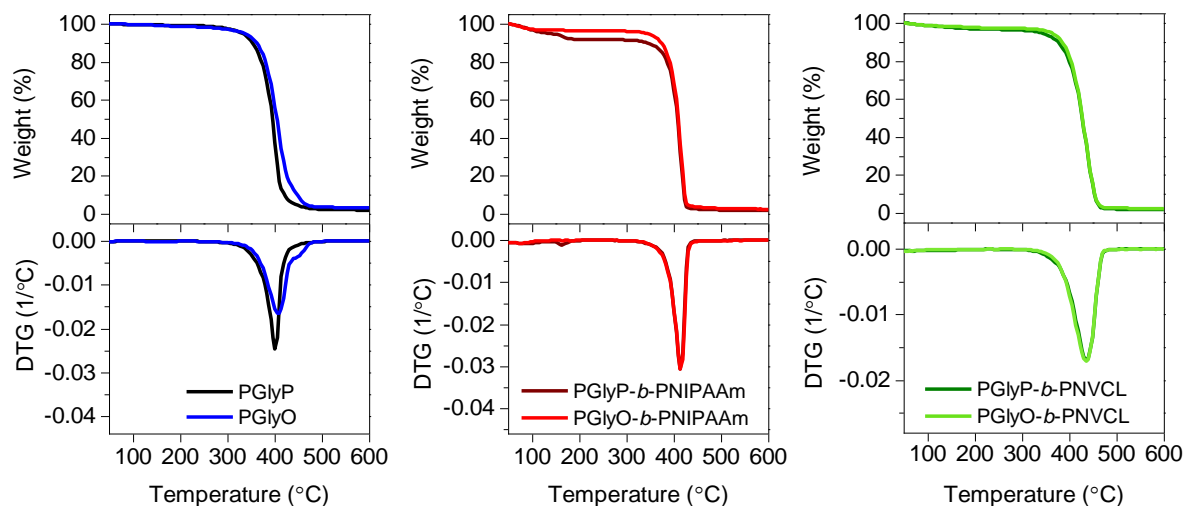


Figure 26. TGA (top panels) and DTG (bottom panels) of the studied homopolymers and copolymers.

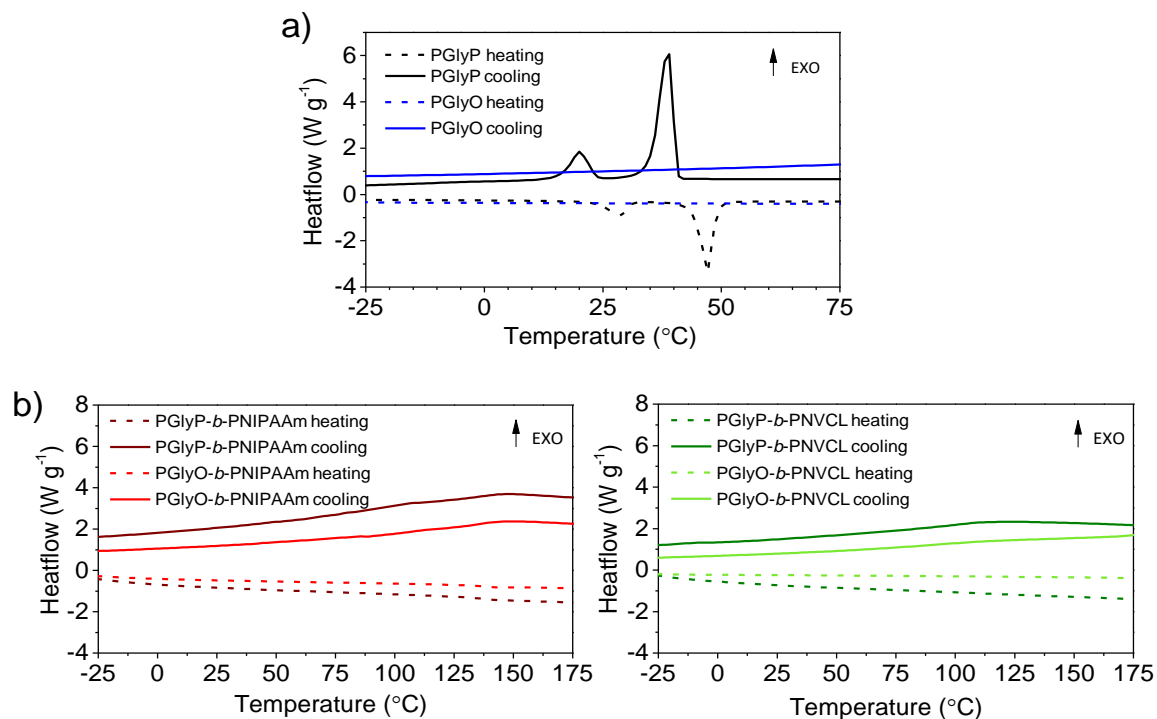


Figure 27. DSC curves (the second heating and cooling run) of the studied a) homopolymers and b) copolymers.

The copolymers synthesized in this work consist of hydrophilic (PNIPAAm or PNVCL) and hydrophobic segments (the diglyceride of palmitic or oleic acid), allowing for their self-organization in an aqueous solution. Similar to the investigations in the previous section on diglyceride end-capped homopolymers, these properties were also examined.

The CMC values were determined by fluorescence analysis from the plot of the intensity ratio of pyrene versus polymer concentration. The observed CMC value was $\sim 7 \cdot 10^{-3}$ mg mL⁻¹ for the copolymers containing PNVCL and $\sim 1.4 \cdot 10^{-2}$ mg mL⁻¹ for those based on PNIPAAm (Table 7, Figure 28). Thus, the CMC values for copolymers containing PNVCL block are lower than those with PNIPAAm, which, as previously mentioned, can be correlated to the lower hydrophilicity of PNVCL compared to PNIPAAm. However, no significant differences were observed between the CMC values, depending on the type of hydrophobic lipidated block.

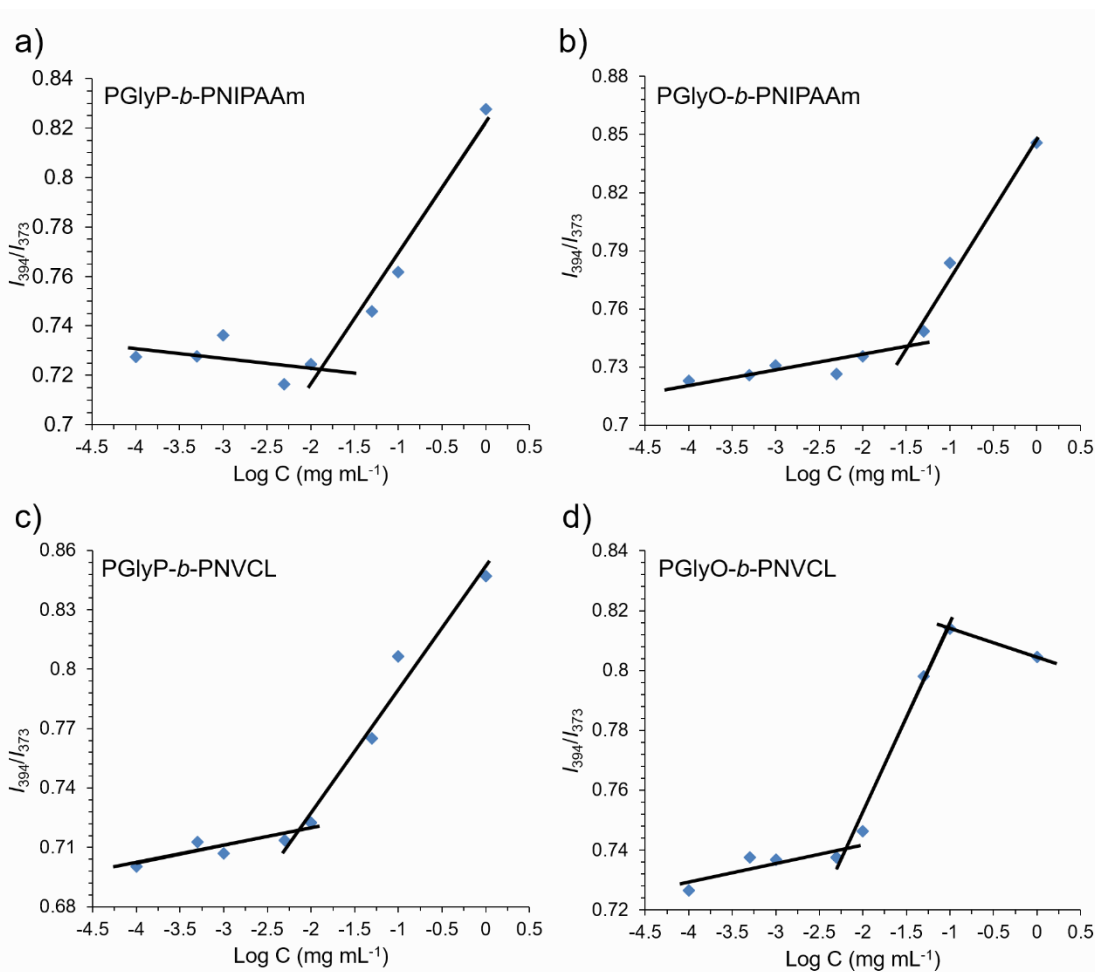


Figure 28. Critical micelle concentration measurements of copolymers a) PGlyP-*b*-PNIPAAm, b) PGlyO-*b*-PNIPAAm, c) PGlyP-*b*-PNVCL, and d) PGlyO-*b*-PNVCL.

Summary

This chapter delves into the synthesis, characterization, and applications of original chain transfer agents (CTAs) and monomers derived from diglycerides containing palmitic or oleic acid moieties for use in RAFT polymerization. These CTAs and monomers were developed through multistep synthetic pathways using solketal as the starting material. The successful synthesis of monomers and CTAs was confirmed using several techniques such as ^1H NMR, ^{13}C NMR, ATR-FTIR, TGA, DSC, and MS. The original diglyceride-based CTAs and monomers set the stage for synthesizing polymers containing one or more diglyceride molecules within their structures using the RAFT method.

DG-based CTAs were used to polymerize *N*-isopropylacrylamide (NIPAAm) and *N*-vinylcaprolactam (NVCL) with molar masses of 2, 5, 10, and 20 kg mol $^{-1}$. Synthesized polymers were characterized using SEC, ^1H NMR, ATR-FTIR, TGA, and DSC. The SEC results indicated that diglyceride-based CTAs effectively controlled the polymerizations. Furthermore, NMR and ATR-FTIR analyses confirmed the presence of diglyceride tails at the chain end of polymers. The DSC results showed an increase in the glass transition temperature (T_g) with the molar mass of PNIPAAm or PNVCL.

Polymers with multiple diglyceride molecules in their side chains were also successfully synthesized in two steps. First, diglyceride-based monomers were polymerized to yield PGlyP or PGlyO homopolymers. Narrow molar mass distributions ($\mathcal{D} < 1.3$) were detected, and there was consistency between theoretical and experimental molar masses determined by SEC. The formation of homopolymers was confirmed by ^1H NMR and ATR-FTIR spectroscopy. Subsequently, NIPAAm and NVCL were polymerized in the presence of PGlyP and PGlyO as macro-CTAs. The resulting copolymers were then characterized using various techniques, including SEC, ^1H NMR, ATR-FTIR, TGA, and DSC. The SEC showed that the molar masses of PNIPAAm block copolymers were in line with theoretical predictions, while those of PNVCL-based copolymers were slightly lower. In particular, all copolymers maintained narrow molar mass distributions ($\mathcal{D} < 1.4$). TGA and DSC analyses indicated uniform decomposition patterns and similar T_g values for the copolymers containing blocks of PNIPAAm or PNVCL. The ^1H NMR and ATR-FTIR analyses further affirmed the successful synthesis of block copolymers, showing specific signals corresponding to both blocks.

The amphiphilic characteristics of these copolymers, derived from the presence of hydrophilic (PNIPAAm or PNVCL) and hydrophobic (diglyceride of palmitic or oleic acid)

chain-end or block, prompted their self-organization in aqueous media. This behavior was investigated by estimating the hydrophilic-lipophilic balance and analyzing the critical micelle concentration. The CMC and HLB values for DG-terminated PNIPAAm and PNVCL varied depending on the length of the hydrophilic block. For all copolymers, the HLB values were similar. Notably, PNVCL-based copolymers had higher CMC values than their PNIPAAm counterparts, but the lipidated hydrophobic block did not significantly impact these values.

These amphiphilic properties of polymers could potentially facilitate the encapsulation of biologically active, water-insoluble substances within polymers.

The studies outlined in this chapter have been published in:

- 1) I. Kurowska, K. H. Markiewicz, K. Niemirowicz-Laskowska, P. Misiak, M. Destarac, P. Wielgat, I. Misztalewska-Turkowicz, G. Siemiaszko, H. Car, A. Z. Wilczewska, *European Polymer Journal* **2022**, *169*, 111154.
- 2) I. Kurowska, K. H. Markiewicz, K. Niemirowicz-Laskowska, M. Destarac, P. Wielgat, I. Misztalewska-Turkowicz, P. Misiak, H. Car, A. Z. Wilczewska, *Biomacromolecules* **2023**, *24*, 4854.

CHAPTER 3. POLYMERIC NANOPARTICLES BASED ON POLYMERS WITH DIGLYCERIDE MOIETIES

This chapter focuses on the formation and physicochemical characterization of water-soluble polymeric nanoparticles (PNPs) derived from polymers with one or multiple diglyceride molecules within their structure. Additionally, it highlights their thermoresponsive properties and potential as drug carriers.

The presence of diglyceride moieties in PNPs enhances the biocompatibility and affinity to cell membranes. Notably, this study incorporates two types of diglycerides within the PNP structure: saturated, derived from palmitic acid, and unsaturated, derived from oleic acid. As mentioned in the literature review, palmitic acid moieties contribute to stability and rigidity, while oleic acid moieties have the ability to introduce fluidity and flexibility into the PNPs. This comparative analysis specifically assesses how diglycerides with saturated and unsaturated chains influence the physicochemical properties of PNPs and, subsequently, their effectiveness in therapeutic applications. Furthermore, this investigation contrasts two types of thermoresponsive polymers integrated into the PNPs: PNIPAAm and PNVCL. These polymers undergo phase transitions in response to temperature changes, a characteristic that can be utilized to facilitate controlled drug release. The dual comparison of the diglyceride types and the thermoresponsive polymers provides a comprehensive overview of how each component's characteristics can be optimized to enhance the design and functionality of polymeric nanoparticles for targeted drug delivery applications.

Polymeric nanoparticles are one of the most explored platforms for targeted and controlled drug delivery. PNPs offer various benefits compared to other nanoparticulate systems, including high stability in the body, prolonged storage stability, and increased biocompatibility and biodegradability under certain conditions.³⁰⁷ Additionally, they offer a high surface area-to-volume ratio, enabling efficient loading and release of drugs.^{130,308}

Previous research in the Department of Polymers and Organic Synthesis of the University of Białystok demonstrated that micelles obtained from cholesterol-terminated polymers by direct dissolution in water were unstable and heterogeneous.²⁹⁰ Therefore, in this work, lipid-polymer nanoparticles were prepared using a simple and commonly used nanoprecipitation method (Figure 29a). Nanoprecipitation, also called the solvent displacement method, involves fast diffusion of the polymer-containing organic solution into an aqueous phase.^{309,310} Colloidal particles of a polymer with a well-defined size and a narrow size distribution form instantaneously as they minimize contact with water

molecules.^{310,311} An advantage of nanoprecipitation is the ability to incorporate various types of drugs and other biomolecules into nanoparticles. This can be achieved by adding the drug or biomolecule to the polymer solution prior to precipitation (Figure 29b).

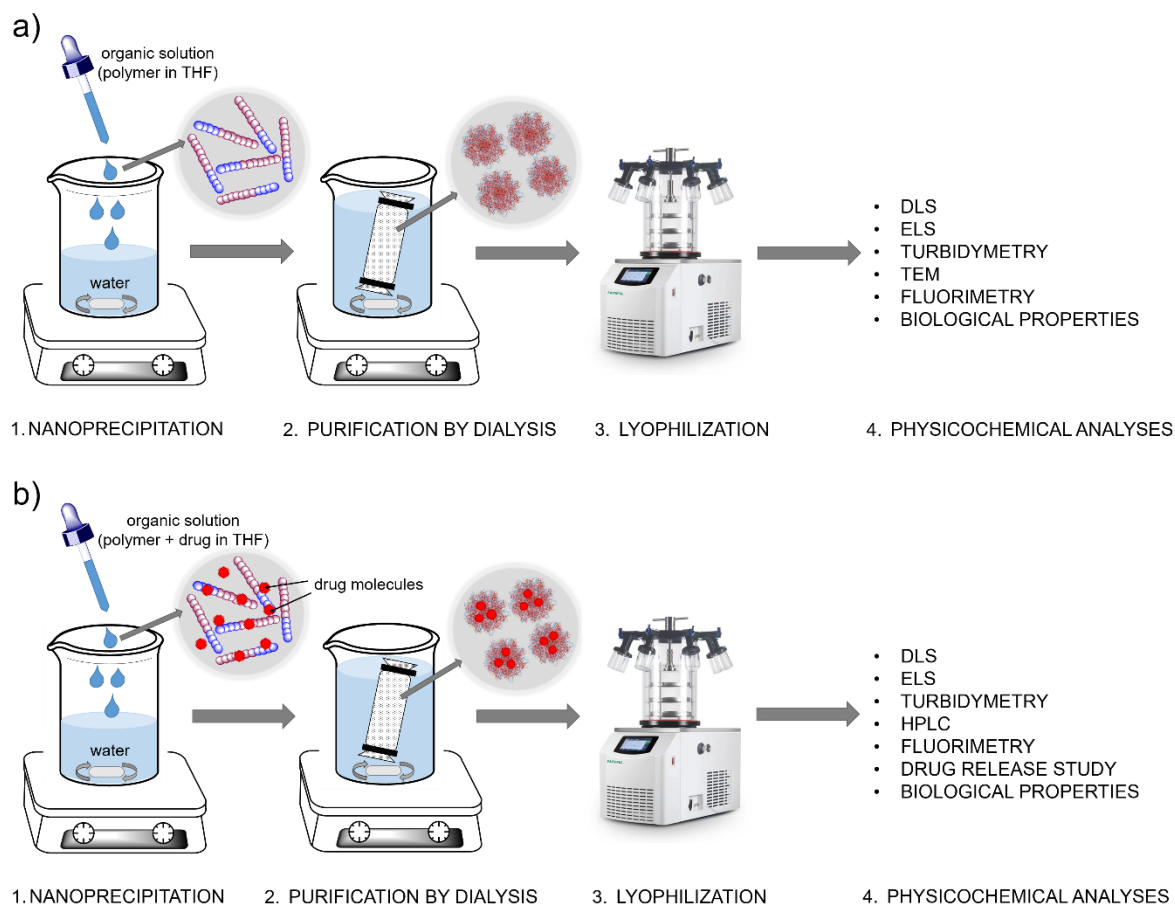


Figure 29. Schematic representation of nanoprecipitation method.

3.1. Polymeric nanoparticles based on homopolymers with DGs in the main chain

As mentioned, the polymeric nanoparticles were prepared using the nanoprecipitation method (Figure 29a). Polymers were dissolved in THF and, after 3 hours, added dropwise to water. The resulting homogeneous solutions were then dialyzed against distilled water to remove the organic solvent, freeze-dried, redispersed in water or phosphate buffered saline (PBS), and analyzed in terms of their properties. Multiangle dynamic light scattering (MADLS) was used to determine the size (hydrodynamic diameter) of the resulting lipid-polymer nanoparticles. MADLS is a new approach to the traditional DLS technique, introduced with the new Zetasizer Ultra system (Malvern Panalítica). Compared to the DLS method, the measurement using MADLS is acquired with three different detection angles (back, side, and forward) and combines the information obtained into one angle-independent

high-resolution result.^{312,313} As shown in Figure 30 and Table 8, the MADLS measurements of nanoparticles in PBS showed a narrow monomodal size distribution ranging from 16.96 ± 0.37 nm to 25.08 ± 0.44 nm for PNIPAAm-based particles and from 11.62 ± 0.30 nm to 20.14 ± 0.47 nm for PNVCL-based particles. The influence of the length of the polymer chain on the size of the particles was evident. As expected, the size of the nanoparticles increased with the molar mass of PNIPAAm or PNVCL.^{314,315} It was observed that the hydrodynamic diameter of the particles varied depending on the type of thermoresponsive block (PNIPAAm or PNVCL). Diglycerides-terminated PNVCL-based particles exhibited smaller sizes in comparison to their PNIPAAm-based counterparts. This may be correlated with the lower hydrophilicity of PNVCL compared to PNIPAAm.^{158,303,304} However, no significant differences were observed between the sizes of the polymeric nanoparticles depending on the lipidated chain-end.

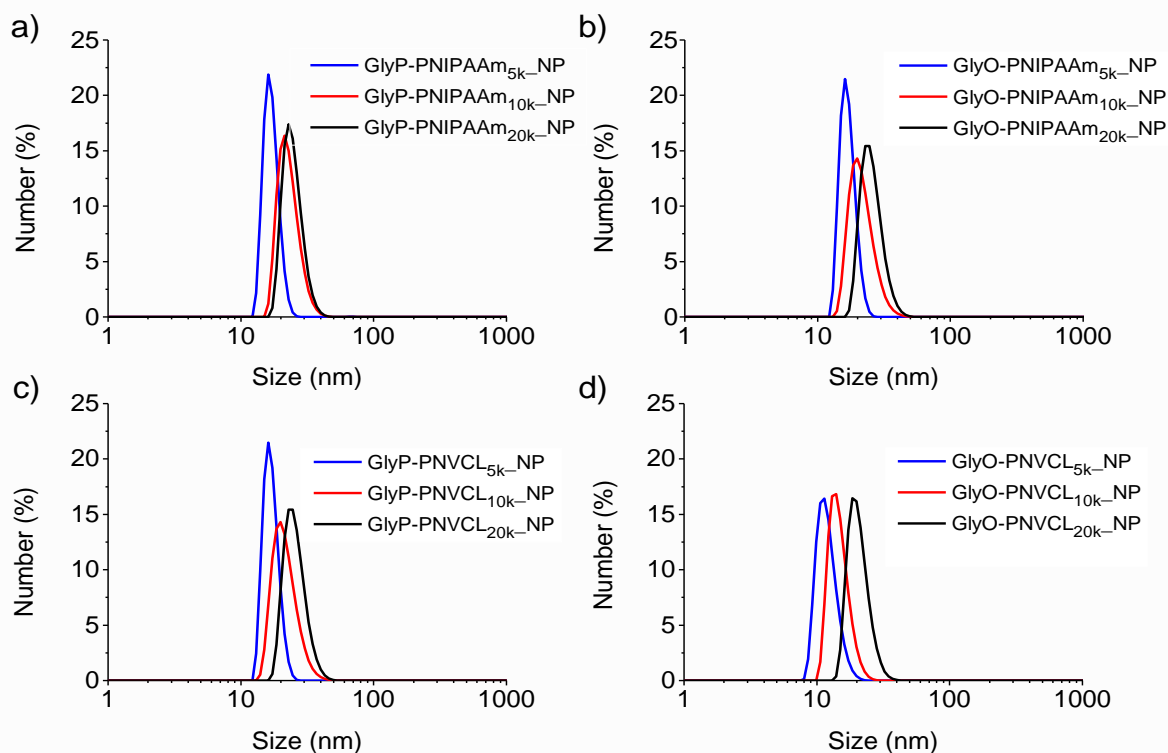


Figure 30. Number size distribution measured by MADLS (PBS, 25 °C, $C = 1$ mg mL⁻¹), a) GlyP-PNIPAAm_NP, b) GlyO-PNIPAAm_NP, c) GlyP-PNVCL_NP, d) GlyO-PNVCL_NP.

The use of DLS in combination with polarization filters allows for detailed characterization of the shape of particles in solution. Briefly, the shape is determined by two measurements, one using vertically polarized light and the other with horizontally polarized light. If the values of both measures overlap, there are spherical objects in the analyzed solution. For all samples, the plots obtained from the vertical and horizontal traces were

superposed, indicating the formation of spherical particles. Typical results for selected PNIPAAm- and PNVCL-based nanoparticles are shown in Figure 31.

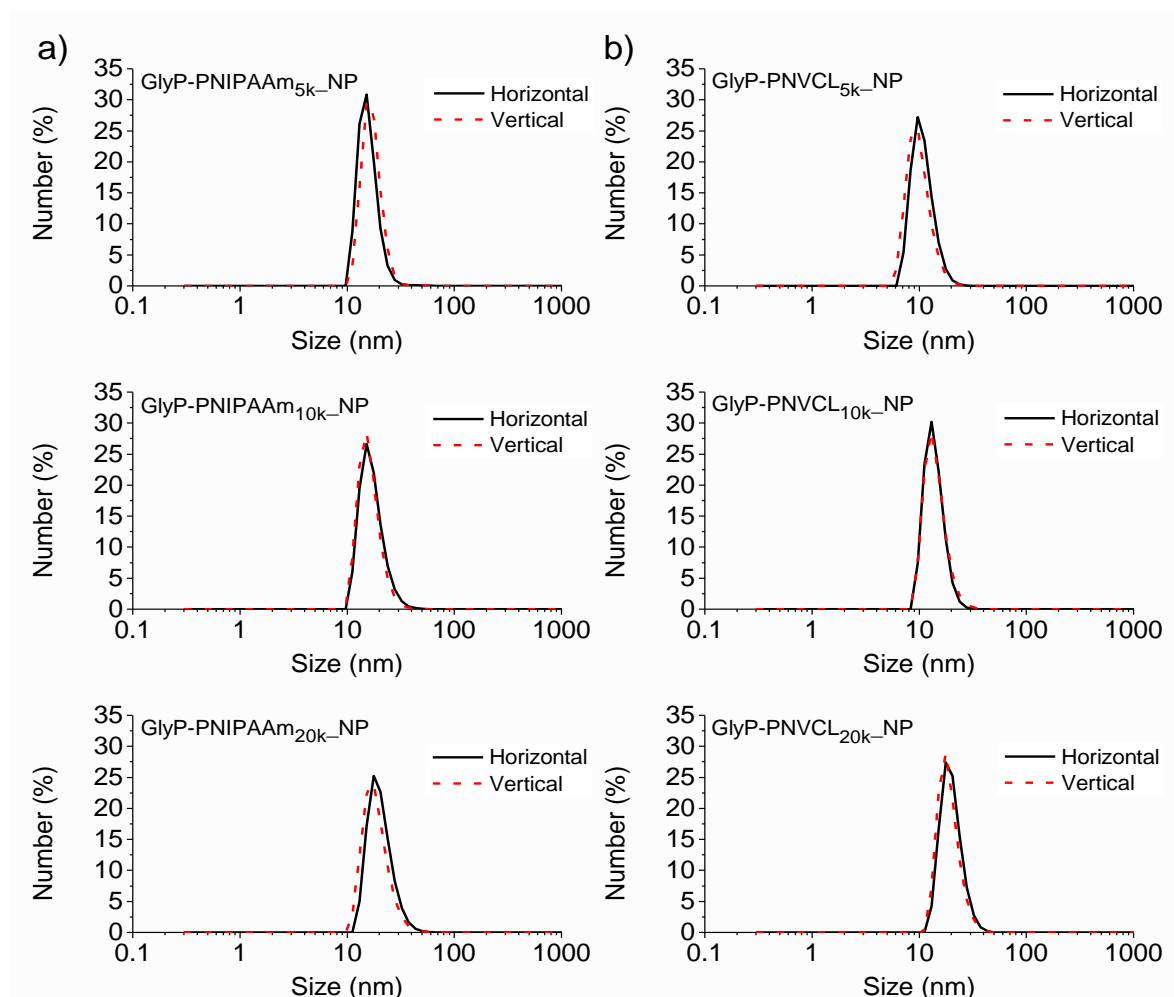


Figure 31. Determination of the shape of polymeric nanoparticles using horizontal and vertical measurements: a) GlyP-PNIPAAm_NP and b) GlyP-PNVCL_NP (PBS, 25 °C, $C = 1 \text{ mg mL}^{-1}$).

The morphology of polymeric structures in an aqueous solution was also examined by transmission electron microscopy (TEM) imaging. For this purpose, a drop of aqueous PNPs solution was applied to the copper grid. The grid with the sample was then immersed in liquid nitrogen and dried under a vacuum. Representative TEM images are shown in Figure 32. In images labeled as a) and b), the particles displayed spherical shapes but overlapped, forming larger aggregates. This overlap is probably related to the sample preparation methodology. Because of the limited number of nanoparticles in these images, it was impossible to perform reliable statistical calculations. For sample c), the images show homogeneous and well-dispersed nanoparticles with a diameter of $10.72 \pm 0.33 \text{ nm}$. As expected, the size obtained from TEM was lower than that obtained from MADLS measurement (14.45 ± 0.26). This discrepancy can be attributed to the fact that MADLS

measures the hydrodynamic radius of particles, which can be influenced by solvation layers in suspension, whereas TEM directly images dried particles.³¹⁶

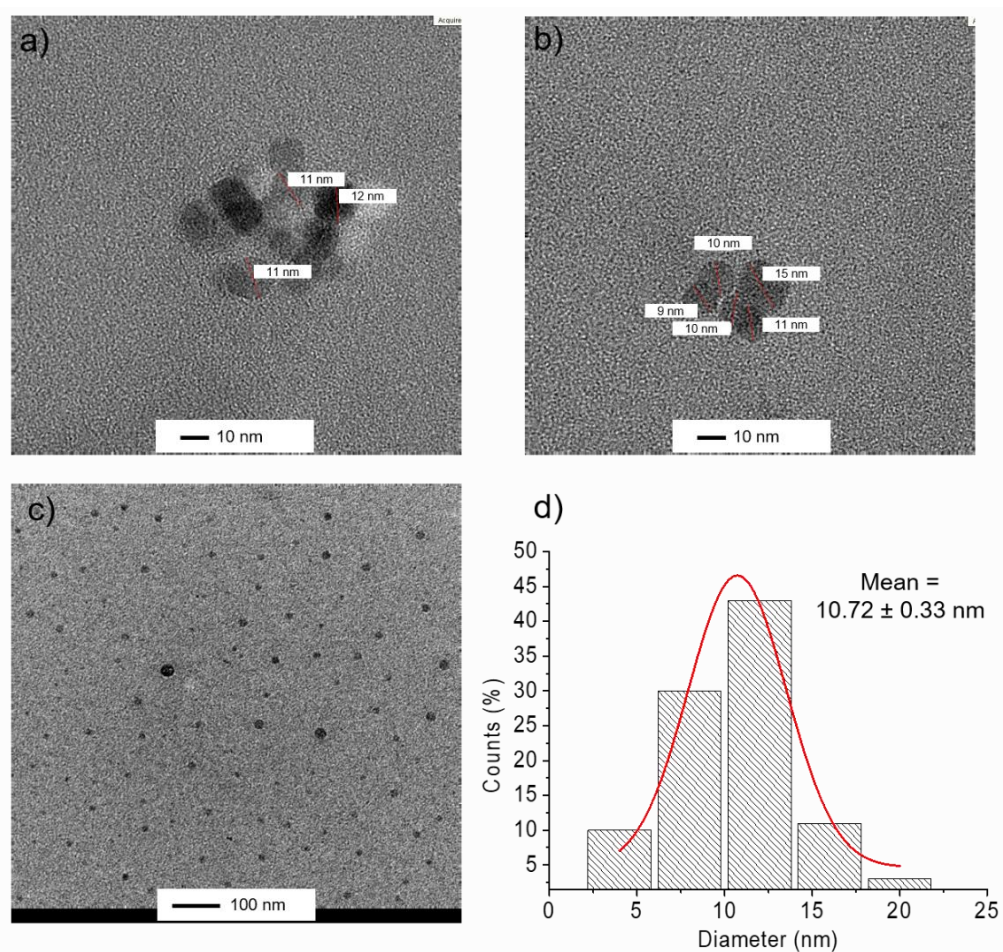


Figure 32. TEM images of selected polymeric nanoparticles in two different magnitudes: a) GlyP-PNIPAAm_{20k}_NP, b) GlyO-PNVCL_{5k}_NP, c) GlyO-PNVCL_{10k}_NP, d) distribution of measured diameter for GlyO-PNVCL_{10k}_NP.

PNIPAAm and PNVCL are thermoresponsive polymers with a lower critical solution temperature (LCST) in an aqueous solution. The cloud point temperature (T_{CP}) is a crucial parameter that indicates the onset of phase separation in polymer solutions. Another closely related term is the aggregation temperature, commonly denoted T_{Agg} , which explicitly refers to the onset of polymer aggregation. Various instrumental methods are available for measuring these temperatures, including UV-Vis spectrophotometry, DLS (dynamic light scattering), DSC (differential scanning calorimetry), and NMR (nuclear magnetic resonance).¹⁵⁹ Among these methods, the most commonly used are UV-Vis and DLS. UV-Vis spectrophotometry, coupled with a Peltier system for controlled temperature changes, is employed to monitor the light transmittance of the polymer solution, thus establishing T_{CP} .

The maximum light transmittance corresponds to the complete solution transparency, indicating full polymer solubility, while the minimum transmittance indicates turbidity. On the other hand, DLS enables a more sensitive determination of the phase transition onset by detecting aggregates even before solution clouding or significant changes in UV-Vis signals occur, marking T_{Agg} . Below this temperature, polymer chains exist as dissolved coils with a small hydrodynamic radius. The coil-to-globule transition leads to dehydration, collapse, and aggregation of the polymer chain into larger globules.^{159,160}

At first, the cloud point temperatures were determined by turbidimetry in water (Table 8). For polymeric nanoparticles based on PNIPAAm, the cloud point temperature increased with the increasing length of the hydrophilic block, which involves a change in the relationship between the hydrophilic/hydrophobic of the polymer. This finding is consistent with existing literature, as exemplified by results from cholesterol end-functionalized PNIPAAms.²⁹⁰ Conversely, for PNPs incorporating PNVCL, the polymer length also affected T_{CP} , especially in series terminated with oleic moieties. Within the GlyP-PNVCL series, the sample with a molar mass of 5 kg mol^{-1} had the lowest T_{CP} ($33 \text{ }^{\circ}\text{C}$), whereas the samples with a molar mass of 10 and 20 kg mol^{-1} showed identical T_{CP} values. The influence of the lipid moiety was of the most significant importance for PNPs containing polymers of the lowest molar mass (5 kg mol^{-1}). Specifically, the sample with the palmitic moiety exhibited a T_{CP} of $1.5 \text{ }^{\circ}\text{C}$ higher than its oleic acid derivative counterpart. Although these phase transition studies were conducted under salt-free conditions, it is essential to consider their effects when aiming for biomedical applications with these thermoresponsive polymers. Therefore, T_{CP} and T_{Agg} were measured in PBS (pH ~ 7.4), where the osmolarity and ion concentrations mimic those of the human body.

Turbidimetric measurements indicated that homopolymers terminated with diglycerides had a lower T_{CP} in PBS than in water. In contrast, pure PNIPAAm and PNVCL showed higher T_{CP} values under salt conditions than in water. With no surprise, the T_{Agg} determined from DLS manifested at temperatures lower than the cloudiness for all samples, with a temperature difference ranging between 0.5 to $2 \text{ }^{\circ}\text{C}$ (Figure 33). Diglyceride-terminated PNIPAAms and PNVCLs consistently displayed lower T_{CP} s in PBS than bare PNIPAAm and PNVCL procured through radical polymerization. In the context of *N*-isopropylacrylamide polymers, the differences in T_{CP} were around $2\text{--}3 \text{ }^{\circ}\text{C}$. For poly(*N*-vinylcaprolactam), the variance exceeded $10 \text{ }^{\circ}\text{C}$. This phenomenon can be explained by the hydrophobic nature of the end-groups, which tend to lower the T_{CP} .¹⁵⁶

For particles based on PNIPAAm, T_{CP} in PBS showed a behavior similar to that in pure water, and the values increased with increasing hydrophobic/hydrophilic ratio and molar mass. However, for PNVCL-based particles, the influence of HLB on the T_{CP} was less pronounced. As mentioned earlier in this work, unlike PNIPAAm, PNVCL exhibits a "classical" Flory-Huggins thermoresponsive phase separation behavior. Consequently, its LCST value depends on the length of the polymer chain as well as its concentration.^{284,306}

Table 8. Physicochemical parameters of the studied homopolymers.

Polymer	Size by number ^a (nm)	T_{CP} ^b (°C)	T_{CP} ^c (°C)	T_{Agg} ^d (°C)
PNIPAAm	-	34.0 ± 0.5	34.5 ± 0.5	31 ± 1
GlyP-PNIPAAm _{2k} _NP	-	-	-	-
GlyP-PNIPAAm _{5k} _NP	17.20 ± 0.41	32.0 ± 0.5	31.0 ± 0.5	30 ± 1
GlyP-PNIPAAm _{10k} _NP	22.42 ± 0.60	33.5 ± 0.5	31.0 ± 0.5	31 ± 1
GlyP-PNIPAAm _{20k} _NP	25.08 ± 0.44	35.5 ± 0.5	33.0 ± 0.5	31 ± 1
GlyO-PNIPAAm _{2k} _NP	-	-	-	-
GlyO-PNIPAAm _{5k} _NP	16.96 ± 0.37	30.5 ± 0.5	30.0 ± 0.5	30 ± 1
GlyO-PNIPAAm _{10k} _NP	20.50 ± 1.16	33.5 ± 0.5	31.5 ± 0.5	31 ± 1
GlyO-PNIPAAm _{20k} _NP	23.96 ± 0.36	35.0 ± 0.5	32.5 ± 0.5	31 ± 1
PNVCL	-	42.0 ± 0.5	44.5 ± 0.5	41 ± 1
GlyP-PNVCL _{2k} _NP	-	-	-	-
GlyP-PNVCL _{5k} _NP	12.44 ± 0.12	33.0 ± 0.5	32.5 ± 0.5	31 ± 1
GlyP-PNVCL _{10k} _NP	15.23 ± 0.52	34.5 ± 0.5	32.5 ± 0.5	32 ± 1
GlyP-PNVCL _{20k} _NP	20.14 ± 0.47	34.5 ± 0.5	33.5 ± 0.5	33 ± 1
GlyO-PNVCL _{2k} _NP	-	-	-	-
GlyO-PNVCL _{5k} _NP	11.62 ± 0.30	34.0 ± 0.5	32.0 ± 0.5	31 ± 1
GlyO-PNVCL _{10k} _NP	14.45 ± 0.26	35.0 ± 0.5	34.5 ± 0.5	34 ± 1
GlyO-PNVCL _{20k} _NP	19.34 ± 0.28	36.5 ± 0.5	33.5 ± 0.5	32 ± 1

Notes: ^adetermined by MADLS (PBS, 25 °C, $C = 1 \text{ mg mL}^{-1}$), ^bcloud point temperature determined by turbidimetry in water (25 °C, $C = 0.5 \text{ mg mL}^{-1}$), ^ccloud point temperature determined by turbidimetry in PBS (25 °C, $C = 0.5 \text{ mg mL}^{-1}$), ^daggregation temperature determined by DLS (PBS, 25 °C, $C = 0.5 \text{ mg mL}^{-1}$).

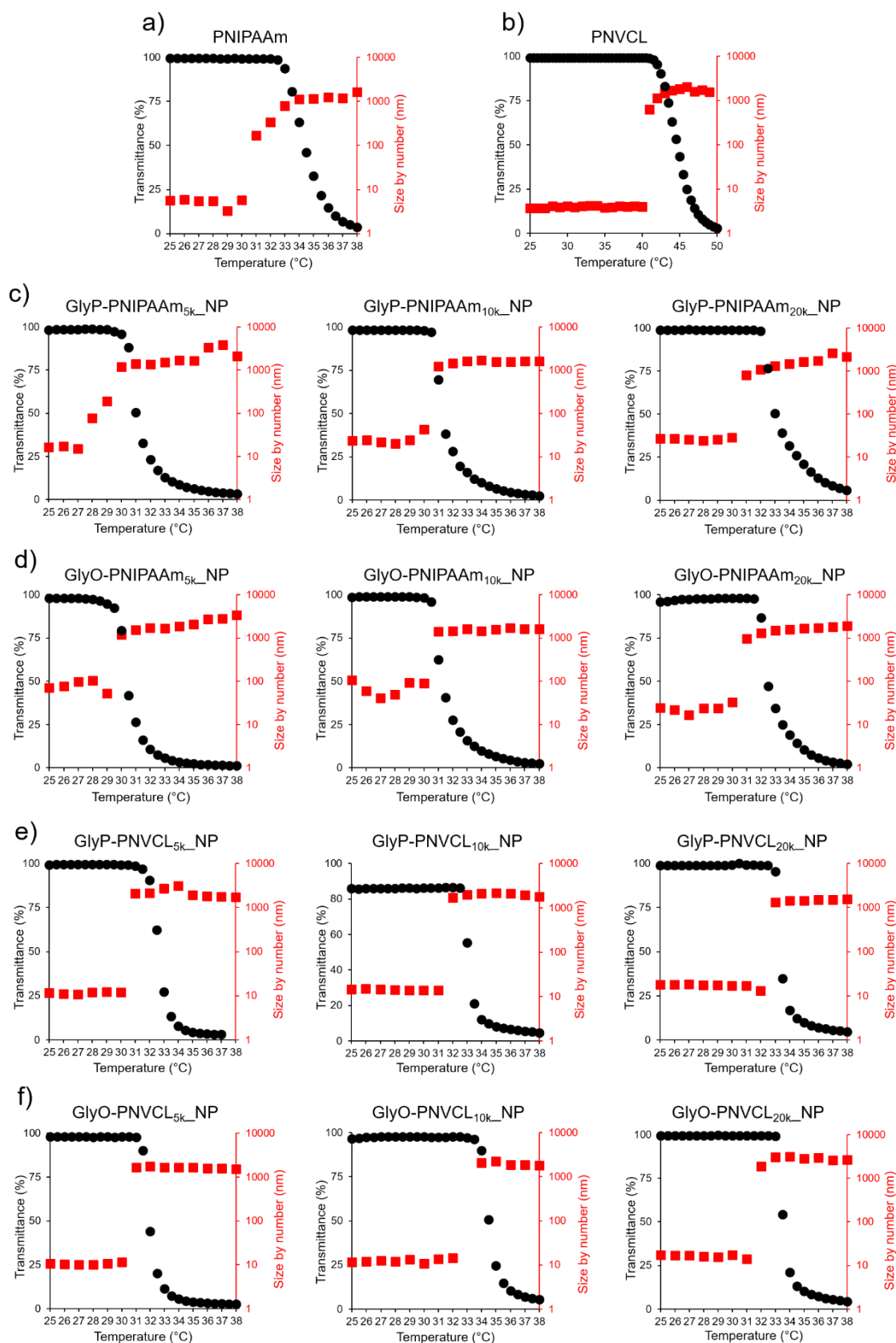


Figure 33. Evolution of transmittance measured by turbidimetry and number size distribution measured by DLS as a function of temperature for polymers: a) PNIPAAm, b) PNVCL, and polymeric nanoparticles, c) GlyP-PNIPAAm_{NP}, d) GlyO-PNIPAAm_{NP}, e) GlyP-PNVCL_{NP}, f) GlyO-PNVCL_{NP} (PBS, 25 °C, $C = 0.5 \text{ mg mL}^{-1}$).

In cooperation with the Medical University of Białystok, polymeric nanoparticles were tested regarding their biological properties. The research focused on the interaction of PNPs with red blood cells and representatives of immune cells (monocyte/macrophage THP-1 cells). The results showed that the particles were non-hemolytic and non-toxic. None of the tested compounds disrupted the membranes of red blood cells (hemolysis rates were lower than 5%) and did not affect the metabolic activity of THP-1 cells.

Based on these studies, polymers consisting of a diglyceride moiety and a thermoresponsive block are the promising basis for designing drug delivery systems. More information about biological studies can be found in the article published by our group.¹⁹⁸

3.2. Polymeric nanoparticles based on copolymers with DGs in the side chains

Polymeric nanoparticles based on copolymers (PGlyP-*b*-PNIPAAm, PGlyO-*b*-PNIPAAm, PGlyP-*b*-PNVCL, and PGlyO-*b*-PNVCL), as previously mentioned, were prepared by the nanoprecipitation method (Figure 29a). Polymers were dissolved in THF, added dropwise to water, dialyzed, and freeze-dried. After lyophilization, the nanoparticles were redispersed in water or PBS at a concentration of 1 mg mL⁻¹ and subsequently analyzed by multiangle dynamic light scattering (MADLS). Compared to PNPs based on homopolymers, the colloidal stability of polymeric nanoparticles containing several diglyceride repeat units was investigated. The samples were analyzed after 24 hours, 7 days, and 30 days. The colloidal stability of all solutions, regardless of the solvent used, was excellent, as indicated by the correlograms, which demonstrated high similarity even after one month of storage (Figure 34). The particle size distributions of the nanoparticle suspensions are shown in Table 9.

Table 9. Size distribution of polymeric nanoparticles in water or PBS (25 °C, $C = 1 \text{ mg mL}^{-1}$).

Polymer	H ₂ O 24 h	H ₂ O 7 days	H ₂ O 30 days	PBS 24 h	PBS 7 days	PBS 30 days
PGlyP- <i>b</i> -PNIPAAm_NP	34.25 ± 1.59	33.04 ± 0.38	31.36 ± 2.78	34.40 ± 1.76	30.94 ± 1.95	31.36 ± 0.19
PGlyO- <i>b</i> -PNIPAAm_NP	42.11 ± 0.64	39.93 ± 3.97	39.84 ± 1.74	32.59 ± 1.33	30.94 ± 0.96	37.55 ± 0.85
PGlyP- <i>b</i> -PNVCL_NP	22.34 ± 1.34	34.15 ± 1.40	29.48 ± 0.78	27.41 ± 1.90	28.21 ± 1.89	31.61 ± 0.79
PGlyO- <i>b</i> -PNVCL_NP	24.00 ± 0.90	23.04 ± 1.31	22.34 ± 0.99	23.20 ± 1.10	23.15 ± 3.73	26.40 ± 1.25

The shape of the obtained particles was determined using backscattering DLS measurements with vertically and horizontally polarized light. The curves obtained from both measurements overlapped, indicating the formation of spherical particles (Figure 34).

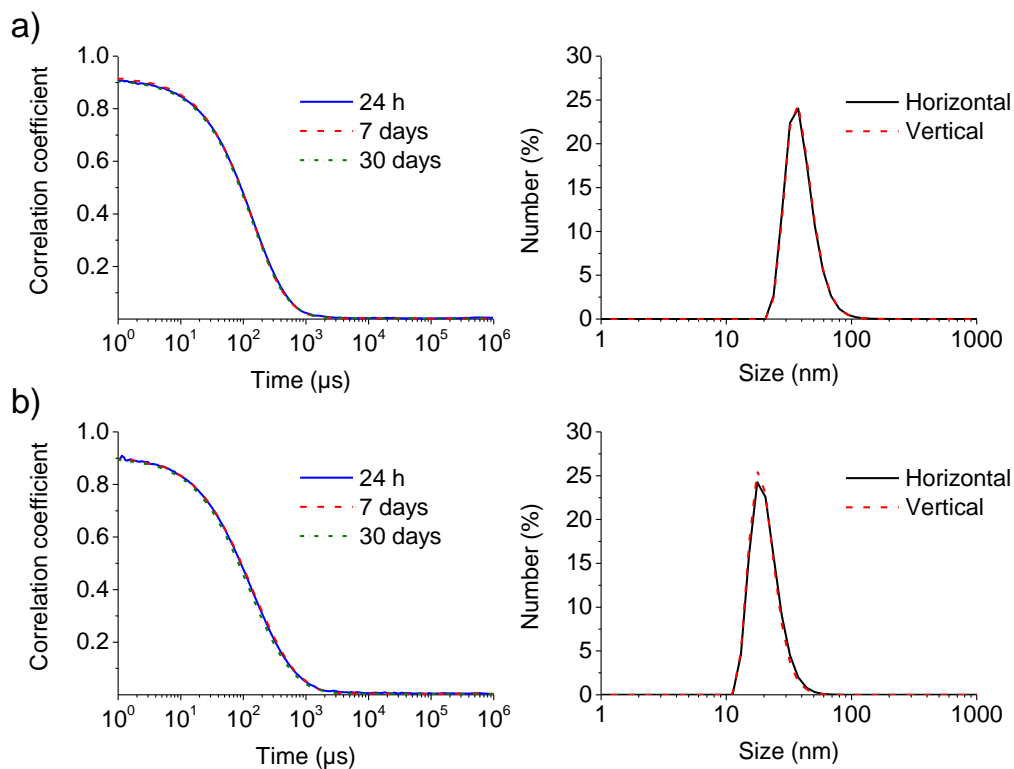


Figure 34. Correlograms obtained from DLS experiments with a scattering angle of 173 ° (PBS, 25 °C, $C = 1 \text{ mg mL}^{-1}$) and horizontal and vertical measurements for polymeric nanoparticles a) PGlyP-*b*-PNIPAAm and b) PGlyO-*b*-PNVCL.

TEM imaging confirmed the morphology of polymeric structures (Figure 35). The monodisperse, spherical shapes were observed.

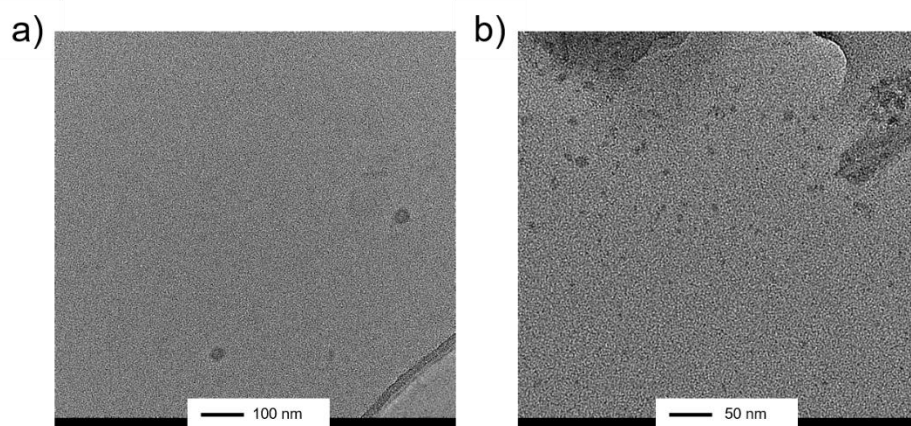


Figure 35. TEM images for a) PGlyP-*b*-PNIPAAm_NP and b) PGlyO-*b*-PNIPAAm_NP.

3.2.1. Drug encapsulation and characterization of drug-loaded nanoparticles

The ability to form polymeric nanoparticles, combined with the long-term stability of the systems at pH 7.4, makes them promising candidates for further biomedical applications as drug carriers. Two anticancer drugs with low water solubility, doxorubicin (DOX) and tamoxifen (TAM), were encapsulated into polymeric nanoparticles to explore this potential. As mentioned earlier in this work, the encapsulation strategy not only enhances the therapeutic index of drugs but also addresses challenges such as solubility and side effects, making treatments more efficient and patient-friendly.

The structures of doxorubicin and tamoxifen are depicted in Figure 36. DOX is an anthracycline drug known for its ability to intercalate DNA, which subsequently inhibits replication and transcription processes, leading to cell death.³¹⁷ It is commonly used in the treatment of various cancers, including breast, prostate, liver, and stomach cancers. However, the main challenges associated with doxorubicin usage are its cardiotoxicity and toxicity on non-cancerous cells.³¹⁸ Tamoxifen, on the other hand, is a selective estrogen receptor modulator (SERM) that primarily acts on breast tissue. It binds to estrogen receptors, inhibiting the growth of hormone-sensitive tumor cells.³¹⁹ The main issues related to TAM are its hydrophobic nature and specific side effects, such as an increased risk of endometrial cancer and thromboembolic disorders.^{319–321}

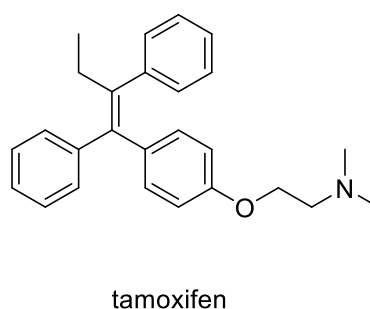
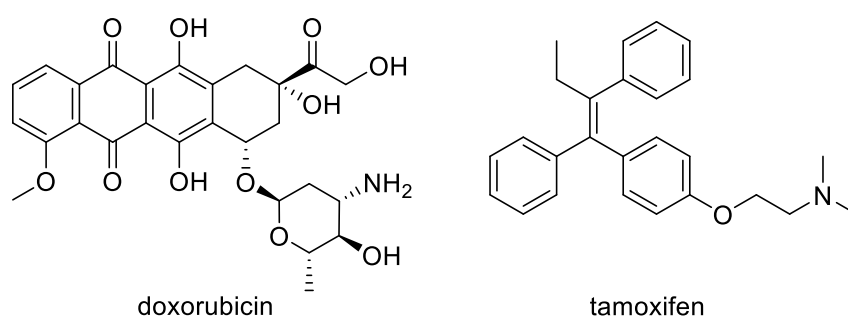


Figure 36. The structure of doxorubicin and tamoxifen.

Doxorubicin and tamoxifen were incorporated into polymeric nanoparticles using the nanoprecipitation method (Figure 29b). During this process, the drug is entrapped by the hydrophobic segment of the copolymers.

The quantity of doxorubicin encapsulated in polymeric nanoparticles was determined using the spectrofluorometric method based on the standard curve equation (shown in the experimental part).^{134,322} The content of tamoxifen in PNPs was determined by high-performance liquid chromatography (HPLC). The values were converted to the

concentrations of DOX and TAM contained in the 1 mg mL⁻¹ solution of the polymers obtained after redispersion in PBS. The concentrations of the encapsulated drugs are present in Table 10. The amount of DOX encapsulated in PNPs ranged from 0.164 to 0.425 μM mL⁻¹. The concentration of TAM encapsulated was markedly higher than that of DOX, with values ranging from 30.46 to 38.01 μM mL⁻¹.

To assess the efficiency of drug encapsulation, the drug loading efficiency (DLE) and drug loading content (DLC) were calculated for both DOX and TAM in the respective polymeric carriers. DLE and DLC are crucial parameters in the design, evaluation, and optimization of drug delivery systems. Drug loading efficiency (often called encapsulation efficiency)³²³ represents the percentage of drug successfully incorporated into the drug delivery system compared to the total amount of drug initially used during the formulation process. On the other hand, drug loading content describes the amount of drug present in the drug delivery system relative to the total weight of the drug carrier. The DLE and DLC can be calculated according to equations (1) and (2).

$$\text{DLE (\%)} = \frac{\text{Weight of loaded drug}}{\text{Initial weight of drug used for loading}} \times 100 \quad (1)$$

$$\text{DLC (\%)} = \frac{\text{Weight of loaded drug}}{\text{Total weight of drug-loaded system}} \times 100 \quad (2)$$

The DLE and DLC values for all polymeric nanoparticles are presented in Table 10. For example, for PGlyP-*b*-PNIPAAm_NPDOX, the DLE for DOX was 0.13%, indicating that only a small fraction of the added DOX was successfully encapsulated. The DLC for DOX in the same polymeric nanoparticle was 0.009%. A similar trend was observed for all copolymers containing doxorubicin. On the contrary, TAM exhibited much higher DLE and DLC values in all polymeric nanoparticles. For example, PGlyP-*b*-PNIPAAm_NPTAM showed a DLE of 12.10 % and a DLC of 1.30%.

These observations highlight the role of the carrier structure in drug encapsulation and the necessity for the customization of carriers for different drugs. The compatibility between the physicochemical properties of the drugs and the structure of the carriers significantly influences the stability and distribution of the drugs within the polymeric system.^{324,325} Additionally, it is also important to note that the method used for drug loading^{111,326} along with external factors such as temperature,³²⁷ pH,^{328,329} ionic strength,³³⁰ and mechanical agitation during the encapsulation process can also affect the overall efficiency of drug loading^{331,332}.

The obtained drug-loaded nanoparticles were further analyzed by MADLS. The size of drug-loaded polymeric nanoparticles after 7 days was slightly larger than their blank counterparts, as presented in Table 10. This can be explained by increasing the inner space of the nanoparticles after drug encapsulation.³³³ Notably, the hydrodynamic diameters of the drug-loaded nanoparticles ranged from 28.70 ± 1.11 to 44.06 ± 3.38 nm, making them ideally suited for drug delivery applications. Furthermore, the morphology of the particles remained spherical after drug encapsulation, as evidenced by DLS measurements. Zeta potential was measured by electrophoretic light scattering (ELS). The observed values for empty and drug-loaded polymeric nanoparticles were negative in the range of -3.22 to -7.32 mV. Regarding the surface charge, it is reported that neutral and slightly negative particles (defined as having ζ potential of -10 to +10 mV) have the longest half-lives in circulation.^{118,127,129}

In the following research step, the cloud point temperatures (T_{CP}) and the aggregation temperature (T_{Agg}) of empty and drug-loaded nanoparticles were investigated in PBS at a concentration of 0.5 mg mL^{-1} . The results are shown in Table 10 and Figure 37. The phase separation temperatures for all nanoparticles formed from copolymers were lower than those of pure PNIPAAm or PNVCL. Compared to end-capped diglyceride PNVCLs and PNIPAAms presented in the previous section of this work, incorporating diglycerides as repeating units into the polymer structure did not significantly change the value of the cloud point temperatures.

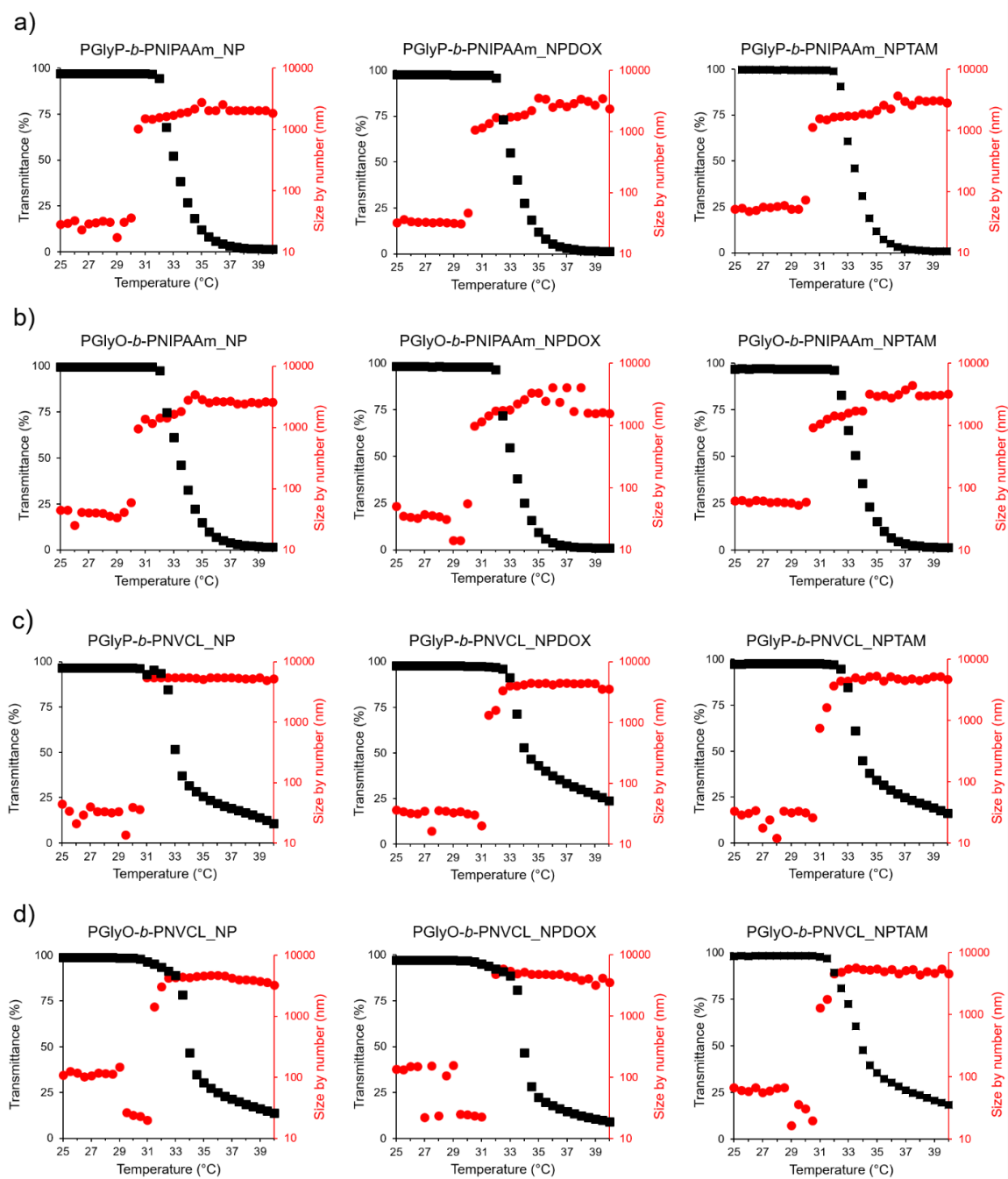


Figure 37. Evolution of transmittance measured by turbidimetry and number size distribution measured by DLS as a function of temperature for empty and drug-loaded polymeric nanoparticles (PBS, 25 °C, $C = 0.5 \text{ mg mL}^{-1}$).

Table 10. Physicochemical parameters of the studied polymers.

Polymer	Amount of DOX ($\mu\text{M mL}^{-1}$)	DLE (%)	DLC (%)	Amount of TAM ($\mu\text{M mL}^{-1}$)	DLE (%)	DLC (%)	Zeta potential ^a (mV)	Size by number ^b (nm)	T_{CP}^c (°C)	T_{Agg}^d (°C)
PNIPAAm	-	-	-	-	-	-	-	-	34.5 ± 0.5	31.0 ± 0.5
PGlyP- <i>b</i> -PNIPAAm_NP	-	-	-	-	-	-	-6.30 ± 0.10	30.94 ± 1.95	33.0 ± 0.5	30.5 ± 0.5
PGlyP- <i>b</i> -PNIPAAm_NPDOX	0.164	0.130	0.009	-	-	-	-5.19 ± 0.51	41.56 ± 1.38	33.5 ± 0.5	30.5 ± 0.5
PGlyP- <i>b</i> -PNIPAAm_NPTAM	-	-	-	34.60	12.10	1.30	-3.40 ± 0.45	41.43 ± 3.34	33.5 ± 0.5	30.5 ± 0.5
PGlyO- <i>b</i> -PNIPAAm_NP	-	-	-	-	-	-	-7.32 ± 0.13	30.94 ± 0.96	33.5 ± 0.5	30.5 ± 0.5
PGlyO- <i>b</i> -PNIPAAm_NPDOX	0.255	0.182	0.015	-	-	-	-5.32 ± 0.51	37.47 ± 1.80	33.5 ± 0.5	30.5 ± 0.5
PGlyO- <i>b</i> -PNIPAAm_NPTAM	-	-	-	30.46	10.40	1.10	-3.86 ± 0.56	42.18 ± 2.14	33.5 ± 0.5	30.5 ± 0.5
PNVCL	-	-	-	-	-	-	-	-	44.5 ± 0.5	41.0 ± 0.5
PGlyP- <i>b</i> -PNVCL_NP	-	-	-	-	-	-	-3.22 ± 0.18	28.21 ± 1.89	33.0 ± 0.5	31.0 ± 0.5
PGlyP- <i>b</i> -PNVCL_NPDOX	0.268	0.199	0.016	-	-	-	-4.67 ± 0.36	44.06 ± 3.38	34.0 ± 0.5	31.5 ± 0.5
PGlyP- <i>b</i> -PNVCL_NPTAM	-	-	-	36.15	11.95	1.30	-6.23 ± 0.16	32.19 ± 0.67	33.5 ± 0.5	31.0 ± 0.5
PGlyO- <i>b</i> -PNVCL_NP	-	-	-	-	-	-	-3.67 ± 0.39	23.15 ± 3.73	34.0 ± 0.5	31.5 ± 0.5
PGlyO- <i>b</i> -PNVCL_NPDOX	0.425	0.282	0.025	-	-	-	-7.09 ± 0.66	28.70 ± 1.11	34.0 ± 0.5	31.5 ± 0.5
PGlyO- <i>b</i> -PNVCL_NPTAM	-	-	-	38.01	12.30	1.30	-6.34 ± 0.55	28.87 ± 0.63	33.5 ± 0.5	31.0 ± 0.5

Notes: ^a determined by ELS (measured after 7 days, PBS, 25 °C, $C = 1 \text{ mg mL}^{-1}$), ^b determined by MADLS (measured after 7 days, PBS, 25 °C, $C = 1 \text{ mg mL}^{-1}$), ^c cloud point temperature determined by turbidimetry (PBS, 25 °C, $C = 0.5 \text{ mg mL}^{-1}$), ^d aggregation temperature determined by DLS (PBS, 25 °C, $C = 0.5 \text{ mg mL}^{-1}$).

3.2.2. Drug release study

This part of the work delves into analyzing the temperature-induced drug release from polymeric nanoparticles loaded with DOX and TAM. Understanding the release profile is important in optimizing drug delivery systems for effective therapies.

The small quantities of encapsulated doxorubicin made it impossible to determine the drug release profile accurately. However, it should be emphasized that both the TAM-loaded and DOX-loaded carriers were thoroughly purified by 24-hour dialysis. This step ensured the removal of unbound drugs from the PNPs. As a result, it was possible to focus exclusively on the drugs remaining encapsulated within the nanoparticles.

As presented in Figure 38, the drug release study of TAM was successfully conducted using the most versatile and popular dialysis method (DM).³³⁴ Predetermined amounts of tamoxifen-loaded nanoparticles were dissolved in water and transferred to dialysis bags. The dialysis bags were immersed in beakers containing release medium (water) and subjected to agitation using a magnetic stirrer. The drug release experiments were conducted at a constant temperature of 37 °C, which is above the phase transition temperature of the polymers and closely simulates human body conditions. At specific time intervals (5, 15, 30, 60, 120, 240, and 1440 min), the dialysis membranes were removed from the release medium, and the release medium was lyophilized and further analyzed. The concentration of tamoxifen released from the nanoparticles was quantified using high-performance liquid chromatography (HPLC).

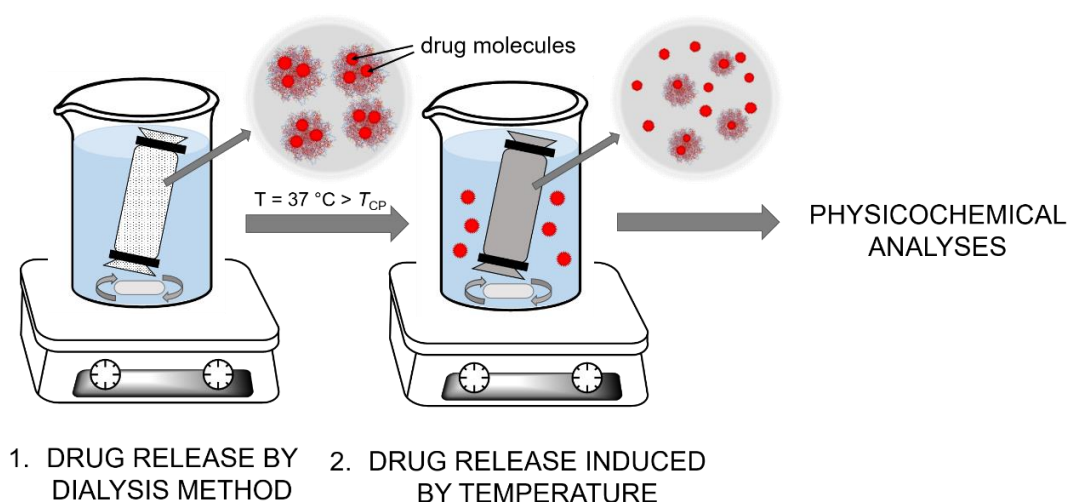


Figure 38. Schematic representation of temperature-induced drug release.

The resulting drug release profiles are demonstrated in Figure 39. The results revealed the controlled release of TAM from polymeric nanoparticles. An initial burst release was noted in the first 60 minutes, attributed to the phase transition behavior of PNIPAAm or PNVCL. This led to the collapse and shrinkage of the polymeric nanoparticles, facilitating drug diffusion. During the early time points (5 and 15 minutes), a slight variation in the initial release rate was observed among different nanoparticles. PNVCL-based nanoparticles exhibited a more rapid initial release compared to those based on PNIPAAm. As time progressed, all formulations showed a similar pattern of release. In all cases, approximately 60% of the drug was released in 240 minutes. The data also indicated no significant increase in TAM release after 24 hours. Approximately 40% of the encapsulated drug in the tested systems remained attached to the polymeric structure.

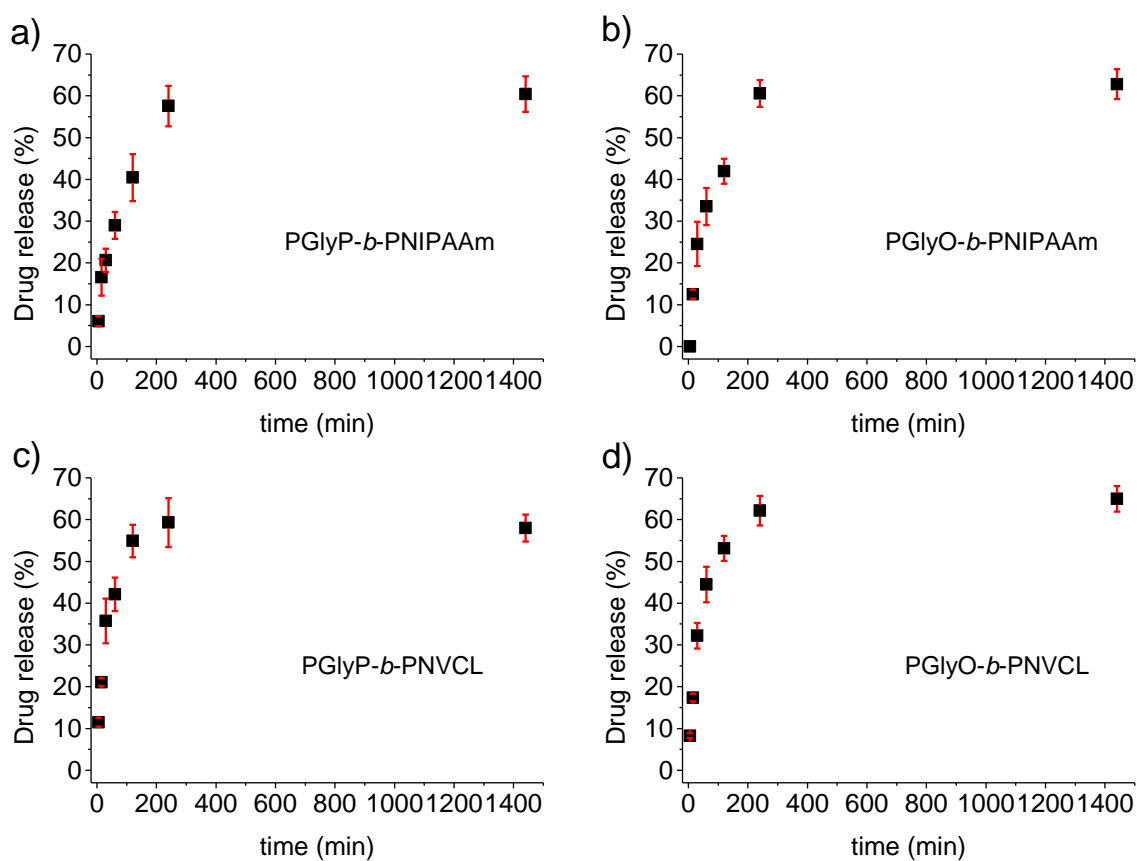


Figure 39. Release profiles of tamoxifen from thermoresponsive polymeric nanoparticles: a) PGlyP-*b*-PNIPAAm_NPTAM, b) PGlyO-*b*-PNIPAAm_NPTAM, c) PGlyP-*b*-PNVCL_NPTAM, d) PGlyO-*b*-PNVCL_NPTAM.

3.2.3. Biological studies

Polymeric nanoparticles, empty and DOX-loaded, were tested regarding their biological properties. The experiments were carried out at the Medical University of Bialystok. Human RBC cells, monocytic/macrophage, myocardial cells, and two types of human breast cancer cells were treated with varying doses of empty and drug-loaded PNPs. The study sought to examine the hemocompatibility, impact on cell viability, and anticancer potential of polymeric nanoparticles.

Regarding hemolysis, both the bare and DOX-loaded PNPs were found to be non-hemolytic, exhibiting only about 1% hemolysis. This is vital to prevent severe hematological complications, such as acute immune hemolytic anemia (AIHA), during anticancer treatments.³³⁵ Further evaluations revealed no significant activity against THP-1 monocytic cells and H9c2(2-1) cardiomyocyte cells.

Given that breast cancer remains one of the most frequently diagnosed cancers in women worldwide, the efficacy of these PNPs in drug delivery was studied using two types of breast cancer cells: estrogen-dependent, noninvasive MCF-7 cells and more aggressive, hormone-independent MDA-MB-231 cells. Notably, the cytotoxic effect on cancer cell lines varied based on the chemical composition of the carriers (type of diglyceride and the thermoresponsive segment). The findings revealed that the empty PNPs comprising the PGlyP block did not manifest a cytotoxic impact on both cell lines at concentrations of 0.05 and 0.1 mg mL⁻¹, with about 90% cell viability observed. PGlyO-containing PNPs had a significant cytotoxic effect on MCF-7 cells. There was a notable decrease in viable cells when treated with PGlyO-*b*-PNVCL_NP compared to PGlyO-*b*-PNIPAAm_NP.

The addition of DOX to the PNPs significantly fortified their cytotoxic effect. The viability of MCF-7 cells treated with DOX-loaded carriers showed a substantial decrease, by 40–55% and 70–85%, respectively, at concentrations of 0.1 and 0.5 mg mL⁻¹, compared to untreated control cells. Polymeric nanoparticles based on PNIPAAm manifested a significant reduction in the viability of MCF-7 cells at a concentration of 0.1 mg mL⁻¹ and for PNVCL-based carriers at 0.5 mg mL⁻¹.

When analyzing the behavior against the more aggressive MDA-MB-231 cell line, all DOX-loaded particles revealed markedly better efficacy compared to their empty counterparts. The cytotoxic effects were concentration-dependent, except PGlyO-*b*-PNVCL_NPDOX. This suggests that lower concentrations of this carrier could be utilized while still maintaining efficacy. This is a crucial finding, as it highlights the potential to

minimize carrier dosage (and encapsulated drug), thus improving compatibility and reducing the risk of side effects.

The biological study also explored the mechanism of cell death induced by these polymeric nanoparticles. Evaluations were performed to determine whether treated cells underwent apoptosis (programmed cell death) or necrosis (unprogrammed cell death). The implications of inducing apoptosis versus necrosis in cancer treatment remain a subject of ongoing debate, as both pathways have distinct impacts on the body's immune system and overall cancer treatment efficacy.³³⁶ Bioluminescent-based assays demonstrated that both bare and DOX-loaded PNIPAAm-based PNPs induced significant apoptosis in treated cells. The impact of the diglyceride moiety on the induction of apoptosis was also studied, revealing a higher level of apoptotic cells after treatment with PNPs containing the palmitic moiety. Interestingly, carriers containing PNVCL segments were more potent in inducing necrotic cell death than those with PNIPAAm. Furthermore, the presence of DOX increased the ability to induce necrosis in estrogen-dependent cells. These findings suggest that the carriers' mechanism of action depends on the presence of the PNVCL or PNIPAAm block.

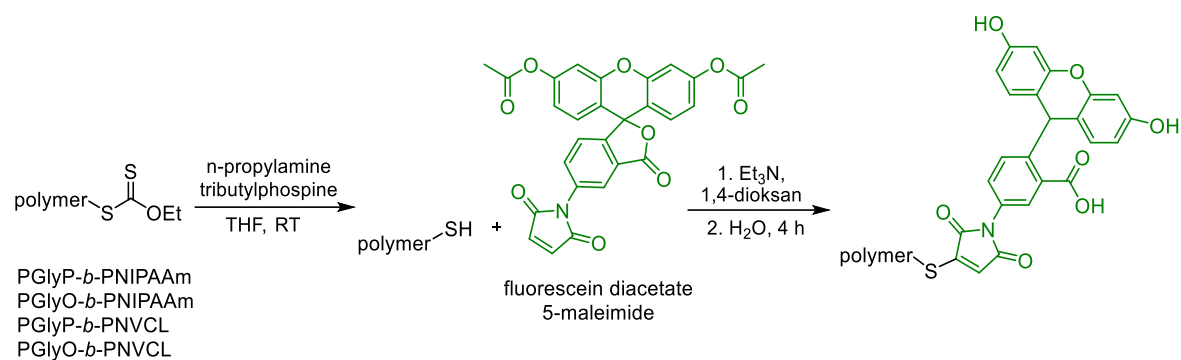
It was concluded that the phase transition property of the hydrophilic PNIPAAm and PNVCL-based copolymers below body temperature played a pivotal role in the drug delivery process. At body temperature, the hydrophilic segments of PNPs were in a dehydrated state, enhancing their hydrophobic character. This increased hydrophobicity promoted the disruption of the cancer cell membranes by the diglyceride-based block and the effective delivery of DOX directly into the cancer cells.

A deeper insight into the biological properties of empty and DOX-loaded nanoparticles can be found in the recently published manuscript by our group.³⁰

TAM-loaded nanoparticles are the focus of current research that examines their biological properties. The initial results of this research are very promising and will be detailed in a scientific publication.

3.2.4. The modification of the polymer chain-end with a fluorescent probe

In addition, a study was conducted to examine the internalization of PNPs by breast cancer cells. The ends of the polymer chains were modified with a fluorescent dye to investigate this specific behavior of polymeric nanoparticles in biological systems. As outlined in Scheme 15, a two-step postpolymerization labeling procedure was employed for this purpose.



Scheme 15. Modification of polymer chain-end with fluorescent dye.

First, the terminal dithiocarbonate group was reduced to the thiol moiety through a simple aminolysis using *n*-propylamine in the presence of tributylphosphine.⁷¹ The complete removal of the dithiocarbonate group was confirmed by UV-Vis spectroscopy by the disappearance of characteristic absorption at 280 nm. A representative UV-Vis spectrum is shown in Figure 40. The polymers terminated with the –SH group were subsequently modified with a fluorescein diacetate 5-maleimide through Michael addition.³³⁷ Following this, simple hydrolysis was performed to obtain the fluorescein-labeled polymers.^{338,339}

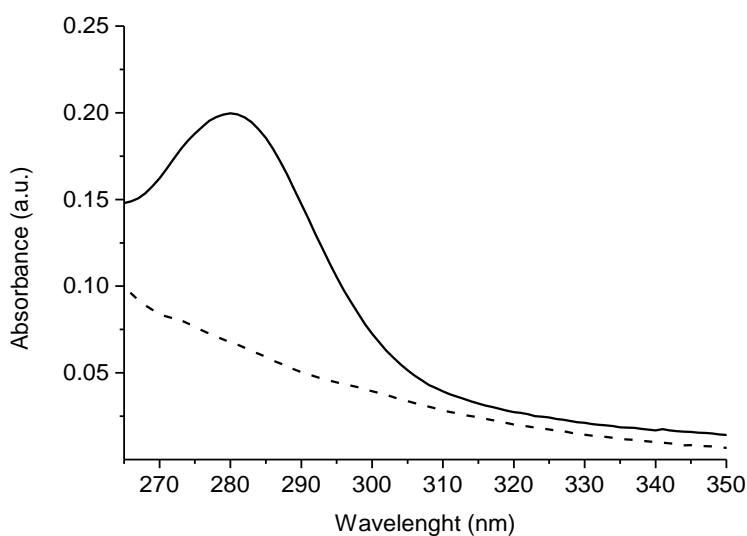


Figure 40. Representative of UV-Vis spectrum of polymer (PGlyP-*b*-PNIPAAm) terminated with dithiocarbonate (solid line) and reduced to thiol (dashed line).

Using the nanoprecipitation method, dye-labeled polymers were then utilized to fabricate lipid-polymer nanoparticles (empty and drug-loaded). The fluorescent properties of linear fluorescein-labeled polymers and their corresponding polymeric nanoparticles were investigated. Figure 41 shows that the fluorescence intensity was higher for all polymeric

nanoparticles. These results can be attributed to the compact structure of the nanoparticles, which facilitates the accumulation of dyes in a confined space.³⁴⁰

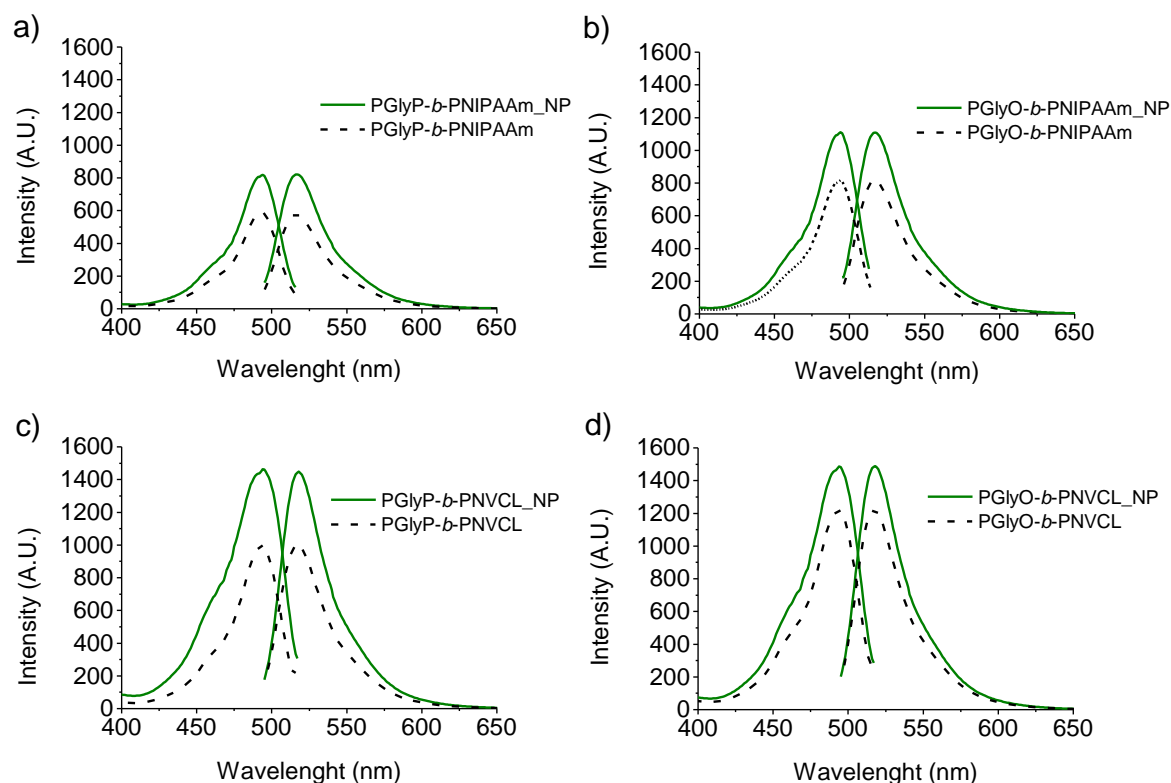
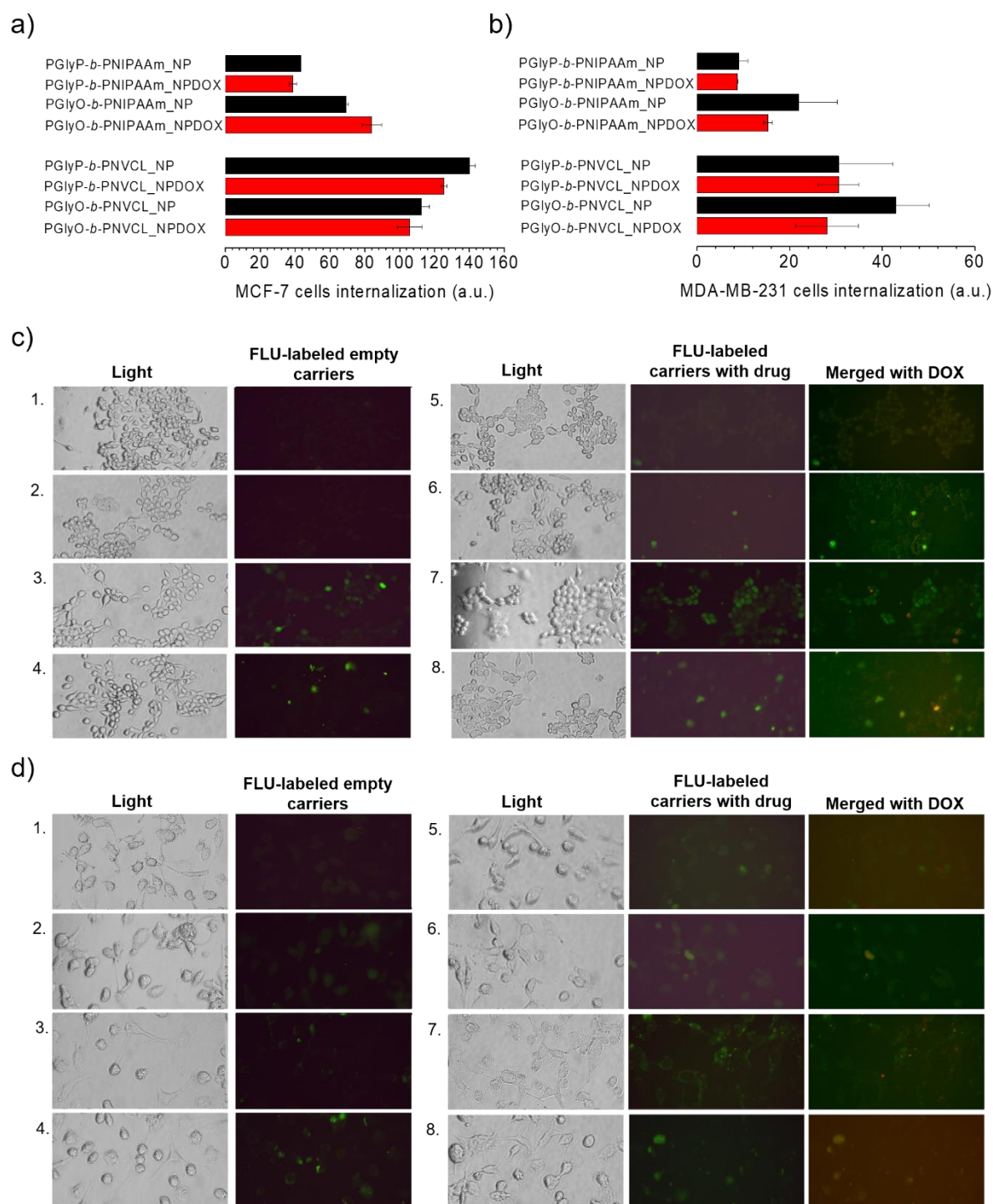


Figure 41. Fluorescence properties of polymers and corresponding fluorescein-labeled polymeric nanoparticles ($C = 0.1 \text{ mg mL}^{-1}$, PBS, $\lambda_{\text{ex}} = 494 \text{ nm}$ and $\lambda_{\text{em}} = 518 \text{ nm}$).

Microscopic examinations and fluorescence studies of dye-labeled PNPs confirmed that DOX-loaded nanoparticles effectively penetrated breast cancer cells, significantly reducing their viability (Figure 42). The results revealed that internalization depended on the type of thermoresponsive segment. In particular, carriers with a PNVCL block exhibited better penetration than PNPs with the PNIPAAm segment. The analysis further revealed that the diglyceride part modulates the internalization of PNIPAAm-based PNPs, with an increased internalization observed for carriers containing an unsaturated diglyceride moiety.



Abbreviations: 1. PGlyP-*b*-PNIPAAm_NP; 2. PGlyO-*b*-PNIPAAm_NP; 3. PGlyP-*b*-PNVCL_NP; 4. PGlyO-*b*-PNVCL_NP; 5. PGlyP-*b*-PNIPAAm_NPDOX; 6. PGlyO-*b*-PNIPAAm_NPDOX; 7. PGlyP-*b*-PNVCL_NPDOX; 8. PGlyO-*b*-PNVCL_NPDOX.

Figure 42. Internalization of fluorescein (FLU)-labeled empty and DOX-loaded PNPs into breast cancer cells. Fluorescence intensity of fluorescein-labeled empty and DOX-loaded PNPs in a) MCF-7 cells and b) MDA-MB-231 cells. Microscopic analysis of fluorescein-labeled empty and DOX-loaded PNPs localization into c) MCF-7 cells and d) MDA-MB-231 cells; 200x magnification.

Summary

This chapter extensively investigates the properties of water-soluble thermoresponsive polymeric nanoparticles formed using homopolymers or copolymers containing either PNIPAAm or PNVCL, which incorporate one or more diglyceride moieties in the structure, respectively. PNPs were produced via a straightforward nanoprecipitation method.

The size of homopolymer-based PNPs, assessed using MADLS, revealed a narrow size distribution influenced by the thermoresponsive block type and the molar mass of the polymer. The spherical shape of nanoparticles was corroborated using DLS with polarization filters and TEM. UV-Vis spectroscopy and DLS were employed to determine thermoresponsive properties. It was found that the T_{CP} changed based on molar mass, hydrophobic/hydrophilic ratio, and environmental factors such as salt presence. In PBS, the diglyceride-terminated PNIPAAm and PNVCL particles displayed lower T_{CP} s than their bare counterparts, indicating the role of the end groups in influencing the thermal response. Collaborative studies with the Medical University of Bialystok revealed the hemocompatibility of nanoparticles. They did not cause hemolysis in red blood cells or affect the metabolic activity of THP-1 cells.

The spherical shape of copolymers-based PNPs was confirmed using backscattering DLS measurements and TEM imaging. Given their excellent long-term stability at pH 7.4, these nanoparticles were ideal for biomedical applications as drug carriers. The successful encapsulation of two low water-soluble anticancer drugs, doxorubicin (DOX) and tamoxifen (TAM), into these nanoparticles was achieved. The structure of PNPs has been proven to influence drug encapsulation efficiency. The PNPs demonstrated a significantly higher encapsulation efficiency for TAM than DOX. The hydrodynamic diameter of drug-loaded nanoparticles was within the 10–200 nm range, which is ideal for drug delivery. Furthermore, they maintained a spherical shape and exhibited a negative zeta potential, which is favorable for extended circulation half-lives. Additionally, T_{CP} and T_{Agg} of nanoparticles were studied. The phase separation temperatures for all nanoparticles were lower than those of pure PNIPAAm or PNVCL. The thermoresponsive properties of PNPs enabled controlled drug release in response to temperature variations. The study of the drug release of TAM from polymeric nanoparticles revealed an initial burst release. Subsequently, the release rate stabilized, with approximately 60% of the drug released within the first 240 minutes and no further significant release. This suggests that approximately 40% of the

encapsulated drug remained within the nanoparticles. The small quantities of encapsulated doxorubicin made it impossible to determine the drug release profile accurately.

Despite the lack of significant differences in the physicochemical properties of PNPs composed of diglycerides with saturated and unsaturated chains (PGlyP and PGlyO) and thermoresponsive blocks (PNIPAAm and PNVCL), their composition influenced their biological properties.

The polymeric nanoparticles (empty and drug-loaded) were compatible with representatives of normal cells, such as human RBC, THP-1 monocytic cells, and H9c2(2-1) cardiomyocyte cells. The cytotoxic efficacy of PNPs on breast cancer cell lines (MCF-7 and MDA-MB-231) varied based on their chemical composition. Empty PNPs with the PGlyP block showed negligible cytotoxic effects on both cell lines. In contrast, empty PNPs containing PGlyO, particularly those combined with PNVCL, showed a marked reduction in viability among MCF-7 cells, suggesting that unsaturated acid moieties and the choice of thermoresponsive block significantly influence cytotoxicity. Despite the low doses of the encapsulated drug, all DOX-loaded PNPs exhibited significant cytotoxic effects against MCF-7 and more aggressive MDA-MB-231 breast cancer cell lines. Moreover, in the case of MDA-MB-231 cells, PGlyO-*b*-PNVCL_NPDOX showed a lack of dose-dependent efficacy, indicating the potential for lower dosage applications without compromising therapeutic outcomes. The efficiency of cancer cell death varied according to the composition of the PNPs and induced apoptosis or necrosis. PNIPAAm-based PNPs induced apoptosis, whereas PNPs containing PNVCL were more potent in inducing necrosis. Furthermore, the uptake of fluorescein-labeled PNPs by breast cancer cells was studied. It was confirmed that they could penetrate the membranes of cancer cells, disintegrating their functions. The results revealed that internalization depended on the type of thermoresponsive segment. In particular, PNPs with a PNVCL block exhibited better penetration than those with the PNIPAAm segment. In the case of PNIPAAm-based PNPs, the unsaturated diglyceride moiety showed increased internalization than their saturated counterparts. The biological properties of TAM-loaded nanoparticles are currently being evaluated.

The investigation of PNPs formulated from thermoresponsive polymers, which incorporate one or multiple diglyceride molecules within their structure, has shed light on their biocompatibility and potential as drug carriers. Furthermore, studies on fluorescently labeled PNPs have determined their ability to penetrate the membranes of cancer cells. This underscores the potential of dye-labeled polymeric nanoparticles not only in analyzing their biodistribution and metabolism but also as valuable tools in theranostics and diagnostics.

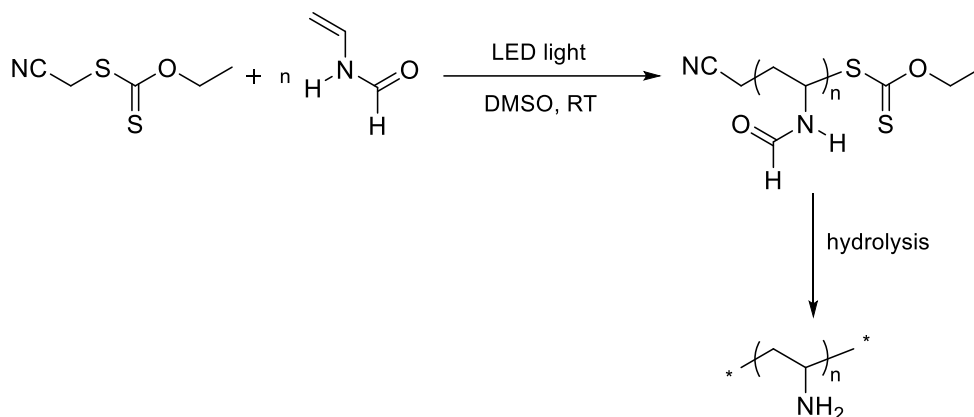
The results presented in this chapter establish a foundational platform for further research. Future studies may explore varied polymer compositions, molar masses, and types of encapsulated drugs to increase the therapeutic potential of these nanocarriers. Moreover, additional research is necessary to optimize the design and evaluate the *in vivo* behavior of these nanoparticles for clinical applications.

Part of the results of this chapter have been published in:

- 1) I. Kurowska, K. H. Markiewicz, K. Niemirowicz-Laskowska, P. Misiak, M. Destarac, P. Wielgat, I. Misztalewska-Turkowicz, G. Siemiaszko, H. Car, A. Z. Wilczewska, *European Polymer Journal* **2022**, *169*, 111154.
- 2) I. Kurowska, K. H. Markiewicz, K. Niemirowicz-Laskowska, M. Destarac, P. Wielgat, I. Misztalewska-Turkowicz, P. Misiak, H. Car, A. Z. Wilczewska, *Biomacromolecules* **2023**, *24*, 4854.

CHAPTER 4. POLYVINYLAMIDES AND POLYVINYLAMINES

This part of the doctoral dissertation aimed to determine optimal parameters for the polymerization of *N*-vinylformamide (NVF) employing a photoiniferter reversible addition-fragmentation chain transfer (PI-RAFT) technique (Scheme 16). Additionally, this chapter explores the potential for preparing block copolymers with a poly(*N*-vinylformamide) segment and their subsequent hydrolysis to create tailor-made polyvinylamines.



Scheme 16. General scheme of PI-RAFT polymerization of NVF under LED irradiation and hydrolysis of PNVF to corresponding polyvinylamine.

4.1. Photoreactors

All polymerizations were conducted in homemade photoreactors. As an example, the purple photoreactor is shown in Figure 43. Light-emitting diodes (LEDs) were chosen as the light source because of their numerous advantages. LEDs emit light at specific wavelengths with a narrow half-width, which is crucial for photopolymerization, where only a particular wavelength might initiate the reaction.^{82,341} They operate at low voltages, leading to reduced electricity consumption. Furthermore, the minimal heat generated by LEDs eliminates the need for additional cooling measures or more complex equipment.³⁴² Their durability, extended lifespan, and cost-effectiveness, compared to other light sources, further underscore their suitability for photochemical applications.^{82,85} The purple LED light strip ($\lambda = 395\text{--}400\text{ nm}$) was wound inside an aluminum can with a diameter of 8.5 cm and a height of 9.5 cm. The LED light strip was connected to the power with a power supply. A cooling fan placed at the bottom of the photoreactor ensured constant airflow. The polymerization kinetics were evaluated in sealed glass tubes placed 2.5 cm from the light source. The samples were withdrawn at different intervals and analyzed by ¹H NMR and SEC.

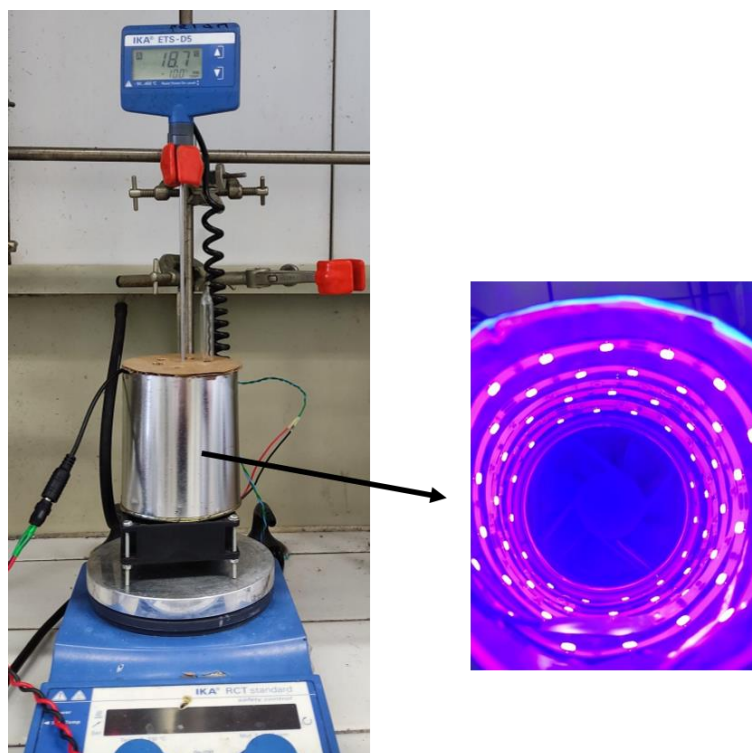


Figure 43. Purple LEDs-based photoreactor for polymerization studies.

4.2. The influence of light wavelength on polymerization

The *S*-(cyanomethyl) *O*-ethyl carbonate dithionite (CTA2) absorbs light in the UV region (260–320 nm) due to the spin allowed $\pi \rightarrow \pi^*$ electronic transition of the thiocarbonyl group. Absorption in the visible light region (340–420 nm) is caused by the spin forbidden $n \rightarrow \pi^*$ electronic transition (Figure 44). The $n \rightarrow \pi^*$ absorption of CTA2 with a maximum of around 360 nm suggested that purple LED light is more appropriate for NVF polymerization. However, examples can be found in the literature where blue LED light was used to initiate polymerization with a dithiocarbonate chain transfer agent.¹⁰⁶ It is worth mentioning that recently, Barner-Kowollik and coworkers explored the wavelength-dependent behavior of photoinduced ATRP, demonstrating a red shift in the action spectrum relative to the absorption spectrum of a copper(II) catalyst.³⁴³ This finding is particularly relevant to this study as it suggests that the most effective wavelength for polymerization might not directly align with the peak absorption wavelength of the chain transfer agent used. Therefore, the investigation began by identifying optimal parameters for polymerization. At first, two varying wavelengths of light, 395–400 nm (purple) and 460 nm (blue), were tested as a light source in the PI-RAFT polymerization of NVF for $M_{n,th} = 20 \text{ kg mol}^{-1}$. The number of LEDs in both photoreactors was 66.

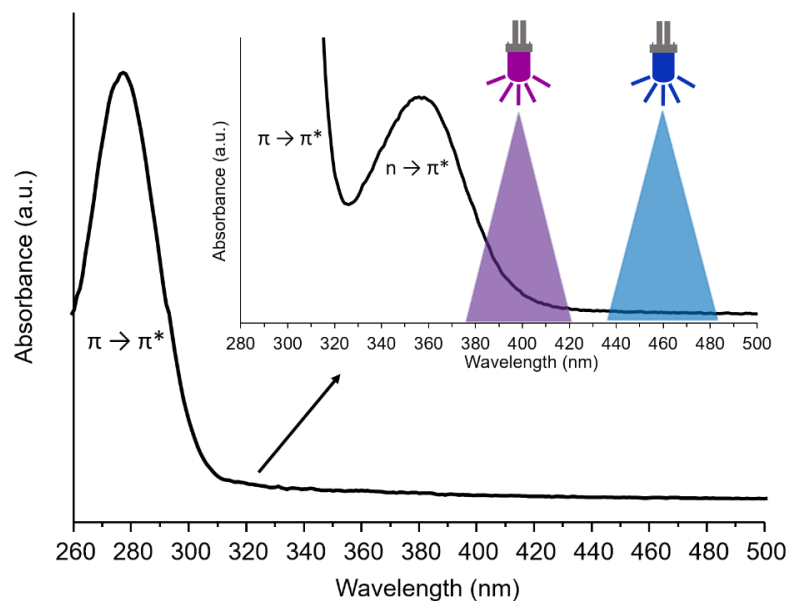


Figure 44. UV-Vis spectrum of *S*-(cyanomethyl) *O*-ethyl carbonodithioate.

As expected, the polymerization rate was much faster with purple light. High conversion (80%) was obtained after 4 h of irradiation with purple light. Achieving such a value with blue light required 40 h of irradiation (Figure 45).

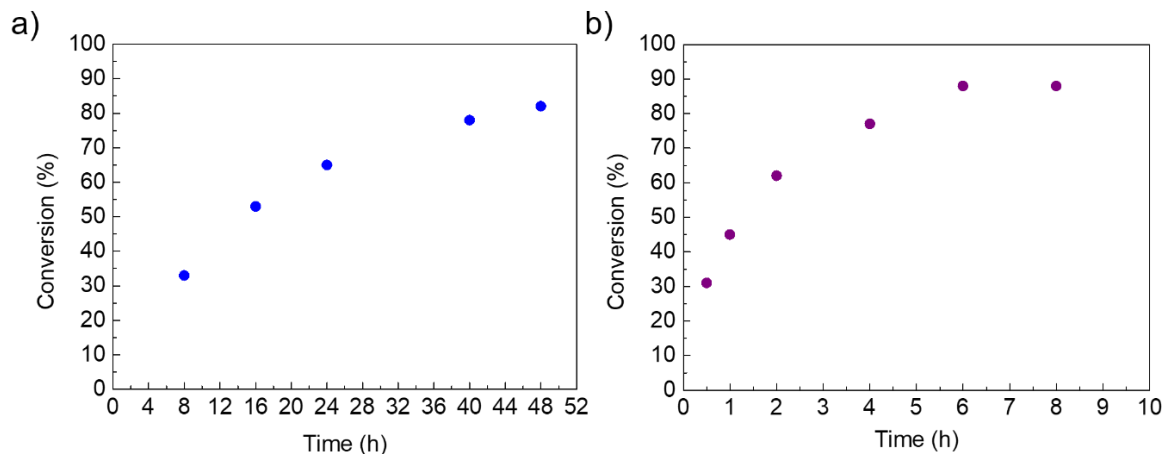


Figure 45. The effect of light wavelength on NVF conversion over time.

This finding was further justified through the comparison of chromatograms (Figure 46). Although all of the traces were monomodal, they did not shift toward lower elution times in the case of polymerization carried out with blue light. The molar masses determined by SEC did not increase with conversion, hinting at a lack of control (Figure 47, Table 11).

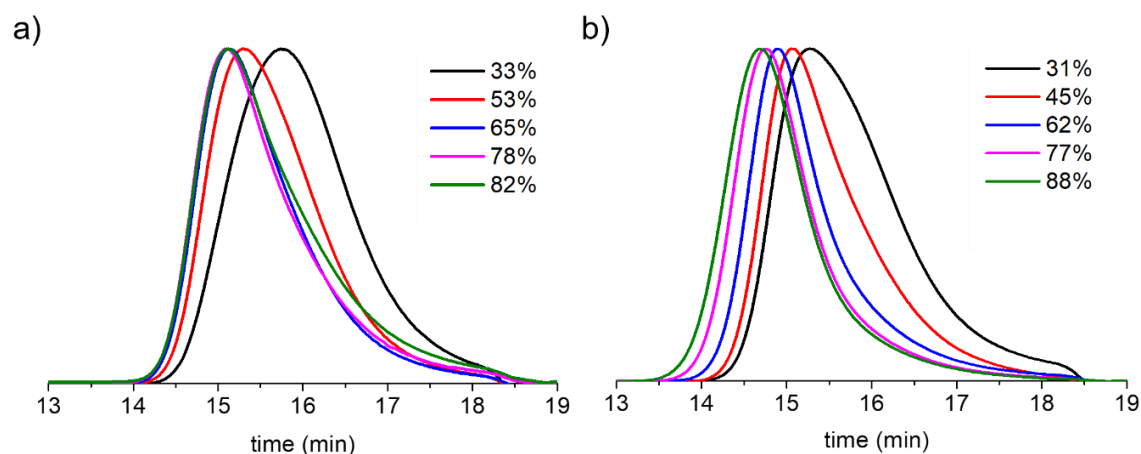


Figure 46. Evolution of SEC-RI chromatograms of PNVF with NVF conversion for polymerizations carried out with a) blue light and b) purple light.

In the case of reactions carried out with purple LED light, the increase in molar mass showed a nearly linear relationship with the irradiation time. However, the molar masses determined by SEC were slightly higher than the theoretical values. Furthermore, a gradual increase in dispersities with conversion was observed (1.53 at 87% conversion). This may be attributed to a gradual loss of RAFT end-groups due to high light intensity during polymerization.⁴⁵

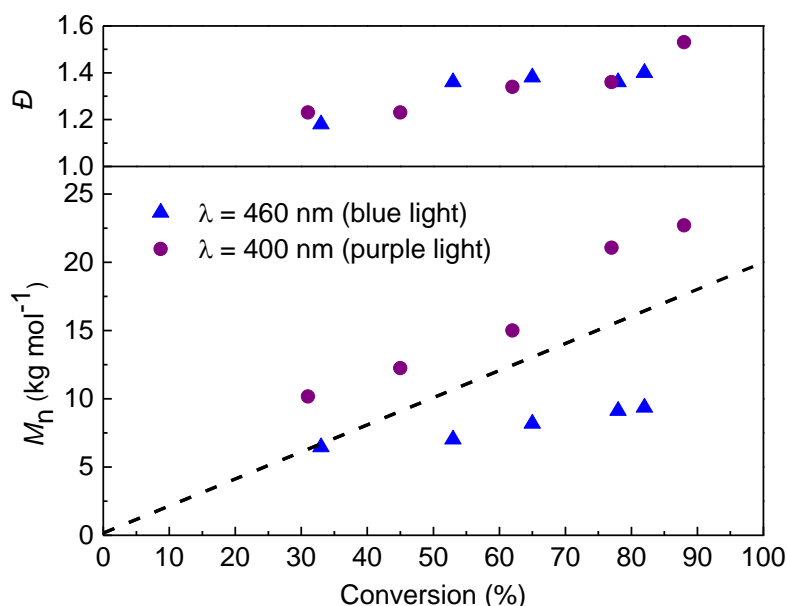


Figure 47. Evolution of M_n and \bar{D} during PI-RAFT polymerization of NVF with different light sources.

In addition, the analysis of SEC-UV traces of two samples with similar conversion (more than 60%) prepared with two different light sources clearly showed a much weaker UV signal for polymerization carried out with blue light than with purple light (Figure 48). This indicates degradation of the CTA end-groups and, thus, a lack of livingness of the polymers.

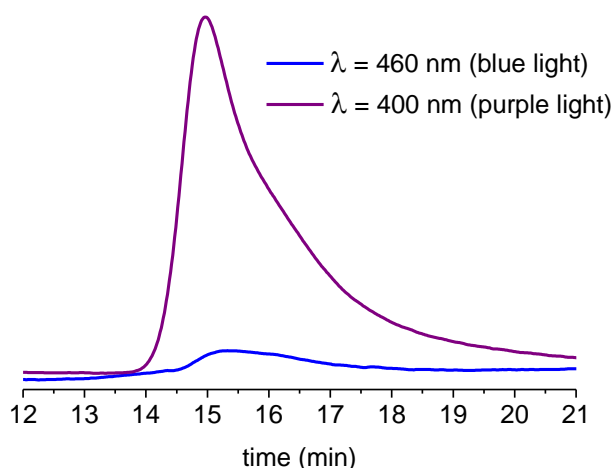


Figure 48. SEC-UV chromatograms of PNVF.

These results determined that purple light was a better choice for further experiments as it demonstrated better control over the polymerization than blue light.

4.3. The influence of light intensity on polymerization

Given the results of the previous section, it was deemed necessary to examine the influence of purple light intensity on the polymerization of NVF. The light intensity was adjusted by changing the number of LEDs in the photoreactor. Figure 49 shows that a higher intensity of purple LEDs resulted in a higher radical concentration and faster polymerization in the initial stages, with differences disappearing at the final polymerization stage.

As depicted in Figure 50 and Table 12, reducing the light intensity resulted in better control over the polymerization. $M_{n,SEC}$ values were closer to theoretical expectations, and the dispersities remained at a similar level (\mathcal{D} between 1.19 and 1.32) throughout the process. The $M_{n,SEC}$, and \mathcal{D} values did not exhibit significant variations between the experiments conducted with 30 and 12 LEDs. Therefore, a reactor with 30 LEDs was selected for further research as the optimal compromise between polymerization control and ease of manipulation.

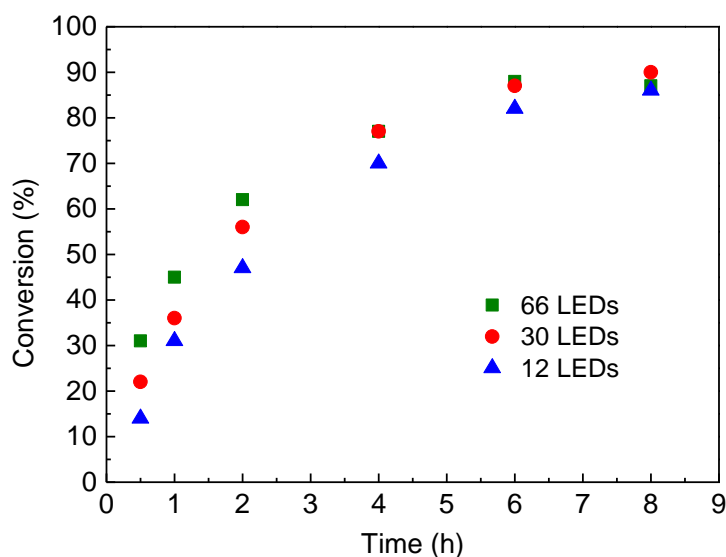


Figure 49. The effect of purple light intensity on NVF conversion with time.

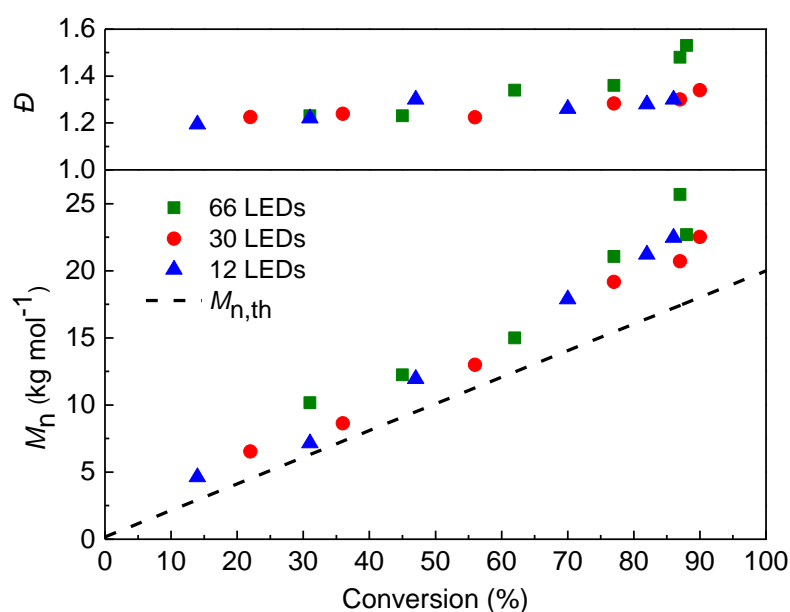


Figure 50. The effect of purple light intensity on M_n and dispersities versus conversion.

4.4. Polymerization with different targeted molar masses

To investigate the behavior of *N*-vinylformamide (NVF) during PI-RAFT, three different initial concentrations of CTA2 ($[CTA2]_0 = 66.5, 16.2, \text{ and } 6.45 \text{ mmol L}^{-1}$) were used, corresponding to the theoretical M_n of 5, 20, and 50 kg mol^{-1} . The controlled nature of the polymerization was confirmed in all cases. The obtained polymers showed a linear increase in $M_{n,SEC}$ with monomer conversion and agreed with the theoretical values (Figure

51 and Table 13). However, dispersity values increased as the initial concentration of CTA2 decreased.

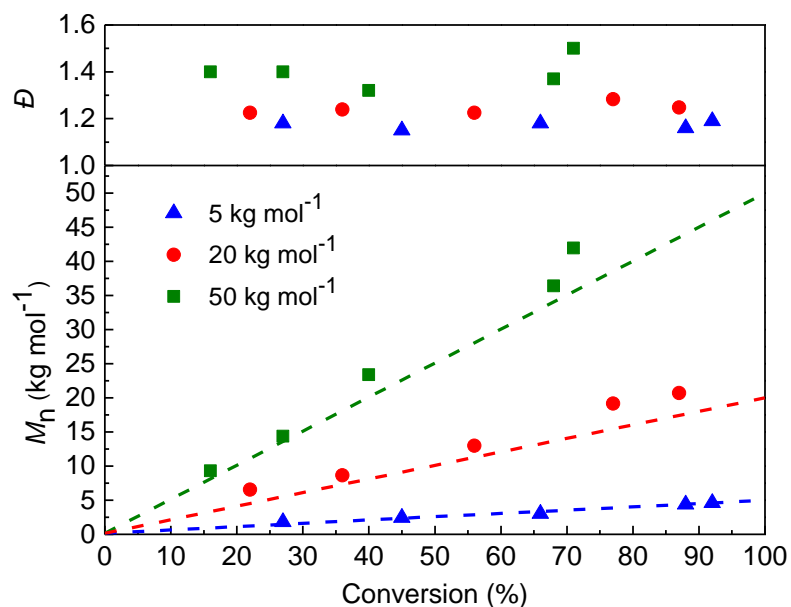


Figure 51. Evolution of M_n and \bar{D} during PI-RAFT polymerization of NVF for different targeted molar masses.

The evolution of SEC-RI chromatograms with conversion also confirmed the controlled character of the polymerization. The SEC traces were monomodal throughout polymerization and shifted toward a lower elution time with increasing monomer conversion (Figure 52).

As shown in Figure 53, the kinetic study revealed that the polymerization rate increased with the increasing initial concentration of the chain transfer agent ($[CTA2]_0$). After 6 hours of irradiation, a high conversion of approximately 90% was observed for polymers of molar mass 5 and 20 kg mol^{-1} . Polymers were characterized by low dispersity ($\bar{D} \sim 1.2$). However, for 50 kg mol^{-1} , the monomer conversion was slightly lower (70%) after the same period, and the dispersities slightly increased (Figure 51). This can be explained by the dual role of CTA, which acts as both a chain transfer agent and the only source of radicals in PI-RAFT polymerization. When the concentration of CTA is lower, the number of radicals produced also decreases, affecting the polymerization process.

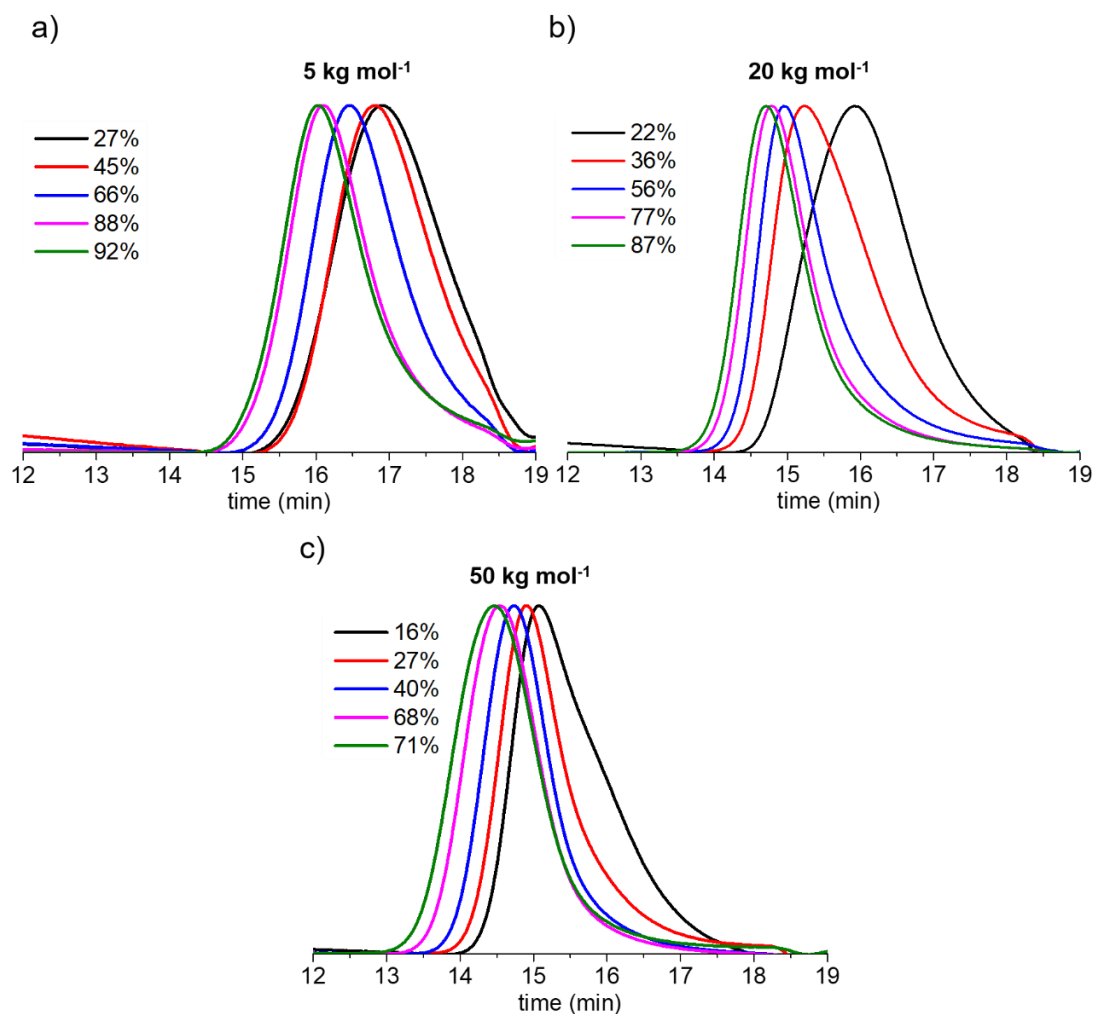


Figure 52. Evolution of the SEC-RI chromatograms of PNVF with NVF conversion for different molar masses.

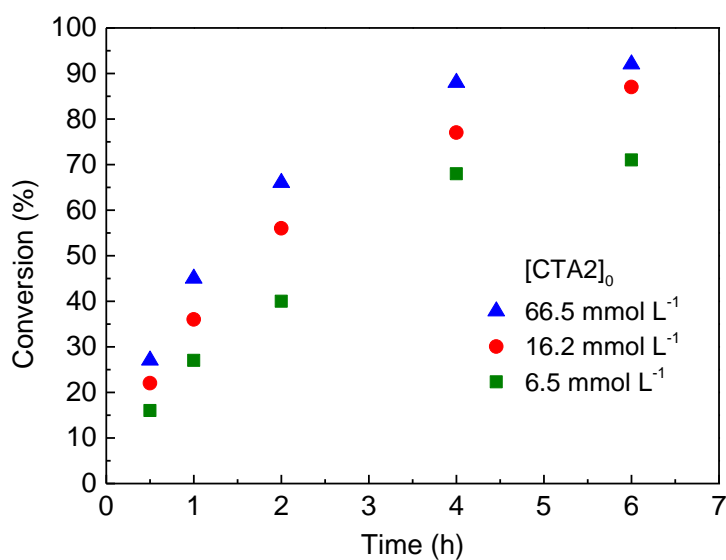


Figure 53. Effect of the initial concentration of CTA2 on PI-RAFT polymerization in DMSO at ambient temperature ($[NVF]_0 = 4.53 \text{ mol L}^{-1}$).

4.5. Dithiocarbonate and light-free experiments

In order to determine the essential role of the RAFT agent and purple light in the polymerization process, experiments without these components were conducted. In the dithiocarbonate-free experiment, no polymerization occurred even after 16 hours of exposure to purple light (Figure 54a). Similarly, no polymerization occurred when the reaction mixture containing dithiocarbonate and NVF in DMSO was exposed to daylight for 48 hours (Figure 54b).

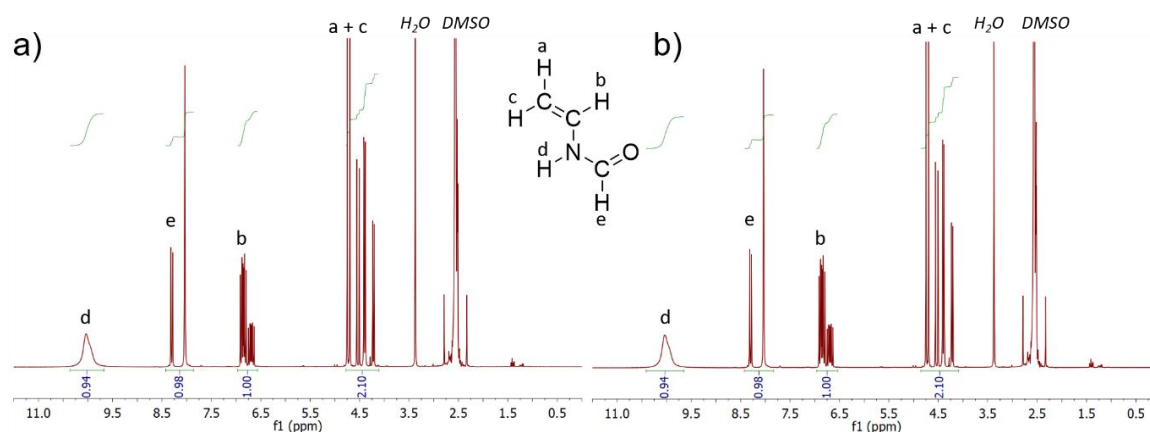


Figure 54. ^1H NMR spectra of a) a dithiocarbonate-free experiment and b) a light-free experiment (300.13 MHz, DMSO).

4.6. Temporal control

Temporal control in photoinduced polymerization offers significant advancement, using light as an on-demand switch to initiate or stop the process instantaneously. Polymerization is in progress when the light is on, whereas when it is off, the process is suspended. The experiment was carried out in an NMR tube with deuterated DMSO for the targeted $M_n = 20 \text{ kg mol}^{-1}$. Figure 55 shows the evolution of the NVF conversion over time during purple LED irradiation. The conversion value remains unchanged at specific intervals, such as 2 to 3 hours, 4 to 5 hours, 6 to 8 hours, and 9 to 11 hours. This indicates periods when the LED irradiation was turned off (represented as gray areas). On the contrary, when the light source was activated (shown as white areas), a linear increase in conversion was evident, signaling the continuation of the polymerization process.

Temporal control is beneficial in the production of block copolymers because it allows for the sequential addition of different monomers. A new monomer can be added by pausing the polymerization process, and then the process can be restarted by turning the light source

back on. This precise control over the polymerization process facilitates the creation of complex polymeric structures.

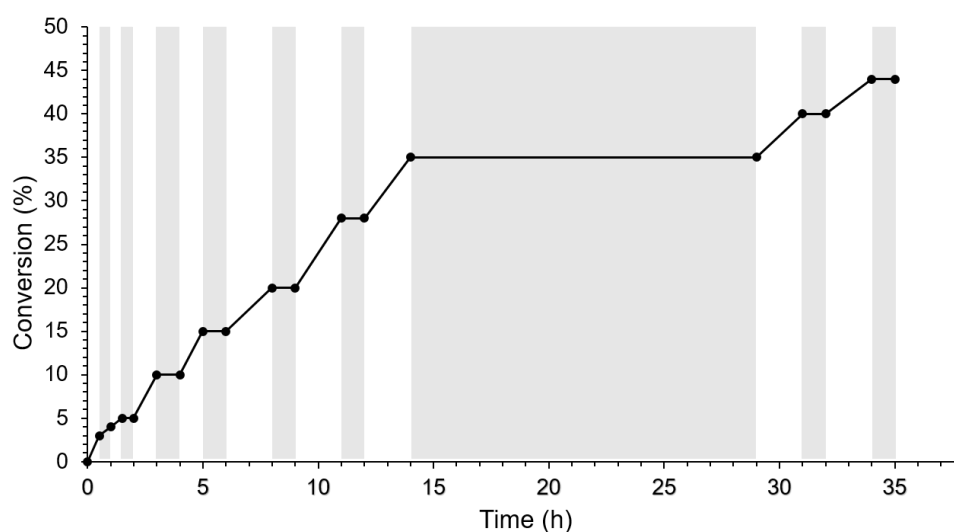


Figure 55. Temporal control of PI-RAFT polymerization. Evolution of NVF conversion over time during purple LED irradiation (ON: white area) and without irradiation (OFF: gray area).

4.7. The nature of end-groups

To verify the livingness of the polymer by the presence of the dithiocarbonate as the end-group, a low molar mass PNVF-CTA2, was synthesized, purified by precipitation in cold acetone, and subsequently analyzed by SEC, matrix-assisted laser desorption ionization time-of-flight mass spectrometry (MALDI-TOF MS), ^1H NMR, and electrospray-ionization time-of-flight mass spectrometry (ESI-TOF MS). The molar mass determined by SEC ($M_{n,\text{SEC}} = 2.2 \text{ kg mol}^{-1}$, $D = 1.08$) was in good agreement with the expected $M_{n,\text{th}} = 1.8 \text{ kg mol}^{-1}$. The MALDI-TOF MS spectrum, presented in Figure 56, showed two populations.

The major population, with a general formula of $\text{C}_2\text{H}_2\text{N}-(\text{C}_3\text{H}_5\text{NO})_{n-1}-\text{CH}_2=\text{CH}_2-\text{NHCHO}$, was identified as the sodium adduct of a PNVF terminated by a double bond due to the decomposition of the dithiocarbonate group under the MALDI-TOF laser. This phenomenon is commonly observed for other poly(*N*-vinylamides).^{230,344} The minor population could not be identified but did not correspond to thiol nor hydrogen-terminated chains. However, confirmation of the presence of the dithiocarbonate group as the chain-end was achieved through ^1H NMR spectroscopy, where characteristic signals at 4.5–4.7 ppm and 1.4 ppm corresponding to the methylene and methyl protons of the *O*-ethyl dithiocarbonate group were observed (Figure 57).

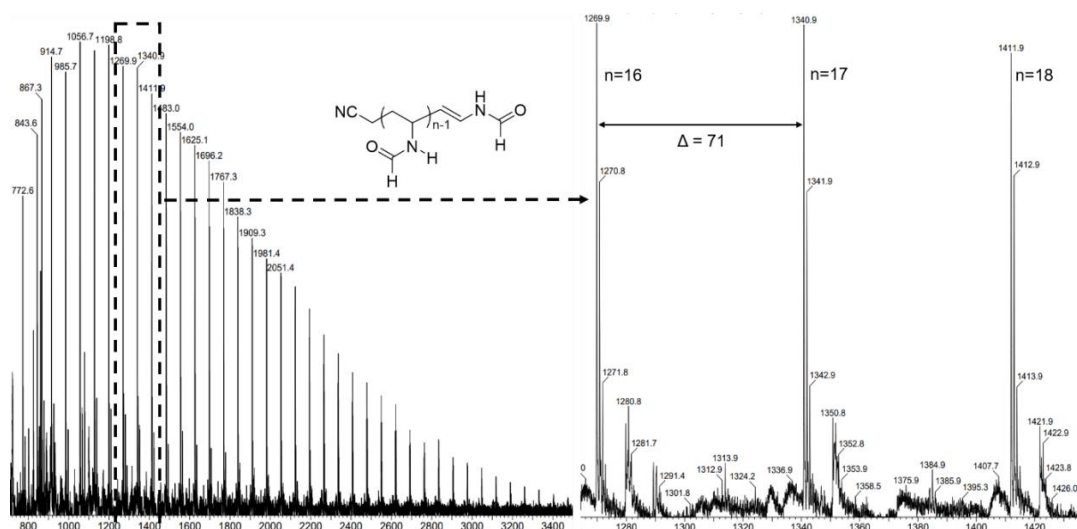


Figure 56. MALDI-TOF MS spectrum of PNVF-CTA2 ($M_{n,SEC} = 2.2 \text{ kg mol}^{-1}$, $D = 1.08$).

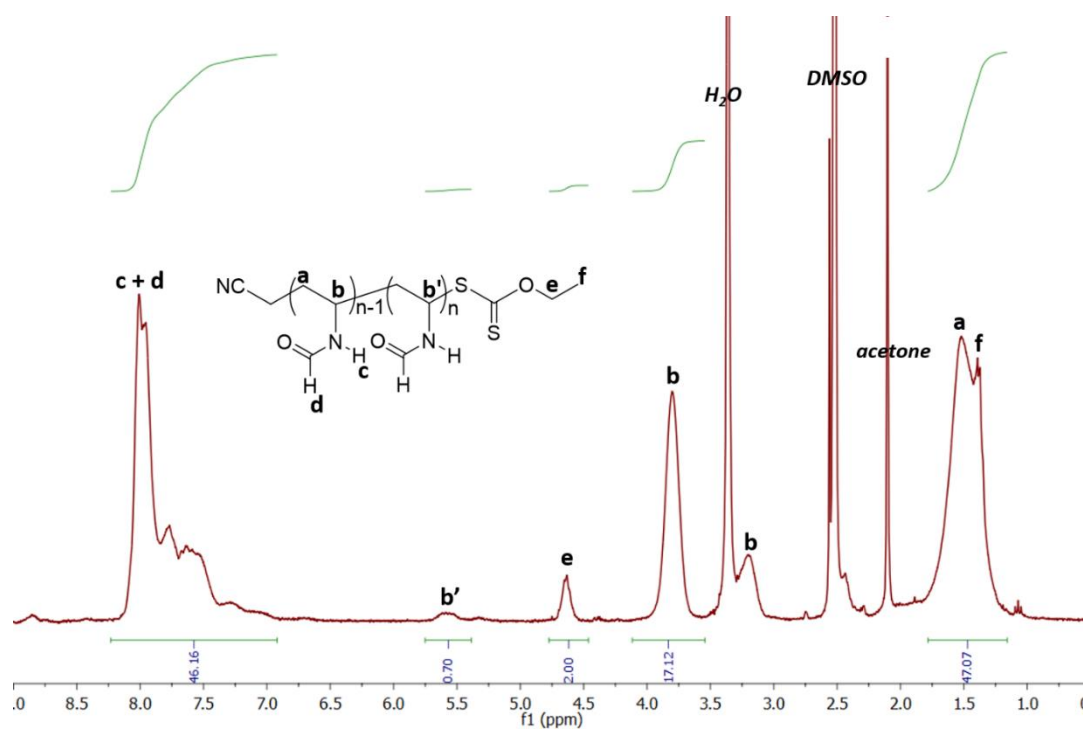


Figure 57. ^1H NMR spectrum of PNVF-CTA2 of low molar mass ($M_{n,SEC} = 2.2 \text{ kg mol}^{-1}$, $D = 1.08$), (300.13 MHz, DMSO).

The ESI-TOF MS spectrum of low molar mass PNVF-CTA2 was more complex and detected five distinct populations. (Figure 58). Three of these populations were ascribed to a polymer that ended with a dithiocarbonate group ($\text{C}_2\text{H}_2\text{N}-(\text{C}_3\text{H}_5\text{NO})_n-\text{S}(\text{C}=\text{S})\text{OCH}_2\text{CH}_3$) cationized with hydrogen or sodium. The remaining two minor populations were related to a polymer terminated with a double bond from dithiocarbonate decomposition.

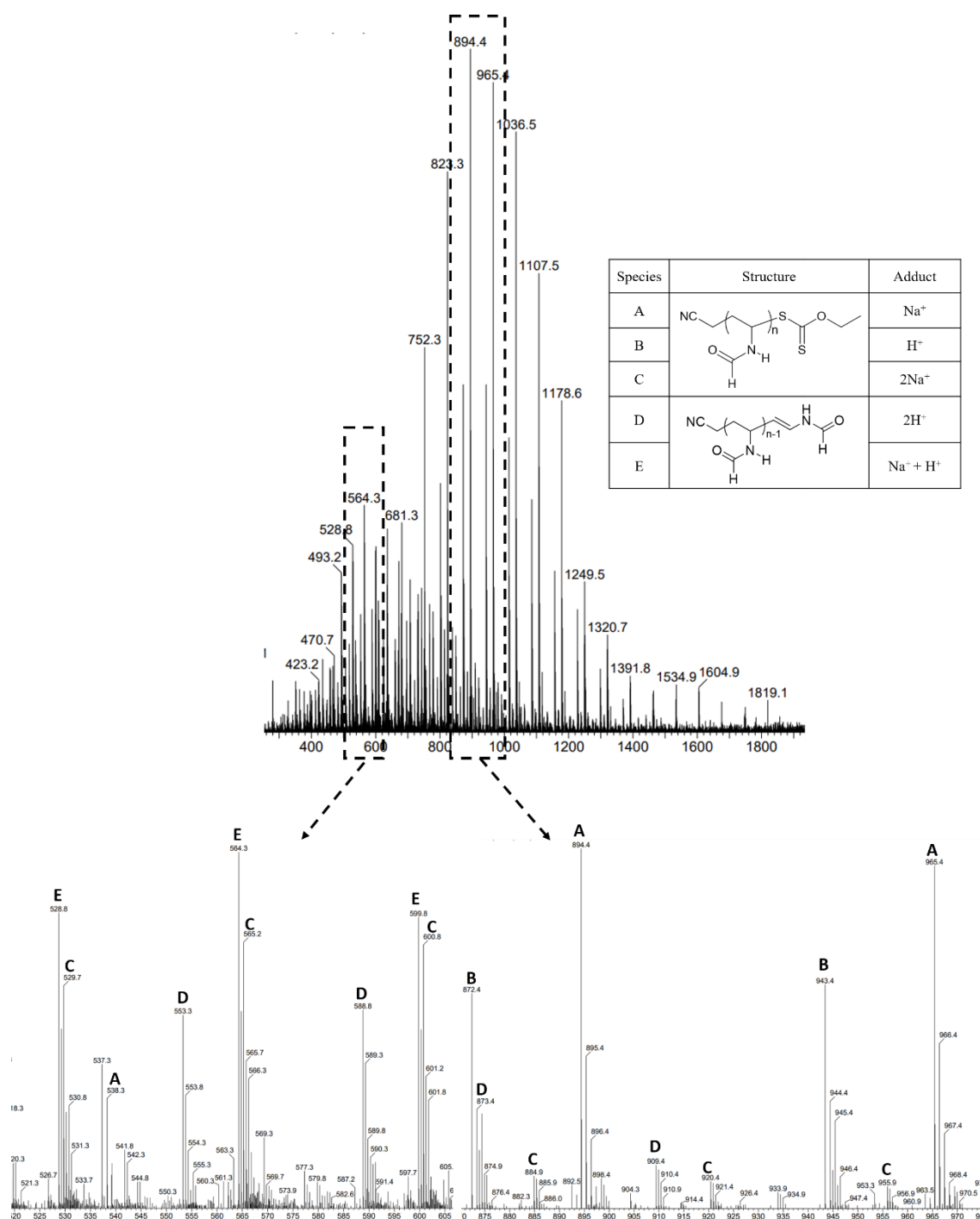


Figure 58. ESI-TOF MS spectrum of PNVF-CTA2 ($M_{n,SEC} = 2.2 \text{ kg mol}^{-1}$, $D = 1.08$).

The chain-end fidelity of the RAFT groups was further confirmed by a chain extension experiment from a well-characterized PNVF-CTA2 macro-CTA (Table 14). SEC chromatograms of the chain extended PNVF shifted to a lower elution time with the increasing conversion, while the initial trace of PNVF-CTA2 disappeared completely (Figure 59a). Additionally, $M_{n,SEC}$ were in accordance with theoretical values with consistently low dispersities ($D < 1.25$), as demonstrated in Figure 59b and Table 14.

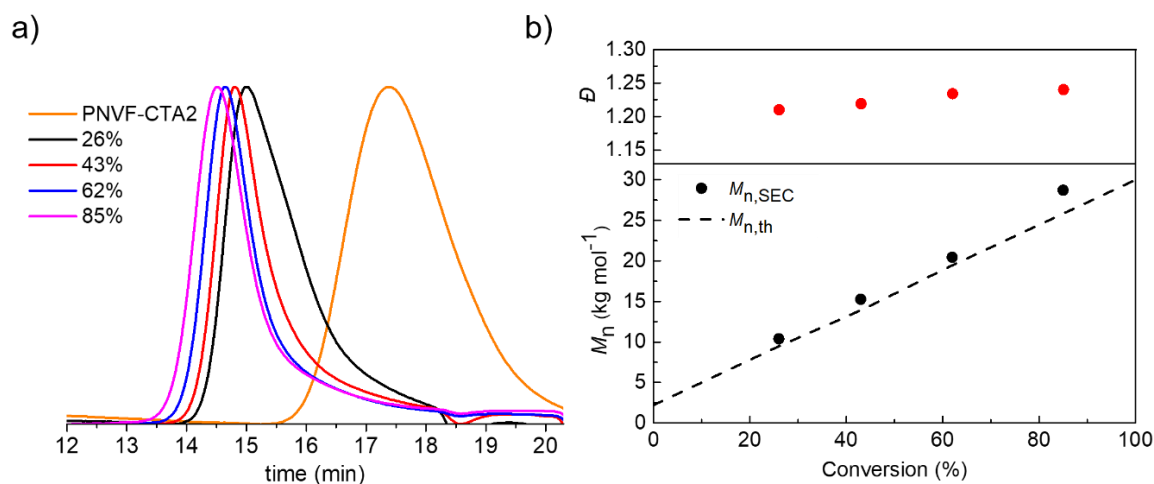


Figure 59. a) Evolution of SEC-RI chromatograms of PNVF with NVF conversion during chain extension experiment. b) Evolution of M_n and dispersity versus conversion during chain extension of PNVF.

Based on these findings, it can be concluded that PI-RAFT is an effective method of NVF polymerization, which creates the possibility of preparing block copolymers with a PNVF segment.

4.8. Block copolymerization

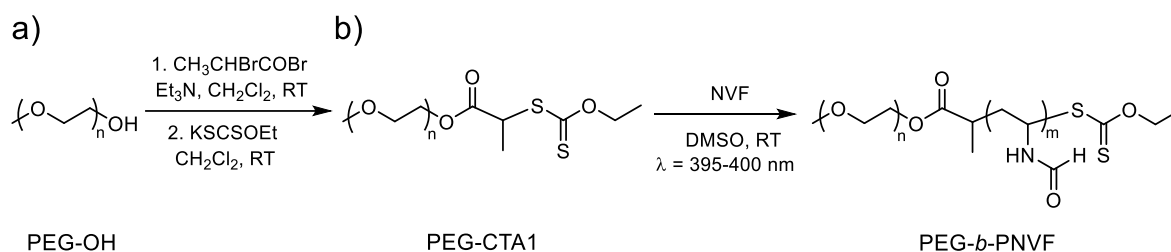
Two block copolymers containing a PNVF segment were synthesized by PI-RAFT polymerization of NVF with two different macro-CTAs. The well-known poly(ethylene glycol) (PEG) and poly(*N*-vinyl pyrrolidone) (PVP) were selected as the first blocks.

4.8.1. Polymerization with PEG as macro-CTA

Poly(ethylene glycol) (PEG) is a versatile polymer with many applications, for example, in the medical, industrial, and cosmetic fields. PEG is soluble in both aqueous and organic solvents, exhibits biocompatibility, and has received approval from the Food and Drug Administration (FDA).^{345,346}

A macro-CTA, based on PEG, was synthesized using a two-step procedure from commercially available ω -hydroxy-terminated PEG (PEG-OH) with a molar mass of 5 kg mol⁻¹ (Scheme 17a).³⁴⁷ Briefly, PEG-OH was modified with 2-bromopropionyl bromide to obtain PEG-Br. This compound then reacted with ethyl potassium dithiocarbonate, resulting in the dithiocarbonate-functionalized macro-CTA marked as PEG-CTA1. Subsequently,

PEG-CTA1 was used to polymerize NVF, targeting a molar mass of 25 kg mol^{-1} at complete conversion (Scheme 17b).



Scheme 17. General scheme of copolymerization with PEG ac macro-CTA.

The copolymerization proceeded in a controlled manner, with the NVF conversion reaching 87% after 6 hours of irradiation under purple LED light. The molar masses of the copolymer, as determined by aqueous SEC, increased linearly with conversion and were closely aligned with theoretical predictions (Figure 60a, Table 15). SEC chromatograms of copolymers were monomodal and shifted toward a lower elution time with increasing monomer conversion. (Figure 60b). The shoulder visible in the chromatogram of PEG-CTA1 is more likely to originate from the starting material (PEG-OH), which has also been observed in previously reported studies.³⁴⁷

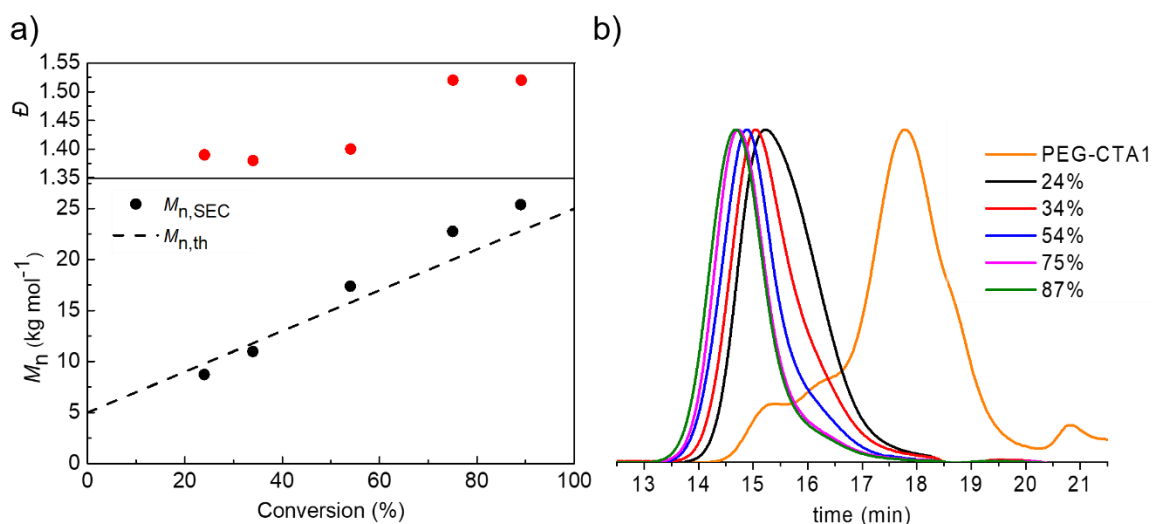


Figure 60. a) Evolution of M_n and D versus conversion determined by aqueous SEC. b) Evolution of SEC-RI chromatograms of PEG-*b*-PNVF copolymers with NVF conversion during PI-RAFT polymerization.

4.8.2. Polymerization with PVP as macro-CTA

Poly(*N*-vinyl pyrrolidone) (PVP) is a biocompatible, non-toxic, and water-soluble polymer.³⁴⁸ Initially developed as a plasma substitute, PVP has significantly broadened its scope. It now plays an important role in many sectors, such as pharmaceuticals, biomedical devices, laboratory analysis, cosmetics, food products, adhesives, textile processing, fuel cells, batteries, metal nanoparticle synthesis, and environmental protection.²²⁵

4.8.2.1. Polymerization of *N*-vinylpyrrolidone (NVP)

In the case of PVP-based macro-CTA, its synthesis with PI-RAFT was more challenging. Although the polymerization of NVP with RAFT is well described, only a few publications have shown attempts to polymerize this monomer using light. Gibson and coworkers discussed the application of PI-RAFT in PVP synthesis utilizing blue LED light.³⁴⁹ However, the monomer conversion reached a maximum of 44% after 24 hours of irradiation, while the molar masses measured by SEC were higher than theoretical values. Zhu et al. demonstrated the lack of NVP homopolymerization upon exposure to purple or blue LED light, whereas only oligomers were obtained under UV light irradiation.¹⁰⁴ However, when NVP was used as a second block in PI-RAFT to extend the chain of macro-CTA from poly(*n*-butyl acrylate) (P*n*BA), poly(methyl acrylate) (PMA), and polystyrene (PS), well-defined block copolymers were produced. These results encouraged the testing of purple light to drive NVP polymerization.

Preliminary research focused on the identification of suitable polymerization conditions. At first, polymerization was carried out in bulk with *S*-(cyanomethyl) *O*-ethyl carbonate dithionate (CTA2) as a chain transfer agent. After only a short time of irradiation with purple light (10 minutes), it was noticed that the reaction mixture became dense. Surprisingly, the ¹H NMR analysis showed that NVP did not polymerize but instead underwent dimerization (Figure 61). It is known that the dimerization of NVP can occur in the presence of water and/or acidic functional groups,^{350,351} although neither of these factors was present in this case. The reaction was performed several times with freshly distilled NVP, and the dimerization occurred each time. Contamination of the chain transfer agent with alkyl halides was also considered as a potential cause of dimerization. However, this possibility was ruled out as CTA2 from the same batch was successfully used in the polymerization of *N*-vinylformamide, which is also sensitive to acid as a monomer from the

N-vinylamides family.^{229,351} To date, no explanation for this unexpected behavior of CTA2 with NVP has been identified.

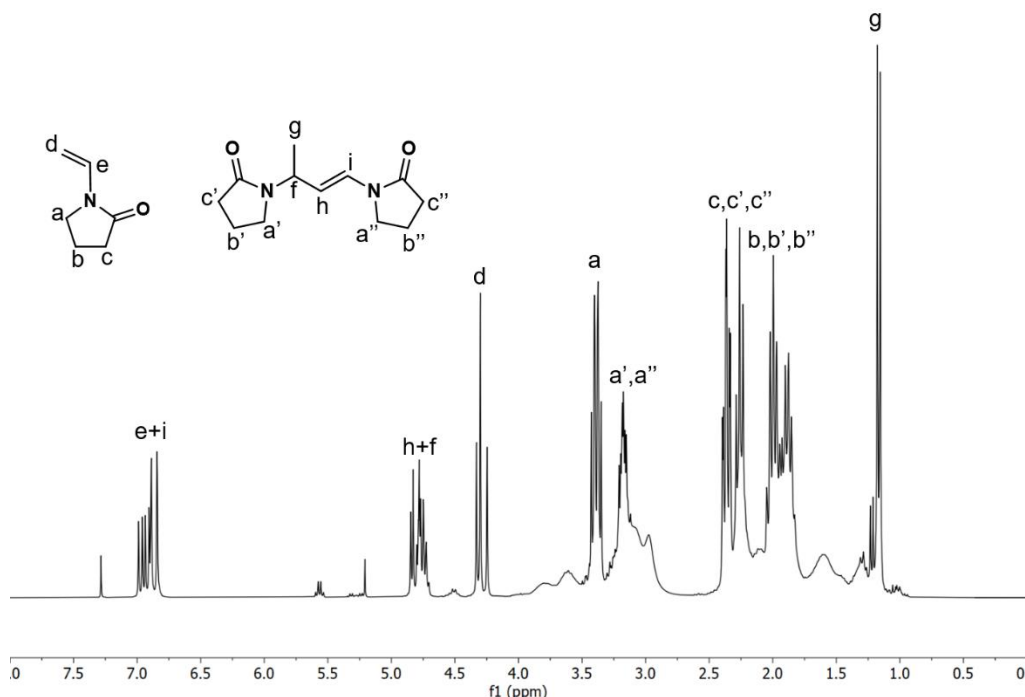
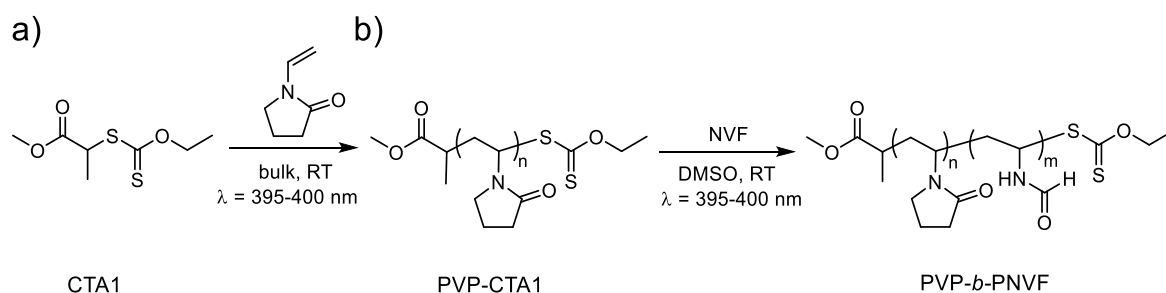


Figure 61. ¹H NMR spectrum of PI-RAFT polymerization of NVP with CTA2 (300.13 MHz, CDCl₃).

Based on these findings, the chain transfer agent was changed to 2-((ethoxycarbonothioyl)thio)propanoate (CTA1), previously reported as a good CTA in RAFT polymerization of NVP (Scheme 18a).²²⁸



Scheme 18. General scheme for block copolymerization with PVP as macro-CTA.

The polymerization with CTA1 proceeded in a controlled manner and, surprisingly, was extremely fast, with 94% conversion after 30 min of irradiation under purple light. As depicted in Figure 62a, SEC chromatograms were monomodal and shifted toward a lower elution time with increasing monomer conversion. Molar masses determined in DMF displayed a linear relationship with conversion and were nearly identical to theoretical expectations. Also, dispersities remained low ($D < 1.2$) throughout polymerization (Figure 62b, Table 16).

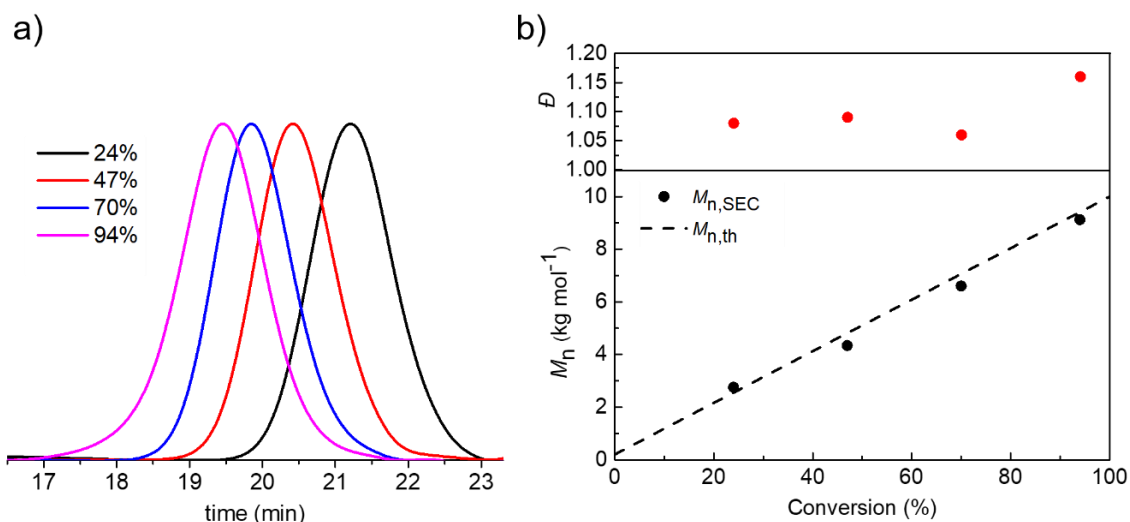


Figure 62. a) Evolution of SEC-RI chromatograms of PVP with NVP conversion during PI-RAFT polymerization. b) Evolution of M_n and dispersity versus conversion during PI-RAFT polymerization.

4.8.2.2. Block copolymerization with NVF

Subsequently, PVP-CTA1 ($M_{n,SEC} = 5.1 \text{ kg mol}^{-1}$, $\mathcal{D} = 1.11$) was synthesized and further used as a macro-CTA in the polymerization of NVF targeting a $M_{n,th} = 30 \text{ kg mol}^{-1}$ at complete conversion (Scheme 18b). Polymerization exhibited a controlled nature, and molar masses determined under aqueous conditions followed a linear trend while maintaining low dispersities ($\mathcal{D} < 1.2$) (Figure 63a, Table 17). The monomodal SEC traces shifted toward lower elution time with increasing monomer conversion (Figure 63b).

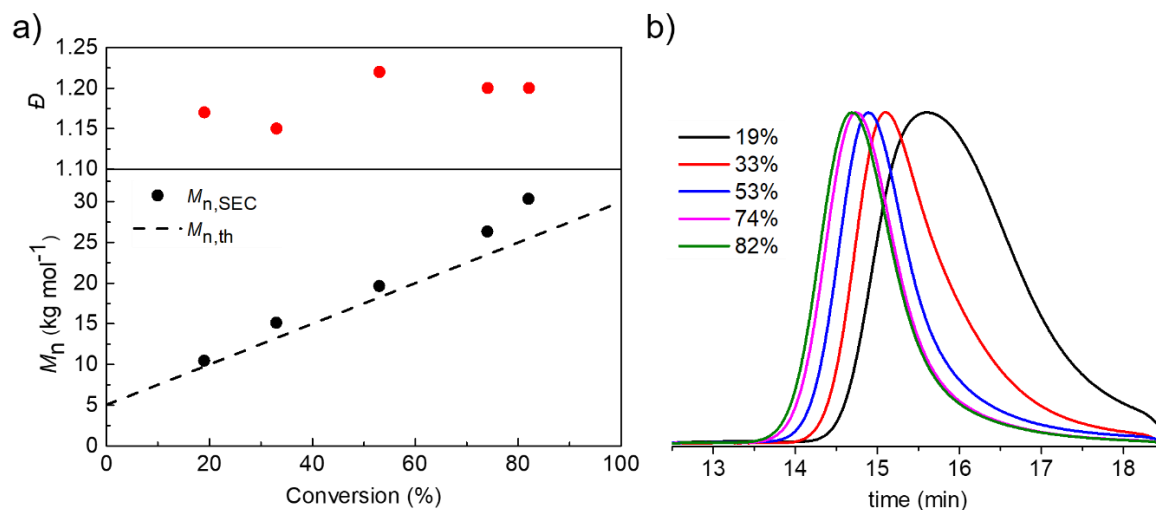


Figure 63. a) Evolution of M_n and \mathcal{D} versus conversion determined by aqueous SEC. b) Evolution of SEC-RI chromatograms of PVP-*b*-PNVF copolymers with NVF conversion during PI-RAFT polymerization.

However, due to differences in solubility between the first block (PVP-CTA1) and the copolymer (PVP-*b*-PNVF), the successful chain extension of macro-CTA could not be demonstrated by SEC analysis. Analysis of the PVP homopolymer using aqueous SEC was impossible as the sample exhibits a strong tendency to interact and adsorb on the SEC columns.³⁵² While DMF is a common solvent for PVP analysis, the PVP-*b*-PNVF copolymer, with a high content of PNVF, was not soluble in DMF and had to be analyzed in water instead.

To overcome this limitation and gain further insight into block copolymer formation, alternative characterization techniques such as the asymmetric flow field-flow fractionation (AF4) technique and diffusion-ordered spectroscopy nuclear magnetic resonance (DOSY NMR) were employed.

Asymmetric flow field flow fractionation (AF4) is a powerful analytical technique to separate and characterize polymers and other macromolecules. AF4 has several advantages, including the absence of a stationary phase, which reduces interactions between the sample and the column packing.^{352–354} In the AF4 method, the sample is introduced into a separation channel where a longitudinal laminar flow of a carrier liquid through the channel is combined with a perpendicular cross flow. This crossflow forces the sample components toward an ultrafiltration membrane, where they are confined to a thin, concentrated layer. The sample is separated based on size, with larger molecules moving slower and eluting later than smaller molecules.^{354,355} This is opposite to size exclusion chromatography (SEC), where large molecules elute first. It is important to note that the AF4 method has already been successfully used to analyze both PVP³⁵⁵ and PNVF³⁵².

AF4 analysis of PVP-CTA1 and PVP-*b*-PNVF showed a clear shift between the fractogram of PVP-CTA1 and the copolymer. The absence of any residual trace of the first block indicated the effective synthesis of the diblock copolymer (Figure 64). Although the M_n determined for the PVP block by AF4 was slightly higher ($M_{n,AF4} = 6.0 \text{ kg mol}^{-1}$, $D = 1.12$) than the value measured by SEC ($M_{n,SEC} = 5.1 \text{ kg mol}^{-1}$, $D = 1.11$), the two values were still closely correlated. For the PVP-*b*-PNVF, $M_{n,AF4} = 22.6 \text{ kg mol}^{-1}$ ($D = 1.26$) was nearly identical to the theoretical value ($M_{n,th} = 22.5 \text{ kg mol}^{-1}$).

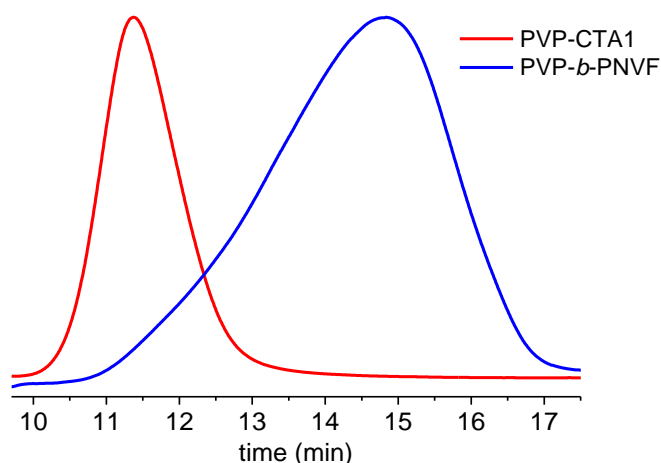


Figure 64. A4F fractograms of PVP-CTA1 and PVP-*b*-PNVF.

Diffusion-ordered spectroscopy nuclear magnetic resonance (DOSY NMR) is an effective analytical technique that provides valuable information about block copolymer synthesis. As an alternative to chromatographic methods, this technique allows for the analysis of molecular diffusion in solution, providing diffusion coefficients (D) of molecules related to their hydrodynamic radius. The results are presented as a two-dimensional map. The horizontal axis displays the conventional chemical shift spectra, while the vertical axis shows the spectra of the diffusion coefficients. DOSY NMR is especially valuable for detecting by-products or impurities, including unreacted monomers, residual homopolymers, and degradation products, providing information on the polymerization process and the quality of the final product.^{356–359}

Analysis of PVP-CTA1 and PVP-*b*-PNVF using DOSY NMR confirmed the successful synthesis of a block copolymer (Figure 65). This conclusion was drawn from the distinct diffusion coefficients observed for each sample in the spectrum. PVP-CTA1 was characterized by a higher diffusion coefficient ($D = 49 \mu\text{m}^2 \text{s}^{-1}$) due to its lower hydrodynamic radius. Conversely, PVP-*b*-PNVF displayed a lower diffusion coefficient ($D = 6 \mu\text{m}^2 \text{s}^{-1}$). Additionally, no residual signals from the first block were detected in the NMR spectrum of the copolymer.

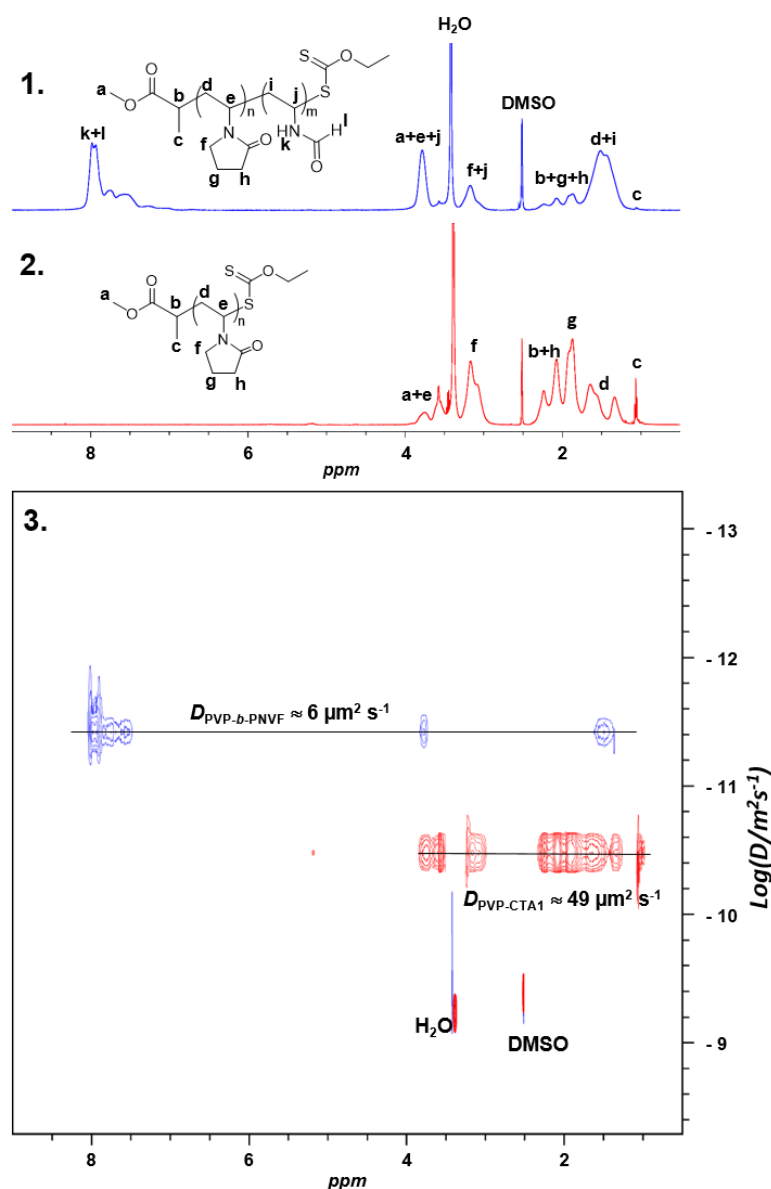
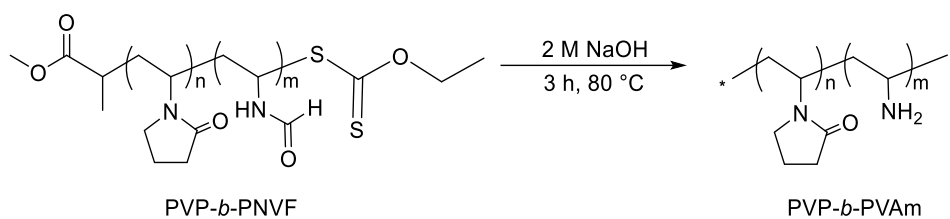


Figure 65. ^1H DOSY NMR spectra (500 MHz, DMSO).

4.8.2.3. Hydrolysis of the PNVF segment

Poly(*N*-vinylformamide) can be converted to PVAm through hydrolysis in either acidic or basic conditions.^{229,360} Acidic hydrolysis results in cationic polymers, which may hinder the complete transformation of PNVF into PVAm due to electrostatic repulsion between cationic amine groups and proton hydrates. In contrast, basic hydrolysis leads to the formation of polymers with free amine functional groups, making the process generally more effective with almost complete conversion. In the present study, the hydrolysis of the PNVF block was carried out under basic conditions (Scheme 19). PVP-*b*-PNVF was dissolved in 2 M sodium hydroxide (NaOH), and the solution was heated at 80 °C for 3 h. Afterward, the copolymer was purified by dialysis to remove the forming by-product (sodium formate salt).



Scheme 19. The hydrolysis of the PNVF segment.

Confirmation of the quantitative conversion of PVP-*b*-PNVF to PVP-*b*-PVAm was achieved using ^1H NMR spectroscopy of purified polymers. This was evident from the complete disappearance of a broad signal corresponding to the formyl group (k), previously visible in the range of 7.7–8.1 ppm, and the shift of signals corresponding to methylene (i) and methyne (j) from 1.5 to 1.1 ppm and from 3.8 to 2.8 ppm, respectively (Figure 66).

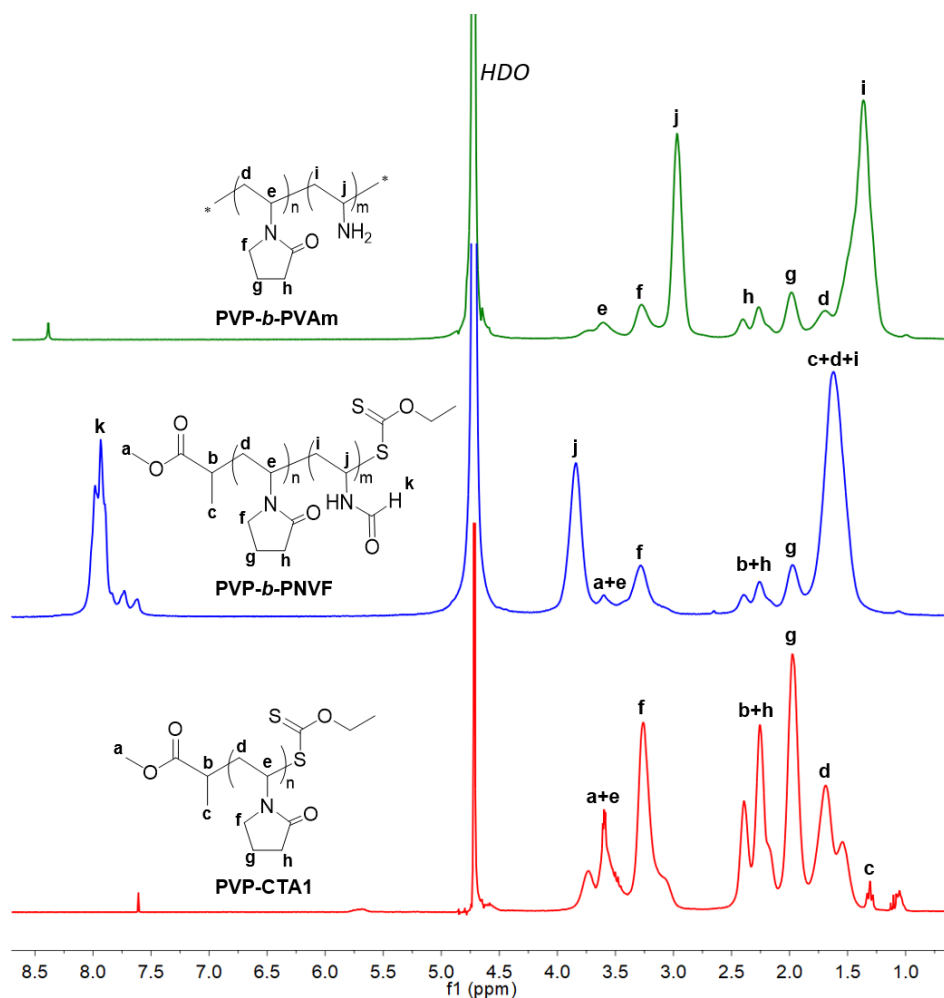


Figure 66. Comparison of ^1H NMR spectra of PVP-CTA1, PVP-*b*-PNVF, and PVP-*b*-PVAm (300.13 MHz, D_2O).

Summary

This chapter of the doctoral dissertation focused on the polymerization of *N*-vinylformamide (NVF) using the photoiniferter reversible addition-fragmentation chain transfer (PI-RAFT) technique in a custom photoreactor with LEDs. Purple LEDs (395–400 nm) were more effective than blue (460 nm), achieving 80% conversion in 4 hours, compared to 40 hours with blue light. Molar mass analyses further showed that purple LED light provided better control over polymerization. Adjusting the intensity showed that, while higher intensities led to faster polymerization, a moderate intensity (using 30 LEDs) provided a balance between speed and control. Further investigation was conducted on the polymerization behavior of NVF under PI-RAFT at different targeted molar masses (5, 20, and 50 kg mol⁻¹). The results highlighted the controlled nature of the polymerization process, with the obtained polymers showing a linear correlation of molar mass with monomer conversion. Experiments were also conducted to understand the importance of the RAFT agent and purple light in the polymerization process. No polymerization occurred in tests where either the dithiocarbonate (a RAFT agent) was excluded or the mixture was exposed to daylight. Highlighting the significance of light in this process, it was found that light could serve as a temporal switch, initiating or halting polymerization instantaneously. The study also delved into analyzing the end groups of the polymer to confirm its "living" nature. Several techniques were used, including MALDI-TOF MS, ESI-TOF MS, and ¹H NMR. The results confirmed the presence of dithiocarbonate as a chain-end group in the synthesized polymer. These findings were further validated with a chain extension experiment, demonstrating that PI-RAFT is a potent method for NVF polymerization, enabling the potential synthesis of block copolymers with a PNVF segment.

Two block copolymers containing PNVF segments were successfully synthesized via PI-RAFT polymerization with macro-CTAs based on poly(ethylene glycol) (PEG) and poly(*N*-vinylpyrrolidone) (PVP). For polymerization with PEG, an 87% NVF conversion was achieved after 6 hours under purple light irradiation. As validated by aqueous SEC, the molar masses of the resulting copolymer agreed with the theoretical predictions. In the case of the PVP-based macro-CTA, PI-RAFT polymerization was initially challenging. However, after changing the chain transfer agent to 2-(ethoxycarbonothioyl)thio)propanoate (CTA1), polymerization was rapid and controlled, with 94% conversion after 30 minutes of purple light irradiation. A PVP-CTA1 was then synthesized and used as a macro-CTA for NVF polymerization, displaying controlled polymerization behavior. Despite challenges in

solubility during SEC analysis, the synthesis of the PVP-*b*-PNVF block copolymer was confirmed using alternative techniques such as asymmetric flow field flow fractionation (AF4) and diffusion-ordered nuclear magnetic resonance (DOSY NMR). Lastly, the hydrolysis of the PNVF segment was performed under basic conditions using 2 M sodium hydroxide. The resultant copolymer underwent complete conversion from PVP-*b*-PNVF to PVP-*b*-PVAm, which was confirmed using ¹H NMR spectroscopy.

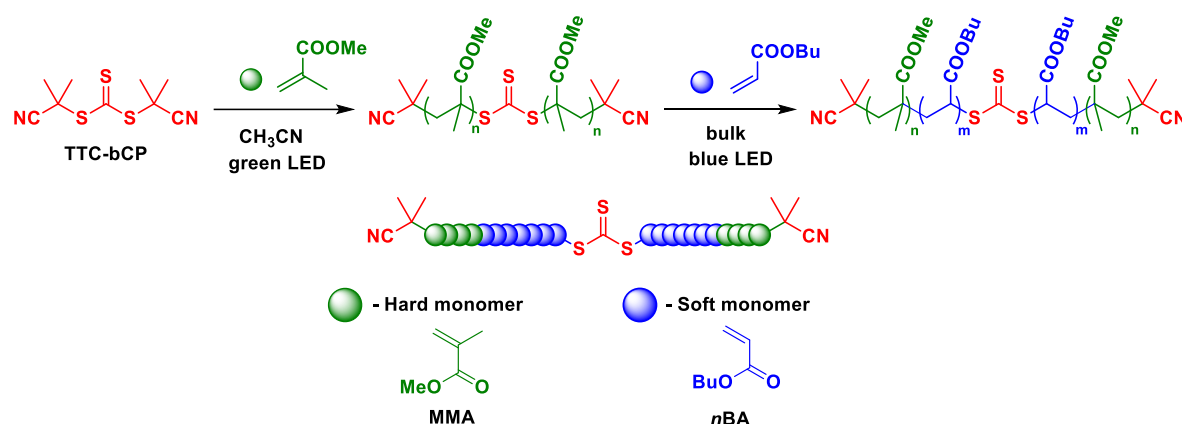
In summary, barriers in NVF polymerization were overcome by conducting an eco-friendly PI-RAFT polymerization under mild conditions influenced by purple light. The PI-RAFT approach enabled the synthesis of well-defined PNVF-based homopolymers and copolymers. Moreover, the transformation of PNVF to PVAm through basic hydrolysis was a foundational step toward future advances in the synthesis and potential applications of PVAm.

Part of the results of this chapter have been published in:

1) I. Kurowska, A. Dupre–Demorsy, S. Balayssac, M. Henriet, A. Ric, V. Bourdon, T. Ando, H. Ajiro, O. Coutelier, M. Destarac, *Macromolecular Rapid Communications* **2023**, *44*, 2200729.

CHAPTER 5. SYNTHESIS OF ABA TRIBLOCK COPOLYMERS

This part of the work aims to expand the knowledge on synthesizing homopolymers based on poly(methyl methacrylate) (PMMA) or poly(*n*-butylacrylate) (P*n*BA) and their methacrylate–acrylate–methacrylate (hard–soft–hard) ABA triblock copolymers as a potential thermoplastic elastomer (TPE). Polymerizations were performed using PI-RAFT polymerization with a new symmetrical RAFT agent called bis-(2-methylpropanenitrile) trithiocarbonate (TTC-bCP, CTA3) (Scheme 20).²⁴⁶ PMMA with T_g in the range of 120–135 °C was selected as a hard block (A), and P*n*BA with T_g of approximately -40 °C as a soft block (B).²⁴³ It is important to highlight that the key to achieving the desired properties of methacrylate–acrylate–methacrylate copolymers, such as high elongation, flexibility, UV, and scratch resistance, lies in the precise combination of methacrylate and acrylate blocks. The performance of these materials as TPEs depends on the ratio of hard to soft blocks, with optimal properties observed when the hard phase accounts for about 15 to 30% of the composition.^{259,361–364}



Scheme 20. General scheme for the synthesis of ABA triblock copolymers using PI-RAFT.²⁴⁶

5.1. Synthesis of a hard block: PMMA

5.1.1. The influence of light wavelength on polymerization

Bis-(2-methylpropanenitrile)trithiocarbonate (TTC-bCP) absorbs light in the UV region (265–365 nm) due to the spin allowed $\pi \rightarrow \pi^*$ electronic transition of the thiocarbonyl group and the absorption in the visible light region (385–545 nm) is caused by the spin forbidden $n \rightarrow \pi^*$ electronic transition (Figure 67). Thus, it can be excited by either blue or green light.

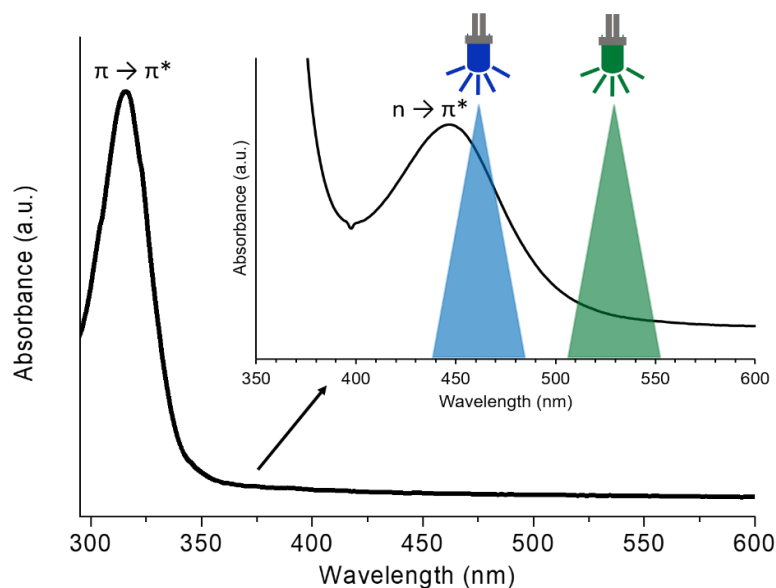


Figure 67. UV-Vis spectrum of bis-(2-methylpropanenitrile)trithiocarbonate (TTC-bCP).

Therefore, first, two varying wavelengths of light, 460 nm (blue) and 530 nm (green), were tested to drive methyl methacrylate (MMA) polymerization targeting $M_{n,th} = 50 \text{ kg mol}^{-1}$. MMA polymerizations were carried out in a 50% w/w acetonitrile (CH_3CN) solution for 16 hours, using photoreactors equipped with 60 LEDs. Using blue light during the polymerization resulted in a higher conversion of 81%, while green light yielded a conversion of 61%. However, SEC analysis revealed that the control of the polymerizations was notably different for these two samples. The molar mass of PMMA polymerized with green light showed good agreement between M_n obtained from SEC ($M_{n,SEC} = 28.0 \text{ kg mol}^{-1}$, $\mathcal{D} = 1.22$) and the theoretical value ($M_{n,th} = 30.6 \text{ kg mol}^{-1}$). On the other hand, $M_{n,SEC} = 29.8 \text{ kg mol}^{-1}$ of the polymer obtained using blue light was lower than the expected value ($M_{n,th} = 40.6 \text{ kg mol}^{-1}$) and was characterized by a much higher dispersity ($\mathcal{D} = 1.62$). This was further supported by comparing SEC-RI (Figure 68, solid lines) chromatograms, which showed a broader and bimodal profile for blue light-initiated polymerization. The TTC mid-chain fragments were also detected in green light-initiated polymerization through SEC-UV traces (Figure 68, dashed lines), where a strong UV absorbance at a wavelength of 290 nm was observed. However, no signal was detected for the polymer polymerized with blue LEDs, indicating the photodegradation of TTC fragments and a lack of control over the process.

Based on these results, it was concluded that using the green light offered a better potential for the polymerization of MMA with CTA3 as a chain transfer agent and was chosen for further investigations.

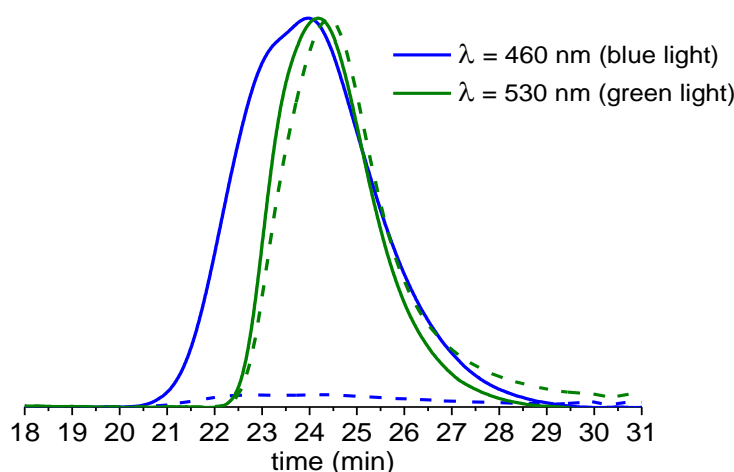


Figure 68. SEC chromatograms of PMMA obtained with different sources of light (SEC-RI trace: solid line, SEC-UV trace: dashed line).

5.1.2. The influence of monomer concentration on polymerization

The following research stage assessed the impact of monomer concentration on polymerization. Different concentrations of MMA in acetonitrile (70% w/w and 50% w/w) were tested to achieve a theoretical molar mass of 200 kg mol^{-1} . Polymerizations proceeded for 32 hours, achieving the same final conversions of 85%. However, when using a monomer concentration of 50% w/w, the molar masses determined by SEC were notably lower than the theoretical values (Figure 69 and Table 18). On the other hand, employing a higher concentration of MMA (70% w/w) and, therefore, increasing the concentration of radicals originating from CTA3 led to a better relationship of the molar masses measured by SEC with theoretical values. Nevertheless, longer irradiation times resulted in bimodal chromatograms because of the degradation of the TTC fragments (Figure 70). Despite this, the concentration of 70% w/w was selected for further research. Based on the findings from the previous part of the doctoral thesis on PI-RAFT polymerization of NVF, it was found that the bimodal character of the chromatogram combined with broad dispersity ($\mathcal{D} \sim 1.5$) could be attributed to the too high light intensity utilized in the system. Thus, as before, in the case of polymerization of NVF, it was decided to reduce the number of LEDs in the photoreactor to address this issue.

It is also worth mentioning that attempts to polymerize MMA in bulk were made. The results were quite promising. For example, for the theoretical molar mass ($M_{n,\text{th}}$) of 400 kg mol^{-1} , the conversion reached 52% after 16 hours of irradiation. The molar mass determined by SEC ($M_{n,\text{SEC}} = 192.4 \text{ kg mol}^{-1}$) was close to the theoretical assumption ($M_{n,\text{th}} = 208.1 \text{ kg mol}^{-1}$).

mol^{-1}). The dispersity was also low ($\bar{D} = 1.24$), and the chromatogram exhibited a monomodal distribution (Figure 71). However, this method was subsequently abandoned because of the difficulties in solubilizing the polymer samples for SEC or NMR analysis.

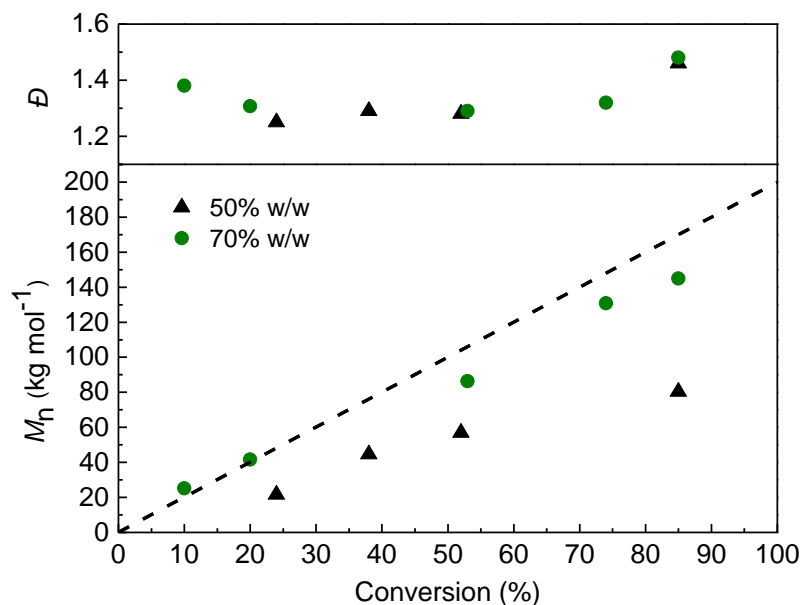


Figure 69. Evolution of M_n and \bar{D} during PI-RAFT polymerization with different concentrations of MMA in acetonitrile.

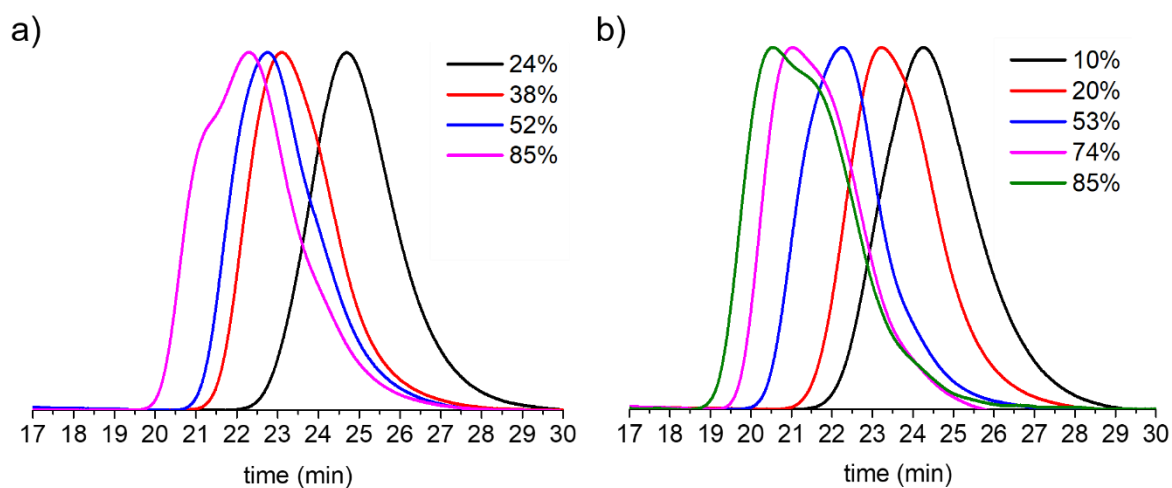


Figure 70. Evolution of PMMA SEC-RI chromatograms with MMA conversion for polymerizations carried out with a) 50% w/w and b) 70% w/w of MMA in acetonitrile.

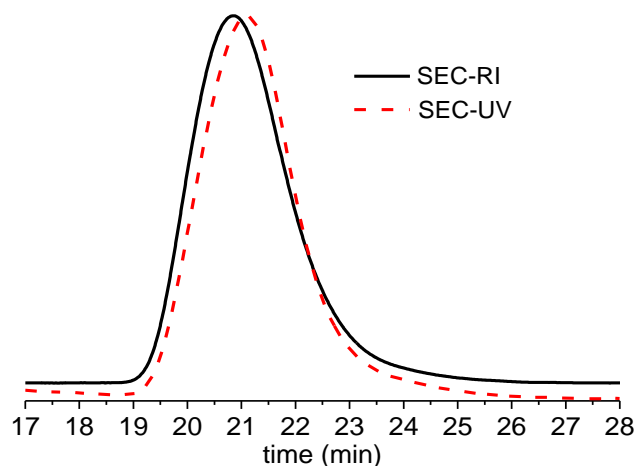


Figure 71. SEC chromatograms of PMMA prepared by bulk polymerization.

5.1.3. The influence of light intensity on the polymerization of MMA

As expected, reducing the light intensity by changing the number of LEDs to 30 caused better control over the polymerization of MMA. To investigate the behavior of methyl methacrylate during PI-RAFT, three different theoretical M_n of PMMA (50, 200, and 400 kg mol⁻¹) were selected for this study. The obtained polymers showed a linear increase in $M_{n,SEC}$ with monomer conversion and were in good agreement with theoretical values (shown in Figure 72 and Table 19).

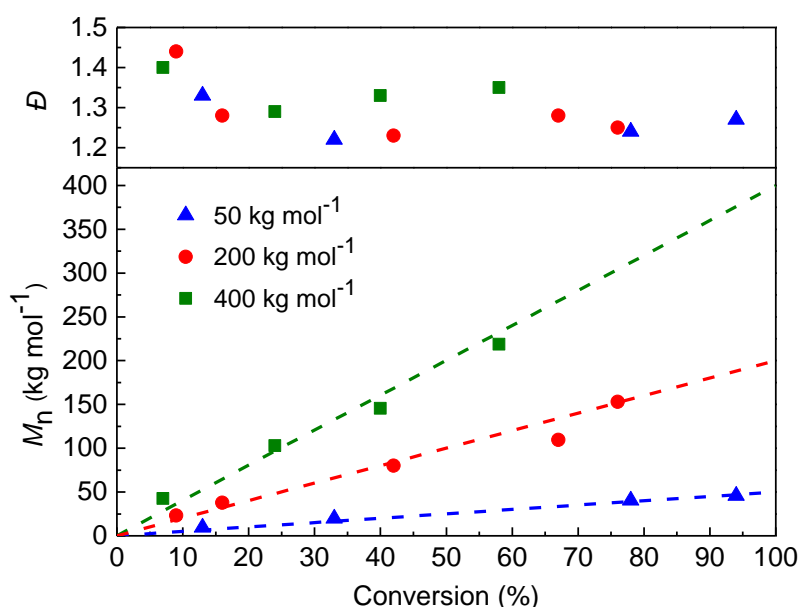


Figure 72. Evolution of M_n and \bar{D} during PI-RAFT polymerization for different targeted molar masses.

The dispersities values, $\mathcal{D} < 1.5$, also confirmed the controlled character of the polymerization. SEC traces were monomodal throughout polymerization and shifted toward a lower elution time with increasing monomer conversion (Figure 73). The polymerization rate increased with increasing initial concentration of the chain transfer agent. The pattern found here corresponded to that of experiments with *N*-vinylformamide. After 32 hours of irradiation, the conversion reached 94% for $M_{n,th} = 50 \text{ kg mol}^{-1}$. In contrast, for $M_{n,th} = 400 \text{ kg mol}^{-1}$, the monomer conversion was lower (58%) after the same period. Also, dispersities for polymers of $M_{n,th} = 50 \text{ kg mol}^{-1}$ were lower than those of $M_{n,th} = 400 \text{ kg mol}^{-1}$. The designed method enabled the synthesis of PMMA with a high molar mass of up to $M_n \sim 200 \text{ kg mol}^{-1}$ and low dispersities ($\mathcal{D} < 1.4$).

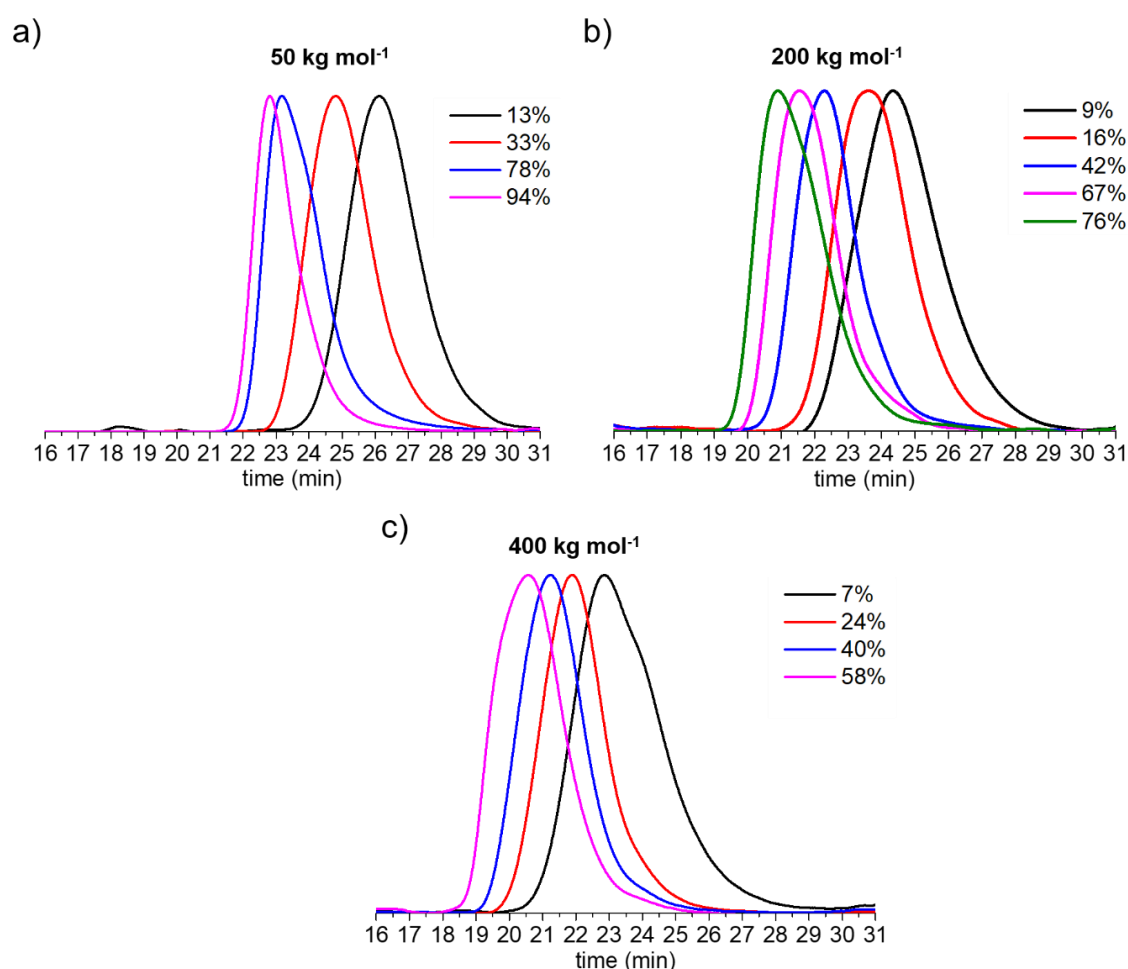


Figure 73. SEC-RI chromatograms of PMMA with MMA conversion for different molar masses.

5.2. Synthesis of a soft block: PnBA

The primary attempt to drive the polymerization of *n*-butyl acrylate via exposure to green light yielded no evidence of polymerization. Therefore, it was chosen to change the

reaction conditions and test the blue light. The reactions were carried out in bulk in a photoreactor equipped with 60 LEDs. The polymerization process was very effective. The molar masses of the polymers determined by SEC increased linearly with monomer conversion and matched theoretical predictions (Figure 74, Table 20). At the initial stage of all polymerization, dispersities were higher and tended to decrease quickly with monomer conversion. The average number of *n*BA units propagated between two reversible transfer events decreased with monomer concentration, which led to a decrease in dispersities over the course of polymerization.²⁴⁶ Then, after reaching approximately 30% of the monomer conversion, they stabilized at a lower level of < 1.07. The polymerization rate increased with increasing initial concentration of the chain transfer agent. The results were consistent with the previous results from NVF and MMA polymerization using PI-RAFT. After 24 hours of irradiation, the conversion reached almost 90% for 200 kg mol⁻¹. Polymers were characterized by exceptionally low dispersity (between 1.05 and 1.02). In contrast, for 1,500 kg mol⁻¹, the monomer conversion was nearly twice lower (48%) after the same period. However, dispersities remained at a similarly low level (between 1.10 and 1.02). SEC-RI traces also confirmed the controlled character of the polymerization. SEC chromatograms were symmetrical and monomodal in all cases and shifted toward a lower elution time with increasing monomer conversion (Figure 75).

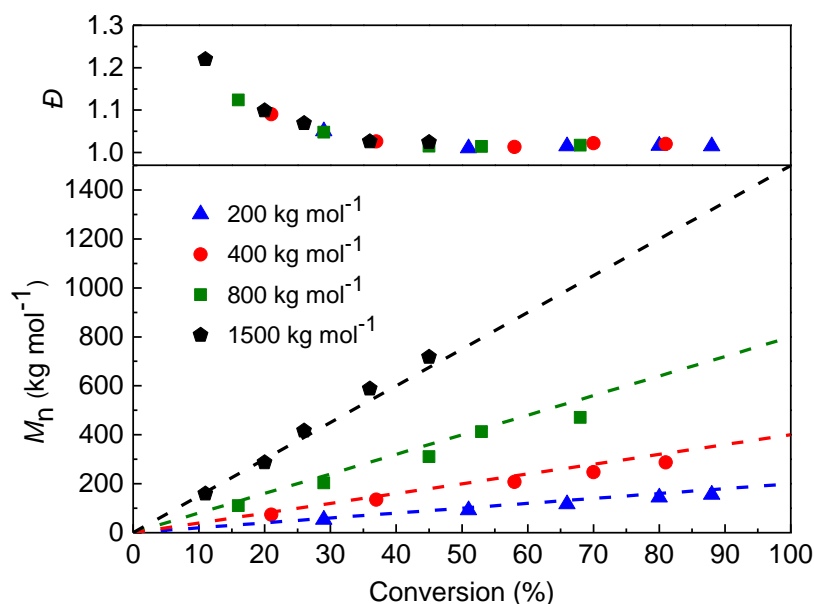


Figure 74. Evolution of M_n and \bar{D} during PI-RAFT polymerization for different targeted molar masses.

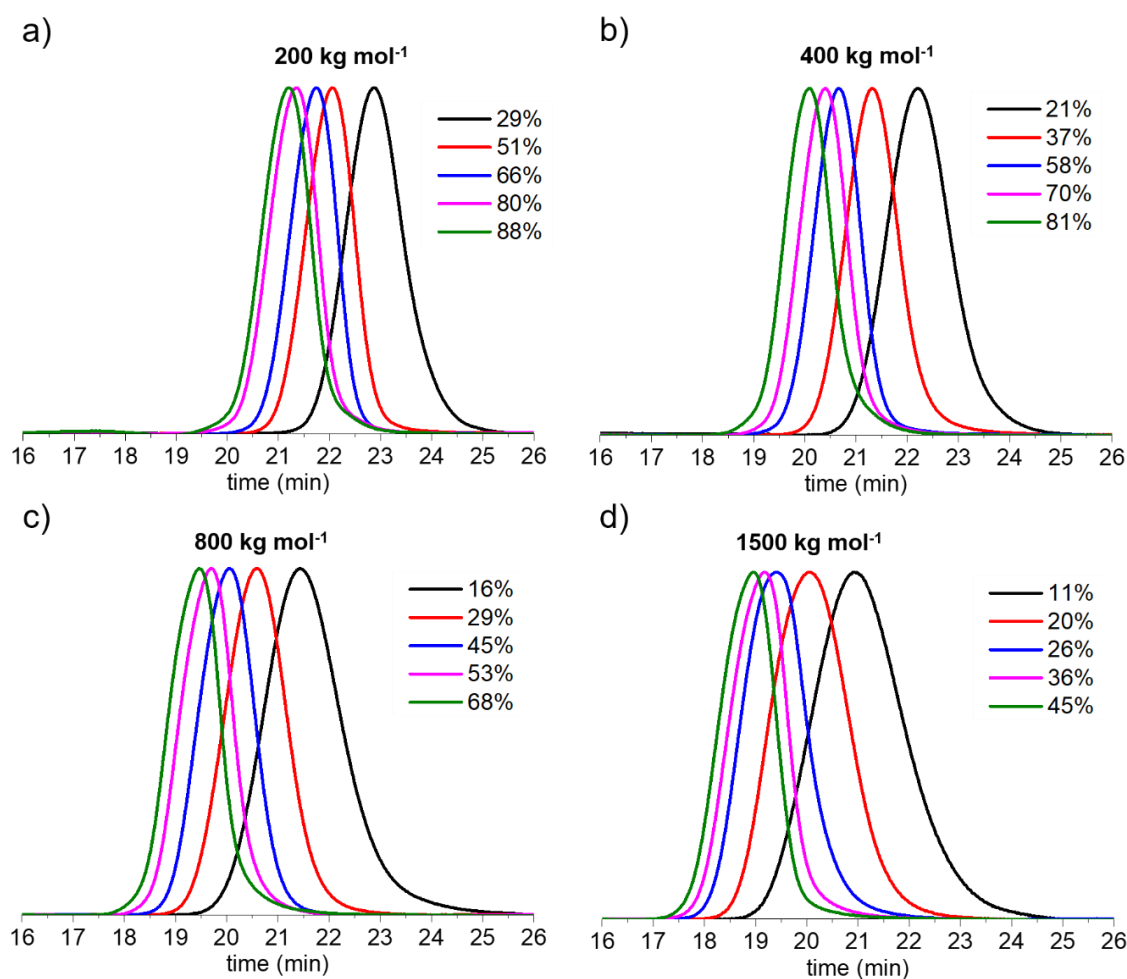


Figure 75. Evolution of SEC-RI chromatograms of PnBA with nBA conversion for different molar masses.

The PI-RAFT approach enhanced the accessibility of HMM PnBA ($M_n \sim 700 \text{ kg mol}^{-1}$) with low dispersity under mild conditions, compared to polymers obtained from RDRP methods reported in the literature. For example, PnBA of molar mass ($M_n = 612 \text{ kg mol}^{-1}$) with $\mathcal{D} = 1.25$ was prepared by ATRP under a high-pressure condition (5 kbar).³⁶⁵ PnBA with $M_n > 500 \text{ kg mol}^{-1}$ was also synthesized by TERP, but polymers were characterized by higher dispersity (~ 1.4).²⁶⁸

Based on these findings, it can be concluded that the choice of the light wavelength depends not only on the type of chain transfer agent but also on the character of the monomer and its reactivity. Acrylates and methacrylates differ significantly in their radical formation during polymerization. As mentioned in the literature introduction, acrylates form secondary radicals during polymerization, while methacrylates produce more stable tertiary radicals. The C–S bond dissociation energy increases with the insertion of a monomer that provides less stabilization (PnBA-CTA3).⁸³ Therefore, the green light was insufficient in the

polymerization of *n*BA. In the case of PMMA-CTA3, which has a weaker C–S bond dissociation energy, blue light is too energetic, as indicated by the lack of control over the polymerization process.

5.3. Synthesis of the ABA triblock copolymer

The possibility of using PI-RAFT to synthesize triblock polymers was examined in the next part of the work. PMMA-CTA3, obtained through a PI-RAFT polymerization optimized in the previous part of this work (green light, 30 LEDs, 30% w/w CH₃CN, 24 hours of irradiation), was selected as the first block. After purification by precipitation in toluene, PMMA-CTA3 ($M_n = 109.4 \text{ kg mol}^{-1}$, $D = 1.28$) was used in chain extension with *n*-butyl acrylate targeting a $M_{n,\text{th}} = 800 \text{ kg mol}^{-1}$. Polymerization was carried out in bulk for 4 h with blue LEDs as a light source, which was identified as suitable for the polymerization of *n*BA in the previous part of the work. The conversion of *n*BA was calculated from the ¹H NMR spectrum and reached 20%. The SEC analysis showed the formation of the triblock copolymer (Figure 76). However, a shoulder at 22 min corresponding to unreacted PMMA was observed. Due to the lack of a SEC-UV signal in this shoulder (red trace, dashed line), it was assumed that the extended irradiation time (24 h) during the synthesis of PMMA-CTA3, led to the degradation of the thiocarbonylthio group, which decreased the livingness of PMMA-macroCTA3.³⁶⁶ The dead polymer chains could not initiate polymerization, leading to the higher molar mass obtained from SEC ($M_{n,\text{SEC}} = 518.9 \text{ kg mol}^{-1}$) than the theoretical value ($M_{n,\text{th}} = 247.5 \text{ kg mol}^{-1}$). The polymer was also characterized by high dispersity $D = 1.59$.

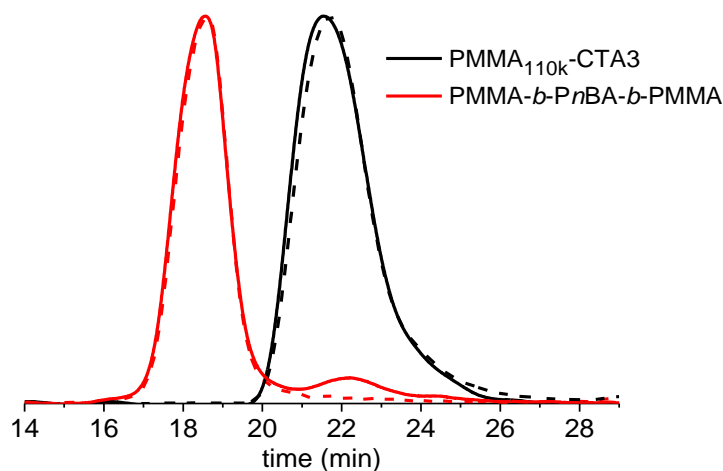


Figure 76. SEC chromatograms of PMMA110k-CTA3 and the corresponding ABA triblock copolymer.

To limit the possibility of macro-CTA photodegradation, PMMA-CTA3 ($M_{n,SEC} = 80.8 \text{ kg mol}^{-1}$, $\mathcal{D} = 1.21$), which was synthesized by being exposed to light for a shorter time (16 h), was used as the first block in chain extension with *n*-butyl acrylate. The conversion of *n*BA was 21%. The SEC analysis revealed the successful formation of the triblock copolymer, with a clear shift of the chromatograms and no residual of the starting PMMA (Figure 77). Furthermore, the molar mass determined by SEC ($M_{n,SEC} = 217.7 \text{ kg mol}^{-1}$) was in good agreement with the expected $M_{n,th} = 231.9 \text{ kg mol}^{-1}$, and the polymer was characterized by low dispersity ($\mathcal{D} = 1.13$). Compared to the previous report, where PMMA-*b*-P*n*BA-*b*-PMMA ($M_n = 135 \text{ kg mol}^{-1}$, $\mathcal{D} = 1.04$) was obtained by the traditional azo-initiated polymerization,²⁴⁶ the M_n obtained with the PI-RAFT approach was twice higher while maintaining a similar level of control. This modification is particularly significant as it suggests potential changes in TPE properties, such as increased chain entanglement in both the hard and soft phases.

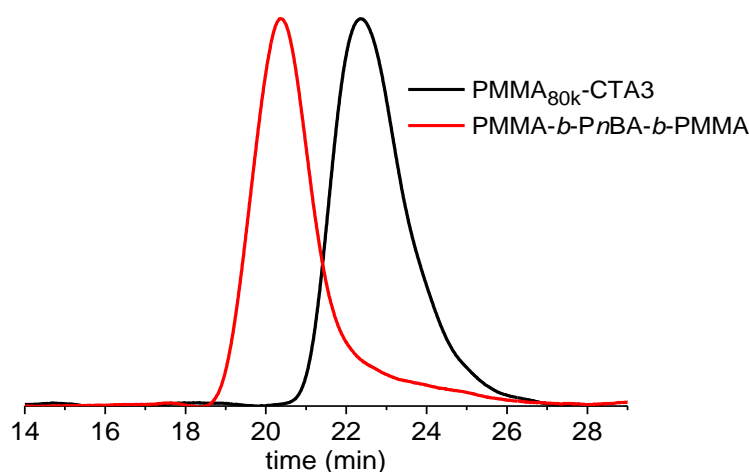


Figure 77. SEC-RI chromatograms of PMMA_{80k}-CTA3 and the corresponding ABA triblock copolymer.

The promising results of this part of the doctoral dissertation will continue in the SOFTMAT laboratory. The synthesis conditions for triblock copolymers will be optimized, as this may facilitate the production of well-defined polymers with higher molar masses and, thus, intriguing properties. Additionally, ABA triblock polymers will be tested regarding their thermomechanical properties in order to reveal their TPE behavior.

Summary

This chapter of the doctoral thesis evaluates the synthesis of homopolymers and (meth)acrylic ABA triblock copolymers using PI-RAFT polymerization. The work targets the creation of potential thermoplastic elastomers using poly(methyl methacrylate) (PMMA) and poly(*n*-butylacrylate) (*Pn*BA) as hard and soft blocks, respectively. A key objective was synthesizing high molar mass (HMM) polymers to enhance mechanical and thermal properties.

At first, the effects of variables such as light wavelength, monomer concentration, and light intensity on the polymerization of MMA were examined. Experiments with blue (460 nm) and green (530 nm) light showed significant differences in polymerization. Green light was more suitable for the controlled polymerization of MMA, as indicated by closer agreement of the molar masses obtained by SEC with theoretical values, lower dispersity, and the presence of TTC mid-chain fragments in the SEC-UV chromatograms. Next, the monomer concentration in acetonitrile (70% w/w and 50% w/w) on polymerization was investigated. A higher monomer concentration improved the alignment of $M_{n,SEC}$ with theoretical values but caused bimodal chromatograms due to TTC fragment degradation. It was found that high light intensity could contribute to the bimodal character of chromatograms, leading to a decision to reduce the number of LEDs in the photoreactor. Reducing light intensity led to improved control over MMA polymerization. A closer alignment of the observed molar masses with theoretical values, lower dispersities, and monomodal SEC traces evidenced this. This approach enabled the synthesis of PMMA with a high molar mass of $218.8 \text{ kg mol}^{-1}$ and relatively low dispersity ($D = 1.35$).

Polymerization *n*BA was initially unsuccessful under green light, prompting a switch to blue light. This change significantly improved polymerization, yielding polymers with molar masses obtained from SEC in agreement with theoretical values and exceptionally low dispersity. This approach resulted in the HMM *Pn*BA with the highest molar mass of $718.2 \text{ kg mol}^{-1}$ with $D = 1.02$.

The final section explored the synthesis of ABA triblock polymers. The process involved extending PMMA-CTA3 with *n*-butyl acrylate using blue light. Two different approaches using PMMA-CTA3 prepared by exposure to green light for varying durations (16 h and 24 h) were tested. The study finds that longer irradiation led to degradation of the thiocarbonylthio group in PMMA-macroCTA3. However, using PMMA obtained by being

exposed to light for a shorter duration shows the successful formation of triblock copolymers with molar mass determined by SEC closely matched to theoretical predictions.

In conclusion, this chapter presents comprehensive insights into the influence of light wavelength, monomer concentration, light intensity, and irradiation time on the polymerization of MMA, *n*BA, and their PMMA-*b*-P*n*BA-*b*-PMMA triblock copolymer. Notably, the PI-RAFT approach enabled the doubling of the M_n of PMMA-*b*-P*n*BA-*b*-PMMA copolymer, compared to the previous report.²⁴⁶ A key advancement demonstrated in this chapter is the development of an initiator-free RAFT methodology for the preparation of high molar mass homopolymers and triblock copolymers. The PI-RAFT method, utilizing milder conditions such as LED light, room temperature, and a limited amount of solvent, marks a significant improvement over the previous technique. These findings open pathways for producing well-defined ABA triblock polymers with potential applications as thermoplastic elastomers.

CONCLUSIONS AND PERSPECTIVES

This dissertation demonstrates the versatile application of reversible addition-fragmentation chain transfer (RAFT) polymerization to synthesize polymers with the desired properties and architecture. It specifically explores the applications of RAFT polymerization in three areas: developing thermoresponsive drug delivery systems based on diglycerides, achieving controlled polymerization of *N*-vinylformamide, and enhancing the synthesis of (meth)acrylic ABA triblock copolymers. Each part of the research addressed the stated hypotheses. The key findings of this dissertation are summarized below.

PART I. Developing thermoresponsive drug delivery systems based on diglycerides.

RAFT polymerization allowed the obtaining of homopolymers and block copolymers, which contained one or several diglyceride molecules in their structure, and thermoresponsive blocks based on poly(*N*-isopropylacrylamide) (PNIPAAm) or poly(*N*-vinylcaprolactam) (PNVCL). Despite the benefits of using diglycerides in drug delivery systems, such as enhancing interactions with the cell membrane, this research was the first to present water-soluble block copolymers with diglycerides in the side chains.

Polymeric nanoparticles formed from homopolymers and block copolymers were stable in an aqueous environment, demonstrated sensitivity within a narrow temperature range, and possessed ideal physicochemical parameters required for drug carriers. It was demonstrated that copolymers-based nanoparticles can efficiently encapsulate poorly water-soluble anticancer drugs and control the release of therapeutic agents in response to temperature variations. Furthermore, the structure of these nanoparticles has been proven to influence drug encapsulation efficiency and drug release profiles. The PNPs demonstrated a significantly higher encapsulation efficiency for tamoxifen compared to doxorubicin, underscoring the role of polymer design in optimizing drug delivery systems. Integrating diglyceride moieties within PNPs has enhanced their biocompatibility and interaction with cellular membranes. Despite the lack of significant differences in the physicochemical properties of PNPs composed of diglycerides with saturated and unsaturated chains (PGlyP and PGlyO) and thermoresponsive blocks (PNIPAAm and PNVCL), their composition influenced their biological properties. Although low doses of the encapsulated drug, DOX-loaded carriers exhibited significant cytotoxic effects against MCF-7 and MDA-MB-231 breast cancer cell lines. Simultaneously, they maintained compatibility with representatives

of normal cells. It was also demonstrated that fluorescein-labeled PNPs could penetrate the membranes of breast cancer cells, thereby disintegrating their functions.

These results indicate that thermoresponsive polymers with diglyceride moieties are valuable tools as drug carriers. Moreover, fluorescein-labeled PNPs can be utilized as theranostic agents, providing simultaneous therapeutic and diagnostic functions.

PART II. Exploring the polymerization of *N*-vinylformamide by PI-RAFT polymerization.

Barriers in NVF polymerization were overcome by conducting PI-RAFT polymerization under mild conditions influenced by the light of a specific wavelength. Until recently, the controlled synthesis of poly(*N*-vinylformamide) (PNVF) has been a synthetic challenge. The research validated that the purple LED light effectively initiated NVF polymerization, yielding polymers with predetermined molar masses and low molar mass distribution. Experiments established the essential role of dithiocarbonate and purple light in polymerization, as evidenced by the absence of polymerization when the RAFT agent was excluded, or the mixture was exposed to daylight. The presence of dithiocarbonate end-groups in the polymers synthesized through the PI-RAFT technique proved their "living" nature. The synthesis of original block copolymers with the PNVF segment utilizing PEG and PVP as macro-CTAs (PEG-*b*-PNVF, PVP-*b*-PNVF) proceeded in a controlled manner. Moreover, it has been shown that the selective hydrolysis of PNVF led to the corresponding polyvinylamine (PVAm) segment.

The development of a fast and effective method for synthesizing PNVF homopolymers and copolymers containing the PNVF block paved the way for creating new materials based on PVAm.

PART III. Investigating the synthesis of high molar mass (meth)acrylic ABA triblock copolymers employing the PI-RAFT technique.

The application of the new RAFT agent TTC-bCP in PI-RAFT polymerization enabled the synthesis of PMMA, *Pn*BA, and their triblock ABA copolymer under mild conditions. The use of varied light wavelengths, monomer concentration, and light intensities allowed the optimization of the PI-RAFT process and successful synthesis of PMMA-*b*-*Pn*BA-*b*-PMMA with a molar mass significantly higher than that reported in previous studies.

This advancement underscores the potential of initiator-free, light-mediated polymerization in creating more efficient and environmentally friendly synthetic routes for ABA triblock copolymers with application as high-performance materials.

Further investigation of the long-term therapeutic effectiveness and safety of synthesized drug delivery systems is essential. Furthermore, exploring the full potential of PNVF and PVAm-based materials in various applications could yield groundbreaking results. More research should look into high molar mass ABA triblock copolymer properties as thermoplastic elastomers, e.g., rheology studies. Future research should also focus on refining the PI-RAFT technique to broaden its applicability. Expanding the range of monomers and conditions used in PI-RAFT polymerization could lead to the discovery of new polymeric materials.

In conclusion, this dissertation has significantly advanced the field of polymer science by demonstrating the applications of RAFT polymerization in creating a broad range of polymers with desired properties and architectures. This research not only addressed the original objectives but also opened new horizons in macromolecular design. The approaches adopted in this study for synthesizing thermoresponsive drug delivery systems, controlling *N*-vinylformamide polymerization, and developing (meth)acrylic ABA triblock copolymers underscore the vast potential of RAFT polymerization in medicinal and industrial applications. The implications of these findings offer a foundation for future explorations and innovations in the dynamic and ever-evolving realm of polymer chemistry.

SUMMARY IN BULLET POINTS

PART I. Developing thermoresponsive drug delivery systems based on diglycerides.

1. The following compounds have been synthesized:
 - a) 2 diglyceride-based chain transfer agents (GlyP-X, GlyO-X),
 - b) 2 diglyceride-based monomers (GlyP-A, GlyO-A),
 - c) 1 chain transfer agent (CTA1),
 - d) 20 homopolymers, including:
 - 8 diglyceride end-capped homopolymers of PNIPAAm (GlyP-PNIPAAm, GlyO-PNIPAAm),
 - 8 diglyceride end-capped homopolymers of PNVCL (GlyP-PNVCL, GlyO-PNVCL),
 - 2 diglyceride-based homopolymers (PGlyP, PGlyO),
 - PNIPAAm obtained by radical polymerization,
 - PNVCL obtained by radical polymerization,
 - e) 4 copolymers (PGlyP-*b*-PNIPAAm, PGlyP-*b*-PNVCL, PGlyO-*b*-PNIPAAm, PGlyO-*b*-PNVCL),
 - f) 4 fluorescently labeled copolymers (PGlyP-*b*-PNIPAAm, PGlyP-*b*-PNVCL, PGlyO-*b*-PNIPAAm, and PGlyO-*b*-PNVCL).
2. The following nanoparticles have been prepared:
 - a) 20 empty polymeric nanoparticles, including:
 - 12 polymeric nanoparticles prepared from thermoresponsive diglyceride end-capped homopolymers of PNIPAAm or PNVCL,
 - 4 polymeric nanoparticles prepared from thermoresponsive copolymers with diglyceride-based segment,
 - 4 fluorescently-labeled polymeric nanoparticles prepared from thermoresponsive copolymers with diglyceride-based segment.
 - b) 16 drug-loaded polymeric nanoparticles, including:
 - 4 polymeric nanoparticles with encapsulated doxorubicin,
 - 4 polymeric nanoparticles with encapsulated tamoxifen,
 - 4 fluorescently-labeled polymeric nanoparticles with encapsulated doxorubicin,
 - 4 fluorescently-labeled polymeric nanoparticles with encapsulated tamoxifen.

3. The structures of the monomers and chain transfer agents were confirmed using ^1H NMR, ^{13}C NMR, ATR-FTIR, and MS.
4. Polymers were characterized by ^1H NMR, ATR-FTIR, SEC, UV-VIS, fluorimetry, TGA, and DSC.
5. Polymeric nanoparticles based on diglyceride end-capped homopolymers of PNIPAAm or PNVCL were characterized by DLS, TEM, and turbidimetry.
6. Polymeric nanoparticles derived from thermoresponsive copolymers with diglyceride-based segments were characterized by DLS, ELS, TEM, fluorimetry, and turbidimetry.
7. The release of the drug (tamoxifen) from four thermoresponsive polymeric nanoparticles was investigated.
8. Selected polymeric nanoparticles were tested regarding their biological properties.

PART II. Exploring the polymerization of *N*-vinylformamide by PI-RAFT polymerization.

1. The effects of light wavelength and light intensity on polymerization NVF were investigated.
2. The following compounds have been synthesized:
 - a) PNVF with different targeted molar masses (5, 20, and 50 kg mol⁻¹),
 - b) 1 chain transfer agent (CTA2),
 - c) 3 macro-CTAs (PNVF-CTA2, PEG-CTA1, PVP-CTA1),
 - d) 2 copolymers with PNVF segment (PEG-*b*-PNVF, PVP-*b*-PNVF),
 - e) 1 copolymer with PVAm segment (PVP-*b*-PVAm).
3. Polymers were characterized by ^1H NMR, SEC, AF4, and DOSY-NMR.
4. Dithiocarbonate and light-free experiments were performed.
5. The nature of the end-groups of PNVF was confirmed by the chain extension experiment, MALDI-TOF MS, ESI-TOF MS, and ^1H NMR.
6. PVP-*b*-PNVF was hydrolyzed to the corresponding PVP-*b*-PVAm.

PART III. Investigating the synthesis of high molar mass (meth)acrylic ABA triblock copolymers employing the PI-RAFT technique.

1. The effects of light wavelength, light intensity, and monomer concentration on polymerization of MMA were investigated.
2. The effect of light wavelength on the polymerization of *n*BA was investigated.
3. PMMA with different targeted molar masses (50, 200, and 400 kg mol⁻¹) was synthesized via the PI-RAFT method using green light.

4. PnBA with different targeted molar masses (200, 400, 800, and 1,500 kg mol⁻¹) was synthesized via the PI-RAFT method using blue light.
5. Methacrylate–acrylate–methacrylate ABA triblock copolymer with high molar mass was synthesized via the PI-RAFT method using blue light.

EXPERIMENTAL PART

CHAPTER 6. METHODS

The obtained compounds, polymers, and polymeric materials were identified and characterized using the scientific and research equipment listed below.

Asymmetrical flow field flow fractionation (AF4) coupled with multiangle light scattering and differential refractometer. AF4 analyses were performed using a Thermo Scientific Dionex UltiMate3000 HPLC System with pump, thermostated autosampler (set at 25 °C), and UV detector (set at 290 nm). The pump was coupled with Eclipse AF4 (Wyatt Technology) to regulate flows in the separation channel (long channel, Wyatt Technology). An ultrafiltration membrane of regenerated cellulose material with a cut-off at 2 kDa (Wyatt Technology) was used. A 350 μm thick Mylar spacer of trapezoidal geometry (length of 23.6 cm, initial breadth of 2.1 cm, and final breadth of 0.6 cm) was inserted between the membrane and the upper glass plate. A multi-detection system, including an 8-angle Dawn8+ MALS detector and an Optilab T-rEX dRI (Wyatt Technology), was coupled with the AF4 system. The Chromeleon 7.2.10 software was used to control the autosampler, pump, and Eclipse flows. Acquisition of UV, MALS-Qels, and dRI data was performed using Astra 7.1.2.5 software. The Zimm model was used to obtain the average molecular mass M_n via MALS.³⁶⁷ dn/dc of the homopolymer and copolymer were measured on the same Optilab T-rEX dRI detector (Wyatt Technology), $(\text{dn}/\text{dc})_{\text{PVP-CTAI}} = 0.159 \text{ mL g}^{-1}$; $(\text{dn}/\text{dc})_{\text{PVP-}b\text{-PNVF}} = 0.167 \text{ mL g}^{-1}$. The system was calibrated using a standard bovine serum albumin (BSA) solution. The eluent comprised Milli-Q Water with 0.1 mol L⁻¹ sodium nitrate and sodium azide. For separation, the detector flow rate was maintained at 1 mL min⁻¹. During the focus/injection step, the focus-flow rate was set at 3 mL min⁻¹. After 1 min, samples were injected at 0.2 mL min⁻¹ over 4 min. The focus flow was then maintained for 2 min. During the elution step, the cross-flow was set at 5 mL min⁻¹ and decreased exponentially to reach 0.1 mL min⁻¹ after 16 min. It was then maintained at 0.1 mL min⁻¹ for 5 min. The system was rinsed with eluent for 28 min after each sample. The measurements were taken at the Institut National Polytechnique de Toulouse by Dr. Alexis Dupre–Demorsey.

Attenuated total reflectance Fourier transform infrared spectroscopy (ATR-FTIR). All ATR-FTIR spectra were performed using a Thermo Scientific Nicolet 6700 FTIR

spectrophotometer equipped with diamond ATR. Spectra were compared with background spectra, and 32 scans were taken from 400 to 4000 cm^{-1} .

Differential scanning calorimetry (DSC). Measurements were made using a Mettler Toledo Star DSC unit. A sample (2–3 mg) was placed in an aluminum crucible and sealed. An empty pan was used as the reference. The samples were measured using the following procedure: heated from 25 to 200 $^{\circ}\text{C}$ at a rate of 10 $^{\circ}\text{C min}^{-1}$, held isothermally for 5 min, and then cooled to -100 $^{\circ}\text{C}$ at a rate of -20 $^{\circ}\text{C min}^{-1}$. Two heating/cooling cycles were performed under an argon flow rate of 200 ml min^{-1} . The glass transition temperature (T_g) was taken as the change in the midpoint of the heat capacity in the second heating run. The measurements were made at the Faculty of Chemistry of the University of Białystok by Prof. Agnieszka Z. Wilczewska or Dr. Karolina H. Markiewicz.

Dynamic light scattering (DLS). The colloidal stability and phase separation of the obtained polymeric systems was studied using a Zetasizer Ultra (Malvern Instruments, UK) equipped with a He-Ne laser ($\lambda = 633 \text{ nm}$). Polymeric nanoparticles were redispersed in PBS or water at a concentration of 0.5 mg mL^{-1} to determine the size. Polymeric nanoparticles were prepared in water or PBS at a concentration of 0.5 mg mL^{-1} to study phase separation. Measurements were carried out in the temperature range from 25 to 40 $^{\circ}\text{C}$ with a heating step of 0.5 $^{\circ}\text{C}$. The aggregation temperature (T_{Agg}) was determined based on size versus temperature plots and was taken as an inflection point of the curve.

Electrospray ionization-time of flight mass spectrometry (ESI-TOF MS). ESI-TOF mass spectra were acquired with a QTOF Premier mass spectrometer (Waters) in positive mode. The sample was dissolved in water, diluted at 1/20 in methanol, and then NaI was added. The resulting samples were infused directly into the source. The source and desolvation temperatures were 110 $^{\circ}\text{C}$ and 200 $^{\circ}\text{C}$, respectively, and the cone voltage was optimized at 30 V. The measurements were made at Institut de Chimie de Toulouse by Dr. Valérie Bourdon.

Fluorescence measurements. A. Critical micelle concentration (CMC). The critical micelle concentration values of copolymers were determined by fluorescence spectroscopy using pyrene as a hydrophobic probe. Ten microliters of pyrene stock solution in acetone (0.15 mM) were poured into vials, and acetone was entirely evaporated by an argon stream. Then, 3 mL of aqueous polymer solutions of various concentrations (10^{-4} to 1 mg mL^{-1}) were added to the vials and vigorously stirred. The mixtures were stored overnight in the dark to achieve equilibrium. Then emission spectra were recorded on Hitachi F-7000

Fluorescence Spectrophotometer in the range from 360 to 550 nm ($\lambda_{\text{ex}} = 339$ nm, the slit width = 2.5 nm). The ratios between intensities of emission peaks at 373 and 393 nm (I_{373}/I_{393}) were plotted as a function of the polymer concentration. The CMC values were determined based on eight measuring points from the intersection between the regression straight lines of the linearly dependent region. **B. Determination of the quantity of encapsulated doxorubicin in polymeric nanoparticles.** A calibration curve was measured with different concentrations (0.0005 to 1 mg mL⁻¹) of DOX solutions in PBS (Figure 78). Emission spectra were recorded within a range of 460–700 nm with an excitation wavelength of 490 nm and a slit width of 5 nm. Polymeric nanoparticles with encapsulated doxorubicin were then dissolved in PBS at a concentration of 1 mg mL⁻¹, and fluorescence measurements were taken. **C. Fluorescence spectra of dye-labeled polymers.** Fluorescence spectra were recorded in PBS at a concentration of 0.1 mg mL⁻¹, ($\lambda_{\text{ex}} = 494$ nm, $\lambda_{\text{em}} = 518$ nm, split = 2.5 nm).

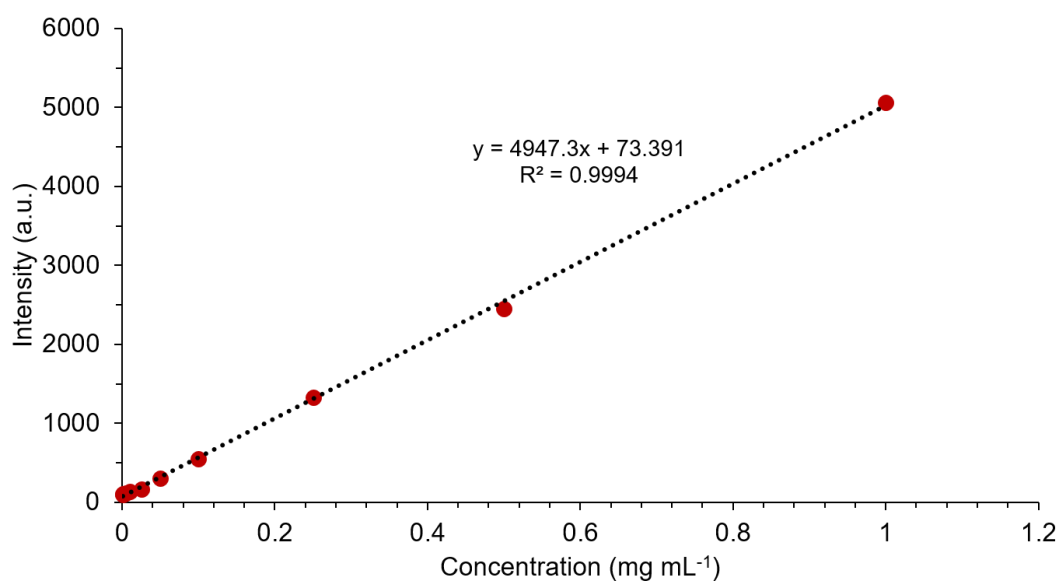


Figure 78. Calibration curve for doxorubicin.

High-performance liquid chromatography (HPLC). A. Determination of the quantity of encapsulated tamoxifen in polymeric nanoparticles. A calibration curve was measured with different concentrations (0.005 to 1 mg mL⁻¹) of TAM solutions in methanol (Figure 79). A Gemini[®] NX-C18 110 Å column (4.6 × 150 mm, 3 μm) was used for separation, maintaining the column temperature at 20 °C. The samples were analyzed using water/methanol mobile phase (0 min – 5:95, 2 min – 92:8, 6 min – 75:25) at a flow rate of 0.6 mL min⁻¹. The injection volume was 20 μL. The peak of TAM was detected at

a wavelength of 240 nm. **B. Study of drug release.** Predetermined amounts of tamoxifen-loaded nanoparticles (2–3 mg) were dissolved in water at a concentration of 1 mg mL⁻¹ and transferred into dialysis bags (MWCO = 3.5 kDa). The dialysis bags were immersed in a beaker containing 60 mL of water maintained at 37 °C and placed on a magnetic stirrer. At specific time intervals (5, 15, 30, 60, 120, 240, and 1440 minutes), dialysis membranes were removed from the release medium, and the release medium was lyophilized. The residues were dissolved in 1 mL of methanol and filtered through a 0.45 µm PTFE filter. The samples were analyzed using water/methanol mobile phase (0 min – 5:95, 2 min – 92:8, 6 min – 75:25) at a flow rate of 0.6 mL min⁻¹. The injection volume was 20 µL. The peak of TAM was detected at a wavelength of 240 nm. The measurements were made at the Faculty of Chemistry of the University of Białystok by Dr. Michał Sienkiewicz.

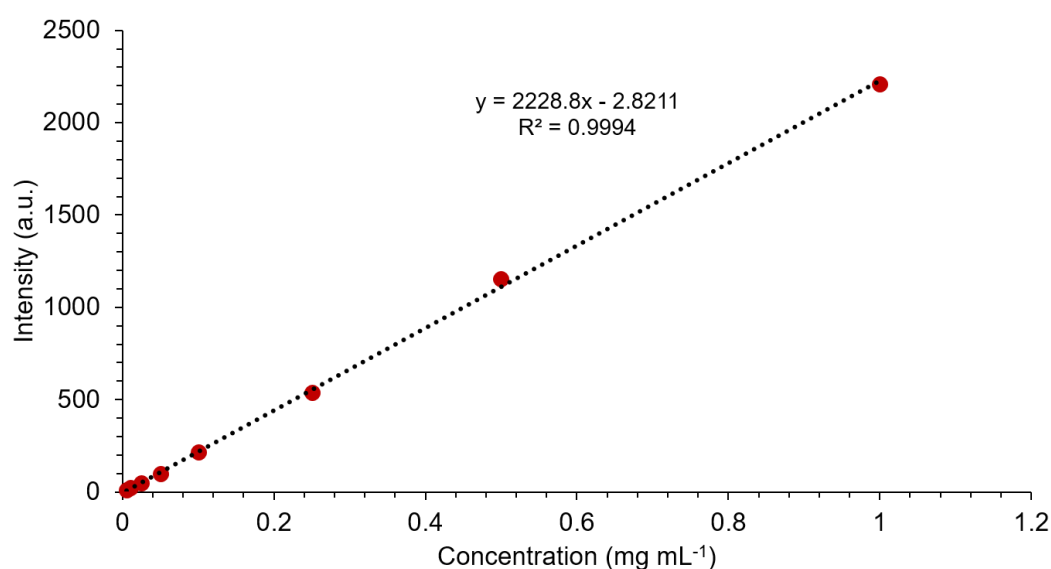


Figure 79. Calibration curve for tamoxifen.

Mass spectrometry (MS-ESI). Spectra were obtained on the Agilent 6530 Accurate-Mass Q-TOF ESI. The measurements were made at the Faculty of Chemistry of the University of Białystok by Dr. Michał Sienkiewicz.

Matrix-assisted laser desorption/ionization-time of flight mass spectrometry (MALDI-TOF MS). MALDI-TOF MS analysis was performed on Waters MALDI-TOF Micro MX equipped with a nitrogen laser emitting at $\lambda = 337$ nm. Analysis was conducted with α -cyano-4-hydroxycinnamic acid (HCCA) as matrix and NaI salt as cationizing agents. The acquisition software was Masslynx (Waters), and the spectra were processed using Masslynx

and Polymerix 3.0 (Sierra Analytics). The measurements were made at Institut de Chimie de Toulouse by Dr. Valérie Bourdon.

Medium pressure liquid chromatography (MPLC). MPLC was performed with a Buchi MSDF 2000 apparatus with pump module C-605 and fraction collector C-660.

Nuclear magnetic resonance (NMR). The ^1H and ^{13}C NMR spectra of diglyceride-based compounds and polymers were recorded at 25 °C with a Bruker Avance II 400 MHz spectrometer, using CDCl_3 solutions with TMS as the internal standard. Measurements were made at the Faculty of Chemistry of the University of Bialystok by Dr. Eng. Leszek Siergiejczyk or Dr. Jolanta Magnuszewska.

^1H NMR spectra of PNVF-based compounds, PnBA, PMMA, and ABA triblock copolymers were recorded at 25 °C with a Bruker Avance 300 MHz instrument at an operating frequency of 300.13 MHz. The resonance multiplicities are described as s (singlet), d (doublet), t (triplet), q (quartet), or m (multiplet). Chemical shifts δ are reported in parts per million (ppm) and are referenced to the residual solvent peak (DMSO: H = 2.5 ppm, CDCl_3 : H = 7.26 ppm, HDO: H = 4.79 ppm).

^1H and 2D DOSY NMR analyses were acquired on a Bruker Avance 500 spectrometer with a 5 mm dual ^1H - ^{13}C TCI cryoprobe at 5 °C. Samples were dissolved in dimethylsulfoxide (DMSO)- d_6 at a concentration of 100 mg mL^{-1} . ^1D ^1H NMR profiles were obtained using a classical NMR pulse sequence with a relaxation delay of 2 s, a flip angle of 90 °, an acquisition time of 5.45 s, and a spectral width of 12 ppm. The self-diffusion coefficients (D) can be measured with specific pulsed field gradient NMR sequences by increasing the gradient strength for a series of 1D spectra and fitting the NMR signal attenuation decay behavior with the Stejskal-Tanner equation.³⁶⁸

$$I = I_0 e^{[-(\gamma g \delta)^2 (\Delta - \frac{\delta}{3}) D]}$$

Where I is the signal intensity, I_0 is the signal intensity without gradient, γ the gyromagnetic ratio, g and δ the strength and the length of the pulsed field gradient, Δ the diffusion time, and D is the self-diffusion coefficient. Diffusion ^1H NMR spectra were recorded with bipolar pulse pairs stimulated echo pulse sequence with longitudinal eddy current delay and convection compensation (dstebpgp3s in the Bruker library).³⁶⁹ The acquisition parameters were as follows: 64K data points, acquisition time 5.45 s, spectral width 12 ppm, number of scans 16, relaxation delay 3 s, and recovery delay after each gradient 3 ms. The length of the

field gradient and diffusion time were 5.4 ms and 400 ms for PVP-CTA1 and 10 ms and 1000 ms for PVP-*b*-PNVF, respectively. The spoiler gradients were 0.6 ms long with a field strength of -9.26, -8.32, and -7.12 G cm⁻¹. Twenty experiments were recorded with linear gradient sampling from 5 to 95%. The gradient system was calibrated to 54.1 G cm⁻¹ at maximum intensity. DOSY NMR data were processed with the DOSY workup module, including in the Topspin 3.2 software. The data sets of the diffusion NMR experiments were generated and extracted with Topspin 3.2 software and transferred to the Origin 9.1 software. The exponential fit tool was then used to determine the values of the *D* using the equation: $y = a \cdot \exp(-D \cdot x)$, where $y = I$, $a = I_0$, and $x = [(\gamma g \delta)^2 (\Delta - \delta / 3)]$. The measurements were made at the SOFTMAT laboratory of Paul Sabatier University by Dr. Stéphane Balayssac.

Polymeric nanoparticles formation and drug encapsulation. 10 mg of the polymer was dissolved in 1 mL of THF and stirred for 3 h. Next, the obtained solution was added dropwise to 10 mL of deionized water with constant stirring. After 30 minutes, the solution was transferred to a dialysis membrane (MWCO 3.5 kDa) and dialyzed against 1 L of distilled water for 24 hours, changing the water twice (after 1 h and 3 h). The aqueous content of the dialysis membranes was frozen with liquid nitrogen and lyophilized overnight on Christ Alpha 1-2 LDplus with a double-chamber. The obtained polymeric nanoparticles were marked as NP. Drug-encapsulated polymeric nanoparticles were formed similarly. 10 mg of the polymer was dissolved in 1 mL of a solution of doxorubicin hydrochloride (DOX) or tamoxifen (TAM) in THF ($C = 1 \text{ mg mL}^{-1}$) and added dropwise to 10 mL of distilled water with constant stirring. Next, it was dialyzed against 1 L of distilled water for 24 hours, changing it twice (after 1 h and 3 h). The membrane content was freeze-dried and further analyzed.

Size exclusion chromatography (SEC). The molecular masses and molecular mass distributions of homopolymers and copolymers with diglyceride moieties, *Pn*BA, PMMA, and ABA triblock copolymers were determined by size exclusion chromatography (SEC) using THF as an eluent at a flow rate of 1.0 mL min⁻¹ at 25 °C. Before the analysis, the polymers were carefully dissolved in the eluent (the final concentration was 5 mg mL⁻¹) and filtered through a 0.45 μm PTFE filter. The samples were analyzed using a two-column set Styragel HR3 and HR4 (Waters) coupled with a three-detector system: refractometer thermostated at 35 °C (Optilab Rex, Wyatt technology), a UV detector (Prostar, Varian) set at 254 nm, and a multiangle laser light scattering detector (Mini Dawn, 3 angles, Wyatt technology). The dn/dc of the diglyceride end-capped homopolymers was assumed to be

equal to PNIPAAm (0.107)³⁷⁰ or PNVCL (0.137)³⁷¹. The dn/dc of the copolymers were calculated based on the weight fraction of PNIPAAm or PNVCL and diglyceride-based block. The refractive index increment (dn/dc) of PGlyP5k (0.076 mL g⁻¹) was measured at 620 nm using a DNDC-2010 differential refractometer by Dr. Karolina H. Markiewicz at the SOFTMAT laboratory of Paul Sabatier University. The dn/dc for PMMA (0.085) and PnBA (0.067) were adopted from the literature.^{361,363} The dn/dc of the ABA triblock copolymers were calculated based on the weight fraction of PMMA and PnBA.

Average molar masses and molar mass distributions of PNVF-based homopolymers and copolymers were determined using water + 0.2 M NaCl + 0.025 M NaH₂PO₄ + 0.025 M Na₂HPO₄ as an eluent at a flow rate of 1 mL min⁻¹ at 35 °C. Before analysis, polymers were dissolved in the eluent (the final concentration was 10 mg mL⁻¹) and filtered through a 0.45 μm cellulose filter. Analysis was performed on a system composed of a SB-G precolumn and a set of two SB-806M HQ and SB-802.5 HQ columns (Shodex). Detections were conducted using a Wyatt Optilab® rEX refractive index detector, a Varian ProStar UV detector (dual wavelength analysis at 290 and 254 nm), and a Wyatt DAWN-Heleos-II multiangle light scattering detector. The dn/dc (0.13 mL g⁻¹) of PEG was adopted from the literature.³⁷² The dn/dc of PNVF (0.162 mL g⁻¹) was measured at 620 nm with a PSS DnDc-2010 differential refractometer by Dr. Alexis Dupre-Demorsey at the SOFTMAT laboratory of Paul Sabatier University.

Average molar masses and molar mass distributions of PVP-based homopolymers were determined by using 10 mM LiBr solution in DMF as an eluent at a flow rate of 1 mL min⁻¹ at 55 °C. Before the analysis, polymers were dissolved in the eluent (final concentration was 10 mg mL⁻¹) and filtered through a 0.45 μm PTFE filter. Analysis was carried out on a system composed of an Agilent technologies guard column (PLGel20 μm, 50 × 7.5 mm) and a set of two KD-804 and KD-805L columns (SHODEX). Detections were performed using a Wyatt Optilab® rEX refractive index detector, a Varian ProStar UV detector (dual wavelength analysis at 290 and 254 nm), and a Wyatt MiniDawn TREOS multiangle light scattering detector. The dn/dc (0.093 mL g⁻¹) of PVP was adopted from the literature.³⁷³

Thermogravimetric (TGA) analysis. Measurements were carried out using a Mettler Toledo Star TGA/DSC unit. A sample weighing 2–3 mg was placed in an aluminum oxide crucible and heated from 50 °C to 600 °C. A heating rate of 10 °C min⁻¹ and an argon flow

rate of 40 mL min^{-1} were applied. An empty pan was used as a reference. The measurements were made at the Faculty of Chemistry of the University of Białystok by Prof. Agnieszka Z. Wilczewska or Dr. Karolina H. Markiewicz.

Transmission electron microscopy (TEM). Polymeric nanoparticles were redispersed in deionized water at a concentration of 0.1 mg mL^{-1} . Then, $5 \mu\text{l}$ of the solution was applied to a holey carbon copper grid, and the excess solution was removed. The process was repeated twice. Grids were then immersed in liquid nitrogen and lyophilized overnight on Christ Alpha 1-2 LDplus. TEM images were taken using a Tecnai G2 X-Twin microscope. Images were recorded at an accelerating voltage of 200 kV using a copper trap equipped with an LN2 Dewar as a cooling tool for the microscope column. The measurements were made at the Faculty of Chemistry of the University of Białystok by Dr. Iwona Misztalewska-Turkowicz.

Turbidimetry. Cloud points were determined by UV-Vis spectroscopy with the Peltier system on a Jasco V-670 Spectrophotometer in absorbance mode at a wavelength of 700–800 nm, a heating rate of $0.5 \text{ }^\circ\text{C min}^{-1}$ in the temperature range from 25 to $40 \text{ }^\circ\text{C}$. Polymeric nanoparticles were prepared in PBS at a concentration of 0.5 mg mL^{-1} . T_{CP} was determined based on transmittance versus temperature plots. T_{CP} was taken at 50% of transmittance at a wavelength of 750 nm.

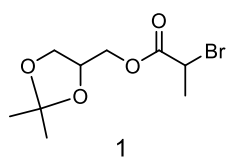
CHAPTER 7. SYNTHETIC PROTOCOLS

7.1. Materials

- *N*-isopropylacrylamide (NIPAAm, 99%, Acros) was recrystallized twice from toluene-hexane (6:4, v/v) before use.
- *N*-vinylcaprolactam (NVCL) was recrystallized from hexane at room temperature three times before use.
- *N*-vinylformamide (NVF, Sigma-Aldrich, 98%) and *N*-vinylpyrrolidone (NVP, Sigma-Aldrich, 99%) were distilled under reduced pressure before use.
- *n*-Butyl acrylate (*n*BA, $\geq 99\%$, Sigma-Aldrich) and methyl methacrylate (MMA, $>99\%$, Sigma-Aldrich) were purified by passing through neutral aluminum oxide.
- Bis-(2-methylpropanenitrile)trithiocarbonate (TTC-bCP, CTA3)²⁴⁶ and PEG-CTA1³⁴⁷ were synthesized according to previously described protocols.
- 2,2'-Azobis(2-methylpropionitrile) (AIBN, 98%, Merck) was recrystallized from methanol.
- Dialysis membranes with a molecular weight cut-off (MWCO) of 1 or 3.5 kDa were purchased from Spectra/Por.
- Purple LED light strip ($\lambda = 395\text{--}400$ nm) and green LED light strip ($\lambda = 530$ nm) were purchased from www.boulevard-des-leds.fr. The blue LED light strip ($\lambda = 460$ nm) was purchased from Amazon.
- Acryloyl chloride (96%, Alfa Aesar), benzyl bromide (99%, Alfa Aesar), boron trichloride solution (BCl_3 , 1.0 M in methylene chloride, Sigma-Aldrich), bromoacetonitrile (Sigma-Aldrich), 2-bromopropionic acid bromide (97%, Sigma-Aldrich), doxorubicin hydrochloride (DOX, AmBeed), fluorescein diacetate 5-maleimide (Sigma-Aldrich), 4-dimethylaminopyridine (DMAP, 99%, Sigma-Aldrich), *N,N'*-dicyclohexylcarbodiimide (DCC, 99%, Aldrich), oleic acid (90%, Sigma-Aldrich), palladium on activated charcoal (Pd/C, 5% Pd basis, Sigma-Aldrich), palmitic acid (99%, Sigma-Aldrich, 99%), Phosphate Buffer Saline (PBS, pH = 7.4, Gibco), potassium *O*-ethyl dithiocarbonate (96%, Sigma-Aldrich), *n*-propylamine (PROSYNTH), sodium hydride (60% dispersion in mineral oil, Sigma-Aldrich), solketal (97%, Alfa Aesar), tamoxifen (TAM, Carbosynth), triethylamine (Et_3N , Avantor), tributylphosphine (97%, Sigma-Aldrich) were used as received.

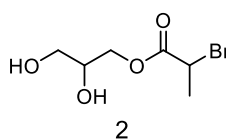
7.2. Drug delivery systems based on polymers with diglyceride moieties

7.2.1. Synthesis of (2,2-dimethyl-1,3-dioxolan-4-yl)methyl 2-bromopropanoate (1)



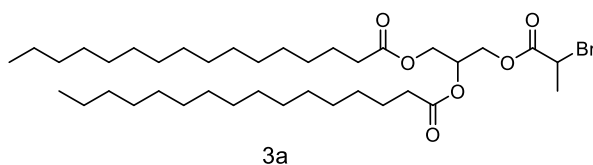
Solketal (5 g, 37.8 mmol) was dissolved in anhydrous DCM (170 mL), and then Et₃N (10.5 mL, 76 mmol, 2 equiv) was added. After being placed in an ice bath, 2-bromopropionic acid bromide (5.55 mL, 53 mmol, 1.4 equiv) was added dropwise over 30 minutes. The reaction temperature was maintained at 0 °C for 2 hours, following which the reaction mixture was warmed slowly to room temperature. After being stirred for an additional 14 hours, 150 mL of 1 M HCl solution was added. The product was extracted with DCM (3 x 100 mL). The combined organic layers were washed with brine, dried over Na₂SO₄, and concentrated in a vacuum. The product was purified by medium pressure liquid chromatography (MPLC) (hexane/EtOAc 8:2). The product was obtained as a pale yellow oil in 83%, 8.4 g. ¹H NMR (400 MHz, CDCl₃): δ 4.41 (q, *J* = 7.0 Hz, 1H, CH₃CHBr), 4.34 (dt, *J* = 10.6, 5.3 Hz, 1H, C(=O)OCH₂CHCH₂), 4.22 (dd, *J* = 8.8, 5.0 Hz, 2H, C(=O)OCH₂CHCH₂), 4.13–4.06 (m, 1H, C(=O)OCH₂CHCH₂), 3.79 (dd, *J* = 14.5, 6.1 Hz, 1H, C(=O)OCH₂CHCH₂), 1.84 (d, *J* = 6.9 Hz, 3H, CH₃CHBr), 1.44 (s, 3H, CH₃), 1.37 (s, 3H, CH₃). ¹³C NMR (101 MHz, CDCl₃): δ 170.0 (C=O), 109.2 (C), 73.2 (CH), 66.2 (CH₂), 65.9 (CH₂), 65.5 (CH₂), 39.5 (CH), 26.6 (CH₃), 25.3 (CH₃), 21.5 (CH₃). ATR-FTIR (cm⁻¹): ν 2985, 2940, 2880, 1740 (C=O), 1445, 1370, 1330 (C–Br), 1210, 1155, 995, 973, 840.

7.2.2. Synthesis of 2,3-dihydroxypropyl 2-bromopropanoate (2)



1 (8 g, 30 mmol) was dissolved in AcOH/H₂O 4:1 (100 mL) and stirred for 2 hours at 65 °C. The reaction mixture was neutralized with saturated aqueous NaHCO₃ solution (100 mL) and extracted with dichloromethane (3 × 100 mL). The organic layer was dried over anhydrous Na₂SO₄ and concentrated in vacuo. The product was purified by MPLC (hexane/EtOAc, 4:6). The isolated product was obtained as a pale yellow oil in 84%, 5.7 g. ¹H NMR (400 MHz, CDCl₃): δ 4.43 (q, *J* = 6.9 Hz, 1H, CH₃CHBr), 4.32–4.18 (m, 2H), 4.03–3.95 (m, 1H), 3.74 (dd, *J* = 11.6, 3.6 Hz, 1H), 3.63 (dt, *J* = 11.4, 5.5 Hz, 1H), 3.21 (s, 2H, OH), 1.84 (d, *J* = 6.9 Hz, 3H, CH₃CHBr). ¹³C NMR (101 MHz, CDCl₃): δ 170.5 (C=O), 69.8 (CH), 66.2 (CH₂), 63.2 (CH₂), 39.7 (CH), 21.4 (CH₃). ATR-FTIR (cm⁻¹): ν 3355 (OH), 2930, 2880, 1730 (C=O), 1445, 1380, 1340 (C–Br), 1220, 1160, 1100, 1055, 995.

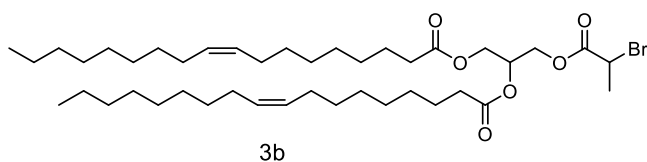
7.2.3. Synthesis of 3-((2-bromopropanoyl)oxy)propane-1,2-diyl dipalmitate (3a)



DCC (3 g, 14.6 mmol, 2.2 equiv) was added to a stirred solution of **2** (1.5 g, 6.64 mmol) and DMAP (0.243 g, 2 mmol, 0.3 equiv) in 140 mL of anhydrous DCM at 0 °C. After

being stirred for 1 hour, palmitic acid (3.74 g, 14.6 mmol, 2.2 equiv) was added portionwise, and the mixture was stirred at room temperature overnight. The solid was removed by filtration through celite, and the filtrate was concentrated under reduced pressure. The product was purified by MPLC (hexane/EtOAc 9.6:0.4). The product was obtained as a white solid in 63%, 2.94 g. $^1\text{H NMR}$ (400 MHz, CDCl_3): δ 5.35–5.25 (m, 1H, $\text{C(=O)OCH}_2\text{CHCH}_2$), 4.46–4.21 (m, 4H, $\text{C(=O)OCH}_2\text{CHCH}_2$), 4.17 (ddd, $J = 11.9, 5.8, 2.0$ Hz, 1H, CH_3CHBr), 2.32 (td, $J = 7.6, 2.7$ Hz, 4H, $\text{CH}_2\text{C(=O)}$), 1.82 (dd, $J = 6.9, 1.7$ Hz, 3H, C(=O)CHCH_3), 1.62 (m, 4H, $\text{CH}_2\text{CH}_2\text{C(=O)}$), 1.27 (d, $J = 10.9$ Hz, 48H, CH_2), 0.88 (t, $J = 6.8$ Hz, 6H, CH_3). $^{13}\text{C NMR}$ (101 MHz, CDCl_3): δ 173.2 (C=O), 172.8 (C=O), 169.7 (C=O), 68.5 (CH), 63.5 (CH_2), 61.8 (CH_2), 39.3 (CH), 34.1 (CH_2), 31.9 (CH_2), 29.7 (CH_2), 29.6 (CH_2), 29.5 (CH_2), 29.4 (CH_2), 29.3 (CH_2), 29.2 (CH_2), 29.1 (CH_2), 29.0 (CH_2), 24.8 (CH_2), 22.7 (CH_2), 21.5 (CH_3), 14.1 (CH_3). **ATR-FTIR** (cm^{-1}): ν 2954 (C–H), 2917 (C–H), 2848 (C–H), 1735 (C=O), 1463 (C–H), 1380, 1265, 1220, 1160, 1100.

7.2.4. Synthesis of 3-((2-bromopropanoyl)oxy)propane-1,2-diyl dioleate (3b)

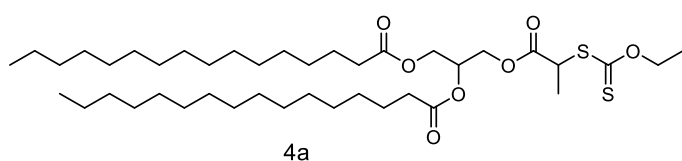


DCC (4 g, 19.5 mmol, 2.2 equiv) was added to a stirred solution of **2** (2 g, 8.85 mmol) and DMAP (0.324 g, 2.65 mmol, 0.3 equiv) in 200 mL of

anhydrous DCM at 0 °C. After being stirred for 1 hour, oleic acid (4.4 g, 19.5 mmol, 2.2 equiv) was added portionwise, and the mixture was stirred at room temperature overnight. The solid was removed by filtration through celite, and the filtrate was concentrated under reduced pressure. The product was purified by MPLC (hexane/EtOAc 9.9:0.1). The product was obtained as a pale yellow oil in 53%, 3.56 g. $^1\text{H NMR}$ (400 MHz, CDCl_3): δ 5.41–5.24 (m, 5H, $\text{C(=O)OCH}_2\text{CH=CHCH}_2$, $\text{C(=O)OCH}_2\text{CHCH}_2$), 4.46–4.21 (m, 4H, $\text{C(=O)OCH}_2\text{CHCH}_2$), 4.17 (ddd, $J = 11.9, 5.8, 1.8$ Hz, 1H, CH_3CHBr), 2.32 (td, $J = 7.6, 2.5$ Hz, 4H, $\text{CH}_2\text{C(=O)}$), 2.01 (d, $J = 5.9$ Hz, 8H, $\text{CH}_2\text{CH=CHCH}_2$), 1.82 (dd, $J = 6.9, 1.5$ Hz, 3H, C(=O)CHCH_3), 1.68–1.54 (m, 4H, $\text{CH}_2\text{CH}_2\text{C(=O)}$), 1.28 (d, $J = 13.9$ Hz, 40H, CH_2), 0.88 (t, $J = 6.7$ Hz, 6H, CH_3). $^{13}\text{C NMR}$ (101 MHz, CDCl_3): δ 173.2 (C=O), 172.8

(C=O), 169.7 (C=O), 130.0 (CH), 129.7 (CH), 68.6 (CH), 63.5 (CH₂), 61.8 (CH₂), 39.3 (CH), 34.1 (CH₂), 34.0 (CH₂), 31.9 (CH₂), 30.0 (CH₂), 29.6 (CH₂), 29.5 (CH₂), 29.3 (CH₂), 29.1 (CH₂), 29.0 (CH₂), 28.9 (CH₂), 27.2 (CH₂), 24.8 (CH₂), 22.6 (CH₂), 21.5 (CH₃), 14.1 (CH₃). **ATR-FTIR** (cm⁻¹): ν 3005 (C–H), 2920 (C–H), 2850 (C–H), 1740 (C=O), 1455 (C–H), 1380, 1340, 1220, 1155, 1095.

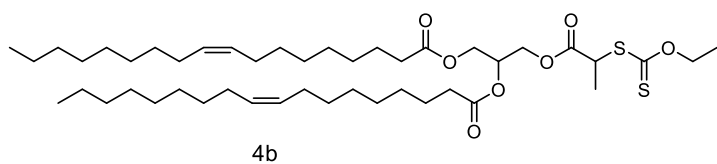
7.2.5. Synthesis of 3-((2-((ethoxycarbonothioyl)thio)propanoyl)oxy)propane-1,2-diyl dipalmitate (4a)



Potassium *O*-ethyl carbonodithioate (0.74 g, 4.63 mmol, 1.3 equiv) was added slowly to a stirred solution of **3a** (2.5 g, 3.6 mmol) in acetone (100

mL) at 0 °C. After stirring overnight, the mixture was filtered to remove the formed KBr. The solvent was concentrated under reduced pressure. The product was purified by MPLC (hexane/EtOAc 9.5:0.5). The product was obtained as a white solid in 92%, 2.41 g. ¹H NMR (400 MHz, CDCl₃): δ 5.33–5.23 (m, 1H, C(=O)OCH₂CHCH₂), 4.63 (qd, *J* = 7.1, 1.3 Hz, 2H, OCH₂CH₃), 4.44–4.34 (m, 2H, C(=O)OCH₂CHCH₂), 4.30 (dt, *J* = 11.8, 4.5 Hz, 1H, CH₃CHSC(=S)), 4.26–4.10 (m, 2H, C(=O)OCH₂CHCH₂), 2.37–2.26 (td, *J* = 7.6, 1.8 Hz, 4H, CH₂C(=O)), 1.69–1.59 (m, 4H, CH₂CH₂C(=O)), 1.57 (dd, *J* = 7.4, 1.1 Hz, 3H, C(=O)CHCH₃), 1.41 (t, *J* = 7.1 Hz, 3H, OCH₂CH₃), 1.27 (d, *J* = 10.2 Hz, 48H, CH₂), 0.88 (t, *J* = 6.8 Hz, 6H, CH₃). ¹³C NMR (101 MHz, CDCl₃): δ 211.8 (C=S), 173.2 (C=O), 172.8 (C=O), 171.0 (C=O), 70.3 (CH₂), 68.6 (CH), 63.3 (CH₂), 61.9 (CH₂), 47.0 (CH), 34.0 (CH₂), 31.9 (CH₂), 29.7 (CH₂), 29.6 (CH₂), 29.4 (CH₂), 29.3 (CH₂), 29.2 (CH₂), 29.1 (CH₂), 29.0 (CH₂), 24.8 (CH₂), 22.6 (CH₂), 16.7 (CH₃), 14.1 (CH₃), 13.6 (CH₃). **ATR-FTIR** (cm⁻¹): ν 2954 (C–H), 2917 (C–H), 2848 (C–H), 1735 (C=O), 1463, 1380, 1220 (C–O–C), 1170, 1060 (C=S). **MS (ESI)**: *m/z* calculated 767.5000 (M + Na)⁺, found 767.4950.

7.2.6. Synthesis of 3-((2-((ethoxycarbonothioyl)thio)propanoyl)oxy)propane-1,2-diyl dioleate (4b)

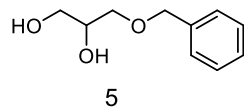


Potassium *O*-ethyl carbonodithioate (0.55 g, 3.4 mmol, 1.3 equiv) was added slowly to a stirred solution of **4a**

(2 g, 2.6 mmol) in acetone (80 mL) at 0 °C. After stirring overnight, the mixture was filtered to remove the formed KBr. The solvent was concentrated under reduced pressure. The

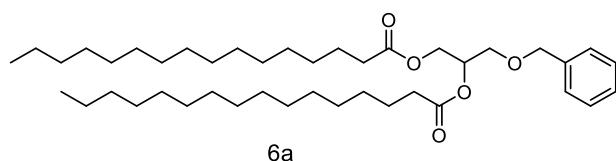
product was purified by MPLC (hexane/EtOAc 9.5:0.5). The product was obtained as a yellow oil in 93%, 1.95 g. $^1\text{H NMR}$ (400 MHz, CDCl_3): δ 5.42–5.23 (m, 5H, $\text{C(=O)OCH}_2\text{CH}=\text{CHCH}_2$, $\text{C(=O)OCH}_2\text{CHCH}_2$), 4.63 (qd, $J = 7.1, 1.4$ Hz, 2H, OCH_2CH_3), 4.45–4.34 (m, 2H, $\text{C(=O)OCH}_2\text{CHCH}_2$), 4.45–4.34 (m, 2H, $\text{C(=O)OCH}_2\text{CHCH}_2$), 4.30 (dt, $J = 11.9, 4.5$ Hz, 1H, $\text{CH}_3\text{CHSC(=S)}$), 4.25–4.11 (m, 2H, $\text{C(=O)OCH}_2\text{CHCH}_2$), 2.31 (dd, $J = 10.5, 4.6$ Hz, 4H, $\text{CH}_2\text{C(=O)}$), 2.01 (d, $J = 5.9$ Hz, 8H, $\text{CH}_2\text{CH}=\text{CHCH}_2$), 1.61 (m, 4H, $\text{CH}_2\text{CH}_2\text{C(=O)}$), 1.57 (dd, $J = 7.4, 1.3$ Hz, 3H, C(=O)CHCH_3), 1.42 (t, $J = 7.1$ Hz, 3H, OCH_2CH_3), 1.28 (d, $J = 14.0$ Hz, 40H, CH_2), 0.88 (t, $J = 6.8$ Hz, 6H, CH_3). $^{13}\text{C NMR}$ (101 MHz, CDCl_3): δ 211.8 (C=S), 173.1 (C=O), 172.7 (C=O), 171.0 (C=O), 130.0 (CH), 129.7 (CH), 70.3 (CH_2), 68.6 (CH), 63.3 (CH_2), 61.9 (CH_2), 47.0 (CH), 34.0 (CH_2), 31.9 (CH_2), 30.9 (CH_2), 29.7 (CH_2), 29.5 (CH_2), 29.3 (CH_2), 29.1 (CH_2), 27.1 (CH_2), 24.8 (CH_2), 22.6 (CH_2), 16.6 (CH_3), 14.1 (CH_3), 13.6 (CH_3). **ATR-FTIR** (cm^{-1}): ν 3005 (C–H), 2920 (C–H), 2850 (C–H), 1740 (C=O), 1460, 1380, 1220 (C–O–C), 1110, 1050 (C=S). **MS (ESI)**: m/z calculated 819.5345 ($\text{M} + \text{Na}$) $^+$, found 819.5250.

7.2.7. Synthesis of 3-(benzyloxy)propane-1,2-diol (5)



Sodium hydride (60% wt. in mineral oil, 3.3 g, 1.3 equiv) was washed with hexane (20 mL x 3) and dissolved in THF (200 mL). Solketal (9.4 mL, 7.65 mmol) was then added at 0 °C, and the reaction mixture was stirred for 1 hour. Next, benzyl bromide (10.83 mL, 0.09 mol, 1.2 equiv) was added at 0 °C, and the reaction mixture was warmed to room temperature. After being stirred overnight, the saturated NH_4Cl (150 mL) solution was added. The product was extracted with Et_2O (3 x 150 mL). The combined organic layer was dried over anhydrous Na_2SO_4 and concentrated in vacuo. The residue was dissolved in $\text{AcOH}/\text{H}_2\text{O}$ 4:1 (100 mL), and the reaction mixture was stirred at 65 °C for 3 hours. The mixture was neutralized with saturated aqueous NaHCO_3 solution (150 mL) and extracted with dichloromethane (3 x 150 mL). The organic layer was dried over anhydrous Na_2SO_4 and concentrated in vacuo. The product was purified by MPLC with hexane/EtOAc (6.5:3.5 and 0:10). The product was obtained as a pale yellow oil in 71%, 9.703 g. $^1\text{H NMR}$ (400 MHz, CDCl_3) δ 7.51–7.17 (m, 5H, C_6H_5), 4.53 (s, 2H, $\text{CH}_2\text{C}_6\text{H}_5$), 3.95–3.80 (m, 1H, $\text{COCH}_2\text{CHCH}_2$), 3.66 (dd, $J = 11.5, 3.6$ Hz, 2H, HOCH_2CH), 3.61–3.52 (m, 2H, CHCH_2O), 3.50 (dd, $J = 5.2, 3.3$ Hz, 2H, CHCH_2O). $^{13}\text{C NMR}$ (101 MHz, CDCl_3): δ 137.6 (C), 128.4 (CH), 127.7 (CH), 73.4 (CH_2), 71.5 (CH_2), 70.7 (CH), 63.9 (CH_2). **ATR-FTIR** (cm^{-1}): ν 3335 (O–H), 3065, 3030, 2925, 2870 (C–H), 1715, 1450, 1275, 1095, 1055, 740, 700.

7.2.8. Synthesis of 3-(benzyloxy)propane-1,2-diyl dipalmitate (6a)

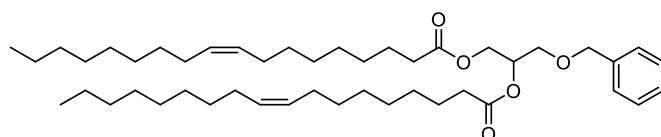


6a

DCC (7.08 g, 34.6 mmol, 2.5 equiv) was added to a stirred solution of **5** (2.5 g, 13.73 mmol), and DMAP (0.67 g, 5.5 mmol, 0.4 equiv) in 200 mL of dry DCM

at 0 °C. After being stirred for 1 hour, palmitic acid (3.74 g, 16.6 mmol, 2.2 equiv) was added portionwise, and the mixture was stirred at room temperature overnight. The solid was removed by filtration through celite, and the filtrate was concentrated under reduced pressure. The product was purified by MPLC (hexane/EtOAc 9.5:0.5). The product was obtained as a white solid in 90%, 8.16 g. $^1\text{H NMR}$ (400 MHz, CDCl_3): δ 7.38–7.26 (m, 5H, C_6H_5), 5.29–5.22 (m, 1H, $\text{COCH}_2\text{CHCH}_2$), 4.54 (d, $J = 5.6$ Hz, 2H, $\text{CH}_2\text{C}_6\text{H}_5$), 4.36 (dd, $J = 11.9, 3.8$ Hz, 2H, $\text{CHCH}_2\text{C}(=\text{O})$), 4.20 (dd, $J = 11.9$ Hz, 6.4 Hz, 2H, $\text{CHCH}_2\text{C}(=\text{O})$), 3.60 (m, 2 H, $\text{CHCH}_2\text{OCH}_2$), 2.31 (dt, $J = 17.0, 7.5$ Hz, 4H, $\text{CH}_2\text{C}(=\text{O})$), 1.70–1.53 (m, 4 H, $\text{CH}_2\text{CH}_2\text{C}(=\text{O})$), 1.28 (s, 48 H, CH_2), 0.89 (t, $J = 6.8$ Hz, 6 H, CH_3). $^{13}\text{C NMR}$ (101 MHz, CDCl_3): δ 173.4 (C=O), 173.1 (C=O), 137.7 (C), 128.4 (CH), 127.8 (CH), 127.60 (CH), 73.3 (CH_2), 70.0 (CH), 68.2 (CH_2), 62.6 (CH_2), 34.3 (CH_2), 34.1(CH_2), 31.9 (CH_2), 29.7 (CH_2), 29.6 (CH_2), 29.5 (CH_2), 29.4 (CH_2), 29.3 (CH_2), 29.1 (CH_2), 29.0 (CH_2), 25.0 (CH_2), 24.9 (CH_2), 22.7 (CH_2), 14.1 (CH_3). **ATR-FTIR** (cm^{-1}): ν 2955 (C–H), 2920 (C–H), 2850 (C–H), 1740, 1720, 1450, 1375, 1350, 1240, 1220, 1150, 1120, 1090, 730.

7.2.9. Synthesis of 3-(benzyloxy)propane-1,2-diyl dioleate (6b)



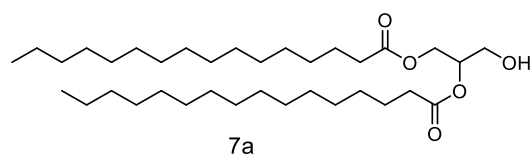
6b

DCC (6.8 g, 32.9 mmol, 2.5 equiv) was added to a stirred solution of **5** (2.5 g, 13.2 mmol, 1 equiv), and DMAP (0.671 g, 5.5 mmol, 0.4 equiv)

in 200 mL of dry DCM at 0 °C. After being stirred for 1 hour, oleic acid (9.98 mL, 31.6 mmol, 2.2 equiv) was added portionwise, and the mixture was stirred at room temperature overnight. The solid was removed by filtration through celite, and the filtrate was concentrated under reduced pressure. The product was purified by MPLC (hexane/EtOAc 9.7:0.3). The product was obtained as a pale yellow oil in 85%, 8.30 g. $^1\text{H NMR}$ (400 MHz, CDCl_3): δ 7.42–7.22 (m, 5H, C_6H_5), 5.45–5.30 (m, 4H, $\text{OCH}_2\text{CH}=\text{CHCH}_2$), 5.26 (m, 1H, $\text{COCH}_2\text{CHCH}_2$), 4.55 (d, $J = 5.5$ Hz, 2H, $\text{CH}_2\text{C}_6\text{H}_5$), 4.36 (dd, $J = 11.9, 3.8$ Hz, 2H, $\text{CHCH}_2\text{C}(=\text{O})$), 4.20 (dd, $J = 11.9, 6.4$ Hz, 2H, $\text{CHCH}_2\text{C}(=\text{O})$), 3.60 (d, $J = 5.2$ Hz, 2H, $\text{CHCH}_2\text{OCH}_2$), 2.31 (dt, $J = 17.1, 7.5$ Hz, 4H, $\text{CH}_2\text{C}(=\text{O})$), 2.14–1.93 (m, 8H,

$\text{CH}_2\text{CH}=\text{CHCH}_2$), 1.68–1.53 (m, 4H, $\text{CH}_2\text{CH}_2\text{C}(=\text{O})$), 1.31 (s, 20H, CH_2), 1.28 (s, 20H, CH_2), 0.90 (t, $J = 6.8$ Hz, 6H, CH_3). ^{13}C NMR (101 MHz, CDCl_3) δ 173.3 (C=O), 173.0 (C=O), 137.7 (C), 130.0 (CH), 129.7 (CH), 128.4 (CH), 127.7 (CH), 127.6 (CH), 73.2 (CH_2), 70.0 (CH), 68.2 (CH_2), 62.6 (CH_2), 34.2 (CH_2), 34.0 (CH_2), 31.9 (CH_2), 29.7 (CH_2), 29.5 (CH_2), 29.3 (CH_2), 29.2 (CH_2), 29.1 (CH_2), 29.0 (CH_2), 27.2 (CH_2), 27.1 (CH_2), 24.9 (CH_2), 24.8 (CH_2), 22.6 (CH_2), 14.1 (CH_3). ATR-FTIR (cm^{-1}): ν 3004 (C–H), 2920 (C–H), 2850 (C–H), 1740, 1455, 1365, 1350, 1240, 1160, 1095, 730, 700.

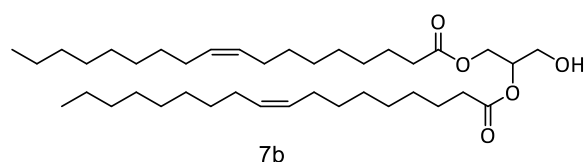
7.2.10. Synthesis of 3-hydroxypropane-1,2-diyl dipalmitate (7a)



A solution of **6a** (6.0 g, 10.0 mmol), 5% Pd/C (800 mg) in a mixture of glacial acetic acid (20 mL) and ethanol (100 mL) was stirred under a hydrogen atmosphere at room temperature.

The reaction progress was monitored by TLC. When the reaction was complete, the mixture was diluted with CH_2Cl_2 , and the catalysts were removed by celite filtration. The filtrate was evaporated under reduced pressure, and the crude product was purified by MPLC (hexane/EtOAc 9.6:0.4). The product was obtained as a white solid in 86%, 4.45 g. ^1H NMR (400 MHz, CDCl_3) δ 5.13–5.02 (m, 1H, $\text{COCH}_2\text{CHCH}_2$), 4.32 (dd, $J = 11.9, 4.3$ Hz, 2H, $\text{CHCH}_2\text{C}(=\text{O})$), 4.24 (dd, $J = 11.6, 5.6$ Hz, 2H, $\text{CHCH}_2\text{C}(=\text{O})$), 3.79–3.63 (m, 2H, CHCH_2OH), 2.35 (td, $J = 12.0, 5.9$ Hz, 4 H, $\text{CH}_2\text{CH}_2\text{C}(=\text{O})$), 1.66–1.58 (m, 4H, $\text{CH}_2\text{CH}_2\text{C}(=\text{O})$), 1.25 (s, 48H, CH_2), 0.88 (t, $J = 6.8$ Hz, 6H, CH_3). ^{13}C NMR (101 MHz, CDCl_3): δ 173.9 (C=O), 68.3 (CH), 65.0 (CH_2), 34.1 (CH_2), 29.7 (CH_2), 29.6 (CH_2), 29.5 (CH_2), 29.4 (CH_2), 29.3 (CH_2), 29.2 (CH_2), 29.1 (CH_2), 24.9 (CH_2), 22.6 (CH_2), 14.1 (CH_3). ATR-FTIR (cm^{-1}): ν 3500 (OH), 2955 (C–H), 2920 (C–H), 2850, 1730, 1710, 1470, 1380, 1290, 1265, 1220, 1180, 1090, 1065, 720.

7.2.11. Synthesis of 3-hydroxypropane-1,2-diyl dioleate (7b)

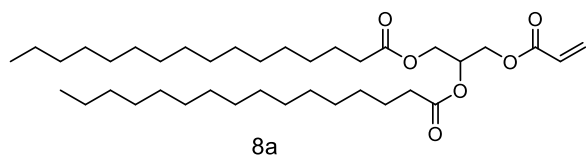


To a solution of **6b** (1.5 g, 0.0021 mol, 1 equiv) in 50 mL CH_2Cl_2 at -78°C , boron trichloride (5.3 mL, 0.053 mol, 2.5 equiv) (1 M in CH_2Cl_2) was added over 15 minutes.

The reaction was stirred for 1 hour under argon. The flask contents were poured over ice water (50 mL) and warmed to room temperature. The product was extracted with DCM (3 x 50 mL). The combined organic layer was dried over anhydrous Na_2SO_4 and concentrated in

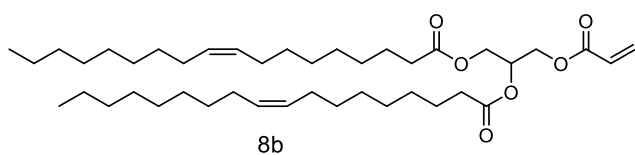
vacuo. The product was purified by MPLC (hexane/EtOAc 9.7:0.3). The product was obtained as a pale yellow oil in 54%, 712 mg. $^1\text{H NMR}$ (400 MHz, CDCl_3) δ 5.46–5.21 (m, 5H, $\text{CH}_2\text{CH}=\text{CHCH}_2$, $\text{COCH}_2\text{CHCH}_2$), 4.29–4.00 (m, 4H, $\text{CHCH}_2\text{C}(=\text{O})$, CHCH_2OH), 2.60 (d, $J = 4.8$ Hz, 2H), 2.35 (t, $J = 7.6$ Hz, 8H), 2.04–1.99 (m, 8H, $\text{CH}_2\text{CH}=\text{CHCH}_2$, 1.65–1.61 (m, 4H, $\text{CH}_2\text{CH}_2\text{C}(=\text{O})$), 1.31 (s, 20H, CH_2), 1.28 (s, 20H, CH_2), 0.90 (t, $J = 6.8$ Hz, 6H, CH_3). $^{13}\text{C NMR}$ (101 MHz, CDCl_3) δ 173.8 (C=O), 130.0 (CH), 129.7 (CH), 68.3 (CH), 65.0 (CH_2), 34.0 (CH_2), 31.9 (CH_2), 29.7 (CH_2), 29.6 (CH_2), 29.5 (CH_2), 29.3 (CH_2), 29.1 (CH_2), 29.0 (CH_2), 27.2 (CH_2), 27.1 (CH_2), 22.6 (CH_2), 14.1 (CH_3). **ATR-FTIR** (cm^{-1}): ν 3450 (OH), 3004 (C–H), 2920, 2850, 1740, 1455, 1370, 1240, 1065, 720, 700.

7.2.12. Synthesis of 3-(acryloyloxy)propane-1,2-diyl dipalmitate (**8a**)



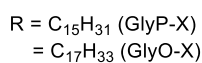
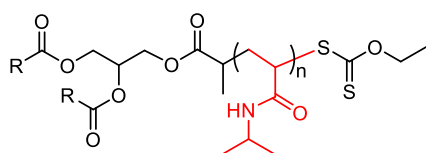
Compound **7a** (4.3 g, 7.5 mmol) was dissolved in dried DCM (200 mL), and then Et_3N (2 mL, 15 mmol, 2 equiv) was added. After 30 minutes, acryloyl chloride (0.75 mL, 9 mmol, 1.2 equiv) was added dropwise at 0 °C over 30 minutes. The reaction temperature was maintained at 0 °C for 3 hours. After being stirred for an additional 16 hours at room temperature, 150 mL 1 M HCl solution was added. The product was extracted with DCM (3 x 100 mL). The combined organic layers were washed with brine, dried over Na_2SO_4 , and concentrated in vacuo. The product was purified by MPLC (hexane/EtOAc, 9.6:0.4). The product was obtained as a white solid in 89%, 5.3 g. $^1\text{H NMR}$ (400 MHz, CDCl_3) δ 6.43 (d, $J = 17.3$ Hz, 1H, $\text{CH}_2=\text{CH}_2$), 6.13 (dd, $J = 17.3, 10.4$ Hz, 1H, $\text{CH}_2=\text{CH}_2$), 5.88 (d, $J = 10.5$ Hz, 1H, $\text{CH}_2=\text{CH}_2$), 5.58–5.03 (m, 1H, $\text{COCH}_2\text{CHCH}_2$), 4.47–4.23 (m, 2H, $\text{CHCH}_2\text{C}(=\text{O})$), 4.17 (dd, $J = 11.9, 5.9$ Hz, 2H, $\text{CHCH}_2\text{C}(=\text{O})$), 2.32 (td, $J = 7.5, 2.6$ Hz, 4H, $\text{CH}_2\text{C}(=\text{O})$), 1.63–1.59 (m, 4H, $\text{CH}_2\text{CH}_2\text{C}(=\text{O})$), 1.25 (s, 48H, CH_2), 0.89 (t, $J = 6.6$ Hz, 6H, CH_3). $^{13}\text{C NMR}$ (101 MHz, CDCl_3): δ 173.2 (C=O), 172.8 (C=O), 165.5 (C=O), 131.5 (CH_2), 127.7 (CH), 68.8 (CH), 62.4 (CH_2), 62.0 (CH_2), 34.2 (CH_2), 34.0 (CH_2), 31.9 (CH_2), 29.7 (CH_2), 29.6 (CH_2), 29.5 (CH_2), 29.4 (CH_2), 29.3 (CH_2), 29.2 (CH_2), 29.1 (CH_2), 29.0 (CH_2), 24.9 (CH_2), 24.8 (CH_2), 22.7 (CH_2), 14.1 (CH_3). **ATR-FTIR** (cm^{-1}): ν 2955, 2920, 2850, 1740, 1720, 1635 (C=O), 1460, 1360, 1260, 1170, 1085, 810. **MS (ESI)**: m/z calculated 645.5000 ($\text{M} + \text{Na}$) $^+$, found 645.5101.

7.2.13. Synthesis of 3-(acryloyloxy)propane-1,2-diyl dioleate (8b)



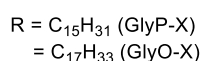
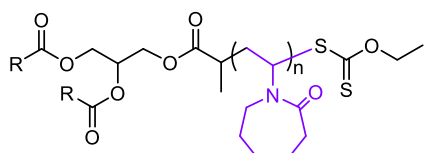
Compound **7b** (2.5 g, 4 mmol) was dissolved in dried DCM (85 mL), and then Et₃N (1.12 mL, 8 mmol, 2 equiv) was added. After 30 minutes, acryloyl chloride (0.43 mL, 5.2 mmol, 1.3 equiv) was added dropwise at 0 °C over 30 minutes. The reaction temperature was maintained at 0 °C for 3 hours. After being stirred for an additional 3 hours at room temperature, 100 mL 1 M HCl solution was added. The product was extracted with DCM (3 x 80 mL). The combined organic layers were washed with brine, dried over Na₂SO₄, and concentrated in vacuo. The product was purified by MPLC (hexane/EtOAc 9.6:0.4). The product was obtained as yellow oil in 49%, 1.3 gFSTEGL

7.2.14. General procedure for RAFT polymerization of NIPAAm with diglyceride-based chain transfer agents



Appropriate amounts of GlyP-X or GlyO-X, NIPAAm, solution of AIBN in THF, and THF were placed in a Schlenk flask equipped with a magnetic stirrer. The resulting mixture was degassed by bubbling with argon for 30 minutes. The reaction flask was placed in an oil bath preheated to 70 °C. After stirring for 3 hours, the polymerization was stopped by cooling in an ice bath. Then, THF was evaporated on a rotary evaporator. Products with higher molar masses (5, 10, 20 kg mol⁻¹) were dissolved in chloroform, precipitated in cold hexane twice, filtered, and dried. The polymers with 2 kg mol⁻¹ could not be purified by precipitation.

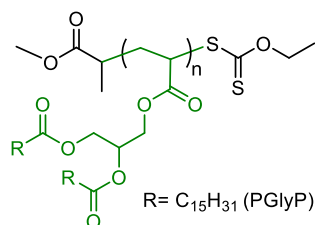
7.2.15. General procedure for RAFT polymerization of NVCL with diglyceride-based chain transfer agents



Appropriate amounts of GlyP-X or GlyO-X, NVCL, solution of AIBN in THF, and THF were placed in a Schlenk flask equipped with a magnetic stirrer. The resulting mixture was degassed by bubbling with argon for 30 minutes. The reaction flask was placed in an oil bath preheated to 70 °C. After stirring for 16 hours, the polymerization was stopped by cooling in an ice bath. Then, THF was evaporated on a rotary evaporator. Products with higher molar masses (5, 10, 20 kg mol⁻¹) were dissolved in chloroform, precipitated in cold

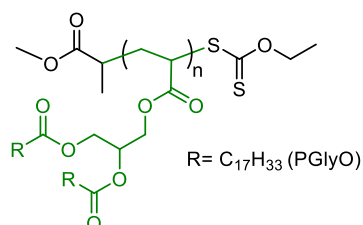
pentane twice, filtered, and dried. The polymers of molar mass 2 kg mol^{-1} could not be purified by precipitation.

7.2.16. General procedure for RAFT polymerization with GlyP acrylate



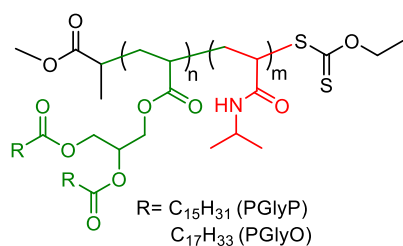
Appropriate amounts of CTA1, GlyP-A, and AIBN were placed in a Schlenk flask equipped with a magnetic stirrer. The resulting mixture was degassed by bubbling with argon for 30 minutes. The reaction flask was placed in an oil bath preheated to 70 °C. After stirring for 6 hours, the polymerization was stopped by cooling in an ice bath. THF was evaporated on a rotary evaporator. Finally, the product was dissolved in chloroform, precipitated in cold methanol four times, filtered, and dried.

7.2.17. General procedure for RAFT polymerization with GlyO acrylate



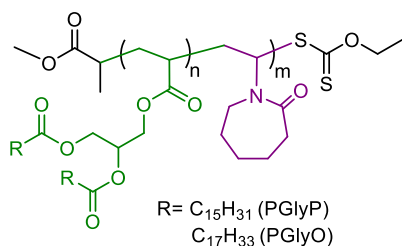
Appropriate amounts of CTA1, GlyO-A, and AIBN were placed in a Schlenk flask equipped with a magnetic stirrer. The resulting mixture was degassed by bubbling with argon for 30 minutes. The resulting solution was heated to 70 °C in an oil bath. After stirring for 16 hours, the polymerization was stopped by cooling in an ice bath. THF was evaporated on a rotary evaporator. Finally, the product was dissolved in acetone, precipitated in cold methanol four times, and dried under a high vacuum.

7.2.18. General procedure for RAFT copolymerization with NIPAAm



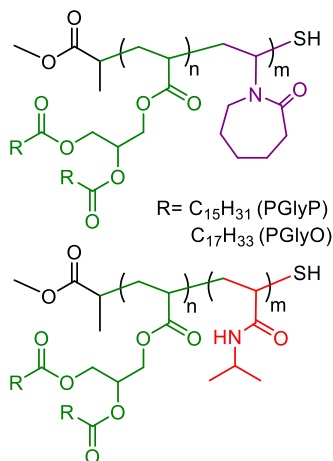
Appropriate amounts of PGlyP-macroCTA, or PGlyO-macroCTA, NIPAAm, and AIBN were placed in a Schlenk flask equipped with a magnetic stirrer. The resulting mixture was degassed by bubbling with argon for 30 minutes. The resulting solution was heated to 70 °C in an oil bath. After stirring for 6 hours, the polymerization was stopped by cooling in an ice bath. THF was evaporated on a rotary evaporator. Finally, products were dissolved in chloroform, precipitated in cold hexane twice, filtered, and dried.

7.2.19. General procedure for RAFT copolymerization with NVCL



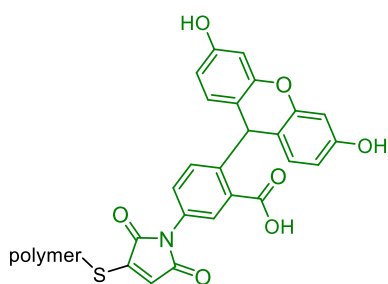
Appropriate amounts of PGlyP-X or PGlyO-X, NVCL, and AIBN were placed in a Schlenk flask equipped with a magnetic stirrer. The resulting mixture was degassed by bubbling with argon for 30 minutes. The resulting solutions were heated to 70 °C in an oil bath. After stirring for 16 hours, the polymerization was stopped by cooling in an ice bath. THF was evaporated on a rotary evaporator. Finally, products were dissolved in chloroform, precipitated in cold pentane twice, filtered, and dried.

7.2.20. Removing the dithiocarboante-end group by aminolysis



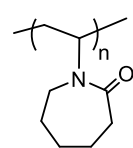
Removing the dithiocarboante end-group was conducted according to the previously described protocol.⁷¹ The 100 mg of PGlyP-*b*-PNIPAAm, PGlyO-*b*-PNIPAAm, PGlyP-*b*-PNVCL, and PGlyO-*b*-PNVCL were placed in a vial equipped with a magnetic stirrer and dissolved in 1 mL of THF. The solutions were degassed by bubbling with argon for 30 minutes. Then, *n*-propylamine (9 equiv) and tributylphosphine (9 equiv) were added. The resulting mixtures were stirred for 40 hours at room temperature. THF was evaporated on a rotary evaporator. Finally, products were dissolved in chloroform, precipitated in cold pentane (3 x 15 mL), filtered, and dried.

7.2.21. The modification of the polymer chain ends with a fluorescent dye



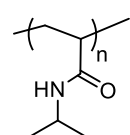
50 mg of PGlyP-*b*-PNIPAAm, PGlyO-*b*-PNIPAAm, PGlyP-*b*-PNVCL, and PGlyO-*b*-PNVCL terminated with -SH group were placed in a vial equipped with a magnetic stirrer and dissolved in 1 mL of dioxane. The solutions were degassed by bubbling with argon for 10 minutes. Then, triethylamine (3 equiv) and fluorescein diacetate 5-maleimide (5 equiv) were then added. The resulting mixtures were stirred for 48 hours at room temperature. Then, a few drops of water were added, and the mixture was stirred for another 4 h. Finally, products were precipitated in cold pentane (3 x 15 mL), filtered, and dried.

7.2.22. Radical polymerization of NVCL



NVCL (0.5 g, 3.6 mmol), AIBN (1 mg, 1.44 mmol) solution in 0.1 mL THF, and THF (0.9 mL) were placed in a Schlenk flask equipped with a magnetic stirrer. The mixture was degassed by bubbling with argon for 30 minutes. The reaction flask was placed in an oil bath preheated to 70 °C. After stirring for 16 hours, the polymerization was stopped by cooling in an ice bath. Then, THF was evaporated on a rotary evaporator. The product was dissolved in chloroform, precipitated in cold pentane twice, filtered, and dried. SEC: $M_n = 7.6 \text{ kg mol}^{-1}$, $D = 1.6$. $^1\text{H NMR}$ (400 MHz, CDCl_3): δ 4.55–4.20 (m, $\text{CHN}(\text{CO})$), 3.3–3.0 (m, $\text{CH}_2\text{N}(\text{CO})$), 2.60–2.20 (m, $\text{N}(\text{CO})\text{CH}_2$), 2.0–1.5 (m, $\text{CH}_2\text{CH}_2\text{N}$, $\text{CH}_2\text{CH}_2\text{CH}_2\text{N}$, $\text{CH}_2\text{CH}_2\text{CH}_2\text{CH}_2\text{N}$, CH_2CHN). ATR-FTIR (cm^{-1}): ν 3450, 2922, 2853, 1626, 1476, 1440, 1420, 1350, 1332, 1302, 1261, 1195, 1150, 973.

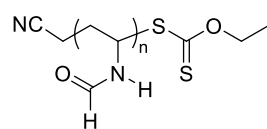
7.2.23. Radical polymerization of NIPAAm



NIPAAm (0.2 g, 1.77 mmol), AIBN (1 mg, 0.006 mmol), and THF (2 mL) were placed in a Schlenk flask equipped with a magnetic stirrer. The mixture was degassed by bubbling with argon for 30 minutes. The reaction flask was placed in an oil bath preheated to 70 °C. After stirring for 24 hours, the polymerization was stopped by cooling in an ice bath. Then, THF was evaporated on a rotary evaporator. The product was dissolved in DCM, precipitated in cold hexane twice, filtered, and dried. SEC: $M_n = 10.2 \text{ kg mol}^{-1}$, $D = 1.13$. $^1\text{H NMR}$ (400 MHz, CDCl_3): δ 4.00 ($\text{CH}(\text{CH}_3)_2$), 2.40–1.40 (polymer backbone), 1.13 ($\text{CH}(\text{CH}_3)_2$). ATR-FTIR (cm^{-1}): ν 3287, 3075, 2970, 2932, 2873, 1640, 1530, 1455, 1390, 1365, 1715, 1130.

7.3. Polymerization of *N*-vinylformamide via PI-RAFT technique

7.3.1. General procedure for the polymerization of NVF with CTA2



A reaction stock solution consisting of CTA2, NVF, and DMSO was prepared. 1 mL of solution was then added to several glass tubes and degassed by four freeze-pump-thaw cycles. The tubes were sealed with an acetylene/oxygen flame and irradiated in a blue or purple LEDs-based photoreactor. Polymerization was stopped by removing the tube from the light source. For kinetic studies, samples were directly analyzed by $^1\text{H NMR}$ and SEC without purification. NVF conversion was determined by $^1\text{H NMR}$ spectroscopy by comparison of the integration ratio of two protons ($-\text{NHCHO}$) at 7.0–8.2 ppm with the residual vinyl proton at 6.8–6.9 ppm.

Table 11. PI-RAFT polymerization of NVF in DMSO with CTA2 at ambient temperature with different light wavelengths.

Entry	Light wavelength	Time (h)	Conversion ^a (%)	$M_{n,th}^b$ (kg mol ⁻¹)	$M_{n,SEC}^c$ (kg mol ⁻¹)	\bar{D}
1	460 nm	8	33	6.71	6.45	1.18
2		16	53	10.67	7.02	1.36
3		24	65	13.06	8.19	1.38
4		40	78	15.64	9.11	1.36
5		48	82	16.43	9.35	1.40
6	400 nm	0.5	31	6.31	10.16	1.23
7		1	45	9.09	12.25	1.23
8		2	62	12.46	15.00	1.34
9		4	77	15.44	21.06	1.36
10		6	88	17.62	22.69	1.53

Notes: ^acalculated by ¹H NMR in DMSO, ^b $M_{n,th} = [NVF]_0/[CTA]_0 \cdot M_{NVF} \cdot Conv. + M_{CTA}$, ^c $M_{n,SEC}$ measured by aqueous SEC with RI-MALS detection, $[NVF]_0 = 4.53 \text{ mol L}^{-1}$.

Table 12. PI-RAFT polymerization of NVF in DMSO with CTA2 at ambient temperature with different numbers of LEDs.

Entry	Number of LEDs	Time (h)	Conversion ^a (%)	$M_{n,th}^b$ (kg mol ⁻¹)	$M_{n,SEC}^c$ (kg mol ⁻¹)	\bar{D}
1	66	0.5	31	6.31	10.16	1.23
2		1	45	9.09	12.25	1.23
3		2	62	12.46	15.00	1.34
4		4	77	15.44	21.06	1.36
5		6	88	17.62	22.69	1.53
6	30	0.5	22	4.53	6.53	1.22
7		1	36	7.30	8.62	1.24
8		2	56	11.27	12.99	1.22
9		4	77	15.44	19.17	1.28
10		6	87	17.42	20.70	1.25
11	12	8	90	18.02	22.52	1.32
12		0.5	14	2.94	4.61	1.19
13		1	31	6.31	71.60	1.30
14		2	47	9.49	11.95	1.30
15		4	70	14.05	17.87	1.26
16	30	6	82	16.43	21.21	1.28
17		8	86	17.22	22.47	1.30

Notes: ^acalculated by ¹H NMR in DMSO, ^b $M_{n,th} = [NVF]_0/[CTA]_0 \cdot M_{NVF} \cdot Conv. + M_{CTA}$, ^c $M_{n,SEC}$ measured by aqueous SEC with RI-MALS detection, $[NVF]_0 = 4.53 \text{ mol L}^{-1}$.

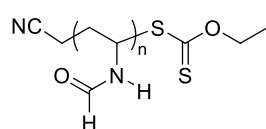
Table 13. PI-RAFT polymerization of NVF in DMSO with CTA2 at ambient temperature with 30 LEDs.

Entry	Targeted M_n (kg mol ⁻¹)	Time (h)	Conversion ^a (%)	$M_{n,th}^b$ (kg mol ⁻¹)	$M_{n,SEC}^c$ (kg mol ⁻¹)	\bar{D}
1	5	0.5	27	1.47	1.82	1.18

2		1	45	2.34	2.42	1.15
3		2	66	3.36	3.03	1.18
4		4	88	4.42	4.37	1.16
5		6	92	4.61	4.60	1.19
6		0.5	22	4.53	6.53	1.22
7		1	36	7.30	8.62	1.24
8	20	2	56	11.27	12.98	1.22
9		4	77	15.44	19.17	1.28
10		6	87	17.42	20.70	1.27
11		0.5	16	8.14	9.28	1.40
12		1	27	13.62	14.37	1.40
13	50	2	40	20.10	23.37	1.32
14		4	68	34.05	36.41	1.37
15		6	71	35.55	41.95	1.50

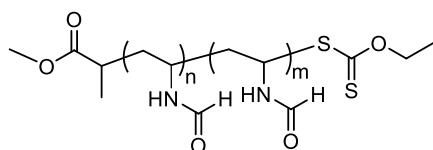
Notes: ^acalculated by ¹H NMR in DMSO, ^b $M_{n,th} = [NVF]_0/[CTA]_0 \cdot M_{NVF} \cdot Conv. + M_{CTA}$, ^c $M_{n,SEC}$ measured by aqueous SEC with RI-MALS detection, $[NVF]_0 = 4.53 \text{ mol L}^{-1}$.

7.3.2. Synthesis of PNVF-CTA2



CTA2 (0.167 g, 1.03 mmol), NVF (5 g, 70.34 mmol), and DMSO (70% w/w, 11.67 g) were added to a Schlenk tube, degassed by four freeze-pump-thaw cycles and irradiated in a purple LED light photoreactor for 45 minutes. The polymerization was stopped by removing the tube from the light source, and a withdrawn sample was analyzed by ¹H NMR to determine conversion (34%). The polymer was purified by three cycles of solubilization in water, precipitation in cold acetone, filtration, and drying under vacuum. SEC: $M_{n,SEC} = 2.2 \text{ kg mol}^{-1}$, $\mathcal{D} = 1.08$.

7.3.3. Chain extension experiment



A reaction stock solution of PNVF-CTA2 (0.155 g, 0.072 mmol), NVF (2 g, 28.14 mmol), and DMSO (70% w/w, 4.69 g) was prepared. 1 mL of solution was then added to several glass tubes and degassed by four freeze-pump-thaw cycles. The tubes were sealed with an acetylene/oxygen flame and irradiated in a purple LEDs-based photoreactor. Polymerization was stopped by removing the tube from the light source. For kinetic studies, samples were directly analyzed by ¹H NMR and SEC without purification.

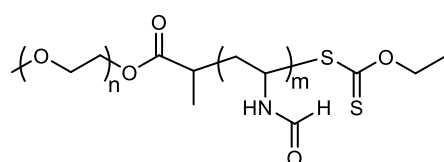
Table 14. PI-RAFT polymerization of NVF in DMSO using a PNVF-CTA2 as a macro-RAFT agent.

Entry	Targeted M_n (kg mol^{-1})	Time (h)	Conversion ^a (%)	$M_{n,th}^b$ (kg mol^{-1})	$M_{n,SEC}^c$ (kg mol^{-1})	\mathcal{D}
1		0.5	26	9.47	10.38	1.21
2	30	1	43	13.90	15.25	1.22
3		2	62	19.46	20.44	1.23

4	4	85	25.84	28.72	1.24
5	6	86	26.12	29.75	1.19

Notes: ^acalculated by ¹H NMR in DMSO, ^b $M_{n,th} = [NVF]_0/[CTA]_0 \cdot M_{NVF} \cdot Conv. + M_{CTA}$, ^c $M_{n,SEC}$ measured by aqueous SEC with a RI-MALS detection, $[NVF]_0 = 4.53 \text{ mol L}^{-1}$.

7.3.4. General procedure for the synthesis of PEG-*b*-PNVF block copolymer



A reaction stock solution consisting of PEG-CTA1 (0.6 g, 0.12 mmol), NVF (3 g, 42.2 mmol), and DMSO (70% w/w, 7 g) was prepared. The 1 mL of solution was then added to several glass tubes and degassed by

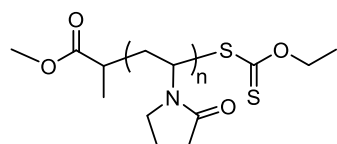
four freeze-pump-thaw cycles. The tubes were sealed with an acetylene/oxygen flame and irradiated in a purple LEDs-based photoreactor. Polymerization was stopped by removing the tube from the light source. For kinetic studies, samples were directly analyzed by ¹H NMR and SEC without purification. Dry polymers could be obtained after purification by dialysis, followed by lyophilization. The dn/dc of the copolymers were calculated based on the weight fraction of the PEG and PNVF block.

Table 15. PI-RAFT polymerization of NVF with PEG-CTA1 under purple light irradiation with 30 LEDs.

Entry	Targeted M_n (kg mol^{-1})	Time (h)	Conversion ^a (%)	$M_{n,th}^b$ (kg mol^{-1})	$M_{n,SEC}^c$ (kg mol^{-1})	dn/dc	\bar{D}
1	25	0.5	24	9.80	8.73	0.1440	1.39
2		1	34	11.80	10.98	0.1502	1.38
3		2	54	15.80	17.38	0.1534	1.40
4		4	75	20.00	22.77	0.1553	1.52
5		8	89	22.80	25.39	0.1560	1.52

Notes: ^acalculated by ¹H NMR in DMSO, ^b $M_{n,th} = [NVF]_0/[CTA]_0 \cdot M_{NVF} \cdot Conv. + M_{CTA}$, ^c $M_{n,SEC}$ measured by aqueous SEC with a RI-MALS detection, $[NVF]_0 = 4.53 \text{ mol L}^{-1}$.

7.3.5. General procedure for the polymerization of NVP with CTA1



A reaction stock solution consisting of CTA1 and NVP was prepared. Then, 1 mL of solution was added to several glass tubes and degassed by four freeze-pump-thaw cycles. The tubes were sealed with an acetylene/oxygen flame and

irradiated in a purple LEDs-based photoreactor. Polymerization was stopped by removing the tube from the light source. For kinetic studies, samples were directly analyzed by

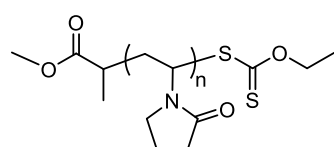
¹H NMR and SEC without purification.

Table 16. PI-RAFT polymerization of NVP in bulk with CTA1 under purple light irradiation with 30 LEDs.

Entry	Targeted M_n (kg mol ⁻¹)	Time (min)	Conversion ^a (%)	$M_{n,th}^b$ (kg mol ⁻¹)	$M_{n,SEC}^c$ (kg mol ⁻¹)	\bar{D}
1	10	7	24	2.56	2.75	1.08
2		15	47	4.81	4.34	1.09
3		22	70	7.06	6.60	1.06
4		30	94	9.41	9.12	1.16
5		60	95	9.51	9.81	1.19

Notes: ^acalculated by ¹H NMR in CDCl₃, ^b $M_{n,th} = [NVP]_0/[CTA]_0 \cdot M_{NVP} \cdot Conv. + M_{CTA}$, ^c $M_{n,SEC}$ measured by SEC in DMF with a RI-MALS detection, $[NVP]_0 = 9.36 \text{ mol L}^{-1}$.

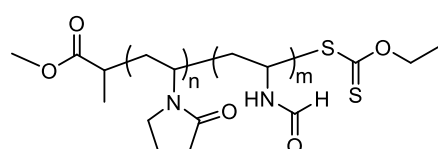
7.3.6. General procedure for the polymerization of PVP-CTA1



NVP (5 g, 44.2 mmol) and CTA1 (0.218 g, 1.04 mmol) were added to a Schlenk tube, degassed by four freeze-pump-thaw cycles, and irradiated in a purple LEDs-based photoreactor for 1 hour. Polymerization was stopped by removing the tube from

the light source, and a withdrawn sample was analyzed by ¹H NMR to determine conversion (88%). The polymer was purified by three cycles of solubilization in chloroform, precipitation in cold diethyl ether, filtration, and drying under vacuum.

7.3.7. General procedure for the synthesis of PVP-*b*-PNVF block copolymer



A reaction stock solution consisting of PVP-CTA1 (0.506 g, 0.1 mmol), NVF (2.5 g, 35.17 mmol), and DMSO (70% w/w, 5.83 g) was prepared. 1 mL of solution was then added to several glass tubes and

degassed by four freeze-pump-thaw cycles. The tubes were sealed with an acetylene/oxygen flame and irradiated in a purple LEDs-based photoreactor. Polymerization was stopped by removing the tube from the light source. For kinetic studies, samples were directly analyzed by ¹H NMR and SEC without purification. Dry polymers could be obtained after purification by three cycles of solubilization in water, precipitation in cold acetone, filtration, and drying under vacuum.

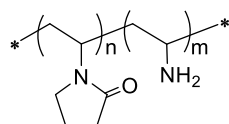
Table 17. Block polymerization of NVF in DMSO with PVP-CTA1 as a macro-CTA.

Entry	Targeted M_n (kg mol ⁻¹)	Time (h)	Conversion ^a (%)	$M_{n,th}^b$ (kg mol ⁻¹)	$M_{n,SEC}^c$ (kg mol ⁻¹)	\bar{D}
1	30	0.5	19	9.75	10.47	1.17

2	1	33	13.25	15.14	1.15
3	2	53	18.25	19.63	1.22
4	4	74	23.50	26.35	1.20
5	6	82	25.50	33.36	1.13

Notes: ^acalculated by ¹H NMR in DMSO, ^b $M_{n,th} = [NVF]_0/[PVP-CTA1]_0 \cdot M_{NVF} \cdot Conv. + M_{n,PVP-CTA1}$, ^c $M_{n,SEC}$ measured by aqueous SEC with a RI-MALS detection, $[NVF]_0 = 4.53 \text{ mol L}^{-1}$.

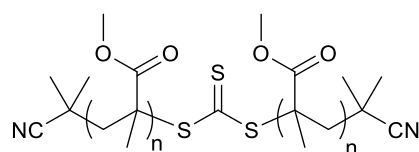
7.3.8. Hydrolysis of PVP-*b*-PNVF



PVP-*b*-PNVF (0.5 g) was dissolved in 10 mL of 2 M NaOH in a round-bottom flask. The resulting solution was heated at 80 °C for 3 hours. After complete hydrolysis confirmed by ¹H NMR, the reaction mixture was dialyzed against 1 L for 60 hours, changing the water several times. The final product was isolated by lyophilization.

7.4. Synthesis of ABA triblock copolymers via PI-RAFT technique

7.4.1. General procedure for the polymerization of MMA with TTC-bCP



A reaction stock solution of TTC-bCP and MMA (70% or 50% w/w) in acetonitrile was prepared. 1 mL of solution was then added to several glass tubes and degassed by three freeze-pump-thaw cycles. The tubes were sealed with an acetylene/oxygen flame and irradiated in a blue or green LEDs-based photoreactor. Polymerization was stopped by removing the tube from the light source. The samples were directly analyzed by ¹H NMR. For SEC analysis, the solvent was evaporated, and polymers were dissolved in THF.

Table 18. PI-RAFT polymerization of MMA with CTA3 at ambient temperature with different MMA concentrations.

Entry	Concentration of MMA in acetonitrile	Time (h)	Conversion ^a (%)	$M_{n,th}^b$ (kg mol ⁻¹)	$M_{n,SEC}^c$ (kg mol ⁻¹)	\bar{D}
1	70% w/w	4	10	20.22	25.11	1.38
2		8	20	40.20	41.54	1.31
3		16	53	106.12	86.35	1.29
4		24	74	148.06	130.80	1.32
5		32	85	170.04	144.90	1.48
6	50% w/w	8	24	48.19	21.65	1.25
7		16	38	76.15	44.57	1.29
8		24	52	104.12	56.87	1.28
9		32	85	170.04	80.41	1.46

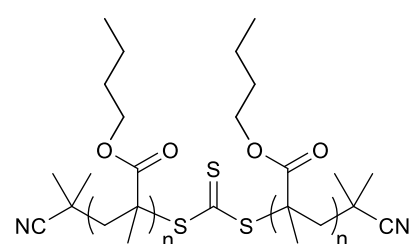
Notes: ^acalculated by ¹H NMR in CDCl₃, ^b $M_{n,th} = [MMA]_0/[CTA3]_0 \cdot M_{MMA} \cdot Conv. + M_{CTA3}$, ^c $M_{n,SEC}$ measured by SEC in THF with a RI-MALS detection.

Table 19. PI-RAFT polymerization of MMA with CTA3 at ambient temperature with 30 LEDs.

Entry	Targeted M_n (kg mol^{-1})	Time (h)	Conversion ^a (%)	$M_{n,th}^b$ (kg mol^{-1})	$M_{n,SEC}^c$ (kg mol^{-1})	\bar{D}
1	50	4	13	6.71	9.36	1.33
2		8	33	16.70	19.80	1.22
3		16	78	39.06	40.29	1.24
4		24	94	47.02	45.87	1.27
6	200	4	9	18.20	23.30	1.44
7		8	16	32.20	37.62	1.28
8		16	42	84.14	80.14	1.23
9		24	67	134.10	109.40	1.28
10	400	32	76	152.06	153.10	1.25
11		4	-	-	-	-
12		8	7	28.23	42.73	1.4
13		16	24	96.19	103.00	1.29
14	400	24	40	160.15	145.40	1.33
15		32	58	232.10	218.80	1.35

Notes: ^acalculated by ¹H NMR in CDCl₃, ^b $M_{n,th} = [\text{MMA}]_0 / [\text{CTA3}]_0 \cdot M_{\text{MMA}} \cdot \text{Conv.} + M_{\text{CTA3}}$, ^c $M_{n,SEC}$ measured by SEC in THF with a RI-MALS detection, $[\text{MMA}]_0 = 6 \text{ mol L}^{-1}$.

7.4.2. General procedure for the polymerization of *n*BA with TTC-bCP



TTC-bCP was carefully dissolved in *n*-butyl acrylate.

1 mL of solution was then added to several glass tubes and degassed by three freeze-pump-thaw cycles. The tubes were sealed with an acetylene/oxygen flame and irradiated in a blue or green LEDs-based photoreactor.

Polymerization was stopped by removing the tube from the light source. Samples were directly analyzed by ¹H NMR. For SEC analysis, the residual *n*BA was evaporated, and polymers were dissolved in THF.

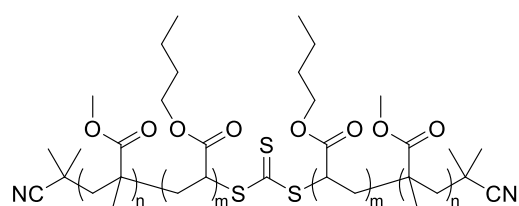
Table 20. PI-RAFT polymerization of *n*BA with CTA3 at ambient temperature.

Entry	Targeted M_n (kg mol^{-1})	Time (h)	Conversion ^a (%)	$M_{n,th}^b$ (kg mol^{-1})	$M_{n,SEC}^c$ (kg mol^{-1})	\bar{D}
1	200	2	29	58.17	52.87	1.05
2		4	51	102.11	92.20	1.01
3		8	66	132.08	116.00	1.02
4		16	80	160.05	144.30	1.02
5		24	88	176.03	155.40	1.02
6	400	2	21	84.20	73.70	1.01
7		4	37	148.16	134.50	1.03
8		8	58	232.10	207.10	1.01
9		16	70	280.08	246.90	1.02
10		24	81	324.05	286.90	1.03
11	800	2	16	128.21	110.10	1.12
12		4	29	232.18	203.50	1.05

13		8	45	360.14	310.11	1.02
14		16	53	424.12	412.60	1.01
15		24	68	544.08	470.55	1.02
16		2	11	165.22	159.10	1.22
17		4	20	300.20	287.40	1.01
18	1,500	8	26	390.18	416.80	1.07
19		16	36	540.16	588.30	1.03
20		24	45	675.14	718.20	1.02

Notes: ^acalculated by ¹H NMR in CDCl₃, ^b $M_{n,th} = [nBA]_0/[CTA3]_0 \cdot M_{nBA} \cdot Conv. + M_{CTA3}$, ^c $M_{n,SEC}$ measured by SEC in THF with a RI-MALS detection, $[nBA]_0 = 6.92 \text{ mol L}^{-1}$.

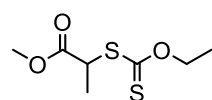
7.4.3. General procedure for ABA triblock copolymer synthesis



PMMA-CTA3 was carefully dissolved in *n*-butyl acrylate. 1 mL of solution was then added to several glass tubes and degassed by three freeze-pump-thaw cycles. The tubes were sealed with an acetylene/oxygen flame and irradiated in a blue

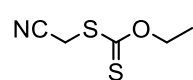
LEDs-based photoreactor. Polymerization was stopped by removing the tube from the light source. Samples were directly analyzed by ¹H NMR. For SEC analysis, the residual *n*BA was evaporated, and polymers were dissolved in THF.

7.5. Synthesis of methyl 2-((ethoxycarbonothioyl)thio)propanoate (CTA1)



This compound was synthesized according to the previously reported method.³⁷⁴ 2-Chloropropionic acid methyl ester (5 g, 41 mmol, 1 equiv) was dissolved in anhydrous acetone (40 mL) and cooled to 0 °C. Then, KSCSOEt (7.5 g, 47 mmol, 1.13 equiv) was added portionwise over 30 minutes. The reaction proceeded at room temperature for 16 hours. The salt (KCl) formed during the reaction was filtered off, and the solvent was evaporated under reduced pressure. The residue was purified by column chromatography with hexane:ethyl acetate (9:1). The final product was obtained as yellow oil in 90% (7.68 g). ¹H NMR (CDCl₃, 400 MHz): δ 4.63 (q, *J* = 7.1 Hz, 2H, CH₂CH₃), 4.40 (q, *J* = 7.4 Hz, 1H, CHCH₃), 3.75 (s, 3H, OCH₃), 1.57 (d, *J* = 7.4 Hz, 3H, CHCH₃), 1.41 (t, *J* = 7.1 Hz, 3H, CH₂CH₃). ¹³C NMR (101 MHz, CDCl₃): δ 211.9 (C=S), 171.8 (C=O), 70.2 (CH₂), 52.6 (CH), 46.9 (CH₃), 16.8 (CH₃), 13.6 (CH₃).

7.6. Synthesis of *S*-(cyanomethyl) *O*-ethyl carbonodithioate (CTA2)



This compound was synthesized according to a previously reported method with slight modifications.³⁷⁵ Bromoacetonitrile (12.4 g, 0.1 mol, 1 equiv) was dissolved in ethanol (200 mL) and cooled to 0 °C. Then, KSCSOEt (18.2 g, 0.114 mol,

1.1 equiv) was added portionwise over 30 minutes. The reaction proceeded at room temperature for 16 hours. The reaction was diluted with water (100 mL) and extracted with diethyl ether (3 x 200 mL). The combined organic layers were washed with water (300 mL), then brine and dried over anhydrous magnesium sulfate. The solvent was evaporated, and the residue was purified by column chromatography with ethyl acetate:petroleum ether (2:8). The compound was obtained as a yellow oil in 85%, 14.1 g. **¹H NMR** (CDCl₃, 300 MHz): δ 1.48 (t, 3H), 3.88 (s, 2H), 4.72 (q, 2H). **¹³C NMR** (101 MHz, CDCl₃): δ 209.2, 115.7, 71.5, 21.3, 13.7.

LIST OF FIGURES

Figure 1.	General chemical structure of RAFT chain transfer agents.....	27
Figure 2.	a) The electronic transitions responsible for C–S bond photolysis. ⁸⁷ b) UV-Vis spectrum of dithiocarbonate (methyl 2-((ethoxycarbonothioyl)thio)propanoate), c) UV-Vis spectrum of trithiocarbonate (bis-(2-methylpropanenitrile) trithiocarbonate).	32
Figure 3.	Complex architectures accessible through the RAFT process.....	35
Figure 4.	Mechanism of action of thermoresponsive amphiphilic polymers.	41
Figure 5.	Schematic illustration of phase diagrams for polymer solution a) lower critical solution temperature (LCST) behavior and b) upper critical solution temperature (UCST) behavior.....	42
Figure 6.	Examples of polymers exhibiting LCST behavior.....	43
Figure 7.	Chemical structures of <i>N</i> -vinylamides.	49
Figure 8.	Structure illustration of thermoplastic elastomers. ²⁵⁷	54
Figure 9.	Comparison of a) ¹ H NMR spectra (400 MHz, CDCl ₃) and b) ¹³ C NMR spectra (100 MHz, CDCl ₃) for the synthetic route of RAFT agent with palmitic acid derivative (GlyP-X).....	68
Figure 10.	Comparison of the a) ¹ H NMR spectra (400 MHz, CDCl ₃) and b) ¹³ C NMR spectra (100 MHz, CDCl ₃) for the synthetic route of RAFT agent with oleic acid derivative (GlyO-X).....	69
Figure 11.	Comparison of ATR-FTIR spectra for the synthetic routes of RAFT agents with a) palmitic acid derivative (GlyP-X) and b) oleic acid derivative (GlyO-X)..	70
Figure 12.	TG and DTG curves of synthesized RAFT agents: GlyP-X and GlyO-X.	71
Figure 13.	DSC curves of chain transfer agents: GlyP-X (black trace) and GlyO-X (red trace).....	71
Figure 14.	Comparison of the a) ¹ H NMR spectra (400 MHz, CDCl ₃) and b) ¹³ C NMR spectra (100 MHz, CDCl ₃) for the synthetic route of monomer with palmitic acid derivative (GlyP-A).....	74
Figure 15.	Comparison of the a) ¹ H NMR spectra (400 MHz, CDCl ₃) and b) ¹³ C NMR spectra (100 MHz, CDCl ₃) for the synthetic route of monomer with oleic acid derivative (GlyO-A).	75
Figure 16.	Comparison of ATR-FTIR spectra for the synthetic routes of monomers with a) palmitic acid derivative (GlyP-A) and b) oleic acid derivative (GlyO-A)..	76
Figure 17.	SEC chromatograms of homopolymers.	80

Figure 18. ^1H NMR spectra (400 MHz, CDCl_3) of homopolymers a) GlyO-PNIPAAm, b) GlyO-PNVCL.	82
Figure 19. ATR-FTIR spectra of homopolymers a) GlyO-PNIPAAm, b) GlyO-PNVCL.	83
Figure 20. TG and DTG curves of the studied homopolymers.	84
Figure 21. Glass transition temperatures of polymers determined by DSC: a) GlyP-PNIPAAm, b) GlyO-PNIPAAm, c) GlyP-PNVCL, and d) GlyO-PNVCL.....	85
Figure 22. Intensity ratios (I_{394}/I_{373}) from pyrene emission spectra plotted with a concentration of polymers a) GlyP-PNIPAAm, b) GlyO-PNIPAAm, c) GlyP-PNVCL, d) GlyO-PNVCL.	87
Figure 23. SEC-RI chromatograms of diglyceride-based homopolymers and copolymers.	89
Figure 24. Comparison of a) ^1H NMR spectra (400 MHz, CDCl_3) and b) ATR-FTIR spectra for polymers containing the palmitic acid derivative (GlyP-A).....	92
Figure 25. Comparison of the a) ^1H NMR spectra (400 MHz, CDCl_3) and b) ATR-FTIR spectra for polymers containing the oleic acid derivative (GlyO-A).	93
Figure 26. TGA (top panels) and DTG (bottom panels) of the studied homopolymers and copolymers.	94
Figure 27. DSC curves (the second heating and cooling run) of the studied a) homopolymers and b) copolymers.	94
Figure 28. Critical micelle concentration measurements of copolymers a) PGlyP- <i>b</i> -PNIPAAm, b) PGlyO- <i>b</i> -PNIPAAm, c) PGlyP- <i>b</i> -PNVCL, and d) PGlyO- <i>b</i> -PNVCL.	95
Figure 29. Schematic representation of nanoprecipitation method.	100
Figure 30. Number size distribution measured by MADLS (PBS, 25 °C, $C = 1 \text{ mg mL}^{-1}$), a) GlyP-PNIPAAm_NP, b) GlyO-PNIPAAm_NP, c) GlyP-PNVCL_NP, d) GlyO-PNVCL_NP.....	101
Figure 31. Determination of the shape of polymeric nanoparticles using horizontal and vertical measurements: a) GlyP-PNIPAAm_NP and b) GlyP-PNVCL_NP (PBS, 25 °C, $C = 1 \text{ mg mL}^{-1}$).	102
Figure 32. TEM images of selected polymeric nanoparticles in two different magnitudes: a) GlyP-PNIPAAm _{20k} _NP, b) GlyO-PNVCL _{5k} _NP, c) GlyO-PNVCL _{10k} _NP, d) distribution of measured diameter for GlyO-PNVCL _{10k} _NP.	103
Figure 33. Evolution of transmittance measured by turbidimetry and number size distribution measured by DLS as a function of temperature for polymers: a) PNIPAAm, b) PNVCL, and polymeric nanoparticles, c) GlyP-PNIPAAm_NP,	

d) GlyO-PNIPAAm_NP, e) GlyP-PNVCL_NP, f) GlyO-PNVCL_NP (PBS, 25 °C, $C = 0.5 \text{ mg mL}^{-1}$).....	106
Figure 34. Correlograms obtained from DLS experiments with a scattering angle of 173° (PBS, 25 °C, $C = 1 \text{ mg mL}^{-1}$) and horizontal and vertical measurements for polymeric nanoparticles a) PGlyP- <i>b</i> -PNIPAAm and b) PGlyO- <i>b</i> -PNVCL... 108	108
Figure 35. TEM images for a) PGlyP- <i>b</i> -PNIPAAm_NP and b) PGlyO- <i>b</i> -PNIPAAm_NP.	108
Figure 36. The structure of doxorubicin and tamoxifen.	109
Figure 37. Evolution of transmittance measured by turbidimetry and number size distribution measured by DLS as a function of temperature for empty and drug-loaded polymeric nanoparticles (PBS, 25 °C, $C = 0.5 \text{ mg mL}^{-1}$).....	112
Figure 38. Schematic representation of temperature-induced drug release.	114
Figure 39. Release profiles of tamoxifen from thermoresponsive polymeric nanoparticles: a) PGlyP- <i>b</i> -PNIPAAm_NPTAM, b) PGlyO- <i>b</i> -PNIPAAm_NPTAM, c) PGlyP- <i>b</i> -PNVCL_NPTAM, d) PGlyO- <i>b</i> -PNVCL_NPTAM.	115
Figure 40. Representative of UV-Vis spectrum of polymer (PGlyP- <i>b</i> -PNIPAAm) terminated with dithiocarbonate (solid line) and reduced to thiol (dashed line).	118
Figure 41. Fluorescence properties of polymers and corresponding fluorescein-labeled polymeric nanoparticles ($C = 0.1 \text{ mg mL}^{-1}$, PBS, $\lambda_{\text{ex}} = 494 \text{ nm}$ and $\lambda_{\text{em}} = 518 \text{ nm}$).....	119
Figure 42. Internalization of fluorescein (FLU)-labeled empty and DOX-loaded PNPs into breast cancer cells. Fluorescence intensity of fluorescein-labeled empty and DOX-loaded PNPs in a) MCF-7 cells and b) MDA-MB-231 cells. Microscopic analysis of fluorescein-labeled empty and DOX-loaded PNPs localization into c) MCF-7 cells and d) MDA-MB-231 cells; 200x magnification.....	120
Figure 43. Purple LEDs-based photoreactor for polymerization studies.....	126
Figure 44. UV-Vis spectrum of <i>S</i> -(cyanomethyl) <i>O</i> -ethyl carbonodithioate.....	127
Figure 45. The effect of light wavelength on NVF conversion over time.	127
Figure 46. Evolution of SEC-RI chromatograms of PNVF with NVF conversion for polymerizations carried out with a) blue light and b) purple light.....	128
Figure 47. Evolution of M_n and \bar{D} during PI-RAFT polymerization of NVF with different light sources.	128
Figure 48. SEC-UV chromatograms of PNVF.....	129
Figure 49. The effect of purple light intensity on NVF conversion with time.....	130

Figure 50. The effect of purple light intensity on M_n and dispersities versus conversion.	130
Figure 51. Evolution of M_n and \mathcal{D} during PI-RAFT polymerization of NVF for different targeted molar masses.	131
Figure 52. Evolution of the SEC-RI chromatograms of PNVF with NVF conversion for different molar masses.	132
Figure 53. Effect of the initial concentration of CTA2 on PI-RAFT polymerization in DMSO at ambient temperature ($[NVF]_0 = 4.53 \text{ mol L}^{-1}$).	132
Figure 54. ^1H NMR spectra of a) a dithiocarbonate-free experiment and b) a light-free experiment (300.13 MHz, DMSO).	133
Figure 55. Temporal control of PI-RAFT polymerization. Evolution of NVF conversion over time during purple LED irradiation (ON: white area) and without irradiation (OFF: gray area).	134
Figure 56. MALDI-TOF MS spectrum of PNVF-CTA2 ($M_{n,SEC} = 2.2 \text{ kg mol}^{-1}$, $\mathcal{D} = 1.08$).	135
Figure 57. ^1H NMR spectrum of PNVF-CTA2 of low molar mass ($M_{n,SEC} = 2.2 \text{ kg mol}^{-1}$, $\mathcal{D} = 1.08$), (300.13 MHz, DMSO).	135
Figure 58. ESI-TOF MS spectrum of PNVF-CTA2 ($M_{n,SEC} = 2.2 \text{ kg mol}^{-1}$, $\mathcal{D} = 1.08$). ..	136
Figure 59. a) Evolution of SEC-RI chromatograms of PNVF with NVF conversion during chain extension experiment. b) Evolution of M_n and dispersity versus conversion during chain extension of PNVF.	137
Figure 60. a) Evolution of M_n and \mathcal{D} versus conversion determined by aqueous SEC. b) Evolution of SEC-RI chromatograms of PEG- <i>b</i> -PNVF copolymers with NVF conversion during PI-RAFT polymerization.	138
Figure 61. ^1H NMR spectrum of PI-RAFT polymerization of NVP with CTA2 (300.13 MHz, CDCl_3).	140
Figure 62. a) Evolution of SEC-RI chromatograms of PVP with NVP conversion during PI-RAFT polymerization. b) Evolution of M_n and dispersity versus conversion during PI-RAFT polymerization.	141
Figure 63. a) Evolution of M_n and \mathcal{D} versus conversion determined by aqueous SEC. b) Evolution of SEC-RI chromatograms of PVP- <i>b</i> -PNVF copolymers with NVF conversion during PI-RAFT polymerization.	141
Figure 64. A4F fractograms of PVP-CTA1 and PVP- <i>b</i> -PNVF.	143
Figure 65. ^1H DOSY NMR spectra (500 MHz, DMSO).	144

Figure 66. Comparison of ^1H NMR spectra of PVP-CTA1, PVP- <i>b</i> -PNVF, and PVP- <i>b</i> -PVAm (300.13 MHz, D_2O).	145
Figure 67. UV-Vis spectrum of bis-(2-methylpropanenitrile)trithiocarbonate (TTC-bCP).	150
Figure 68. SEC chromatograms of PMMA obtained with different sources of light (SEC-RI trace: solid line, SEC-UV trace: dashed line).	151
Figure 69. Evolution of M_n and \bar{D} during PI-RAFT polymerization with different concentrations of MMA in acetonitrile.	152
Figure 70. Evolution of PMMA SEC-RI chromatograms with MMA conversion for polymerizations carried out with a) 50% w/w and b) 70% w/w of MMA in acetonitrile.....	152
Figure 71. SEC chromatograms of PMMA prepared by bulk polymerization.	153
Figure 72. Evolution of M_n and \bar{D} during PI-RAFT polymerization for different targeted molar masses.	153
Figure 73. SEC-RI chromatograms of PMMA with MMA conversion for different molar masses.	154
Figure 74. Evolution of M_n and \bar{D} during PI-RAFT polymerization for different targeted molar masses.	155
Figure 75. Evolution of SEC-RI chromatograms of P <i>n</i> BA with <i>n</i> BA conversion for different molar masses.	156
Figure 76. SEC chromatograms of PMMA _{110k} -CTA3 and the corresponding ABA triblock copolymer.	157
Figure 77. SEC-RI chromatograms of PMMA _{80k} -CTA3 and the corresponding ABA triblock copolymer.	158
Figure 78. Calibration curve for doxorubicin.....	171
Figure 79. Calibration curve for tamoxifen.....	172

LIST OF SCHEMES

Scheme 1.	Mechanism of radical polymerization.....	19
Scheme 2.	Activation-deactivation mechanism in RDRP.....	22
Scheme 3.	Persistent radical effect.....	22
Scheme 4.	Degenerative transfer.....	22
Scheme 5.	Mechanism of reversible addition-fragmentation chain transfer (RAFT) polymerization. ^{23,25,26}	25
Scheme 6.	General guidelines for the selection of the a) Z group and b) R groups.....	29
Scheme 7.	Processes for RAFT end-group modifications (R', radical; [H], hydrogen donor; M, monomer). ⁷⁰	30
Scheme 8.	Mechanism of PI-RAFT. ⁸³	33
Scheme 9.	Imine-enamine tautomerization of vinylamine.....	50
Scheme 10.	Synthesis of ABA-type triblock copolymers via RAFT polymerization using difunctional CTAs: a) R-group approach, b) Z-group approach.....	53
Scheme 11.	Synthesis of chain transfer agents.....	66
Scheme 12.	Synthesis of diglyceride-based monomers.....	72
Scheme 13.	Synthesis of thermoresponsive polymers with diglyceride-based dithiocarbonates by RAFT polymerization.....	77
Scheme 14.	Synthesis of thermoresponsive polymers with diglyceride-based monomers by RAFT polymerization.....	88
Scheme 15.	Modification of polymer chain-end with fluorescent dye.....	118
Scheme 16.	General scheme of PI-RAFT polymerization of NVF under LED irradiation and hydrolysis of PNVF to corresponding polyvinylamine.....	125
Scheme 17.	General scheme of copolymerization with PEG ac macro-CTA.....	138
Scheme 18.	General scheme for block copolymerization with PVP as macro-CTA.....	140
Scheme 19.	The hydrolysis of the PNVF segment.....	145
Scheme 20.	General scheme for the synthesis of ABA triblock copolymers using PI-RAFT. ²⁴⁶	149

LIST OF TABLES

Table 1.	Overview of chain transfer agents, irradiation wavelengths, and monomers in PI-RAFT polymerization.	34
Table 2.	Polymeric nanocarriers developed through the RAFT polymerization.	38
Table 3.	Comprehensive overview of thermoresponsive polymer-based drug delivery systems.	45
Table 4.	Comparison between physicochemical properties of PNIPAAm and PNVCL. ^{156,187}	47
Table 5.	Characteristics and applications of ABA-type triblock copolymers.	57
Table 6.	Comparative properties and synthesis details of polymerizations.	79
Table 7.	Comparative properties and synthetic details of polymerization for PGlyP, PGlyO, and their copolymers.	90
Table 8.	Physicochemical parameters of the studied homopolymers.	105
Table 9.	Size distribution of polymeric nanoparticles in water or PBS (25 °C, $C = 1 \text{ mg mL}^{-1}$).	107
Table 10.	Physicochemical parameters of the studied polymers.	113
Table 11.	PI-RAFT polymerization of NVF in DMSO with CTA2 at ambient temperature with different light wavelengths.	189
Table 12.	PI-RAFT polymerization of NVF in DMSO with CTA2 at ambient temperature with different numbers of LEDs.	189
Table 13.	PI-RAFT polymerization of NVF in DMSO with CTA2 at ambient temperature with 30 LEDs.	189
Table 14.	PI-RAFT polymerization of NVF in DMSO using a PNVF-CTA2 as a macro-RAFT agent.	190
Table 15.	PI-RAFT polymerization of NVF with PEG-CTA1 under purple light irradiation with 30 LEDs.	191
Table 16.	PI-RAFT polymerization of NVP in bulk with CTA1 under purple light irradiation with 30 LEDs.	192
Table 17.	Block polymerization of NVF in DMSO with PVP-CTA1 as a macro-CTA.	192
Table 18.	PI-RAFT polymerization of MMA with CTA3 at ambient temperature with different MMA concentrations.	193
Table 19.	PI-RAFT polymerization of MMA with CTA3 at ambient temperature with 30 LEDs.	194
Table 20.	PI-RAFT polymerization of <i>n</i> BA with CTA3 at ambient temperature.	194

SCIENTIFIC ACHIEVEMENTS

LIST OF PUBLICATIONS

Manuscripts included in the doctoral dissertation:

1. **I. Kurowska**, K.H. Markiewicz, K. Niemirowicz-Laskowska, M. Destarac, P. Wielgat, I. Misztalewska-Turkowicz, P. Misiak, H. Car, A.Z. Wilczewska, Membrane-active thermoresponsive block copolymers containing a diacylglycerol-based segment: RAFT synthesis, doxorubicin encapsulation, and evaluation of cytotoxicity against breast cancer cells, *Biomacromolecules*. 24 (2023) 4854–4868. IF = 6.2, MNISW = 140.
2. **I. Kurowska**, K.H. Markiewicz, K. Niemirowicz-Laskowska, P. Misiak, M. Destarac, P. Wielgat, I. Misztalewska-Turkowicz, G. Siemiaszko, H. Car, A.Z. Wilczewska, Membrane-active diacylglycerol-terminated thermoresponsive polymers: RAFT synthesis and biocompatibility evaluation, *European Polymer Journal*. 169 (2022) 111154. IF = 6.0, MNISW = 100.
3. **I. Kurowska**, A. Dupre–Demorsy, S. Balayssac, M. Hennetier, A. Ric, V. Bourdon, T. Ando, H. Ajiro, O. Coutelier, M. Destarac, Tailor-made poly(vinylamine) via purple LED-activated RAFT polymerization of *N*-vinylformamide, *Macromolecular Rapid Communications*. 44 (2023) 2200729. IF = 4.6, MNISW = 100.

Manuscripts not included in the doctoral dissertation:

4. P. Misiak, K. Niemirowicz-Laskowska, K.H. Markiewicz, P. Wielgat, **I. Kurowska**, R. Czarnomysy, I. Misztalewska-Turkowicz, H. Car, K. Bielawski, A.Z. Wilczewska, Doxorubicin-loaded polymeric nanoparticles containing ketoester-based block and cholesterol moiety as specific vehicles to fight estrogen-dependent breast cancer, *Cancer Nanotechnology*. 14 (2023) 23. IF = 5.7, MNISW = 100.
5. A. Dupre–Demorsy, **I. Kurowska**, S. Balayssac, M. Hennetier, A. Ric, V. Bourdon, T. Ando, H. Ajiro, O. Coutelier, M. Destarac, RAFT polymerisation of *N*-vinylformamide and the corresponding double hydrophilic block copolymers, *Polymer Chemistry*. 13 (2022) 6229–6237. IF = 4.6, MNISW = 140.
6. **I. Kurowska**, B. Amouroux, M. Langlais, O. Coutelier, C. Coudret, M. Destarac, J.-D. Marty, Versatile thiolactone-based conjugation strategies to polymer stabilizers

- for multifunctional upconverting nanoparticles aqueous dispersions, *Nanoscale*. 14 (2022) 2238–2247. IF = 6.7, MNISW = 140.
7. G. Siemiaszko, K. Niemirowicz-Laskowska, K.H. Markiewicz, I. Misztalewska-Turkowicz, E. Dudź, S. Milewska, P. Misiak, **I. Kurowska**, A. Sadowska, H. Car, A.Z. Wilczewska, Synergistic effect of folate-conjugated polymers and 5-fluorouracil in the treatment of colon cancer, *Cancer Nanotechnology*. 12 (2021) 31. IF = 5.7, MNISW = 100.
 8. J. Potaś, E. Szymańska, M. Wróblewska, **I. Kurowska**, M. Maciejczyk, A. Basa, E. Wolska, A.Z. Wilczewska, K. Winnicka, Multilayer films based on chitosan/pectin polyelectrolyte complexes as novel platforms for buccal administration of clotrimazole, *Pharmaceutics*. 13 (2021) 1588. IF = 5.4, MNISW = 140.
 9. P. Misiak, K. Niemirowicz-Laskowska, K.H. Markiewicz, I. Misztalewska-Turkowicz, P. Wielgat, **I. Kurowska**, G. Siemiaszko, M. Destarac, H. Car, A.Z. Wilczewska, Evaluation of cytotoxic effect of cholesterol end-capped poly(*N*-isopropylacrylamide)s on selected normal and neoplastic cells, *International Journal of Nanomedicine*. 15 (2020) 7263–7278. IF = 8.0, MNISW = 140.

*Scores from the Ministry of Science and Higher Education (MNISW).

LIST OF CONFERENCE PRESENTATIONS

List of conference presentations where part of the material included in this doctoral dissertation was presented:

1. **I. Kurowska**, K. H. Markiewicz, K. Niemirowicz-Laskowska, M. Destarac, I. Misztalewska-Turkowicz, P. Misiak, A. Z. Wilczewska, *Termowrażliwe kopolimery zawierające blok na bazie diglicerydów oraz ich koniugaty z doksorubicyną*, 65. Zjazd Naukowy Polskiego Towarzystwa Chemicznego, Toruń, 18–22.09.2023 (poster).
2. **I. Kurowska**, A. Dupre–Demorsy, S. Balayssac, M. Henriet, A. Ric, V. Bourdon, T. Ando, H. Ajiro, O. Coutelier, M. Destarac, *Fotopolimeryzacja PI-RAFT jako narzędzie do otrzymywania poli(*N*-winyloformamidu)*, 65. Zjazd Naukowy Polskiego Towarzystwa Chemicznego, Toruń, 18–22.09.2023 (oral presentation).
3. **I. Kurowska**, K. H. Markiewicz, M. Destarac, I. Misztalewska-Turkowicz, P. Misiak, A. Z. Wilczewska, *Membrane-active thermoresponsive block copolymers*

- containing diacylglycerol-based segment: RAFT synthesis, polymeric nanoparticles formation, and doxorubicin encapsulation*, International conference Recent achievements in nanotechnology – 10th anniversary of BNT Center University of Bialystok, Bialystok, 28.05–01.06.2023 (poster, flash talk).
4. **I. Kurowska**, K.H. Markiewicz, K. Niemirowicz-Laskowska, I. Misztalewska-Turkowicz, P. Misiak, G. Siemiaszko, H. Car, M. Destarac, A. Z. Wilczewska, *Membrane-active diacylglycerol-terminated thermoresponsive polymers: RAFT synthesis and biocompatibility evaluation*, Bordeaux Polymer Conference 2022, Bordeaux, 13–16.06.2022 (poster).
 5. **I. Kurowska**, K. H. Markiewicz, I. Misztalewska-Turkowicz, A. Z. Wilczewska, *Glicerydowe czynniki kontroli polimeryzacji do otrzymywania polimerów termowrażliwych*, e-Zjazd Wiosenny SSPTChem 2021, on-line, 27–29.05.2021 (poster).
 6. **I. Kurowska**, P. Misiak, K. H. Markiewicz, A.Z. Wilczewska, *Synthesis of thermoresponsive polymers with glycerides moieties*, 16th Biennial Bayreuth Polymer Symposium, Bayreuth, 22–24.09.2019 (poster, flash talk).
 7. **I. Kurowska**, D. Szymczuk, P. Misiak, K. H. Markiewicz, A. Z. Wilczewska, *Badanie samoorganizacji polimerów zawierających pochodne glicerydowe*, Związki Biologicznie Czynne – Aktywność, Struktura, Synteza, Białystok, 27–29.06.2019 (poster).

LIST OF INTERNATIONAL INTERNSHIPS

1. Erasmus+ program (February 2020 – March 2020), SOFTMAT laboratory, University Toulouse III - Paul Sabatier, France.
2. Eiffel Excellence scholarship (October 2021 – September 2022), SOFTMAT laboratory, University Toulouse III - Paul Sabatier, France.

REFERENCES

- (1) Moad, G. Radical Polymerization. In *Reference Module in Materials Science and Materials Engineering*; Elsevier, 2016; p B9780128035818013461. <https://doi.org/10.1016/B978-0-12-803581-8.01346-1>.
- (2) Nesvadba, P. Radical Polymerization in Industry. In *Encyclopedia of Radicals in Chemistry, Biology and Materials*; John Wiley & Sons, Ltd, 2012. <https://doi.org/10.1002/9781119953678.rad080>.
- (3) Odian, G. G. *Principles of Polymerization*, 4th ed.; Wiley-Interscience: Hoboken, N.J, 2004.
- (4) Kilbinger, A. F. M. Controlled and Living Polymerizations. From Mechanisms to Applications. Edited by Axel H. E. Müller and Krzysztof Matyjaszewski. *Angewandte Chemie International Edition* **2010**, 49 (7), 1191–1192. <https://doi.org/10.1002/anie.200907064>.
- (5) Matyjaszewski, K.; Davis, T. P. *Handbook of Radical Polymerization*; John Wiley & Sons, 2003.
- (6) Klumperman, B. Reversible Deactivation Radical Polymerization. In *Encyclopedia of Polymer Science and Technology*; John Wiley & Sons, Ltd, 2015; pp 1–27. <https://doi.org/10.1002/0471440264.pst453.pub2>.
- (7) Dworakowska, S.; Lorandi, F.; Gorczyński, A.; Matyjaszewski, K. Toward Green Atom Transfer Radical Polymerization: Current Status and Future Challenges. *Advanced Science* **2022**, 9 (19), 2106076. <https://doi.org/10.1002/advs.202106076>.
- (8) Szwarc, M. ‘Living’ Polymers. *Nature* **1956**, 178 (4543), 1168–1169. <https://doi.org/10.1038/1781168a0>.
- (9) Szwarc, M.; Levy, M.; Milkovich, R. POLYMERIZATION INITIATED BY ELECTRON TRANSFER TO MONOMER. A NEW METHOD OF FORMATION OF BLOCK POLYMERS ¹. *J. Am. Chem. Soc.* **1956**, 78 (11), 2656–2657. <https://doi.org/10.1021/ja01592a101>.
- (10) Hawker, C. J.; Bosman, A. W.; Harth, E. New Polymer Synthesis by Nitroxide Mediated Living Radical Polymerizations. *Chem. Rev.* **2001**, 101 (12), 3661–3688. <https://doi.org/10.1021/cr990119u>.
- (11) Corrigan, N.; Jung, K.; Moad, G.; Hawker, C. J.; Matyjaszewski, K.; Boyer, C. Reversible-Deactivation Radical Polymerization (Controlled/Living Radical Polymerization): From Discovery to Materials Design and Applications. *Progress in Polymer Science* **2020**, 111, 101311. <https://doi.org/10.1016/j.progpolymsci.2020.101311>.
- (12) Moad, G. Living and Controlled RAP (Reversible Activation Polymerization) on the Way to RDRP (Reversible Deactivation Radical Polymerization). No Chance for Immortality. A Mini-review on the Terminological Development of RDRP. *Polymer International* **2022**. <https://doi.org/10.1002/pi.6424>.
- (13) Zetterlund, P. B.; Kagawa, Y.; Okubo, M. Controlled/Living Radical Polymerization in Dispersed Systems. *Chem. Rev.* **2008**, 108 (9), 3747–3794. <https://doi.org/10.1021/cr800242x>.
- (14) Braunecker, W. A.; Matyjaszewski, K. Controlled/Living Radical Polymerization: Features, Developments, and Perspectives. *Progress in Polymer Science* **2007**, 32 (1), 93–146. <https://doi.org/10.1016/j.progpolymsci.2006.11.002>.
- (15) Kamigaito, M.; Satoh, K.; Uchiyama, M. Degenerative Chain-Transfer Process: Controlling All Chain-Growth Polymerizations and Enabling Novel Monomer Sequences. *Journal of Polymer Science Part A: Polymer Chemistry* **2019**, 57 (3), 243–254. <https://doi.org/10.1002/pola.29257>.
- (16) Barton, D. H. R.; McCombie, S. W. A New Method for the Deoxygenation of Secondary Alcohols. *J. Chem. Soc., Perkin Trans. 1* **1975**, No. 16, 1574–1585. <https://doi.org/10.1039/P19750001574>.
- (17) Zard, S. Z. The Genesis of the Reversible Radical Addition–Fragmentation–Transfer of Thiocarbonylthio Derivatives from the Barton–McCombie Deoxygenation: A Brief Account and Some Mechanistic Observations*. *Aust. J. Chem.* **2006**, 59 (10), 663–668. <https://doi.org/10.1071/CH06263>.
- (18) Cacioli, P.; Hawthorne, D. G.; Laslett, R. L.; Rizzardo, E.; Solomon, D. H. Copolymerization of ω -Unsaturated Oligo(Methyl Methacrylate): New Macromonomers. *Journal of*

- Macromolecular Science: Part A - Chemistry* **1986**, *23* (7), 839–852. <https://doi.org/10.1080/00222338608069476>.
- (19) Meijs, G. F.; Rizzardo, E.; Thang, S. H. Preparation of Controlled-Molecular-Weight, Olefin-Terminated Polymers by Free Radical Methods. Chain Transfer Using Allylic Sulfides. *Macromolecules* **1988**, *21* (10), 3122–3124. <https://doi.org/10.1021/ma00188a039>.
- (20) Krstina, J.; Moad, C. L.; Moad, G.; Rizzardo, E.; Berge, C. T.; Fryd, M. A New Form of Controlled Growth Free Radical Polymerization. *Macromol. Symp.* **1996**, *111* (1), 13–23. <https://doi.org/10.1002/masy.19961110104>.
- (21) Chiefari, J.; Chong, Y. K. (Bill); Ercole, F.; Krstina, J.; Jeffery, J.; Le, T. P. T.; Mayadunne, R. T. A.; Meijs, G. F.; Moad, C. L.; Moad, G.; Rizzardo, E.; Thang, S. H. Living Free-Radical Polymerization by Reversible Addition–Fragmentation Chain Transfer: The RAFT Process. *Macromolecules* **1998**, *31* (16), 5559–5562. <https://doi.org/10.1021/ma9804951>.
- (22) Corpart, P.; Charmot, D.; Biadatti, T.; Zard, S.; Michelet, D. Block Polymer Synthesis by Controlled Radical Polymerization. WO9858974, June 23, 1998.
- (23) Perrier, S. 50th Anniversary Perspective: RAFT Polymerization—A User Guide. *Macromolecules* **2017**, *50* (19), 7433–7447. <https://doi.org/10.1021/acs.macromol.7b00767>.
- (24) Tian, X.; Ding, J.; Zhang, B.; Qiu, F.; Zhuang, X.; Chen, Y. Recent Advances in RAFT Polymerization: Novel Initiation Mechanisms and Optoelectronic Applications. *Polymers* **2018**, *10* (3), 318. <https://doi.org/10.3390/polym10030318>.
- (25) Mori, H. Living Radical Polymerization: Reversible Addition-Fragmentation Chain Transfer (RAFT) Polymerization. In *Encyclopedia of Polymeric Nanomaterials*; Kobayashi, S., Müllen, K., Eds.; Springer Berlin Heidelberg: Berlin, Heidelberg, 2015; pp 1148–1155. https://doi.org/10.1007/978-3-642-29648-2_192.
- (26) Moad, G. A Critical Survey of Dithiocarbamate Reversible Addition-Fragmentation Chain Transfer (RAFT) Agents in Radical Polymerization. *J. Polym. Sci. Part A: Polym. Chem.* **2019**, *57* (3), 216–227. <https://doi.org/10.1002/pola.29199>.
- (27) Mitsoni, E.; Roka, N.; Pitsikalis, M. Statistical Copolymerization of N-Vinyl-Pyrrolidone and Alkyl Methacrylates via RAFT: Reactivity Ratios and Thermal Analysis. *J Polym Res* **2019**, *26* (5), 118. <https://doi.org/10.1007/s10965-019-1776-7>.
- (28) Nieswandt, K.; Georgopanos, P.; Abetz, V. Well-Defined Polyvinylpyridine-Block-Polystyrene Diblock Copolymers via RAFT Aqueous-Alcoholic Dispersion Polymerization: Synthesis and Isoporous Thin Film Morphology. *Polym. Chem.* **2021**, *12* (15), 2210–2221. <https://doi.org/10.1039/D1PY00074H>.
- (29) R. Gibson, R.; Fernyhough, A.; M. Musa, O.; P. Armes, S. RAFT Dispersion Polymerization of N, N -Dimethylacrylamide in a Series of n -Alkanes Using a Thermoresponsive Poly(Tert -Octyl Acrylamide) Steric Stabilizer. *Polymer Chemistry* **2021**, *12* (14), 2165–2174. <https://doi.org/10.1039/D1PY00045D>.
- (30) Kurowska, I.; Markiewicz, K. H.; Niemirowicz-Laskowska, K.; Destarac, M.; Wielgat, P.; Misztalewska-Turkowicz, I.; Misiak, P.; Car, H.; Wilczewska, A. Z. Membrane-Active Thermoresponsive Block Copolymers Containing a Diacylglycerol-Based Segment: RAFT Synthesis, Doxorubicin Encapsulation, and Evaluation of Cytotoxicity against Breast Cancer Cells. *Biomacromolecules* **2023**, *24* (11), 4854–4868. <https://doi.org/10.1021/acs.biomac.3c00580>.
- (31) Clothier, G. K. K.; Guimaraes, T. R.; Thompson, S. W.; Rho, J. Y.; Perrier, S.; Moad, G.; Zetterlund, P. B. Multiblock Copolymer Synthesis via RAFT Emulsion Polymerization. *Chem. Soc. Rev.* **2023**. <https://doi.org/10.1039/D2CS00115B>.
- (32) Dai, X.; Yu, L.; Zhang, Y.; Zhang, L.; Tan, J. Polymerization-Induced Self-Assembly via RAFT-Mediated Emulsion Polymerization of Methacrylic Monomers. *Macromolecules* **2019**, *52* (19), 7468–7476. <https://doi.org/10.1021/acs.macromol.9b01689>.
- (33) Derry, M. J.; Fielding, L. A.; Armes, S. P. Polymerization-Induced Self-Assembly of Block Copolymer Nanoparticles via RAFT Non-Aqueous Dispersion Polymerization. *Progress in Polymer Science* **2016**, *52*, 1–18. <https://doi.org/10.1016/j.progpolymsci.2015.10.002>.
- (34) Yang, S.; Zhang, L.; Chen, Y.; Tan, J. Combining Green Light-Activated Photoiniferter RAFT Polymerization and RAFT Dispersion Polymerization for Graft Copolymer

- Assemblies. *Macromolecules* **2022**, *55* (19), 8472–8484. <https://doi.org/10.1021/acs.macromol.2c01529>.
- (35) Hedayati, H. R.; Khorasani, M.; Ahmadi, M.; Ballard, N. Preparation of Well-Defined Poly(Vinyl Alcohol) by Hydrolysis of Poly(Vinyl Acetate) Synthesized by RAFT Suspension Polymerization. *Polymer* **2022**, *246*, 124674. <https://doi.org/10.1016/j.polymer.2022.124674>.
- (36) Biasutti, J. D.; Davis, T. P.; Lucien, F. P.; Heuts, J. P. A. Reversible Addition–Fragmentation Chain Transfer Polymerization of Methyl Methacrylate in Suspension. *Journal of Polymer Science Part A: Polymer Chemistry* **2005**, *43* (10), 2001–2012. <https://doi.org/10.1002/pola.20673>.
- (37) Moad, C. L.; Moad, G. Fundamentals of Reversible Addition–Fragmentation Chain Transfer (RAFT). *Chemistry Teacher International* **2021**, *3* (2), 3–17. <https://doi.org/10.1515/cti-2020-0026>.
- (38) Maksym, P.; Tarnacka, M.; Dzienia, A.; Erfurt, K.; Brzęczek-Szafran, A.; Chrobok, A.; Zięba, A.; Kaminski, K.; Paluch, M. High Pressure RAFT of Sterically Hindered Ionic Monomers. Studying Relationship between Rigidity of the Polymer Backbone and Conductivity. *Polymer* **2018**, *140*, 158–166. <https://doi.org/10.1016/j.polymer.2018.02.030>.
- (39) Wolpers, A.; Bergerbit, C.; Ebeling, B.; D’Agosto, F.; Monteil, V. Aromatic Xanthates and Dithiocarbamates for the Polymerization of Ethylene through Reversible Addition–Fragmentation Chain Transfer (RAFT). *Angewandte Chemie International Edition* **2019**, *58* (40), 14295–14302. <https://doi.org/10.1002/anie.201905629>.
- (40) Fortenberry, A. W.; Jankoski, P. E.; Stacy, E. K.; McCormick, C. L.; Smith, A. E.; Clemons, T. D. A Perspective on the History and Current Opportunities of Aqueous RAFT Polymerization. *Macromolecular Rapid Communications* **2022**, *43* (24), 2200414. <https://doi.org/10.1002/marc.202200414>.
- (41) Santha Kumar, A. R. S.; Singha, N. K. Reversible Addition-Fragmentation Chain Transfer (RAFT) Polymerization in Ionic Liquids: A Sustainable Process. In *Advances in Sustainable Polymers: Synthesis, Fabrication and Characterization*; Katiyar, V., Kumar, A., Mulchandani, N., Eds.; Materials Horizons: From Nature to Nanomaterials; Springer: Singapore, 2020; pp 183–193. https://doi.org/10.1007/978-981-15-1251-3_8.
- (42) Jennings, J.; Beija, M.; Kennon, J. T.; Willcock, H.; O’Reilly, R. K.; Rimmer, S.; Howdle, S. M. Advantages of Block Copolymer Synthesis by RAFT-Controlled Dispersion Polymerization in Supercritical Carbon Dioxide. *Macromolecules* **2013**, *46* (17), 6843–6851. <https://doi.org/10.1021/ma401051e>.
- (43) Allegrezza, M. L.; Konkolewicz, D. PET-RAFT Polymerization: Mechanistic Perspectives for Future Materials. *ACS Macro Lett.* **2021**, *10* (4), 433–446. <https://doi.org/10.1021/acsmacrolett.1c00046>.
- (44) Jiang, Y.; Fan, W.; Tosaka, M.; Cunningham, M. F.; Yamago, S. Fabrication of Structurally Controlled Poly(n-Butyl Acrylate) Particles by Ab Initio Emulsion Organotellurium-Mediated Radical Polymerization. Synthesis of High Molecular Weight Homo and Block Copolymers. *Macromolecules* **2021**. <https://doi.org/10.1021/acs.macromol.1c02037>.
- (45) Hartlieb, M. Photo-Iniferter RAFT Polymerization. *Macromolecular Rapid Communications* **2022**, *43* (1), 2100514. <https://doi.org/10.1002/marc.202100514>.
- (46) Moad, G.; Rizzardo, E.; Thang, S. H. Radical Addition–Fragmentation Chemistry and RAFT Polymerization. In *Reference Module in Materials Science and Materials Engineering*; Elsevier, 2016. <https://doi.org/10.1016/B978-0-12-803581-8.01349-7>.
- (47) Keddie, D. J.; Moad, G.; Rizzardo, E.; Thang, S. H. RAFT Agent Design and Synthesis. *Macromolecules* **2012**, *45* (13), 5321–5342. <https://doi.org/10.1021/ma300410v>.
- (48) Li, Z.; Sarkar, S.; Li, Y.; Tallon, M. A.; Musa, O. M. Synthesis of N-Vinyl Lactam Copolymers by Controlled Radical Polymerizations. In *Handbook of Pyrrolidone and Caprolactam Based Materials*; John Wiley & Sons, Ltd, 2021; pp 843–934. <https://doi.org/10.1002/9781119468769.hpcbm010>.
- (49) Segura, T.; Menes-Arzate, M.; León, F.; Ortega, A.; Burillo, G.; Peralta, R. D. Synthesis of Narrow Molecular Weight Distribution Polyvinyl Acetate by Gamma–Rays Initiated RAFT/MADIX Miniemulsion Polymerization. *Polymer* **2016**, *102*, 183–191. <https://doi.org/10.1016/j.polymer.2016.09.004>.

- (50) Padmakumar, A. K.; Singha, N. K.; Ashokkumar, M.; Leibfarth, F. A.; Qiao, G. G. Ultrasound-Assisted RAFT Polymerization in a Continuous Flow Method. *Macromolecules* **2023**, *56* (17), 6920–6927. <https://doi.org/10.1021/acs.macromol.3c00816>.
- (51) Goodrich, S. L.; Ross, M. E.; Young, J. B.; Sumerlin, B. S. Democratization of Sono-RAFT: Reversible-Deactivation Radical Polymerization with Low-Frequency Ultrasound. *Macromolecules* **2023**, *56* (23), 9350–9358. <https://doi.org/10.1021/acs.macromol.3c01953>.
- (52) Collins, J.; McKenzie, T. G.; Nothling, M. D.; Allison-Logan, S.; Ashokkumar, M.; Qiao, G. G. Sonochemically Initiated RAFT Polymerization in Organic Solvents. *Macromolecules* **2019**, *52* (1), 185–195. <https://doi.org/10.1021/acs.macromol.8b01845>.
- (53) Gu, Y.; Zhao, J.; Liu, Q.; Pan, X.; Zhang, W.; Zhang, Z.; Zhu, X. Zero Valent Metal/RAFT Agent Mediated CRP of Functional Monomers at Room Temperature: A Promising Catalyst System for CRP. *Polym. Chem.* **2014**, *6* (3), 359–363. <https://doi.org/10.1039/C4PY01248H>.
- (54) Gu, Y.; Zhao, J.; Liu, Q.; Zhou, N.; Zhang, Z.; Zhu, X. Zero-Valent Iron (Fe(0)) Mediated RAFT Miniemulsion Polymerization: A Facile Approach for the Fabrication of Fe(0)-Encapsulated Polymeric Nanoparticles. *Polym. Chem.* **2014**, *5* (14), 4215–4218. <https://doi.org/10.1039/C4PY00400K>.
- (55) Zhang, Q.; Zhang, Z.; Wang, W.; Zhu, J.; Cheng, Z.; Zhou, N.; Zhang, W.; Zhu, X. SET-RAFT of MMA Mediated by Ascorbic Acid-Activated Copper Oxide. *Journal of Polymer Science Part A: Polymer Chemistry* **2012**, *50* (7), 1424–1433. <https://doi.org/10.1002/pola.25910>.
- (56) Zhang, W.; Zhang, W.; Zhang, Z.; Zhu, J.; Zhu, X. SET-RAFT Polymerization of Progargyl Methacrylate and a One-Pot/One-Step Preparation of Side-Chain Functionalized Polymers via Combination of SET-RAFT and Click Chemistry. *Macromolecular Rapid Communications* **2010**, *31* (15), 1354–1358. <https://doi.org/10.1002/marc.201000008>.
- (57) Vandenberg, J.; Schweitzer-Chaput, B.; Klussmann, M.; Junkers, T. Acid-Induced Room Temperature RAFT Polymerization: Synthesis and Mechanistic Insights. *Macromolecules* **2016**, *49* (11), 4124–4135. <https://doi.org/10.1021/acs.macromol.6b00192>.
- (58) Aoshima, H.; Uchiyama, M.; Satoh, K.; Kamigaito, M. Inside Cover: Interconvertible Living Radical and Cationic Polymerization through Reversible Activation of Dormant Species with Dual Activity (Angew. Chem. Int. Ed. 41/2014). *Angewandte Chemie International Edition* **2014**, *53* (41), 10830–10830. <https://doi.org/10.1002/anie.201407932>.
- (59) Uchiyama, M.; Satoh, K.; Kamigaito, M. Cationic RAFT Polymerization Using Ppm Concentrations of Organic Acid. *Angewandte Chemie International Edition* **2015**, *54* (6), 1924–1928. <https://doi.org/10.1002/anie.201410858>.
- (60) Liu, Z.; Lv, Y.; An, Z. Enzymatic Cascade Catalysis for the Synthesis of Multiblock and Ultrahigh-Molecular-Weight Polymers with Oxygen Tolerance. *Angewandte Chemie International Edition* **2017**, *56* (44), 13852–13856. <https://doi.org/10.1002/anie.201707993>.
- (61) Shenoy, R.; Tibbitt, M. W.; Anseth, K. S.; Bowman, C. N. Formation of Core-Shell Particles by Interfacial Radical Polymerization Initiated by a Glucose Oxidase-Mediated Redox System. *Chem Mater* **2013**, *25* (5), 761–767. <https://doi.org/10.1021/cm303913f>.
- (62) Li, R.; Zhang, S.; Li, Q.; Qiao, G. G.; An, Z. An Atom-Economic Enzymatic Cascade Catalysis for High-Throughput RAFT Synthesis of Ultrahigh Molecular Weight Polymers. *Angewandte Chemie International Edition* **2022**, *61* (46), e202213396. <https://doi.org/10.1002/anie.202213396>.
- (63) Strover, L. T.; Cantalice, A.; Lam, J. Y. L.; Postma, A.; Hutt, O. E.; Horne, M. D.; Moad, G. Electrochemical Behavior of Thiocarbonylthio Chain Transfer Agents for RAFT Polymerization. *ACS Macro Lett.* **2019**, *8* (10), 1316–1322. <https://doi.org/10.1021/acsmacrolett.9b00598>.
- (64) Clothier, G. K. K.; Guimarães, T. R.; Strover, L. T.; Zetterlund, P. B.; Moad, G. Electrochemically-Initiated RAFT Synthesis of Low Dispersity Multiblock Copolymers by Seeded Emulsion Polymerization. *ACS Macro Lett.* **2023**, *12* (3), 331–337. <https://doi.org/10.1021/acsmacrolett.3c00021>.
- (65) Bray, C.; Li, G.; Postma, A.; Strover, L. T.; Wang, J.; Moad, G. Initiation of RAFT Polymerization: Electrochemically Initiated RAFT Polymerization in Emulsion (Emulsion

- eRAFT), and Direct PhotoRAFT Polymerization of Liquid Crystalline Monomers. *Aust. J. Chem.* **2021**, *74* (1), 56. <https://doi.org/10.1071/CH20260>.
- (66) Whitfield, R.; Parkatzidis, K.; Truong, N. P.; Junkers, T.; Anastasaki, A. Tailoring Polymer Dispersity by RAFT Polymerization: A Versatile Approach. *Chem* **2020**, *6* (6), 1340–1352. <https://doi.org/10.1016/j.chempr.2020.04.020>.
- (67) Destarac, M. On the Critical Role of RAFT Agent Design in Reversible Addition-Fragmentation Chain Transfer (RAFT) Polymerization. *Polymer Reviews* **2011**, *51* (2), 163–187. <https://doi.org/10.1080/15583724.2011.568130>.
- (68) Perrier, S.; Takolpuckdee, P. Macromolecular Design via Reversible Addition–Fragmentation Chain Transfer (RAFT)/Xanthates (MADIX) Polymerization. *Journal of Polymer Science Part A: Polymer Chemistry* **2005**, *43* (22), 5347–5393. <https://doi.org/10.1002/pola.20986>.
- (69) *Handbook of RAFT Polymerization*, 1st ed.; Barner-Kowollik, C., Ed.; Wiley, 2008. <https://doi.org/10.1002/9783527622757>.
- (70) Moad, G.; Rizzardo, E.; Thang, S. H. End-Functional Polymers, Thiocarbonylthio Group Removal/Transformation and Reversible Addition-Fragmentation-Chain Transfer (RAFT) Polymerization: Thiocarbonylthio Group Removal/Transformation. *Polym. Int.* **2011**, *60* (1), 9–25. <https://doi.org/10.1002/pi.2988>.
- (71) Glaria, A.; Beija, M.; Bordes, R.; Destarac, M.; Marty, J.-D. Understanding the Role of ω -End Groups and Molecular Weight in the Interaction of PNIPAM with Gold Surfaces. *Chem. Mater.* **2013**, *25* (9), 1868–1876. <https://doi.org/10.1021/cm400480p>.
- (72) Llauro, M.-F.; Loiseau, J.; Boisson, F.; Delolme, F.; Ladavière, C.; Claverie, J. Unexpected End-Groups of Poly(Acrylic Acid) Prepared by RAFT Polymerization. *Journal of Polymer Science Part A: Polymer Chemistry* **2004**, *42* (21), 5439–5462. <https://doi.org/10.1002/pola.20408>.
- (73) Destarac, M.; Kalai, C.; Wilczewska, A.; Petit, L.; Van Gramberen, E.; Zard, S. Z. Various Strategies for the Chemical Transformation of Xanthate-Functional Chain Termini in MADIX Copolymers. In *Controlled/Living Radical Polymerization*; Matyjaszewski, K., Ed.; ACS Symposium Series; American Chemical Society: Washington, D C, 2006; Vol. 944, pp 564–577. <https://doi.org/10.1021/bk-2006-0944.ch038>.
- (74) Kurowska, I.; Amouroux, B.; Langlais, M.; Coutelier, O.; Coudret, C.; Destarac, M.; Marty, J.-D. Versatile Thiolactone-Based Conjugation Strategies to Polymer Stabilizers for Multifunctional Upconverting Nanoparticles Aqueous Dispersions. *Nanoscale* **2022**, *14* (6), 2238–2247. <https://doi.org/10.1039/D1NR05548H>.
- (75) Willcock, H.; O'Reilly, R. K. End Group Removal and Modification of RAFT Polymers. *Polym. Chem.* **2010**, *1* (2), 149–157. <https://doi.org/10.1039/B9PY00340A>.
- (76) Bousquet, A.; Boyer, C.; Davis, T. P.; Stenzel, M. H. Electrostatic Assembly of Functional Polymer Combs onto Gold Nanoparticle Surfaces: Combining RAFT, Click and LbL to Generate New Hybrid Nanomaterials. *Polym. Chem.* **2010**, *1* (8), 1186–1195. <https://doi.org/10.1039/C0PY00075B>.
- (77) Sinnwell, S.; Inglis, A. J.; Stenzel, M. H.; Barner-Kowollik, C. Access to Three-Arm Star Block Copolymers by a Consecutive Combination of the Copper(I)-Catalyzed Azide–Alkyne Cycloaddition and the RAFT Hetero Diels–Alder Concept. *Macromolecular Rapid Communications* **2008**, *29* (12–13), 1090–1096. <https://doi.org/10.1002/marc.200800233>.
- (78) Yamashina, M.; Sei, Y.; Akita, M.; Yoshizawa, M. Safe Storage of Radical Initiators within a Polyaromatic Nanocapsule. *Nat Commun* **2014**, *5* (1), 4662. <https://doi.org/10.1038/ncomms5662>.
- (79) Otsu, T.; Yoshida, M. Role of Initiator-Transfer Agent-Terminator (Iniferter) in Radical Polymerizations: Polymer Design by Organic Disulfides as Iniferters. *Die Makromolekulare Chemie, Rapid Communications* **1982**, *3* (2), 127–132. <https://doi.org/10.1002/marc.1982.030030208>.
- (80) Xu, J.; Jung, K.; Atme, A.; Shanmugam, S.; Boyer, C. A Robust and Versatile Photoinduced Living Polymerization of Conjugated and Unconjugated Monomers and Its Oxygen Tolerance. *J. Am. Chem. Soc.* **2014**, *136* (14), 5508–5519. <https://doi.org/10.1021/ja501745g>.

- (81) Phommalsack-Lovan, J.; Chu, Y.; Boyer, C.; Xu, J. PET-RAFT Polymerisation: Towards Green and Precision Polymer Manufacturing. *Chem. Commun.* **2018**, *54* (50), 6591–6606. <https://doi.org/10.1039/C8CC02783H>.
- (82) Bellotti, V.; Simonutti, R. New Light in Polymer Science: Photoinduced Reversible Addition-Fragmentation Chain Transfer Polymerization (PET-RAFT) as Innovative Strategy for the Synthesis of Advanced Materials. *Polymers* **2021**, *13* (7), 1119. <https://doi.org/10.3390/polym13071119>.
- (83) Lee, Y.; Boyer, C.; Kwon, M. S. Photocontrolled RAFT Polymerization: Past, Present, and Future. *Chem. Soc. Rev.* **2023**, *52* (9), 3035–3097. <https://doi.org/10.1039/D1CS00069A>.
- (84) Otsu, T.; Yoshida, M.; Tazaki, T. A Model for Living Radical Polymerization. *Die Makromolekulare Chemie, Rapid Communications* **1982**, *3* (2), 133–140. <https://doi.org/10.1002/marc.1982.030030209>.
- (85) Corrigan, N.; Yeow, J.; Judzewitsch, P.; Xu, J.; Boyer, C. Seeing the Light: Advancing Materials Chemistry through Photopolymerization. *Angew Chem Int Ed Engl* **2019**, *58* (16), 5170–5189. <https://doi.org/10.1002/anie.201805473>.
- (86) Xu, J.; Shanmugam, S.; Corrigan, N. A.; Boyer, C. Catalyst-Free Visible Light-Induced RAFT Photopolymerization. In *Controlled Radical Polymerization: Mechanisms*; ACS Symposium Series; American Chemical Society, 2015; Vol. 1187, pp 247–267. <https://doi.org/10.1021/bk-2015-1187.ch013>.
- (87) McKenzie, T. G.; Fu, Q.; Wong, E. H. H.; Dunstan, D. E.; Qiao, G. G. Visible Light Mediated Controlled Radical Polymerization in the Absence of Exogenous Radical Sources or Catalysts. *Macromolecules* **2015**, *48* (12), 3864–3872. <https://doi.org/10.1021/acs.macromol.5b00965>.
- (88) Hart-Smith, G.; Lovestead, T. M.; Davis, T. P.; Stenzel, M. H.; Barner-Kowollik, C. Mapping Formation Pathways and End Group Patterns of Stimuli-Responsive Polymer Systems via High-Resolution Electrospray Ionization Mass Spectrometry. *Biomacromolecules* **2007**, *8* (8), 2404–2415. <https://doi.org/10.1021/bm700526j>.
- (89) McKenzie, T. G.; Fu, Q.; Uchiyama, M.; Satoh, K.; Xu, J.; Boyer, C.; Kamigaito, M.; Qiao, G. G. Beyond Traditional RAFT: Alternative Activation of Thiocarbonylthio Compounds for Controlled Polymerization. *Advanced Science* **2016**, *3* (9), 1500394. <https://doi.org/10.1002/advs.201500394>.
- (90) Hughes, R. W.; Lott, M. E.; Bowman, J. I.; Sumerlin, B. S. Excitation Dependence in Photoiniferter Polymerization. *ACS Macro Lett.* **2023**, *12* (1), 14–19. <https://doi.org/10.1021/acsmacrolett.2c00683>.
- (91) Easterling, C. P.; Xia, Y.; Zhao, J.; Fanucci, G. E.; Sumerlin, B. S. Block Copolymer Sequence Inversion through Photoiniferter Polymerization. *ACS Macro Lett.* **2019**, *8* (11), 1461–1466. <https://doi.org/10.1021/acsmacrolett.9b00716>.
- (92) Bagheri, A.; Engel, K. E.; Bainbridge, C. W. A.; Xu, J.; Boyer, C.; Jin, J. 3D Printing of Polymeric Materials Based on Photo-RAFT Polymerization. *Polym. Chem.* **2020**, *11* (3), 641–647. <https://doi.org/10.1039/C9PY01419E>.
- (93) Zhao, B.; Li, J.; Li, Z.; Lin, X.; Pan, X.; Zhang, Z.; Zhu, J. Photoinduced 3D Printing through a Combination of Cationic and Radical RAFT Polymerization. *Macromolecules* **2022**, *55* (16), 7181–7192. <https://doi.org/10.1021/acs.macromol.2c00841>.
- (94) Arrington, K. J.; Matson, J. B. Assembly of a Visible Light Photoreactor: An Inexpensive Tool for Bottlebrush Polymer Synthesis via Photoiniferter Polymerization. *Polym. Chem.* **2017**, *8* (48), 7452–7456. <https://doi.org/10.1039/C7PY01741C>.
- (95) Yeow, J.; Sugita, O. R.; Boyer, C. Visible Light-Mediated Polymerization-Induced Self-Assembly in the Absence of External Catalyst or Initiator. *ACS Macro Lett.* **2016**, *5* (5), 558–564. <https://doi.org/10.1021/acsmacrolett.6b00235>.
- (96) Ramakers, G.; Rubens, M.; Krivcov, A.; Möbius, H.; Trouillet, V.; Welle, A.; Junkers, T. Photoiniferter Surface Grafting of Poly(Methyl Acrylate) Using Xanthates. *Journal of Polymer Science Part A: Polymer Chemistry* **2019**, *57* (18), 2002–2007. <https://doi.org/10.1002/pola.29405>.
- (97) Bagheri, A.; Sadrearhami, Z.; Adnan, N. N. M.; Boyer, C.; Lim, M. Surface Functionalization of Upconversion Nanoparticles Using Visible Light-Mediated Polymerization. *Polymer* **2018**, *151*, 6–14. <https://doi.org/10.1016/j.polymer.2018.07.054>.

- (98) Carmean, R. N.; Sims, M. B.; Figg, C. A.; Hurst, P. J.; Patterson, J. P.; Sumerlin, B. S. Ultrahigh Molecular Weight Hydrophobic Acrylic and Styrenic Polymers through Organic-Phase Photoiniferter-Mediated Polymerization. *ACS Macro Lett.* **2020**, *9* (4), 613–618. <https://doi.org/10.1021/acsmacrolett.0c00203>.
- (99) Carmean, R. N.; Becker, T. E.; Sims, M. B.; Sumerlin, B. S. Ultra-High Molecular Weights via Aqueous Reversible-Deactivation Radical Polymerization. *Chem* **2017**, *2* (1), 93–101. <https://doi.org/10.1016/j.chempr.2016.12.007>.
- (100) Lehnen, A.-C.; Kurki, J. A. M.; Hartlieb, M. The Difference between Photo-Iniferter and Conventional RAFT Polymerization: High Livingness Enables the Straightforward Synthesis of Multiblock Copolymers. *Polym. Chem.* **2022**, *13* (11), 1537–1546. <https://doi.org/10.1039/D1PY01530C>.
- (101) Ding, C.; Fan, C.; Jiang, G.; Pan, X.; Zhang, Z.; Zhu, J.; Zhu, X. Photocatalyst-Free and Blue Light-Induced RAFT Polymerization of Vinyl Acetate at Ambient Temperature. *Macromolecular Rapid Communications* **2015**, *36* (24), 2181–2185. <https://doi.org/10.1002/marc.201500427>.
- (102) Li, J.; Ding, C.; Zhang, Z.; Pan, X.; Li, N.; Zhu, J.; Zhu, X. Visible Light-Induced Living Radical Polymerization of Butyl Acrylate: Photocatalyst-Free, Ultrafast, and Oxygen Tolerance. *Macromolecular Rapid Communications* **2017**, *38* (13), 1600482. <https://doi.org/10.1002/marc.201600482>.
- (103) Li, J.; Pan, X.; Li, N.; Zhu, J.; Zhu, X. Photoinduced Controlled Radical Polymerization of Methyl Acrylate and Vinyl Acetate by Xanthate. *Polym. Chem.* **2018**, *9* (21), 2897–2904. <https://doi.org/10.1039/C8PY00050F>.
- (104) Wang, Y.; Wang, M.; Bai, L.; Zhang, L.; Cheng, Z.; Zhu, X. Facile Synthesis of Poly(N-Vinyl Pyrrolidone) Block Copolymers with “More-Activated” Monomers by Using Photoinduced Successive RAFT Polymerization. *Polym. Chem.* **2020**, *11* (12), 2080–2088. <https://doi.org/10.1039/C9PY01763A>.
- (105) Bagheri, A.; Bainbridge, C.; Jin, J. Visible Light-Induced Transformation of Polymer Networks. *ACS Appl. Polym. Mater.* **2019**, *1* (7), 1896–1904. <https://doi.org/10.1021/acsapm.9b00458>.
- (106) Li, J.; Ding, C.; Zhang, Z.; Zhu, J.; Zhu, X. Photo-Induced Reversible Addition-Fragmentation Chain Transfer (RAFT) Polymerization of Acrylonitrile at Ambient Temperature: A Simple System to Obtain High-Molecular-Weight Polyacrylonitrile. *Reactive and Functional Polymers* **2017**, *113*, 1–5. <https://doi.org/10.1016/j.reactfunctpolym.2017.02.003>.
- (107) Mazo, A. R.; Tran, T. N.; Zhang, W.; Meng, Y.; Reyhani, A.; Pascual, S.; Fontaine, L.; Qiao, G. G.; Piogé, S. Blue LED Light-Activated RAFT Polymerization of PEG Acrylate with High Chain-End Fidelity for Efficient PEGylation. *Polym. Chem.* **2020**, *11* (32), 5238–5248. <https://doi.org/10.1039/D0PY00838A>.
- (108) Wilczewska, A. Z.; Niemirowicz, K.; Markiewicz, K. H.; Car, H. Nanoparticles as Drug Delivery Systems. *Pharmacological Reports* **2012**, *64* (5), 1020–1037. [https://doi.org/10.1016/S1734-1140\(12\)70901-5](https://doi.org/10.1016/S1734-1140(12)70901-5).
- (109) Alsehli, M. Polymeric Nanocarriers as Stimuli-Responsive Systems for Targeted Tumor (Cancer) Therapy: Recent Advances in Drug Delivery. *Saudi Pharmaceutical Journal* **2020**, *28* (3), 255–265. <https://doi.org/10.1016/j.jsps.2020.01.004>.
- (110) Vasile, C. Polymeric Nanomaterials: Recent Developments, Properties and Medical Applications. In *Polymeric Nanomaterials in Nanotherapeutics*; Vasile, C., Ed.; Micro and Nano Technologies; Elsevier, 2019; pp 1–66. <https://doi.org/10.1016/B978-0-12-813932-5.00001-7>.
- (111) Milewska, S.; Niemirowicz-Laskowska, K.; Siemiaszko, G.; Nowicki, P.; Wilczewska, A. Z.; Car, H. Current Trends and Challenges in Pharmacoeconomic Aspects of Nanocarriers as Drug Delivery Systems for Cancer Treatment. *Int J Nanomedicine* **2021**, *16*, 6593–6644. <https://doi.org/10.2147/IJN.S323831>.
- (112) Guimarães, D.; Cavaco-Paulo, A.; Nogueira, E. Design of Liposomes as Drug Delivery System for Therapeutic Applications. *International Journal of Pharmaceutics* **2021**, *601*, 120571. <https://doi.org/10.1016/j.ijpharm.2021.120571>.

- (113) Liu, P.; Chen, G.; Zhang, J. A Review of Liposomes as a Drug Delivery System: Current Status of Approved Products, Regulatory Environments, and Future Perspectives. *Molecules* **2022**, *27* (4), 1372. <https://doi.org/10.3390/molecules27041372>.
- (114) Zafar, S.; Jain, D.; Ahmad, F. J. Metallic Nanoparticles in Drug Delivery: Concepts, Challenges, and Current Advancement. In *Multifunctional Nanocarriers*; Mehra, N. K., Srivastava, S., Madan, J., Singh, P. kumar, Eds.; Micro and Nano Technologies; Elsevier, 2022; pp 121–148. <https://doi.org/10.1016/B978-0-323-85041-4.00007-X>.
- (115) Chandrakala, V.; Aruna, V.; Angajala, G. Review on Metal Nanoparticles as Nanocarriers: Current Challenges and Perspectives in Drug Delivery Systems. *emergent mater.* **2022**, *5* (6), 1593–1615. <https://doi.org/10.1007/s42247-021-00335-x>.
- (116) Simovic, S.; Ghouchi-Eskandar, N.; Sinn, A. M.; Losic, D.; Prestidge, C. A. Silica Materials in Drug Delivery Applications. *Curr Drug Discov Technol* **2011**, *8* (3), 269–276. <https://doi.org/10.2174/157016311796799026>.
- (117) Şen Karaman, D.; Kettiger, H. Silica-Based Nanoparticles as Drug Delivery Systems: Chances and Challenges. In *Inorganic Frameworks as Smart Nanomedicines*; Grumezescu, A. M., Ed.; William Andrew Publishing, 2018; pp 1–40. <https://doi.org/10.1016/B978-0-12-813661-4.00001-8>.
- (118) Dogra, P.; Adolphi, N. L.; Wang, Z.; Lin, Y.-S.; Butler, K. S.; Durfee, P. N.; Croissant, J. G.; Noureddine, A.; Coker, E. N.; Bearer, E. L.; Cristini, V.; Brinker, C. J. Establishing the Effects of Mesoporous Silica Nanoparticle Properties on in Vivo Disposition Using Imaging-Based Pharmacokinetics. *Nat Commun* **2018**, *9* (1), 4551. <https://doi.org/10.1038/s41467-018-06730-z>.
- (119) Wong, B. S.; Yoong, S. L.; Jagusiak, A.; Panczyk, T.; Ho, H. K.; Ang, W. H.; Pastorin, G. Carbon Nanotubes for Delivery of Small Molecule Drugs. *Adv Drug Deliv Rev* **2013**, *65* (15), 1964–2015. <https://doi.org/10.1016/j.addr.2013.08.005>.
- (120) Bagheri, B.; Surwase, S. S.; Lee, S. S.; Park, H.; Rad, Z. F.; Trevaskis, N. L.; Kim, Y.-C. Carbon-Based Nanostructures for Cancer Therapy and Drug Delivery Applications. *J. Mater. Chem. B* **2022**, *10* (48), 9944–9967. <https://doi.org/10.1039/D2TB01741E>.
- (121) Elmowafy, M.; Shalaby, K.; Elkomy, M. H.; Alsaidan, O. A.; Gomaa, H. A. M.; Abdelgawad, M. A.; Mostafa, E. M. Polymeric Nanoparticles for Delivery of Natural Bioactive Agents: Recent Advances and Challenges. *Polymers* **2023**, *15* (5), 1123. <https://doi.org/10.3390/polym15051123>.
- (122) Prabhu, R. H.; Patravale, V. B.; Joshi, M. D. Polymeric Nanoparticles for Targeted Treatment in Oncology: Current Insights. *Int J Nanomedicine* **2015**, *10*, 1001–1018. <https://doi.org/10.2147/IJN.S56932>.
- (123) Kalhapure, R. S.; Renukuntla, J. Thermo- and pH Dual Responsive Polymeric Micelles and Nanoparticles. *Chemico-Biological Interactions* **2018**, *295*, 20–37. <https://doi.org/10.1016/j.cbi.2018.07.016>.
- (124) Hoshyar, N.; Gray, S.; Han, H.; Bao, G. The Effect of Nanoparticle Size on in Vivo Pharmacokinetics and Cellular Interaction. *Nanomedicine (Lond)* **2016**, *11* (6), 673–692. <https://doi.org/10.2217/nmm.16.5>.
- (125) Liu, Y.; Tan, J.; Thomas, A.; Ou-Yang, D.; Muzykantov, V. R. The Shape of Things to Come: Importance of Design in Nanotechnology for Drug Delivery. *Ther Deliv* **2012**, *3* (2), 181–194.
- (126) He, Y.; Zhang, W.; Xiao, Q.; Fan, L.; Huang, D.; Chen, W.; He, W. Liposomes and Liposome-like Nanoparticles: From Anti-Fungal Infection to the COVID-19 Pandemic Treatment. *Asian Journal of Pharmaceutical Sciences* **2022**, *17* (6), 817–837. <https://doi.org/10.1016/j.ajps.2022.11.002>.
- (127) Mitchell, M. J.; Billingsley, M. M.; Haley, R. M.; Wechsler, M. E.; Peppas, N. A.; Langer, R. Engineering Precision Nanoparticles for Drug Delivery. *Nat Rev Drug Discov* **2021**, *20* (2), 101–124. <https://doi.org/10.1038/s41573-020-0090-8>.
- (128) Ikeda-Imafuku, M.; Wang, L. L.-W.; Rodrigues, D.; Shaha, S.; Zhao, Z.; Mitragotri, S. Strategies to Improve the EPR Effect: A Mechanistic Perspective and Clinical Translation. *Journal of Controlled Release* **2022**, *345*, 512–536. <https://doi.org/10.1016/j.jconrel.2022.03.043>.

- (129) Blanco, E.; Shen, H.; Ferrari, M. Principles of Nanoparticle Design for Overcoming Biological Barriers to Drug Delivery. *Nat Biotechnol* **2015**, *33* (9), 941–951. <https://doi.org/10.1038/nbt.3330>.
- (130) Gagliardi, A.; Giuliano, E.; Venkateswararao, E.; Fresta, M.; Bulotta, S.; Awasthi, V.; Cosco, D. Biodegradable Polymeric Nanoparticles for Drug Delivery to Solid Tumors. *Frontiers in Pharmacology* **2021**, *12*.
- (131) Nguyen, T.-K.; Selvanayagam, R.; K. Ho, K. K.; Chen, R.; K. Kutty, S.; A. Rice, S.; Kumar, N.; Barraud, N.; T. Duong, H. T.; Boyer, C. Co-Delivery of Nitric Oxide and Antibiotic Using Polymeric Nanoparticles. *Chemical Science* **2016**, *7* (2), 1016–1027. <https://doi.org/10.1039/C5SC02769A>.
- (132) Guo, Q.; Guo, H.; Lan, T.; Chen, Y.; Chen, X.; Feng, Y.; Luo, Y.; Yao, Y.; Li, Y.; Pan, X.; Xu, Y.; Tao, L.; Liu, Y.; Shen, X. Co-Delivery of Antibiotic and Baicalein by Using Different Polymeric Nanoparticle Cargos with Enhanced Synergistic Antibacterial Activity. *International Journal of Pharmaceutics* **2021**, *599*, 120419. <https://doi.org/10.1016/j.ijpharm.2021.120419>.
- (133) Asem, H.; Zheng, W.; Nilsson, F.; Zhang, Y.; Hedenqvist, M. S.; Hassan, M.; Malmström, E. Functional Nanocarriers for Drug Delivery by Surface Engineering of Polymeric Nanoparticle Post-Polymerization-Induced Self-Assembly. *ACS Appl. Bio Mater.* **2021**, *4* (1), 1045–1056. <https://doi.org/10.1021/acsabm.0c01552>.
- (134) Misiak, P.; Niemirowicz-Laskowska, K.; Markiewicz, K. H.; Wielgat, P.; Kurowska, I.; Czarnomysy, R.; Misztalewska-Turkowicz, I.; Car, H.; Bielawski, K.; Wilczewska, A. Z. Doxorubicin-Loaded Polymeric Nanoparticles Containing Ketoester-Based Block and Cholesterol Moiety as Specific Vehicles to Fight Estrogen-Dependent Breast Cancer. *Cancer Nanotechnology* **2023**, *14* (1), 23. <https://doi.org/10.1186/s12645-023-00176-9>.
- (135) Wang, H.; Ullah, A. Synthesis and Evaluation of Thermoresponsive Renewable Lipid-Based Block Copolymers for Drug Delivery. *Polymers (Basel)* **2022**, *14* (17), 3436. <https://doi.org/10.3390/polym14173436>.
- (136) Siboro, S. A. P.; Anugrah, D. S. B.; Jeong, Y. T.; Yoo, S. I.; Lim, K. T. Systematic Investigation to the Effects of Near-Infrared Light Exposure on Polymeric Micelles of Poly(Ethylene Glycol)-Block-Poly(Styrene-Alt-Maleic Anhydride) Loaded with Indocyanine Green. *Polymer Degradation and Stability* **2019**, *167*, 241–249. <https://doi.org/10.1016/j.polymdegradstab.2019.07.009>.
- (137) Yu, T.; Zhuang, W.; Su, X.; Ma, B.; Hu, J.; He, H.; Li, G.; Wang, Y. Dual-Responsive Micelles with Aggregation-Induced Emission Feature and Two-Photon Absorption for Accurate Drug Delivery and Bioimaging. *Bioconjugate Chem.* **2019**, *30* (7), 2075–2087. <https://doi.org/10.1021/acs.bioconjchem.9b00364>.
- (138) Wang, X.; Wu, Y.; Shang, H.; Sun, X.; An, K.; Zhang, Q.; Qiao, N. Preparation of pH/Light Dual-Responsive Biocompatible Polymer Micelles: Application to Curcumin Delivery. *Journal of Drug Delivery Science and Technology* **2023**, *86*, 104652. <https://doi.org/10.1016/j.jddst.2023.104652>.
- (139) Hiruta, Y.; Kanda, Y.; Katsuyama, N.; Kanazawa, H. Dual Temperature- and pH-Responsive Polymeric Micelle for Selective and Efficient Two-Step Doxorubicin Delivery. *RSC Advances* **2017**, *7* (47), 29540–29549. <https://doi.org/10.1039/C7RA03579A>.
- (140) Hou, W.; Liu, R.; Bi, S.; He, Q.; Wang, H.; Gu, J. Photo-Responsive Polymersomes as Drug Delivery System for Potential Medical Applications. *Molecules* **2020**, *25* (21), 5147. <https://doi.org/10.3390/molecules25215147>.
- (141) Kozlovskaya, V.; Liu, F.; Yang, Y.; Ingle, K.; Qian, S.; Halade, G. V.; Urban, V. S.; Kharlampieva, E. Temperature-Responsive Polymersomes of Poly(3-Methyl-N-Vinylcaprolactam)-Block-Poly(N-Vinylpyrrolidone) To Decrease Doxorubicin-Induced Cardiotoxicity. *Biomacromolecules* **2019**, *20* (10), 3989–4000. <https://doi.org/10.1021/acs.biomac.9b01026>.
- (142) DiazDuarte-Rodriguez, M.; Cortez-Lemus, N. A.; Licea-Claverie, A.; Licea-Rodriguez, J.; Méndez, E. R. Dual Responsive Polymersomes for Gold Nanorod and Doxorubicin Encapsulation: Nanomaterials with Potential Use as Smart Drug Delivery Systems. *Polymers* **2019**, *11* (6), 939. <https://doi.org/10.3390/polym11060939>.

- (143) Sun, Z.; Liu, G.; Hu, J.; Liu, S. Photo- and Reduction-Responsive Polymersomes for Programmed Release of Small and Macromolecular Payloads. *Biomacromolecules* **2018**, *19* (6), 2071–2081. <https://doi.org/10.1021/acs.biomac.8b00253>.
- (144) Lei, J.; Song, Y.; Li, D.; Lei, M.; Tan, R.; Liu, Y.; Zheng, H. pH-Sensitive and Charge-Reversal Daunorubicin-Conjugated Polymeric Micelles for Enhanced Cancer Therapy. *Journal of Applied Polymer Science* **2022**, *139* (4), 51535. <https://doi.org/10.1002/app.51535>.
- (145) Deng, J.; Liu, S.; Li, G.; Zheng, Y.; Zhang, W.; Lin, J.; Yu, F.; Weng, J.; Liu, P.; Zeng, H. pH-Sensitive Charge-Conversion Cinnamaldehyde Polymeric Prodrug Micelles for Effective Targeted Chemotherapy of Osteosarcoma in Vitro. *Frontiers in Chemistry* **2023**, *11*.
- (146) Chen, K.; Cai, H.; Zhang, H.; Zhu, H.; Gu, Z.; Gong, Q.; Luo, K. Stimuli-Responsive Polymer-Doxorubicin Conjugate: Antitumor Mechanism and Potential as Nano-Prodrug. *Acta Biomaterialia* **2019**, *84*, 339–355. <https://doi.org/10.1016/j.actbio.2018.11.050>.
- (147) Dai, Y.; Ma, X.; Zhang, Y.; Chen, K.; Tang, J. Z.; Gong, Q.; Luo, K. A Biocompatible and Cathepsin B Sensitive Nanoscale System of Dendritic polyHPMA-Gemcitabine Prodrug Enhances Antitumor Activity Markedly. *Biomater. Sci.* **2018**, *6* (11), 2976–2986. <https://doi.org/10.1039/C8BM00946E>.
- (148) Kostka, L.; Kotrchová, L.; Šubr, V.; Libánská, A.; Ferreira, C. A.; Malátová, I.; Lee, H. J.; Barnhart, T. E.; Engle, J. W.; Cai, W.; Šírová, M.; Etrych, T. HPMA-Based Star Polymer Biomaterials with Tuneable Structure and Biodegradability Tailored for Advanced Drug Delivery to Solid Tumours. *Biomaterials* **2020**, *235*, 119728. <https://doi.org/10.1016/j.biomaterials.2019.119728>.
- (149) Selianitis, D.; Katifelis, H.; Gazouli, M.; Pispas, S. Novel Multi-Responsive Hyperbranched Polyelectrolyte Polyplexes as Potential Gene Delivery Vectors. *Pharmaceutics* **2023**, *15* (6), 1627. <https://doi.org/10.3390/pharmaceutics15061627>.
- (150) Fliervoet, L. A. L.; Lisitsyna, E. S.; Durandin, N. A.; Kotsis, I.; Maas-Bakker, R. F. M.; Yliperttula, M.; Hennink, W. E.; Vuorimaa-Laukkanen, E.; Vermonden, T. Structure and Dynamics of Thermosensitive pDNA Polyplexes Studied by Time-Resolved Fluorescence Spectroscopy. *Biomacromolecules* **2020**, *21* (1), 73–88. <https://doi.org/10.1021/acs.biomac.9b00896>.
- (151) Kanto, R.; Yonenuma, R.; Yamamoto, M.; Furusawa, H.; Yano, S.; Haruki, M.; Mori, H. Mixed Polyplex Micelles with Thermoresponsive and Lysine-Based Zwitterionic Shells Derived from Two Poly(Vinyl Amine)-Based Block Copolymers. *Langmuir* **2021**, *37* (10), 3001–3014. <https://doi.org/10.1021/acs.langmuir.0c02197>.
- (152) Zhou, G.; Xu, Y.; Chen, M.; Cheng, D.; Shuai, X. Tumor-Penetrating Peptide Modified and pH-Sensitive Polyplexes for Tumor Targeted siRNA Delivery. *Polym. Chem.* **2016**, *7* (23), 3857–3863. <https://doi.org/10.1039/C6PY00427J>.
- (153) Cao, X.; Wang, C.; Deng, Z.; Zhong, Y.; Chen, H. Efficient Ocular Delivery of siRNA via pH-Sensitive Vehicles for Corneal Neovascularization Inhibition. *International Journal of Pharmaceutics: X* **2023**, *5*, 100183. <https://doi.org/10.1016/j.ijpx.2023.100183>.
- (154) Zhang, Y.; Zhang, D.; Wang, J.-T.; Zhang, X.; Yang, Y. Fabrication of Stimuli-Responsive Nanogels for Protein Encapsulation and Traceless Release without Introducing Organic Solvents, Surfactants, or Small-Molecule Cross-Linkers. *Polym. Chem.* **2021**, *12* (4), 554–563. <https://doi.org/10.1039/D0PY01600D>.
- (155) Stickdorn, J.; Stein, L.; Arnold-Schild, D.; Hahlbrock, J.; Medina-Montano, C.; Bartneck, J.; Ziß, T.; Montermann, E.; Kappel, C.; Hobernik, D.; Haist, M.; Yurugi, H.; Raabe, M.; Best, A.; Rajalingam, K.; Radsak, M. P.; David, S. A.; Koynov, K.; Bros, M.; Grabbe, S.; Schild, H.; Nuhn, L. Systemically Administered TLR7/8 Agonist and Antigen-Conjugated Nanogels Govern Immune Responses against Tumors. *ACS Nano* **2022**, *16* (3), 4426–4443. <https://doi.org/10.1021/acsnano.1c10709>.
- (156) Liu, J.; Debuigne, A.; Detrembleur, C.; Jérôme, C. Poly(N-Vinylcaprolactam): A Thermoresponsive Macromolecule with Promising Future in Biomedical Field. *Adv Healthc Mater* **2014**, *3* (12), 1941–1968. <https://doi.org/10.1002/adhm.201400371>.
- (157) Abulateefeh, S. R.; Spain, S. G.; Aylott, J. W.; Chan, W. C.; Garnett, M. C.; Alexander, C. Thermoresponsive Polymer Colloids for Drug Delivery and Cancer Therapy. *Macromolecular Bioscience* **2011**, *11* (12), 1722–1734. <https://doi.org/10.1002/mabi.201100252>.

- (158) Van Gheluwe, L.; Chourpa, I.; Gaigne, C.; Munnier, E. Polymer-Based Smart Drug Delivery Systems for Skin Application and Demonstration of Stimuli-Responsiveness. *Polymers (Basel)* **2021**, *13* (8), 1285. <https://doi.org/10.3390/polym13081285>.
- (159) Zhang, Q.; Weber, C.; Schubert, U. S.; Hoogenboom, R. Thermoresponsive Polymers with Lower Critical Solution Temperature: From Fundamental Aspects and Measuring Techniques to Recommended Turbidimetry Conditions. *Mater. Horiz.* **2017**, *4* (2), 109–116. <https://doi.org/10.1039/C7MH00016B>.
- (160) Bordat, A.; Boissenot, T.; Nicolas, J.; Tsapis, N. Thermoresponsive Polymer Nanocarriers for Biomedical Applications. *Advanced Drug Delivery Reviews* **2019**, *138*, 167–192. <https://doi.org/10.1016/j.addr.2018.10.005>.
- (161) Doberenz, F.; Zeng, K.; Willems, C.; Zhang, K.; Groth, T. Thermoresponsive Polymers and Their Biomedical Application in Tissue Engineering – a Review. *Journal of Materials Chemistry B* **2020**, *8* (4), 607–628. <https://doi.org/10.1039/C9TB02052G>.
- (162) Peralta, M. E.; Jadhav, S. A.; Magnacca, G.; Scalarone, D.; Mártire, D. O.; Parolo, M. E.; Carlos, L. Synthesis and in Vitro Testing of Thermoresponsive Polymer-Grafted Core-Shell Magnetic Mesoporous Silica Nanoparticles for Efficient Controlled and Targeted Drug Delivery. *Journal of Colloid and Interface Science* **2019**, *544*, 198–205. <https://doi.org/10.1016/j.jcis.2019.02.086>.
- (163) Cortez-Lemus, N. A.; Licea-Claverie, A. Poly(N -Vinylcaprolactam), a Comprehensive Review on a Thermoresponsive Polymer Becoming Popular. *Progress in Polymer Science* **2016**, *53*, 1–51. <https://doi.org/10.1016/j.progpolymsci.2015.08.001>.
- (164) Ghamkhari, A.; Abbasi, F.; Abbasi, E.; Ghorbani, M. A Novel Thermo-Responsive System Based on β -Cyclodextrin-Nanocomposite for Improving the Docetaxel Activity. *International Journal of Polymeric Materials and Polymeric Biomaterials* **2021**, *70* (12), 830–840. <https://doi.org/10.1080/00914037.2020.1765357>.
- (165) Zhou, D.; Fei, Z.; Jin, L.; Zhou, P.; Li, C.; Liu, X.; Zhao, C. Dual-Responsive Polymersomes as Anticancer Drug Carriers for the Co-Delivery of Doxorubicin and Paclitaxel. *J. Mater. Chem. B* **2021**, *9* (3), 801–808. <https://doi.org/10.1039/D0TB02462G>.
- (166) Rabiee, N.; Bagherzadeh, M.; Heidarian Haris, M.; Ghadiri, A. M.; Matloubi Moghaddam, F.; Fatahi, Y.; Dinarvand, R.; Jarahiyan, A.; Ahmadi, S.; Shokouhimehr, M. Polymer-Coated NH₂-UiO-66 for the Codelivery of DOX/pCRISPR. *ACS Appl. Mater. Interfaces* **2021**, *13* (9), 10796–10811. <https://doi.org/10.1021/acsami.1c01460>.
- (167) Farjadian, F.; Ghasemi, S.; Andami, Z.; Tamami, B. Thermo-Responsive Nanocarrier Based on Poly(N-Isopropylacrylamide) Serving as a Smart Doxorubicin Delivery System. *Iran Polym J* **2020**, *29* (3), 197–207. <https://doi.org/10.1007/s13726-020-00785-w>.
- (168) Milewska, S.; Siemiaszko, G.; Wilczewska, A. Z.; Misztalewska-Turkowicz, I.; Markiewicz, K. H.; Szymczuk, D.; Sawicka, D.; Car, H.; Lazny, R.; Niemirowicz-Laskowska, K. Folic-Acid-Conjugated Thermoresponsive Polymeric Particles for Targeted Delivery of 5-Fluorouracil to CRC Cells. *Int J Mol Sci* **2023**, *24* (2), 1364. <https://doi.org/10.3390/ijms24021364>.
- (169) Augustine, R.; Uthaman, S.; Kalva, N.; Eom, K. H.; Huh, K. M.; Pillarisetti, S.; Park, I.-K.; Kim, I. Two-Tailed Tadpole-Shaped Synthetic Polymer Polypeptide Bioconjugate Nanomicelles for Enhanced Chemo-Photothermal Therapy. *Polymer* **2021**, *230*, 124061. <https://doi.org/10.1016/j.polymer.2021.124061>.
- (170) Ghasemi, S.; Ahmadi, L.; Farjadian, F. Thermo-Responsive PNIPAAm-b-PLA Amphiphilic Block Copolymer Micelle as Nanoplatform for Docetaxel Drug Release. *J Mater Sci* **2022**, *57* (36), 17433–17447. <https://doi.org/10.1007/s10853-022-07711-w>.
- (171) Biswas, C. S.; Biswas, A.; Galluzzi, M.; Shekh, M. I.; Wang, Q.; Ray, B.; Maiti, P.; Stadler, F. J. Synthesis and Characterization of Novel Amphiphilic Biocompatible Block-Copolymers of Poly(N-Isopropylacrylamide)-b-Poly(l-Phenylalanine Methyl Ester) by RAFT Polymerization. *Polymer* **2020**, *203*, 122760. <https://doi.org/10.1016/j.polymer.2020.122760>.
- (172) An, H.; Yang, Y.; Zhou, Z.; Bo, Y.; Wang, Y.; He, Y.; Wang, D.; Qin, J. Pectin-Based Injectable and Biodegradable Self-Healing Hydrogels for Enhanced Synergistic Anticancer Therapy. *Acta Biomaterialia* **2021**, *131*, 149–161. <https://doi.org/10.1016/j.actbio.2021.06.029>.
- (173) Zhou, J.; Sun, Y.; Huang, Z.; Luo, Z.; Hu, H. Improved Antifouling and Drug Delivery Properties of Polyvinyl Alcohol Hydrogel by Grafting with N-Isopropylacrylamide via

- Organic Dye Photocatalyzed PET-RAFT Polymerization. *Journal of Applied Polymer Science* **2021**, *138* (47), 51395. <https://doi.org/10.1002/app.51395>.
- (174) Liu, J.; Detrembleur, C.; Pauw-Gillet, M.-C. D.; Mornet, S.; Duguet, E.; Jérôme, C. Gold Nanorods Coated with a Thermo-Responsive Poly(Ethylene Glycol)-b-Poly(N-Vinylcaprolactam) Corona as Drug Delivery Systems for Remotely near Infrared-Triggered Release. *Polym. Chem.* **2013**, *5* (3), 799–813. <https://doi.org/10.1039/C3PY01057K>.
- (175) Niu, S.; Williams, G. R.; Wu, J.; Wu, J.; Zhang, X.; Chen, X.; Li, S.; Jiao, J.; Zhu, L.-M. A Chitosan-Based Cascade-Responsive Drug Delivery System for Triple-Negative Breast Cancer Therapy. *J Nanobiotechnology* **2019**, *17* (1), 95. <https://doi.org/10.1186/s12951-019-0529-4>.
- (176) Siemiaszko, G.; Niemirowicz-Laskowska, K.; Markiewicz, K. H.; Misztalewska-Turkowicz, I.; Dudź, E.; Milewska, S.; Misiak, P.; Kurowska, I.; Sadowska, A.; Car, H.; Wilczewska, A. Z. Synergistic Effect of Folate-Conjugated Polymers and 5-Fluorouracil in the Treatment of Colon Cancer. *Cancer Nanotechnology* **2021**, *12* (1), 31. <https://doi.org/10.1186/s12645-021-00104-9>.
- (177) Cortez-Lemus, N. A.; Licea-Claverie, A. Preparation of a Mini-Library of Thermo-Responsive Star (NVCL/NVP-VAc) Polymers with Tailored Properties Using a Hexafunctional Xanthate RAFT Agent. *Polymers* **2018**, *10* (1), 20. <https://doi.org/10.3390/polym10010020>.
- (178) Liang, X.; Liu, F.; Kozlovskaya, V.; Palchak, Z.; Kharlampieva, E. Thermoresponsive Micelles from Double LCST-Poly(3-Methyl-N-Vinylcaprolactam) Block Copolymers for Cancer Therapy. *ACS Macro Lett.* **2015**, *4* (3), 308–311. <https://doi.org/10.1021/mz500832a>.
- (179) Góis, J. R.; Serra, A. C.; Coelho, J. F. J. Synthesis and Characterization of New Temperature-Responsive Nanocarriers Based on POEOMA-b-PNVCL Prepared Using a Combination of ATRP, RAFT and CuAAC. *European Polymer Journal* **2016**, *81*, 224–238. <https://doi.org/10.1016/j.eurpolymj.2016.06.011>.
- (180) Qian, W.; Xu, P.; Lu, G.; Huang, X. Synthesis of PAA-g-PNVCL Graft Copolymer and Studies on Its Loading of Ornidazole. *Chinese Journal of Chemistry* **2014**, *32* (10), 1049–1056. <https://doi.org/10.1002/cjoc.201400472>.
- (181) Qian, Y.; Wei, J.; Wang, Y.; You, D.; Lin, F.; Yue, W.; Bi, Y. Thermal and Enzymatic Dual-Stimuli Responsive Linear-Dendritic Block Copolymers Based on Poly(N-Vinylcaprolactam). *Polymers for Advanced Technologies* **2020**, *31* (11), 2797–2805. <https://doi.org/10.1002/pat.5006>.
- (182) Song, W.; Wei, J.; Li, L.; Qian, Y.; Wang, Y.; Bi, Y. Cathepsin B and Thermal Dual-Stimuli Responsive Linear-Dendritic Block Copolymer Micelles for Anticancer Drug Delivery. *Polymer International* **2022**, *71* (3), 317–327. <https://doi.org/10.1002/pi.6332>.
- (183) Yang, Y.; Alford, A.; Kozlovskaya, V.; Zhao, S.; Joshi, H.; Kim, E.; Qian, S.; Urban, V.; Crokek, D.; Aksimentiev, A.; Kharlampieva, E. Effect of Temperature and Hydrophilic Ratio on the Structure of Poly(N-Vinylcaprolactam)-Block-Poly(Dimethylsiloxane)-Block-Poly(N-Vinylcaprolactam) Polymersomes. *ACS Appl. Polym. Mater.* **2019**, *1* (4), 722–736. <https://doi.org/10.1021/acsapm.8b00259>.
- (184) Kozlovskaya, V.; Yang, Y.; Liu, F.; Ingle, K.; Ahmad, A.; Halade, G. V.; Kharlampieva, E. Dually Responsive Poly(N-Vinylcaprolactam)-b-Poly(Dimethylsiloxane)-b-Poly(N-Vinylcaprolactam) Polymersomes for Controlled Delivery. *Molecules* **2022**, *27* (11), 3485. <https://doi.org/10.3390/molecules27113485>.
- (185) Das Karmakar, P.; Pal, A.; Bodhak, S.; Pal, S. Reversible Addition–Fragmentation Chain Transfer-Mediated Amphiphilic Copolymeric Composite as a Nanocarrier for Drug Delivery Application. *ACS Appl. Polym. Mater.* **2021**, *3* (11), 5386–5396. <https://doi.org/10.1021/acsapm.1c00584>.
- (186) Beija, M.; Marty, J.-D.; Destarac, M. Thermoresponsive Poly(N-Vinyl Caprolactam)-Coated Gold Nanoparticles: Sharp Reversible Response and Easy Tunability. *Chem. Commun.* **2011**, *47* (10), 2826–2828. <https://doi.org/10.1039/C0CC05184E>.
- (187) Mohammed, M. N.; Yusoh, K. B.; Shariffuddin, J. H. B. H. Poly(N-Vinyl Caprolactam) Thermoresponsive Polymer in Novel Drug Delivery Systems: A Review. *Materials Express* **2018**, *8* (1), 21–34. <https://doi.org/10.1166/mex.2018.1406>.

- (188) Stillwell, W. *An Introduction to Biological Membranes: Composition, Structure and Function*; Elsevier, 2016.
- (189) Misiak, P.; Niemirowicz-Laskowska, K.; Markiewicz, K. H.; Misztalewska-Turkowicz, I.; Wielgat, P.; Kurowska, I.; Siemiaszko, G.; Destarac, M.; Car, H.; Wilczewska, A. Z. Evaluation of Cytotoxic Effect of Cholesterol End-Capped Poly(N-Isopropylacrylamide)s on Selected Normal and Neoplastic Cells. *IJN* **2020**, Volume 15, 7263–7278. <https://doi.org/10.2147/IJN.S262582>.
- (190) Goñi, F. M.; Alonso, A. Structure and Functional Properties of Diacylglycerols in Membranes. *Prog Lipid Res* **1999**, 38 (1), 1–48. [https://doi.org/10.1016/s0163-7827\(98\)00021-6](https://doi.org/10.1016/s0163-7827(98)00021-6).
- (191) Campomanes, P.; Zoni, V.; Vanni, S. Local Accumulation of Diacylglycerol Alters Membrane Properties Nonlinearly Due to Its Transbilayer Activity. *Commun Chem* **2019**, 2 (1), 72. <https://doi.org/10.1038/s42004-019-0175-7>.
- (192) Schuhmacher, M.; Grasskamp, A. T.; Barahtjan, P.; Wagner, N.; Lombardot, B.; Schuhmacher, J. S.; Sala, P.; Lohmann, A.; Henry, I.; Shevchenko, A.; Coskun, Ü.; Walter, A. M.; Nadler, A. Live-Cell Lipid Biochemistry Reveals a Role of Diacylglycerol Side-Chain Composition for Cellular Lipid Dynamics and Protein Affinities. *Proc Natl Acad Sci USA* **2020**, 117 (14), 7729–7738. <https://doi.org/10.1073/pnas.1912684117>.
- (193) Carrasco, S.; Mérida, I. Diacylglycerol, When Simplicity Becomes Complex. *Trends in Biochemical Sciences* **2007**, 32 (1), 27–36. <https://doi.org/10.1016/j.tibs.2006.11.004>.
- (194) Gómez-Fernández, J. C.; Corbalán-García, S. Diacylglycerols, Multivalent Membrane Modulators. *Chemistry and Physics of Lipids* **2007**, 148 (1), 1–25. <https://doi.org/10.1016/j.chemphyslip.2007.04.003>.
- (195) Eichmann, T. O.; Lass, A. DAG Tales: The Multiple Faces of Diacylglycerol--Stereochemistry, Metabolism, and Signaling. *Cell Mol Life Sci* **2015**, 72 (20), 3931–3952. <https://doi.org/10.1007/s00018-015-1982-3>.
- (196) Sen, N.; Hause, G.; Binder, W. H. Membrane Anchored Polymers Modulate Amyloid Fibrillation. *Macromol. Rapid Commun.* **2021**, 42 (12), 2100120. <https://doi.org/10.1002/marc.202100120>.
- (197) Watanabe, A.; Niu, J.; Lunn, D. J.; Lawrence, J.; Knight, A. S.; Zhang, M.; Hawker, C. J. PET-RAFT as a Facile Strategy for Preparing Functional Lipid-Polymer Conjugates. *J. Polym. Sci. Part A: Polym. Chem.* **2018**, 56 (12), 1259–1268. <https://doi.org/10.1002/pola.29007>.
- (198) Kurowska, I.; Markiewicz, K. H.; Niemirowicz-Laskowska, K.; Misiak, P.; Destarac, M.; Wielgat, P.; Misztalewska-Turkowicz, I.; Siemiaszko, G.; Car, H.; Wilczewska, A. Z. Membrane-Active Diacylglycerol-Terminated Thermoresponsive Polymers: RAFT Synthesis and Biocompatibility Evaluation. *European Polymer Journal* **2022**, 169, 111154. <https://doi.org/10.1016/j.eurpolymj.2022.111154>.
- (199) Dizman, B.; Elasmri, M. O.; Mathias, L. J. Synthesis and Characterization of Antibacterial and Temperature Responsive Methacrylamide Polymers. *Macromolecules* **2006**, 39 (17), 5738–5746. <https://doi.org/10.1021/ma0607620>.
- (200) Nakabayashi, K.; Mori, H. Recent Progress in Controlled Radical Polymerization of N-Vinyl Monomers. *European Polymer Journal* **2013**, 49 (10), 2808–2838. <https://doi.org/10.1016/j.eurpolymj.2013.07.006>.
- (201) Santuryan, Y. G.; Malakhova, I. I.; Gorshkov, N. I.; Krasikov, V. D.; Panarin, E. F. Water-Soluble Poly(n-Vinylamides) as a Basis for the Synthesis of Polymeric Carriers of Biologically Active Compounds. *International Journal of Polymer Analysis and Characterization* **2019**, 24 (2), 105–113. <https://doi.org/10.1080/1023666X.2018.1551270>.
- (202) Panarin, E. F. N-Vinylamides and Related Polymers as Delivery Agents of Biologically Active Compounds. *Russ Chem Bull* **2015**, 64 (1), 15–23. <https://doi.org/10.1007/s11172-015-0813-x>.
- (203) Kawatani, R.; Kawata, Y.; Yusa, S.; Kelland, M. A.; Ajiro, H. Synthesis of Thermosensitive Poly(N-Vinylamide) Derivatives Bearing Oligo Ethylene Glycol Chain for Kinetic Hydrate Inhibitor. *Macromolecules* **2018**, 51 (19), 7845–7852. <https://doi.org/10.1021/acs.macromol.8b01573>.

- (204) Kelland, M. A.; Abrahamsen, E.; Ajiro, H.; Akashi, M. Kinetic Hydrate Inhibition with N-Alkyl-N-Vinylformamide Polymers: Comparison of Polymers to n-Propyl and Isopropyl Groups. *Energy Fuels* **2015**, *29* (8), 4941–4946. <https://doi.org/10.1021/acs.energyfuels.5b01251>.
- (205) Lis, M.; Chudzik, K.; Bakierska, M.; Świętosławski, M.; Gajewska, M.; Rutkowska, M.; Molenda, M. Aqueous Binder for Nanostructured Carbon Anode Materials for Li-Ion Batteries. *J. Electrochem. Soc.* **2019**, *166* (3), A5354. <https://doi.org/10.1149/2.0591903jes>.
- (206) Świder, J.; Molenda, M.; Kulka, A.; Molenda, J. Enhancement of Electrochemical Performance of LiFePO₄ Nanoparticles by Direct Nanocoating with Conductive Carbon Layers. *Funct. Mater. Lett.* **2016**, *09* (04), 1641007. <https://doi.org/10.1142/S1793604716410071>.
- (207) Kröner, M.; Dupuis, J.; Winter, M. N-Vinylformamide — Syntheses and Chemistry of a Multifunctional Monomer. *J. prakt. Chem.* **2000**, *342* (2), 115–131. [https://doi.org/10.1002/\(SICI\)1521-3897\(200002\)342:2<115::AID-PRAC115>3.0.CO;2-5](https://doi.org/10.1002/(SICI)1521-3897(200002)342:2<115::AID-PRAC115>3.0.CO;2-5).
- (208) Pelton, R. Polyvinylamine: A Tool for Engineering Interfaces. *Langmuir* **2014**, *30* (51), 15373–15382. <https://doi.org/10.1021/la5017214>.
- (209) Tian, Y.; Zhao, Y.; Yin, C.; Tan, S.; Wang, X.; Yang, C.; Zhang, T.-D.; Zhang, X.; Ye, F.; Xu, J.; Wu, X.; Ding, L.; Zhang, J.; Pei, J.; Wang, X.-T.; Zhang, R. X.; Xu, J.; Wang, W.; Filipe, C. D. M.; Hoare, T.; Yin, D.-C.; Qian, A.; Deng, X. Polyvinylamine with Moderate Binding Affinity as a Highly Effective Vehicle for RNA Delivery. *Journal of Controlled Release* **2022**, *345*, 20–37. <https://doi.org/10.1016/j.jconrel.2022.03.003>.
- (210) Chen, Y.; Sun, P. pH-Sensitive Polyampholyte Microgels of Poly(Acrylic Acid-Co-Vinylamine) as Injectable Hydrogel for Controlled Drug Release. *Polymers* **2019**, *11* (2), 285. <https://doi.org/10.3390/polym11020285>.
- (211) Tachaboonyakiat, W.; Ajiro, H.; Akashi, M. Controlled DNA Interpolyelectrolyte Complex Formation or Dissociation via Stimuli-Responsive Poly(Vinylamine-Co-N-Vinylisobutylamide). *Journal of Applied Polymer Science* **2016**, *133* (35). <https://doi.org/10.1002/app.43852>.
- (212) Ghaffarlou, M.; Sütekin, S. D.; Hammamchi, H.; İlk, S.; Güven, O.; Barsbay, M. Poly(Acrylic Acid)-b-Poly(Vinylamine) Copolymer: Decoration with Silver Nanoparticles, Antibacterial Properties, Quorum Sensing Activity, and Cytotoxicity on Breast Cancer and Fibroblast Cell Lines. *ACS Appl. Polym. Mater.* **2022**, *4* (10), 7268–7281. <https://doi.org/10.1021/acsapm.2c00906>.
- (213) Kobayashi, S.; Suh, K. D.; Shirokura, Y. Chelating Ability of Poly(Vinylamine): Effects of Polyamine Structure on Chelation. *Macromolecules* **1989**, *22* (5), 2363–2366. <https://doi.org/10.1021/ma00195a062>.
- (214) Huang, Y.; Wu, D.; Wang, X.; Huang, W.; Lawless, D.; Feng, X. Removal of Heavy Metals from Water Using Polyvinylamine by Polymer-Enhanced Ultrafiltration and Flocculation. *Separation and Purification Technology* **2016**, *158*, 124–136. <https://doi.org/10.1016/j.seppur.2015.12.008>.
- (215) Romero Nieto, D.; Lindbråthen, A.; Hägg, M.-B. Effect of Water Interactions on Polyvinylamine at Different pHs for Membrane Gas Separation. *ACS Omega* **2017**, *2* (11), 8388–8400. <https://doi.org/10.1021/acsomega.7b01307>.
- (216) Deng, L.; Hägg, M.-B. Techno-Economic Evaluation of Biogas Upgrading Process Using CO₂ Facilitated Transport Membrane. *International Journal of Greenhouse Gas Control* **2010**, *4* (4), 638–646. <https://doi.org/10.1016/j.ijggc.2009.12.013>.
- (217) Shan, B.; Cui, R.; Zhang, S.; Tang, B. Synthesis and Application of Poly(Vinylamine-Co-Acrylic Acid) Macromolecule Dyes with High Light Fastness. *Textile Research Journal* **2020**, *90* (2), 156–165. <https://doi.org/10.1177/0040517519859936>.
- (218) Bortel, E. N-winyloformamid - nowy ekologiczny monomer wodorozpuszczalny. **2007**, 8.
- (219) Pinschmidt Jr, R. K. Polyvinylamine at Last. *Journal of Polymer Science Part A: Polymer Chemistry* **2010**, *48* (11), 2257–2283. <https://doi.org/10.1002/pola.23992>.
- (220) Achari, A. E.; Coqueret, X.; Lablache-Comber, A.; Loucheux, C. Preparation of Polyvinylamine from Polyacrylamide: A Reinvestigation of the Hofmann Reaction. *Die Makromolekulare Chemie* **1993**, *194* (7), 1879–1891. <https://doi.org/10.1002/macp.1993.021940703>.

- (221) Nadal, C.; Gineste, S.; Coutelier, O.; Tourrette, A.; Marty, J.-D.; Destarac, M. A Deeper Insight into the Dual Temperature- and pH-Responsiveness of Poly(Vinylamine)-b-Poly(N-Isopropylacrylamide) Double Hydrophilic Block Copolymers. *Colloids and Surfaces A: Physicochemical and Engineering Aspects* **2022**, *641*, 128502. <https://doi.org/10.1016/j.colsurfa.2022.128502>.
- (222) Maki, Y.; Mori, H.; Endo, T. Xanthate-Mediated Controlled Radical Polymerization of N-Vinylindole Derivatives. *Macromolecules* **2007**, *40* (17), 6119–6130. <https://doi.org/10.1021/ma062839q>.
- (223) Dréan, M.; Guégan, P.; Jérôme, C.; Rieger, J.; Debuigne, A. Far beyond Primary Poly(Vinylamine)s through Free Radical Copolymerization and Amide Hydrolysis. *Polymer Chemistry* **2016**, *7* (1), 69–78. <https://doi.org/10.1039/C5PY01325A>.
- (224) Dréan, M.; Guégan, P.; Detrembleur, C.; Jérôme, C.; Rieger, J.; Debuigne, A. Controlled Synthesis of Poly(Vinylamine)-Based Copolymers by Organometallic-Mediated Radical Polymerization. *Macromolecules* **2016**, *49* (13), 4817–4827. <https://doi.org/10.1021/acs.macromol.6b00992>.
- (225) Roka, N.; Kokkorogianni, O.; Kontoes-Georgoudakis, P.; Choinopoulos, I.; Pitsikalis, M. Recent Advances in the Synthesis of Complex Macromolecular Architectures Based on Poly(N-Vinyl Pyrrolidone) and the RAFT Polymerization Technique. *Polymers* **2022**, *14* (4), 701. <https://doi.org/10.3390/polym14040701>.
- (226) Góis, J. R.; Costa, J. R. C.; Popov, A. V.; Serra, A. C.; Coelho, J. F. J. Synthesis of Well-Defined Alkyne Terminated Poly(N-Vinyl Caprolactam) with Stringent Control over the LCST by RAFT. *RSC Adv.* **2016**, *6* (21), 16996–17007. <https://doi.org/10.1039/C6RA01014H>.
- (227) Shao, L.; Hu, M.; Chen, L.; Xu, L.; Bi, Y. RAFT Polymerization of N-Vinylcaprolactam and Effects of the End Group on the Thermal Response of Poly(N-Vinylcaprolactam). *Reactive and Functional Polymers* **2012**, *72* (6), 407–413. <https://doi.org/10.1016/j.reactfunctpolym.2012.04.002>.
- (228) Zhao, X.; Coutelier, O.; Nguyen, H. H.; Delmas, C.; Destarac, M.; Marty, J.-D. Effect of Copolymer Composition of RAFT/MADIX-Derived N-Vinylcaprolactam/N-Vinylpyrrolidone Statistical Copolymers on Their Thermoresponsive Behavior and Hydrogel Properties. *Polym. Chem.* **2015**, *6* (29), 5233–5243. <https://doi.org/10.1039/C5PY00606F>.
- (229) Fan, W.; Yamago, S. Synthesis of Poly(N-Vinylamide)s and Poly(Vinylamine)s and Their Block Copolymers by Organotellurium-Mediated Radical Polymerization. *Angewandte Chemie International Edition* **2019**, *58* (21), 7113–7116. <https://doi.org/10.1002/anie.201902940>.
- (230) Dupre--Demorsy, A.; Coutelier, O.; Destarac, M.; Nadal, C.; Bourdon, V.; Ando, T.; Ajiro, H. RAFT Polymerization of N-Methyl-N-Vinylacetamide and Related Double Hydrophilic Block Copolymers. *Macromolecules* **2022**, *55* (4), 1127–1138. <https://doi.org/10.1021/acs.macromol.1c01593>.
- (231) Shi, L.; Chapman, T. M.; Beckman, E. J. Poly(Ethylene Glycol)- Block -Poly(N -Vinylformamide) Copolymers Synthesized by the RAFT Methodology. *Macromolecules* **2003**, *36* (7), 2563–2567. <https://doi.org/10.1021/ma025670z>.
- (232) Peng, H.; Xu, W.; Pich, A. Temperature and pH Dual-Responsive Poly(Vinyl Lactam) Copolymers Functionalized with Amine Side Groups via RAFT Polymerization. *Polym. Chem.* **2016**, *7* (31), 5011–5022. <https://doi.org/10.1039/C6PY00885B>.
- (233) Dupre--Demorsy, A.; Kurowska, I.; Balayssac, S.; Henriet, M.; Ric, A.; Bourdon, V.; Ando, T.; Ajiro, H.; Coutelier, O.; Destarac, M. RAFT Polymerisation of N-Vinylformamide and the Corresponding Double Hydrophilic Block Copolymers. *Polym. Chem.* **2022**, *13* (44), 6229–6237. <https://doi.org/10.1039/D2PY00925K>.
- (234) Kurowska, I.; Dupre--Demorsy, A.; Balayssac, S.; Henriet, M.; Ric, A.; Bourdon, V.; Ando, T.; Ajiro, H.; Coutelier, O.; Destarac, M. Tailor-Made Poly(Vinylamine) via Purple LED-Activated RAFT Polymerization of N-Vinylformamide. *Macromolecular Rapid Communications* *n/a* (n/a), 2200729. <https://doi.org/10.1002/marc.202200729>.
- (235) Zhang, M.; June, S. M.; Long, T. E. 5.02 - Principles of Step-Growth Polymerization (Polycondensation and Polyaddition). In *Polymer Science: A Comprehensive Reference*; Matyjaszewski, K., Möller, M., Eds.; Elsevier: Amsterdam, 2012; pp 7–47. <https://doi.org/10.1016/B978-0-444-53349-4.00131-X>.

- (236) Torres, V. M.; LaNasa, J. A.; Vogt, B. D.; Hickey, R. J. Controlling Nanostructure and Mechanical Properties in Triblock Copolymer/Monomer Blends via Reaction-Induced Phase Transitions. *Soft Matter* **2021**, *17* (6), 1505–1512. <https://doi.org/10.1039/D0SM01661F>.
- (237) Park, J.; Jung, J.-Y.; Shin, H.-W.; Park, J.-W.; Bang, J.; Huh, J. Loop and Bridge Conformations of ABA Triblock Comb Copolymers: A Conformational Assessment for Molecular Composites. *Polymers* **2022**, *14* (11), 2301. <https://doi.org/10.3390/polym14112301>.
- (238) Aguilar, N. M.; Perez-Aguilar, J. M.; González-Coronel, V. J.; Martínez-Gutiérrez, H.; Zayas Pérez, T.; González-Vergara, E.; Sanchez-Gaytan, B. L.; Soriano-Moro, G. Reversible Thermo-Optical Response Nanocomposites Based on RAFT Symmetric Triblock Copolymers (ABA) of Acrylamide and N-Isopropylacrylamide and Gold Nanoparticles. *Polymers* **2023**, *15* (8), 1963. <https://doi.org/10.3390/polym15081963>.
- (239) Cao, Y.; Shi, Y.; Wu, X.; Zhang, L. Preparation of ABA Triblock Copolymer Assemblies through “One-Pot” RAFT PISA. *Chinese Chemical Letters* **2020**, *31* (6), 1660–1664. <https://doi.org/10.1016/j.ccl.2019.10.026>.
- (240) Zahoranová, A.; Mrlík, M.; Tomanová, K.; Kronek, J.; Luxenhofer, R. ABA and BAB Triblock Copolymers Based on 2-Methyl-2-Oxazoline and 2-n-Propyl-2-Oxazoline: Synthesis and Thermoresponsive Behavior in Water. *Macromolecular Chemistry and Physics* **2017**, *218* (13), 1700031. <https://doi.org/10.1002/macp.201700031>.
- (241) Zhao, X.; Liu, W.; Chen, D.; Lin, X.; Lu, W. W. Effect of Block Order of ABA- and BAB-Type NIPAAm/HEMA Triblock Copolymers on Thermoresponsive Behavior of Solutions. *Macromolecular Chemistry and Physics* **2007**, *208* (16), 1773–1781. <https://doi.org/10.1002/macp.200700155>.
- (242) Shentu, Z.; Zhang, Z.; Zhao, J.; Chen, C.; Wu, Q.; Wang, L.; Yan, X. Supramolecular Polymer-Assisted Manipulation of Triblock Copolymers: Understanding the Relationships between Microphase Structures and Mechanical Properties. *J. Mater. Chem. A* **2021**, *9* (35), 19619–19624. <https://doi.org/10.1039/D1TA02288A>.
- (243) Wang, W.; Lu, W.; Goodwin, A.; Wang, H.; Yin, P.; Kang, N.-G.; Hong, K.; Mays, J. W. Recent Advances in Thermoplastic Elastomers from Living Polymerizations: Macromolecular Architectures and Supramolecular Chemistry. *Progress in Polymer Science* **2019**, *95*, 1–31. <https://doi.org/10.1016/j.progpolymsci.2019.04.002>.
- (244) Matsuo, Y.; Konno, R.; Ishizone, T.; Goseki, R.; Hirao, A. Precise Synthesis of Block Polymers Composed of Three or More Blocks by Specially Designed Linking Methodologies in Conjunction with Living Anionic Polymerization System. *Polymers* **2013**, *5* (3), 1012–1040. <https://doi.org/10.3390/polym5031012>.
- (245) Agudelo, N. A.; Elsen, A. M.; He, H.; López, B. L.; Matyjaszewski, K. ABA Triblock Copolymers from Two Mechanistic Techniques: Polycondensation and Atom Transfer Radical Polymerization. *Journal of Polymer Science Part A: Polymer Chemistry* **2015**, *53* (2), 228–238. <https://doi.org/10.1002/pola.27300>.
- (246) Ivanchenko, O.; Odnoroh, M.; Mallet-Ladeira, S.; Guerre, M.; Mazières, S.; Destarac, M. Azo-Derived Symmetrical Trithiocarbonate for Unprecedented RAFT Control. *J. Am. Chem. Soc.* **2021**, *143* (49), 20585–20590. <https://doi.org/10.1021/jacs.1c10031>.
- (247) Legge, T. M.; Slark, A. T.; Perrier, S. Novel Difunctional Reversible Addition Fragmentation Chain Transfer (RAFT) Agent for the Synthesis of Telechelic and ABA Triblock Methacrylate and Acrylate Copolymers. *Macromolecules* **2007**, *40* (7), 2318–2326. <https://doi.org/10.1021/ma061372g>.
- (248) Wu, J.; Sun, X.; Zhang, R.; Yuan, S.; Wu, Z.; Lu, Q.; Yu, Y. RAFT Preparation and Self-Assembly Behavior of Thermosensitive Triblock PNIPAAm-b-PODA-b-PNIPAAm Copolymers. *Colloid Polym Sci* **2016**, *294* (12), 1989–1995. <https://doi.org/10.1007/s00396-016-3958-8>.
- (249) Moad, G.; Mayadunne, R. T. A.; Rizzardo, E.; Skidmore, M.; Thang, S. H. Synthesis of Novel Architectures by Radical Polymerization with Reversible Addition Fragmentation Chain Transfer (RAFT Polymerization). *Macromolecular Symposia* **2003**, *192* (1), 1–12. <https://doi.org/10.1002/masy.200390029>.

- (250) Yu, B. *RAFT Synthesis of Water-Soluble, Stimuli-Responsive (Co)Polymers and Post-Polymerization End Group Modification Via the Thiol-Ene Reaction*; Dissertation, The University of Southern Mississippi, 2009.
- (251) Keddie, D. J. A Guide to the Synthesis of Block Copolymers Using Reversible-Addition Fragmentation Chain Transfer (RAFT) Polymerization. *Chem. Soc. Rev.* **2013**, *43* (2), 496–505. <https://doi.org/10.1039/C3CS60290G>.
- (252) Shi, H.; Qiu, T.; Ou-Yang, H. D.; Xu, H.; Lu, Q.; Zheng, Y.; Liu, K.; He, L.; Guo, L.; Li, X. ABA-Type Triblock Copolymer Micellar System with Lower Critical Solution Temperature-Type Sol-Gel Transition. *Journal of Colloid and Interface Science* **2019**, *545*, 220–230. <https://doi.org/10.1016/j.jcis.2019.03.039>.
- (253) Hinton, T. M.; Challagulla, A.; Stewart, C. R.; Guerrero-Sanchez, C.; Grusche, F. A.; Shi, S.; Bean, A. G.; Monaghan, P.; Gunatillake, P. A.; Thang, S. H.; Tizard, M. L. Inhibition of Influenza Virus in Vivo by siRNA Delivered Using ABA Triblock Copolymer Synthesized by Reversible Addition-Fragmentation Chain-Transfer Polymerization. *Nanomedicine* **2014**, *9* (8), 1141–1154. <https://doi.org/10.2217/nnm.13.119>.
- (254) Massey, L. K. Chapter 60 - Thermoplastic Elastomers: Overview. In *The Effects of UV Light and Weather on Plastics and Elastomers (Second Edition)*; Massey, L. K., Ed.; Plastics Design Library; William Andrew Publishing: Norwich, NY, 2007; p 279. <https://doi.org/10.1016/B978-081551525-8.50064-6>.
- (255) Spring, S. W.; Smith-Sweetser, R. O.; Rosenbloom, S. I.; Sifri, R. J.; Fors, B. P. Sustainable Thermoplastic Elastomers Produced via Cationic RAFT Polymerization. *Polym. Chem.* **2021**, *12* (8), 1097–1104. <https://doi.org/10.1039/D0PY01640C>.
- (256) Wang, W.; Lu, W.; Kang, N.-G.; Mays, J.; Hong, K.; Wang, W.; Lu, W.; Kang, N.-G.; Mays, J.; Hong, K. Thermoplastic Elastomers Based on Block, Graft, and Star Copolymers. In *Elastomers*; IntechOpen, 2017. <https://doi.org/10.5772/intechopen.68586>.
- (257) Lewis, P. R.; Price, C. Electron Microscopy of Sym-SBS Block Polymers. *Polymer* **1972**, *13* (1), 20–26. [https://doi.org/10.1016/0032-3861\(72\)90030-4](https://doi.org/10.1016/0032-3861(72)90030-4).
- (258) Gregory, G. L.; Sulley, G. S.; Carrodeguas, L. P.; Chen, T. T. D.; Santmarti, A.; Terrill, N. J.; Lee, K.-Y.; Williams, C. K. Triblock Polyester Thermoplastic Elastomers with Semi-Aromatic Polymer End Blocks by Ring-Opening Copolymerization. *Chem. Sci.* **2020**, *11* (25), 6567–6581. <https://doi.org/10.1039/D0SC00463D>.
- (259) Destarac, M. Industrial Development of Reversible-Deactivation Radical Polymerization: Is the Induction Period Over? *Polym. Chem.* **2018**, *9* (40), 4947–4967. <https://doi.org/10.1039/C8PY00970H>.
- (260) Tu, W.; Maksym, P.; Chat, K.; Biela, T.; Zięba, A.; Kaminski, K.; Adrjanowicz, K. Tacticity Control Approached by Electric-Field Assisted Free Radical Polymerization – the Case of Sterically Hindered Monomers. *Polym. Chem.* **2023**, *14* (30), 3465–3478. <https://doi.org/10.1039/D3PY00484H>.
- (261) Takács, E.; Wojnárovits, L. Comparison of the Reactivity of Acrylate and Methacrylate Monomers. *Radiation Physics and Chemistry* **1995**, *46* (4, Part 2), 1007–1010. [https://doi.org/10.1016/0969-806X\(95\)00310-T](https://doi.org/10.1016/0969-806X(95)00310-T).
- (262) Dirdal, E. G.; Kelland, M. A. Synthesis and Investigation of Polymers of 2-Methacrylamido-Caprolactam as Kinetic Hydrate Inhibitors. *Energy Fuels* **2020**, *34* (6), 6981–6990. <https://doi.org/10.1021/acs.energyfuels.0c00929>.
- (263) Lai, J. T.; Filla, D.; Shea, R. Functional Polymers from Novel Carboxyl-Terminated Trithiocarbonates as Highly Efficient RAFT Agents. *Macromolecules* **2002**, *35* (18), 6754–6756. <https://doi.org/10.1021/ma020362m>.
- (264) Ma, J.; Zhang, H. Kinetic Investigations of RAFT Polymerization: Difunctional RAFT Agent Mediated Polymerization of Methyl Methacrylate and Styrene. *Macromol. Res.* **2015**, *23* (1), 67–73. <https://doi.org/10.1007/s13233-014-2188-5>.
- (265) L. Atkinson, R.; R. Monaghan, O.; T. Elsmore, M.; D. Topham, P.; W. Toolan, D. T.; J. Derry, M.; Taresco, V.; A. Stockman, R.; Focatiis, D. S. A. D.; J. Irvine, D.; M. Howdle, S. RAFT Polymerisation of Renewable Terpene (Meth)Acrylates and the Convergent Synthesis of Methacrylate–Acrylate–Methacrylate Triblock Copolymers. *Polymer Chemistry* **2021**, *12* (21), 3177–3189. <https://doi.org/10.1039/D1PY00326G>.

- (266) Williams, L. G.; Sullivan, K.; Tsanaktsidis, J. *RAFT Agents for Making Well-Defined Functionalized Polymers*. <https://www.sigmaaldrich.com/PL/pl/technical-documents/technical-article/materials-science-and-engineering/polymer-synthesis/raft-agents-for-functionalized-polymers> (accessed 2024-01-14).
- (267) Choi, J.-Y.; Jin, S.-W.; Kim, D.-M.; Song, I.-H.; Nam, K.-N.; Park, H.-J.; Chung, C.-M. Enhancement of the Mechanical Properties of Polyimide Film by Microwave Irradiation. *Polymers (Basel)* **2019**, *11* (3), 477. <https://doi.org/10.3390/polym11030477>.
- (268) Jiang, Y.; Fan, W.; Tosaka, M.; Cunningham, M. F.; Yamago, S. Fabrication of Structurally Controlled Poly(n-Butyl Acrylate) Particles by Ab Initio Emulsion Organotellurium-Mediated Radical Polymerization. Synthesis of High Molecular Weight Homo and Block Copolymers. *Macromolecules* **2021**, *54* (23), 10691–10699. <https://doi.org/10.1021/acs.macromol.1c02037>.
- (269) Vaganov, G.; Simonova, M.; Romasheva, M.; Didenko, A.; Popova, E.; Ivan'kova, E.; Kamalov, A.; Elokhovskiy, V.; Vaganov, V.; Filippov, A.; Yudin, V. Influence of Molecular Weight on Thermal and Mechanical Properties of Carbon-Fiber-Reinforced Plastics Based on Thermoplastic Partially Crystalline Polyimide. *Polymers* **2023**, *15* (13), 2922. <https://doi.org/10.3390/polym15132922>.
- (270) Gong, H.; Gu, Y.; Zhao, Y.; Quan, Q.; Han, S.; Chen, M. Precise Synthesis of Ultra-High-Molecular-Weight Fluoropolymers Enabled by Chain-Transfer-Agent Differentiation under Visible-Light Irradiation. *Angewandte Chemie International Edition* **2020**, *59* (2), 919–927. <https://doi.org/10.1002/anie.201912698>.
- (271) Truong, N. P.; Dussert, M. V.; Whittaker, M. R.; Quinn, J. F.; Davis, T. P. Rapid Synthesis of Ultrahigh Molecular Weight and Low Polydispersity Polystyrene Diblock Copolymers by RAFT-Mediated Emulsion Polymerization. *Polym. Chem.* **2015**, *6* (20), 3865–3874. <https://doi.org/10.1039/C5PY00166H>.
- (272) Arita, T.; Kayama, Y.; Ohno, K.; Tsujii, Y.; Fukuda, T. High-Pressure Atom Transfer Radical Polymerization of Methyl Methacrylate for Well-Defined Ultrahigh Molecular-Weight Polymers. *Polymer* **2008**, *49* (10), 2426–2429. <https://doi.org/10.1016/j.polymer.2008.03.026>.
- (273) Arita, T.; Buback, M.; Janssen, O.; Vana, P. RAFT-Polymerization of Styrene up to High Pressure: Rate Enhancement and Improved Control. *Macromolecular Rapid Communications* **2004**, *25* (15), 1376–1381. <https://doi.org/10.1002/marc.200400204>.
- (274) Spring, S. W.; Smith-Sweetser, R. O.; Rosenbloom, S. I.; Sifri, R. J.; Fors, B. P. Sustainable Thermoplastic Elastomers Produced via Cationic RAFT Polymerization. *Polym. Chem.* **2021**, *12* (8), 1097–1104. <https://doi.org/10.1039/D0PY01640C>.
- (275) Siljanovska Petreska, G.; Arbe, A.; Auschra, C.; Paulis, M. Mechanical and Morphological Properties of Waterborne ABA Hard-Soft-Hard Block Copolymers Synthesized by Means of RAFT Miniemulsion Polymerization. *Polymers* **2019**, *11* (8), 1259. <https://doi.org/10.3390/polym11081259>.
- (276) Kalita, U.; Samanta, S.; Banerjee, S. L.; Das, N. C.; Singha, N. K. Biobased Thermoplastic Elastomer Based on an SMS Triblock Copolymer Prepared via RAFT Polymerization in Aqueous Medium. *Macromolecules* **2021**, *54* (3), 1478–1488. <https://doi.org/10.1021/acs.macromol.0c02169>.
- (277) Guo, Y.; Yu, Y.; Shi, K.; Zhang, W. Synthesis of ABA Triblock Copolymer Nanoparticles by Polymerization Induced Self-Assembly and Their Application as an Efficient Emulsifier. *Polym. Chem.* **2021**, *12* (4), 572–580. <https://doi.org/10.1039/D0PY01498B>.
- (278) Liu, J.; Cui, K.; Zhao, Q.-L.; Huang, J.; Jiang, T.; Ma, Z. New ABA Tri-Block Copolymers of Poly(Tert-Butylacrylate)-b-Poly(2,2,2-Trifluoroethyl Acrylate)-b-Poly(Tert-Butylacrylate): Synthesis, Self-Assembly and Fabrication of Their Porous Films, Spheres, and Fibers. *European Polymer Journal* **2019**, *113*, 52–59. <https://doi.org/10.1016/j.eurpolymj.2019.01.037>.
- (279) Lee, J.-D.; Ueno, M.; Miyajima, Y.; Nakamura, H. Synthesis of Boron Cluster Lipids: Closo-Dodecaborate as an Alternative Hydrophilic Function of Boronated Liposomes for Neutron Capture Therapy. *Org. Lett.* **2007**, *9* (2), 4.
- (280) Vilela, C.; Rua, R.; Silvestre, A. J. D.; Gandini, A. Polymers and Copolymers from Fatty Acid-Based Monomers. *Industrial Crops and Products* **2010**, *32* (2), 97–104. <https://doi.org/10.1016/j.indcrop.2010.03.008>.

- (281) Chira, N.; Nicolescu, A.; Raluca, S.; Rosca, S. Fatty Acid Composition of Vegetable Oils Determined from C-13-NMR Spectra. *Revista de Chimie -Bucharest- Original Edition-* **2016**, *67*, 1257–1263.
- (282) del Río, J. C.; Evaristo, A. B.; Marques, G.; Martín-Ramos, P.; Martín-Gil, J.; Gutiérrez, A. Chemical Composition and Thermal Behavior of the Pulp and Kernel Oils from Macauba Palm (*Acrocomia Aculeata*) Fruit. *Industrial Crops and Products* **2016**, *84*, 294–304. <https://doi.org/10.1016/j.indcrop.2016.02.018>.
- (283) Vilela, C.; Rua, R.; Silvestre, A. J. D.; Gandini, A. Polymers and Copolymers from Fatty Acid-Based Monomers. *Industrial Crops and Products* **2010**, *32* (2), 97–104. <https://doi.org/10.1016/j.indcrop.2010.03.008>.
- (284) Beija, M.; Marty, J.-D.; Destarac, M. Thermoresponsive Poly(N-Vinyl Caprolactam)-Coated Gold Nanoparticles: Sharp Reversible Response and Easy Tunability. *Chem. Commun.* **2011**, *47* (10), 2826. <https://doi.org/10.1039/c0cc05184e>.
- (285) Sistach, S.; Beija, M.; Rahal, V.; Brûlet, A.; Marty, J.-D.; Destarac, M.; Mingotaud, C. Thermoresponsive Amphiphilic Diblock Copolymers Synthesized by MADIX/RAFT: Properties in Aqueous Solutions and Use for the Preparation and Stabilization of Gold Nanoparticles. *Chem. Mater.* **2010**, *22* (12), 3712–3724. <https://doi.org/10.1021/cm100674p>.
- (286) Yin, F.; Behra, J. S.; Beija, M.; Brûlet, A.; Fitremann, J.; Payré, B.; Gineste, S.; Destarac, M.; Lauth-de Viguerie, N.; Marty, J.-D. Effect of the Microstructure of N-Butyl Acrylate/N-Isopropylacrylamide Copolymers on Their Thermo-Responsiveness, Self-Organization and Gel Properties in Water. *Journal of Colloid and Interface Science* **2020**, *578*, 685–697. <https://doi.org/10.1016/j.jcis.2020.06.005>.
- (287) Maiti, B.; Bauri, K.; Nandi, M.; De, P. Surface Functionalized Nano-Objects from Oleic Acid-Derived Stabilizer via Non-Polar RAFT Dispersion Polymerization. *Journal of Polymer Science Part A: Polymer Chemistry* **2017**, *55* (2), 263–273. <https://doi.org/10.1002/pola.28373>.
- (288) Gan, H.; Hutchinson, S. A.; Hurren, C.; Liu, Q.; Wang, X.; Long, R. L. Effect of Oleic Purity on the Chemical Structure, Thermal and Rheological Properties of Bio-Based Polymers Derived from High Oleic Cottonseed Oil via RAFT Polymerization. *Industrial Crops and Products* **2021**, *171*, 113882. <https://doi.org/10.1016/j.indcrop.2021.113882>.
- (289) Kozanoğlu, S.; Özdemir, T.; Usanmaz, A. Polymerization of N-Vinylcaprolactam and Characterization of Poly(N-Vinylcaprolactam). *Journal of Macromolecular Science, Part A* **2011**, *48* (6), 467–477. <https://doi.org/10.1080/10601325.2011.573350>.
- (290) Misiak, P.; Niemirowicz-Laskowska, K.; Markiewicz, K. H.; Misztalewska-Turkiewicz, I.; Wielgat, P.; Kurowska, I.; Siemiaszko, G.; Destarac, M.; Car, H.; Wilczewska, A. Z. Evaluation of Cytotoxic Effect of Cholesterol End-Capped Poly(N-Isopropylacrylamide)s on Selected Normal and Neoplastic Cells. *IJN* **2020**, *Volume 15*, 7263–7278. <https://doi.org/10.2147/IJN.S262582>.
- (291) Santos, S. dos; Medronho, B.; Santos, T. dos; Antunes, F. E. Amphiphilic Molecules in Drug Delivery Systems. In *Drug Delivery Systems: Advanced Technologies Potentially Applicable in Personalised Treatment*; Coelho, J., Ed.; Advances in Predictive, Preventive and Personalised Medicine; Springer Netherlands: Dordrecht, 2013; Vol. 4, pp 35–85. https://doi.org/10.1007/978-94-007-6010-3_2.
- (292) Griffin, W. C. Classification of Surface-Active Agents By. *J. Soc. Cosmet. Chem.* **1949**, *1*, 311–326.
- (293) Cheng, K. C.; Khoo, Z. S.; Lo, N. W.; Tan, W. J.; Chemmangattuvalappil, N. G. Design and Performance Optimisation of Detergent Product Containing Binary Mixture of Anionic-Nonionic Surfactants. *Heliyon* **2020**, *6* (5), e03861. <https://doi.org/10.1016/j.heliyon.2020.e03861>.
- (294) Scharfenberg, M.; Wald, S.; Wurm, F. R.; Frey, H. Acid-Labile Surfactants Based on Poly(Ethylene Glycol), Carbon Dioxide and Propylene Oxide: Miniemulsion Polymerization and Degradation Studies. *Polymers* **2017**, *9* (9), 422. <https://doi.org/10.3390/polym9090422>.
- (295) Barret, R. Importance and Evaluation of Lipophilicity. In *Therapeutic Chemistry*; Elsevier, 2018; pp 53–78. <https://doi.org/10.1016/B978-1-78548-288-5.50003-2>.
- (296) Rotta, J.; Pham, P. D.; Lapinte, V.; Borsali, R.; Minatti, E.; Robin, J.-J. Synthesis of Amphiphilic Polymers Based on Fatty Acids and Glycerol-Derived Monomers - A Study of

- Their Self-Assembly in Water. *Macromol. Chem. Phys.* **2014**, *215* (2), 131–139. <https://doi.org/10.1002/macp.201300483>.
- (297) Heinz, D.; Amado, E.; Kressler, J. Polyphilicity—An Extension of the Concept of Amphiphilicity in Polymers. *Polymers (Basel)* **2018**, *10* (9), 960. <https://doi.org/10.3390/polym10090960>.
- (298) Manfredini, N.; Sponchioni, M.; Moscatelli, D. Recoverable Thermo-Responsive Polymeric Surfactants for the Synthesis of Bulk Plastics from Latexes. *ACS Appl. Polym. Mater.* **2022**, *4* (1), 270–279. <https://doi.org/10.1021/acsapm.1c01266>.
- (299) Lukyanov, A. N.; Torchilin, V. P. Micelles from Lipid Derivatives of Water-Soluble Polymers as Delivery Systems for Poorly Soluble Drugs. *Advanced Drug Delivery Reviews* **2004**, *56* (9), 1273–1289. <https://doi.org/10.1016/j.addr.2003.12.004>.
- (300) Torchilin, V. P.; Levchenko, T. S.; Whiteman, K. R.; Yaroslavov, A. A.; Tsatsakis, A. M.; Rizos, A. K.; Michailova, E. V.; Shtilman, M. I. Amphiphilic Poly-N-Vinylpyrrolidones: Synthesis, Properties and Liposome Surface Modification. *Biomaterials* **2001**, *22* (22), 3035–3044. [https://doi.org/10.1016/s0142-9612\(01\)00050-3](https://doi.org/10.1016/s0142-9612(01)00050-3).
- (301) Volet, G.; Chanthavong, V.; Wintgens, V.; Amiel, C. Synthesis of Monoalkyl End-Capped Poly(2-Methyl-2-Oxazoline) and Its Micelle Formation in Aqueous Solution. *Macromolecules* **2005**, *38* (12), 5190–5197. <https://doi.org/10.1021/ma050407u>.
- (302) Volet, G.; Auvray, L.; Amiel, C. Monoalkyl Poly(2-Methyl-2-Oxazoline) Micelles. A Small-Angle Neutron Scattering Study. *J. Phys. Chem. B* **2009**, *113* (41), 13536–13544. <https://doi.org/10.1021/jp9029634>.
- (303) Kozlovskaya, V.; Kharlampieva, E. Self-Assemblies of Thermoresponsive Poly(*N* -Vinylcaprolactam) Polymers for Applications in Biomedical Field. *ACS Appl. Polym. Mater.* **2020**, *2* (1), 26–39. <https://doi.org/10.1021/acsapm.9b00863>.
- (304) Vihola, H.; Laukkanen, A.; Valtola, L.; Tenhu, H.; Hirvonen, J. Cytotoxicity of Thermosensitive Polymers Poly(N-Isopropylacrylamide), Poly(N-Vinylcaprolactam) and Amphiphilically Modified Poly(N-Vinylcaprolactam). *Biomaterials* **2005**, *26* (16), 3055–3064. <https://doi.org/10.1016/j.biomaterials.2004.09.008>.
- (305) Sun, S.; Wu, P. Infrared Spectroscopic Insight into Hydration Behavior of Poly(*N* -Vinylcaprolactam) in Water. *J. Phys. Chem. B* **2011**, *115* (40), 11609–11618. <https://doi.org/10.1021/jp2071056>.
- (306) Liu, J.; Debuigne, A.; Detrembleur, C.; Jérôme, C. Poly(*N* -Vinylcaprolactam): A Thermoresponsive Macromolecule with Promising Future in Biomedical Field. *Adv. Healthcare Mater.* **2014**, *3* (12), 1941–1968. <https://doi.org/10.1002/adhm.201400371>.
- (307) Dos Santos Ramos, M. A.; Da Silva, P. B.; Spósito, L.; De Toledo, L. G.; Bonifácio, B. V.; Rodero, C. F.; Dos Santos, K. C.; Chorilli, M.; Bauab, T. M. Nanotechnology-Based Drug Delivery Systems for Control of Microbial Biofilms: A Review. *Int J Nanomedicine* **2018**, *13*, 1179–1213. <https://doi.org/10.2147/IJN.S146195>.
- (308) Patra, J. K.; Das, G.; Fraceto, L. F.; Campos, E. V. R.; Rodriguez-Torres, M. del P.; Acosta-Torres, L. S.; Diaz-Torres, L. A.; Grillo, R.; Swamy, M. K.; Sharma, S.; Habtemariam, S.; Shin, H.-S. Nano Based Drug Delivery Systems: Recent Developments and Future Prospects. *Journal of Nanobiotechnology* **2018**, *16* (1), 71. <https://doi.org/10.1186/s12951-018-0392-8>.
- (309) Schubert, S.; Joseph T. Delaney, J.; Schubert, U. S. Nanoprecipitation and Nanoformulation of Polymers: From History to Powerful Possibilities beyond Poly(Lactic Acid). *Soft Matter* **2011**, *7* (5), 1581–1588. <https://doi.org/10.1039/C0SM00862A>.
- (310) Zielińska, A.; Carreiró, F.; Oliveira, A. M.; Neves, A.; Pires, B.; Venkatesh, D. N.; Durazzo, A.; Lucarini, M.; Eder, P.; Silva, A. M.; Santini, A.; Souto, E. B. Polymeric Nanoparticles: Production, Characterization, Toxicology and Ecotoxicology. *Molecules* **2020**, *25* (16), 3731. <https://doi.org/10.3390/molecules25163731>.
- (311) Crucho, C. I. C.; Barros, M. T. Polymeric Nanoparticles: A Study on the Preparation Variables and Characterization Methods. *Materials Science and Engineering: C* **2017**, *80*, 771–784. <https://doi.org/10.1016/j.msec.2017.06.004>.
- (312) Austin, J.; Minelli, C.; Hamilton, D.; Wywijas, M.; Jones, H. J. Nanoparticle Number Concentration Measurements by Multi-Angle Dynamic Light Scattering. *J Nanopart Res* **2020**, *22* (5), 108. <https://doi.org/10.1007/s11051-020-04840-8>.

- (313) Cole, L.; Fernandes, D.; Hussain, M. T.; Kaszuba, M.; Stenson, J.; Markova, N. Characterization of Recombinant Adeno-Associated Viruses (rAAVs) for Gene Therapy Using Orthogonal Techniques. *Pharmaceutics* **2021**, *13* (4), 586. <https://doi.org/10.3390/pharmaceutics13040586>.
- (314) Patterson, J. P.; Kelley, E. G.; Murphy, R. P.; Moughton, A. O.; Robin, M. P.; Lu, A.; Colombani, O.; Chassenieux, C.; Cheung, D.; Sullivan, M. O.; Epps, T. H.; O'Reilly, R. K. Structural Characterization of Amphiphilic Homopolymer Micelles Using Light Scattering, SANS, and Cryo-TEM. *Macromolecules* **2013**, *46* (15), 6319–6325. <https://doi.org/10.1021/ma4007544>.
- (315) Piogé, S.; Fontaine, L.; Gaillard, C.; Nicol, E.; Pascual, S. Self-Assembling Properties of Well-Defined Poly(Ethylene Oxide)-b-Poly(Ethyl Acrylate) Diblock Copolymers. *Macromolecules* **2009**, *42* (12), 4262–4272. <https://doi.org/10.1021/ma802705b>.
- (316) Wilson, B. K.; Prud'homme, R. K. Nanoparticle Size Distribution Quantification from Transmission Electron Microscopy (TEM) of Ruthenium Tetroxide Stained Polymeric Nanoparticles. *Journal of Colloid and Interface Science* **2021**, *604*, 208–220. <https://doi.org/10.1016/j.jcis.2021.04.081>.
- (317) Cagel, M.; Grotz, E.; Bernabeu, E.; Moreton, M. A.; Chiappetta, D. A. Doxorubicin: Nanotechnological Overviews from Bench to Bedside. *Drug Discovery Today* **2017**, *22* (2), 270–281. <https://doi.org/10.1016/j.drudis.2016.11.005>.
- (318) Radu, E. R.; Semenescu, A.; Voicu, S. I. Recent Advances in Stimuli-Responsive Doxorubicin Delivery Systems for Liver Cancer Therapy. *Polymers* **2022**, *14* (23), 5249. <https://doi.org/10.3390/polym14235249>.
- (319) Sani, A.; Pourmadadi, M.; Shaghghi, M.; Mahdi Eshaghi, M.; Shahmollahamsary, S.; Arshad, R.; Fathi-karkan, S.; Rahdar, A.; Medina, D. I.; Pandey, S. Revolutionizing Anticancer Drug Delivery: Exploring the Potential of Tamoxifen-Loaded Nanoformulations. *Journal of Drug Delivery Science and Technology* **2023**, *86*, 104642. <https://doi.org/10.1016/j.jddst.2023.104642>.
- (320) Chao, X.; Zhao, L.; Ma, N.; Mou, Y.; Zhang, P. Nanotechnology-Based Drug Delivery Systems for the Improved Sensitization of Tamoxifen. *Journal of Drug Delivery Science and Technology* **2021**, *61*, 102229. <https://doi.org/10.1016/j.jddst.2020.102229>.
- (321) Parikh, R. P.; Odom, E. B.; Yu, L.; Colditz, G. A.; Myckatyn, T. M. Complications and Thromboembolic Events Associated with Tamoxifen Therapy in Patients with Breast Cancer Undergoing Microvascular Breast Reconstruction: A Systematic Review and Meta-Analysis. *Breast Cancer Res Treat* **2017**, *163* (1), 1–10. <https://doi.org/10.1007/s10549-017-4146-3>.
- (322) Misiak, P.; Niemirowicz-Laskowska, K.; Misztalewska-Turkowicz, I.; Markiewicz, K. H.; Wielgat, P.; Car, H.; Wilczewska, A. Z. Doxorubicin Delivery Systems with an Acetylacetone-Based Block in Cholesterol-Terminated Copolymers: Diverse Activity against Estrogen-Dependent and Estrogen-Independent Breast Cancer Cells. *Chemistry and Physics of Lipids* **2022**, *245*, 105194. <https://doi.org/10.1016/j.chemphyslip.2022.105194>.
- (323) Wallace, S. J.; Li, J.; Nation, R. L.; Boyd, B. J. Drug Release from Nanomedicines: Selection of Appropriate Encapsulation and Release Methodology. *Drug Deliv Transl Res* **2012**, *2* (4), 284–292. <https://doi.org/10.1007/s13346-012-0064-4>.
- (324) Wu, P.; Gao, J.; Prasad, P.; Dutta, K.; Kanjilal, P.; Thayumanavan, S. Influence of Polymer Structure and Architecture on Drug Loading and Redox-Triggered Release. *Biomacromolecules* **2022**, *23* (1), 339–348. <https://doi.org/10.1021/acs.biomac.1c01295>.
- (325) Peng, J.; Qi, T.; Liao, J.; Fan, M.; Luo, F.; Li, H.; Qian, Z. Synthesis and Characterization of Novel Dual-Responsive Nanogels and Their Application as Drug Delivery Systems. *Nanoscale* **2012**, *4* (8), 2694–2704. <https://doi.org/10.1039/C2NR30147D>.
- (326) Souto, E. B.; Fangueiro, J. F.; Fernandes, A. R.; Cano, A.; Sanchez-Lopez, E.; Garcia, M. L.; Severino, P.; Paganelli, M. O.; Chaud, M. V.; Silva, A. M. Physicochemical and Biopharmaceutical Aspects Influencing Skin Permeation and Role of SLN and NLC for Skin Drug Delivery. *Heliyon* **2022**, *8* (2), e08938. <https://doi.org/10.1016/j.heliyon.2022.e08938>.
- (327) Basak, R.; Bandyopadhyay, R. Encapsulation of Hydrophobic Drugs in Pluronic F127 Micelles: Effects of Drug Hydrophobicity, Solution Temperature, and pH. *Langmuir* **2013**, *29* (13), 4350–4356. <https://doi.org/10.1021/la304836e>.

- (328) Trushina, D. B.; Borodina, T. N.; Belyakov, S.; Antipina, M. N. Calcium Carbonate Vaterite Particles for Drug Delivery: Advances and Challenges. *Materials Today Advances* **2022**, *14*, 100214. <https://doi.org/10.1016/j.mtadv.2022.100214>.
- (329) Allen, T. M.; Cullis, P. R. Liposomal Drug Delivery Systems: From Concept to Clinical Applications. *Advanced Drug Delivery Reviews* **2013**, *65* (1), 36–48. <https://doi.org/10.1016/j.addr.2012.09.037>.
- (330) Zhu, Q.; Mao, S. Enhanced Drug Loading Efficiency of Contact Lenses via Salt-Induced Modulation. *Asian J Pharm Sci* **2019**, *14* (2), 204–215. <https://doi.org/10.1016/j.ajps.2018.05.002>.
- (331) Yin, H.; Bae, Y. H. Physicochemical Aspects of Doxorubicin-Loaded pH-Sensitive Polymeric Micelle Formulations from Mixtures of Poly(L-Histidine)-b-Poly(Ethylene Glycol)/ Poly(L-Lactide)-b-Poly(Ethylene Glycol). *Eur J Pharm Biopharm* **2009**, *71* (2), 223–230. <https://doi.org/10.1016/j.ejpb.2008.08.013>.
- (332) Ong, S. G. M.; Ming, L. C.; Lee, K. S.; Yuen, K. H. Influence of the Encapsulation Efficiency and Size of Liposome on the Oral Bioavailability of Griseofulvin-Loaded Liposomes. *Pharmaceutics* **2016**, *8* (3), 25. <https://doi.org/10.3390/pharmaceutics8030025>.
- (333) Zhou, Y.; Yu, J.; Feng, X.; Li, W.; Wang, Y.; Jin, H.; Huang, H.; Liu, Y.; Fan, D. Reduction-Responsive Core-Crosslinked Micelles Based on a Glycol Chitosan–Lipoic Acid Conjugate for Triggered Release of Doxorubicin. *RSC Adv.* **2016**, *6* (37), 31391–31400. <https://doi.org/10.1039/C6RA05501J>.
- (334) D'Souza, S. A Review of *In Vitro* Drug Release Test Methods for Nano-Sized Dosage Forms. *Advances in Pharmaceutics* **2014**, *2014*, e304757. <https://doi.org/10.1155/2014/304757>.
- (335) Doll, D. C.; Weiss, R. B. Hemolytic Anemia Associated with Antineoplastic Agents. *Cancer Treat Rep* **1985**, *69* (7–8), 777–782.
- (336) Bobrin, V. A.; Lin, Y.; He, J.; Qi, Y.; Gu, W.; Monteiro, M. J. Therapeutic Delivery of Polymeric Tadpole Nanostructures with High Selectivity to Triple Negative Breast Cancer Cells. *Biomacromolecules* **2020**, *21* (11), 4457–4468. <https://doi.org/10.1021/acs.biomac.0c00302>.
- (337) Li, M.; De, P.; Gondi, S. R.; Sumerlin, B. S. End Group Transformations of RAFT-generated Polymers with Bismaleimides: Functional Telechelics and Modular Block Copolymers. *J. Polym. Sci. A Polym. Chem.* **2008**, *46* (15), 5093–5100. <https://doi.org/10.1002/pola.22837>.
- (338) Tuccitto, N.; Li-Destri, G.; Messina, G. M. L.; Marletta, G. Reactive Messengers for Digital Molecular Communication with Variable Transmitter–Receiver Distance. *Phys. Chem. Chem. Phys.* **2018**, *20* (48), 30312–30320. <https://doi.org/10.1039/C8CP05643A>.
- (339) Green, V. S.; Stott, D. E.; Diack, M. Assay for Fluorescein Diacetate Hydrolytic Activity: Optimization for Soil Samples. *Soil Biology and Biochemistry* **2006**, *38* (4), 693–701. <https://doi.org/10.1016/j.soilbio.2005.06.020>.
- (340) Reisch, A.; Klymchenko, A. S. Fluorescent Polymer Nanoparticles Based on Dyes: Seeking Brighter Tools for Bioimaging. *Small* **2016**, *12* (15), 1968–1992. <https://doi.org/10.1002/smll.201503396>.
- (341) Sender, M.; Ziegenbalg, D. Light Sources for Photochemical Processes – Estimation of Technological Potentials. *Chemie Ingenieur Technik* **2017**, *89* (9), 1159–1173. <https://doi.org/10.1002/cite.201600191>.
- (342) Leonard, D. L.; Charlton, D. G.; Roberts, H. W.; Cohen, M. E. Polymerization Efficiency of LED Curing Lights. *J Esthet Restor Dent* **2002**, *14* (5), 286–295. <https://doi.org/10.1111/j.1708-8240.2002.tb00524.x>.
- (343) Nardi, M.; Blasco, E.; Barner-Kowollik, C. Wavelength-Resolved PhotoATRP. *Journal of the American Chemical Society* **2022**. <https://doi.org/10.1021/jacs.1c11259>.
- (344) Guinaudeau, A.; Mazières, S.; Wilson, D. J.; Destarac, M. Aqueous RAFT/MADIX polymerisation of N-Vinyl Pyrrolidone at Ambient Temperature. *Polym. Chem.* **2011**, *3* (1), 81–84. <https://doi.org/10.1039/C1PY00373A>.
- (345) Alconcel, S. N. S.; Baas, A. S.; Maynard, H. D. FDA-Approved Poly(Ethylene Glycol)–Protein Conjugate Drugs. *Polym. Chem.* **2011**, *2* (7), 1442–1448. <https://doi.org/10.1039/C1PY00034A>.

- (346) Hoang Thi, T. T.; Pilkington, E. H.; Nguyen, D. H.; Lee, J. S.; Park, K. D.; Truong, N. P. The Importance of Poly(Ethylene Glycol) Alternatives for Overcoming PEG Immunogenicity in Drug Delivery and Bioconjugation. *Polymers (Basel)* **2020**, *12* (2), 298. <https://doi.org/10.3390/polym12020298>.
- (347) Markiewicz, K. H.; Seiler, L.; Misztalewska, I.; Winkler, K.; Harrison, S.; Wilczewska, A. Z.; Destarac, M.; Marty, J.-D. Advantages of Poly(Vinyl Phosphonic Acid)-Based Double Hydrophilic Block Copolymers for the Stabilization of Iron Oxide Nanoparticles. *Polym. Chem.* **2016**, *7* (41), 6391–6399. <https://doi.org/10.1039/C6PY01558A>.
- (348) Kurakula, M.; Rao, G. S. N. K. Pharmaceutical Assessment of Polyvinylpyrrolidone (PVP): As Excipient from Conventional to Controlled Delivery Systems with a Spotlight on COVID-19 Inhibition. *Journal of Drug Delivery Science and Technology* **2020**, *60*, 102046. <https://doi.org/10.1016/j.jddst.2020.102046>.
- (349) Stubbs, C.; Congdon, T. R.; Gibson, M. I. Photo-Polymerisation and Study of the Ice Recrystallisation Inhibition of Hydrophobically Modified Poly(Vinyl Pyrrolidone) Copolymers. *European Polymer Journal* **2019**, *110*, 330–336. <https://doi.org/10.1016/j.eurpolymj.2018.11.047>.
- (350) Pound, G.; Eksteen, Z.; Pfukwa, R.; McKenzie, J. M.; Lange, R. F. M.; Klumperman, B. Unexpected Reactions Associated with the Xanthate-Mediated Polymerization of N-Vinylpyrrolidone. *Journal of Polymer Science Part A: Polymer Chemistry* **2008**, *46* (19), 6575–6593. <https://doi.org/10.1002/pola.22968>.
- (351) Iqbal, N.; Blakstad, G.; Fiksdahl, A. Head-to-Tail Homo- and Heterodimerization of Vinylamides by Hidden Proton Catalysis. *Tetrahedron* **2014**, *70* (6), 1317–1325. <https://doi.org/10.1016/j.tet.2013.12.041>.
- (352) Zataray, J.; Agirre, A.; Carretero, P.; Meabe, L.; De La Cal, J. C.; Leiza, J. R. Characterization of Poly (N -Vinyl Formamide) by Size Exclusion Chromatography-Multiangle Light Scattering and Asymmetric-Flow Field-Flow Fractionation-Multiangle Light Scattering. *J. Appl. Polym. Sci.* **2015**, *132* (34), n/a-n/a. <https://doi.org/10.1002/app.42434>.
- (353) Podzimek, S.; Johann, C. Asymmetric Flow Field-Flow Fractionation: Current Status, Possibilities, Analytical Limitations and Future Trends. *Chromatographia* **2021**, *84* (6), 531–534. <https://doi.org/10.1007/s10337-021-04035-w>.
- (354) Podzimek, S. Asymmetric Flow Field Flow Fractionation. In *Encyclopedia of Analytical Chemistry*; Meyers, R. A., Ed.; John Wiley & Sons, Ltd: Chichester, UK, 2012; p a9289. <https://doi.org/10.1002/9780470027318.a9289>.
- (355) Fuentes, C.; Castillo, J.; Vila, J.; Nilsson, L. Application of Asymmetric Flow Field-Flow Fractionation (AF4) and Multiangle Light Scattering (MALS) for the Evaluation of Changes in the Product Molar Mass during PVP-b-PAMPS Synthesis. *Anal Bioanal Chem* **2018**, *410* (16), 3757–3767. <https://doi.org/10.1007/s00216-018-1039-1>.
- (356) Groves, P. Diffusion Ordered Spectroscopy (DOSY) as Applied to Polymers. *Polym. Chem.* **2017**, *8* (44), 6700–6708. <https://doi.org/10.1039/C7PY01577A>.
- (357) Guinaudeau, A.; Coutelier, O.; Sandeau, A.; Mazières, S.; Nguyen Thi, H. D.; Le Drogo, V.; Wilson, D. J.; Destarac, M. Facile Access to Poly(N-Vinylpyrrolidone)-Based Double Hydrophilic Block Copolymers by Aqueous Ambient RAFT/MADIX Polymerization. *Macromolecules* **2014**, *47* (1), 41–50. <https://doi.org/10.1021/ma4017899>.
- (358) Jiménez-Martínez, T. S.; Romero-Manig, S.; Esturau-Escofet, N.; Briseño-Terán, M. DOSY Experiments to Monitor Block Copolymer Polymerization.
- (359) Viel, S.; Mazarin, M.; Giordanengo, R.; Phan, T. N. T.; Charles, L.; Caldarelli, S.; Bertin, D. Improved Compositional Analysis of Block Copolymers Using Diffusion Ordered NMR Spectroscopy. *Analytica Chimica Acta* **2009**, *654* (1), 45–48. <https://doi.org/10.1016/j.aca.2009.06.049>.
- (360) Gu, L.; Zhu, S.; Hrymak, A. N. Acidic and Basic Hydrolysis of Poly(N-Vinylformamide). *J. Appl. Polym. Sci.* **2002**, *86* (13), 3412–3419. <https://doi.org/10.1002/app.11364>.
- (361) Huo, Z.; Arora, S.; Kong, V. A.; Myrga, B. J.; Statt, A.; Laaser, J. E. Effect of Polymer Composition and Morphology on Mechanochemical Activation in Nanostructured Triblock Copolymers. *Macromolecules* **2023**, *56* (5), 1845–1854. <https://doi.org/10.1021/acs.macromol.2c02475>.

- (362) Moineau, G.; Minet, M.; Teyssié, P.; Jérôme, R. Synthesis of Fully Acrylic Thermoplastic Elastomers by Atom Transfer Radical Polymerization (ATRP), 2. Effect of the Catalyst on the Molecular Control and the Rheological Properties of the Triblock Copolymers. *Macromolecular Chemistry and Physics* **2000**, *201* (11), 1108–1114. [https://doi.org/10.1002/1521-3935\(20000701\)201:11<1108::AID-MACP1108>3.0.CO;2-Y](https://doi.org/10.1002/1521-3935(20000701)201:11<1108::AID-MACP1108>3.0.CO;2-Y).
- (363) Lu, W.; Goodwin, A.; Wang, Y.; Yin, P.; Wang, W.; Zhu, J.; Wu, T.; Lu, X.; Hu, B.; Hong, K.; Kang, N.-G.; Mays, J. All-Acrylic Superelastomers: Facile Synthesis and Exceptional Mechanical Behavior. *Polym. Chem.* **2017**, *9* (2), 160–168. <https://doi.org/10.1039/C7PY01518F>.
- (364) Ruzette, A.-V.; Tencé-Girault, S.; Leibler, L.; Chauvin, F.; Bertin, D.; Guerret, O.; Gérard, P. Molecular Disorder and Mesoscopic Order in Polydisperse Acrylic Block Copolymers Prepared by Controlled Radical Polymerization. *Macromolecules* **2006**, *39* (17), 5804–5814. <https://doi.org/10.1021/ma060541u>.
- (365) Wang, Y.; Schroeder, H.; Morick, J.; Buback, M.; Matyjaszewski, K. High-Pressure Atom Transfer Radical Polymerization of n-Butyl Acrylate. *Macromolecular Rapid Communications* **2013**, *34* (7), 604–609. <https://doi.org/10.1002/marc.201200752>.
- (366) Lehnen, A.-C.; Gurke, J.; Bapolisi, A. M.; Reifarth, M.; Bekir, M.; Hartlieb, M. Xanthate-Supported Photo-Iniferter (XPI)-RAFT Polymerization: Facile and Rapid Access to Complex Macromolecules. *Chem. Sci.* **2023**, *14* (3), 593–603. <https://doi.org/10.1039/D2SC05197D>.
- (367) Zimm, B. H. The Scattering of Light and the Radial Distribution Function of High Polymer Solutions. *J. Chem. Phys.* **1948**, *16* (12), 1093–1099. <https://doi.org/10.1063/1.1746738>.
- (368) Stejskal, E. O.; Tanner, J. E. Spin Diffusion Measurements: Spin Echoes in the Presence of a Time-Dependent Field Gradient. *The Journal of Chemical Physics* **1965**, *42* (1), 288–292. <https://doi.org/10.1063/1.1695690>.
- (369) Jerschow, A.; Müller, N. Suppression of Convection Artifacts in Stimulated-Echo Diffusion Experiments. Double-Stimulated-Echo Experiments. *Journal of Magnetic Resonance* **1997**, *125* (2), 372–375. <https://doi.org/10.1006/jmre.1997.1123>.
- (370) Zhou, S.; Fan, S.; Au-yeung, S. C. F.; Wu, C. Light-Scattering Studies of Poly(N-Isopropylacrylamide) in Tetrahydrofuran and Aqueous Solution. *Polymer* **1995**, *36* (7), 1341–1346. [https://doi.org/10.1016/0032-3861\(95\)95910-S](https://doi.org/10.1016/0032-3861(95)95910-S).
- (371) Siirilä, J.; Häkkinen, S.; Tenhu, H. The Emulsion Polymerization Induced Self-Assembly of a Thermoresponsive Polymer Poly(N-Vinylcaprolactam). *Polym. Chem.* **2019**, *10* (6), 766–775. <https://doi.org/10.1039/C8PY01421C>.
- (372) Nobbmann, U. *Refractive index increment dn/dc values - Materials Talks*. <https://www.materials-talks.com/refractive-index-increment-dn/dc-values/> (accessed 2024-01-14).
- (373) Zhao, X.; Coutelier, O.; Nguyen, H. H.; Delmas, C.; Destarac, M.; Marty, J.-D. Effect of Copolymer Composition of RAFT/MADIX-Derived N-Vinylcaprolactam/N-Vinylpyrrolidone Statistical Copolymers on Their Thermoresponsive Behavior and Hydrogel Properties. *Polymer Chemistry* **2015**, *6* (29), 5233–5243. <https://doi.org/10.1039/C5PY00606F>.
- (374) Liu, X.; Coutelier, O.; Harrisson, S.; Tassaing, T.; Marty, J.-D.; Destarac, M. Enhanced Solubility of Polyvinyl Esters in scCO₂ by Means of Vinyl Trifluorobutyrate Monomer. *ACS Macro Lett.* **2015**, *4* (1), 89–93. <https://doi.org/10.1021/mz500731p>.
- (375) Chiefari, J.; Mayadunne, R. T.; Moad, G.; Rizzardo, E.; Thang, S. H. Polymerization Process with Living Characteristics and Polymers Made Therefrom. US6747111B2, June 8, 2004. <https://patents.google.com/patent/US6747111B2/en> (accessed 2022-07-07).